The investigation of circulating biomarkers and potential mechanisms of resistance in the ATR/CHK1 signalling pathway in response to CHK1 inhibitor therapy

---

Nicola Louise Hannaway

Thesis submission for Doctor of Philosophy

Northern Institute of Cancer Research

July 2022

1. Abstract

The DNA damage response is a network of cell checkpoints leading to cellular repair and genome integrity when DNA insults have occurred. In cancers, enhanced tumour replication stress and genomic instability along with mutations in oncogenes and tumour suppressor genes can lead to disruption of the DNA damage response. Tumour survival becomes dependant on critical checkpoint controls. Drugs to target intact pathways, such as CHK1 inhibitors are therefore desirable and are being evaluated in clinical trials as prospective anticancer therapies. Cancer treatments have moved to a personalised approach based on tumour profiling and circulating biomarkers, such as circulating cell free DNA to predict patient response to targeted treatments. The mechanisms underpinning sensitivity and resistance to CHK1 inhibitor treatment are still unclear.

This project explores three distinct strands of research to examine both primary and acquired mechanisms of CHK1i resistance. Firstly, investigating gene and protein expression changes in Eμ-Myc mouse models of B-Cell lymphoma. Wild type Eμ-Myc mice are sensitive to CHK1i treatment, however by contrast Eμ-Myc NF-κB *c-Rel -/-* and *RelA T505A* lymphomas are CHK1i resistant. Secondly, the generation and characterisation of U2OS osteosarcoma cells with acquired CHK1i resistance. Lastly, investigating if DNA damage response mutations can be isolated from patient cfDNA samples on a CHK1 inhibitor clinical trial.

Results have shown that resistance to CHK1 is complex and that there are multiple resistance mechanisms in place. The Eμ-Myc NF-κB *c-Rel -/-* mice completely downregulate the DNA damage response and this pattern is shared with some resistant cell lines, but alternative mechanisms developed in other models. DDR mutations can be detected and tracked in cfDNA samples and show a large degree of heterogeneity between patients. This study highlights the importance of the ATR/CHK1 DNA damage checkpoint and how drug resistance mechanisms can vary between diverse tumour mutational profiles.

Acknowledgements

This thesis has been funded by Cancer Research UK and I would like to thank them for this research opportunity. I would like to thank my supervisors Prof. Neil Perkins and Dr. Alastair Greystoke for their help and advice during this PhD. Thanks to my panel review members Dr. Yvette Drew and Prof. John Higgins. I would like to express my gratitude to Dr. Jill Hunter for her amazing support and encouragement throughout this project. Many thanks to Dr. Luke Gaughan for his support during my PhD project. I would like to thank members of the Perkins' lab, in particular Dr. Iglika Ivanova and Dr. Adrian Yemm for their help with my project and for the good times within the lab. I would like to thank Dr. Edward Amankwatia from the Biomarkers team for his help and advice at the NICR. I would like to express my thanks to Dr. Raf Hussain, Dr. Jon Coxhead and Leigh Taylor for their assistance at the Genomics Core Facility. Thank you to Dr. Peter Leary for his bioinformatics support throughout this project. Many thanks to the other PhD students for providing the much needed social time outside of the lab. I would like to thank my colleagues at the Northern Centre for Cancer Care for your ongoing support throughout this time. And finally, a big thank you to all of my family and friends who have shown me encouragement throughout this project.

COVID-19 impact statement

Throughout the COVID 19 pandemic I have been working full time in a clinical role in the NHS as a Specialty Registrar. This workload has increased from the pandemic and I have been asked to cover additional roles at times alongside my usual duties. Study leave for the majority of 2020 was cancelled or not permitted.

There has been no direct impact on my research time in the lab, however the increased clinical workload and lack of leave time has had an impact on the time dedicated to writing this thesis. Juggling the additional workload with writing the thesis has increased stress levels during this busy time and I have at times had to focus purely on clinical work to make this manageable. Some areas of the thesis are therefore less developed than others. I have however submitted a full thesis for examination.

Contents

List of Figures

List of tables

Abbreviations

Abbreviation	Explanation
53BP1	p53 binding protein 1
AKT	Protein kinase B
ALK	Anaplastic lymphoma kinase
APE1	AP endonuclease 1
ARF	ADP ribosylation factor
ATM	Ataxia-telangiectasia mutated protein
ATR	Ataxia-telangiectasia and Rad 3 related protein
ATRIP	ATR interacting protein
BEAMing	Beads, emulsion, amplification and magnetics
BER	Base excision repair
BRCA1	Breast cancer susceptibility protein 1
BRCA2	Breast cancer susceptibility protein 2

Abbreviation	Explanation
BRCT	BRCA1 C-terminal
C3D1	Mid study cfDNA sample
CApp-Seq	Cancer personalised profiling by deep sequencing
CCNE1	Cyclin E1
CDC6	Cell division cycle 6
CDC7-DBF4	Cell division cycle 7 with associated subunit
CDC25A	Cell division cycle 25A
CDC45	Cell division cycle 45
CDK	Cyclin-dependent kinase
CDK2	Cell division kinase 2
CDT1	Chromatin licensing and DNA replication factor 1
CETN2	Centrin 2
cfDNA	Circulating cell free DNA

Abbreviation	Explanation
CHK1	Checkpoint protein 1
CHKi	Checkpoint protein 1 inhibitor
CHK2	Checkpoint protein 2
CNVs	Copy number variations
CR	CHK1 resistant U2OS cells
CS	CHK1 suppressed pathway
CSA	Cockayne syndrome WD repeat protein A
CSB	Cockayne syndrome WD repeat protein B
CTCs	Circulating tumour cells
CTCAE	Common Terminology Criteria for Adverse Events
ctDNA	Circulating tumour DNA
D-7to-4	Pre study cfDNA sample
ddPCR	Droplet digital PCR

Abbreviation	Explanation
DDR	DNA damage response
DLT	Dose limiting toxicity
DMEM	Dulbecco's Modified Eagle's Medium
DMSO	Dimethylsulfoxide
DNA	Deoxyribonucleic acid
DNA-PK	DNA dependent protein kinase
DNA-PKcs	DNA-dependent protein kinase catalytic subunit
DSB	Double stranded DNA breaks
DUB	Deubiquitinating enzyme
EOS	End of study cfDNA sample
FA	Fanconi anaemia
FBS	Foetal bovine serum
FOXM1	Forkhead box protein M1

Abbreviation	Explanation
GE	Gene expression
GGNER	Global genome nucleoside excision repair
GINS	DNA replication complex
GSK	Glycogen synthase kinase
GSK3β	Glycogen synthase kinase 3 β
H2AX	H2A histone family member X
HDR	Homology-directed repair
HGSOC	High grade serous ovarian cancer
HMGN1	High mobility group nucleosome-binding domain- containing protein 1
HR	Homologous recombination
HRP	Horseradish peroxidase
ICAM-1	Intracellular adhesion molecule 1
ICLs	Intrastrand crosslinks

Abbreviation	Explanation
IκB	Inhibitors of κB
IKK	IκB kinase complex
IL-1	Interleukin 1
IL-6	Interleukin 6
INDELs	Insertions or deletions of nucleotide bases
IR	Ionising radiation
LIG1	DNA ligase 1
LIG3	DNA ligase 3
LPS	Lipopolysaccharide
MAPK	MAP kinase
MAPKAP2/MK2	MAP kinase activated protein 2
MCM	Minichromosome maintenance complex
MDM2	Mouse double minute 2

Abbreviation	Explanation
MDT	Maximum tolerated dose
miRNA	Micro RNA
MMP	Matrix metalloproteinase
MMR	Mismatch repair
MRN	MRE11-RAD50-NBS1 complex
MSI	Microsatellite instability
NEMO/Iκγ	Nuclear factor (NF)-κB essential modulator
NER	Nucleotide excision repair
NF-κB	Nuclear factor κB
NGS	Next generation sequencing
NHEJ	Non-homologous end-joining
NIK	NF-κB inducing kinase
NSCLC	Non-small cell lung cancer

Abbreviation	Explanation
ORC	Origin recognition complex
PAR	Poly(ADP)ribose
PARP	Poly(ADP)ribose polymerase
PARPi	Poly(ADP)ribose polymerase inhibitor
PBS	Phosphate buffered saline
PCA	Principle components analysis
PCNA	Proliferating cell nuclear antigen
PCR	Polymerase chain reaction
PD-1	Programmed cell death protein 1
PDL-1	Programmed death-ligand 1
PE	Plating effectiveness
PHLPP1	PH domain leucine-rich repeat protein phosphatase 1
PNK	Polynucleotide kinase

Abbreviation	Explanation
PNKP	Polynucleotide Kinase 3'-Phosphatase
Pol-α	DNA polymerase α
Pol-β	DNA polymerase β
Pol-ε	DNA polymerase ε
Pol-δ	DNA polymerase δ
Pol-α-pri	Pol-α complex
PPC3	Primer cocktail 3
QC	Quality control
qPCR	Quantitative PCR
RFC	Replication factor C
RHD	REL homology domain
RIN	RNA integrity number
RNA	Ribonucleic acid

Abbreviation	Explanation
ROS	Reactive oxygen species
RPA	Replication protein A
Safe-SeqS	Safe sequencing system
SCC	Squamous cell carcinoma
SDS-PAGE	Sodium dodecyl sulphate (SDS) polyacrylamide gel electrophoresis
SF	Surviving fraction
siRNA	Small interfering RNA
Skp2	S-Phase Kinase-Associated Protein 2
SMB	Streptavidin magnetic beads
SPB	Sample purification beads
SSB	Single strand DNA breaks
TAD	Transcription activation domain
TAE	Tris Acetate-EDTA buffer

Abbreviation	Explanation
TAm-seq	Tagged-amplicon deep sequencing
TCR	T cell antigen receptor
TE	Tris EDTA buffer
TGCA	The Cancer Genome Atlas Project
TIFIIH	Transcription initiation factor IIH
TIPIN	TIMELESS- interacting protein
TNF-α	Tumour necrosis factor α
TOPBP1	Topoisomerase binding protein 1
UMI	Unique molecular identifiers
USP1	Ubiquitin-specific-processing protease 1
USP7	Ubiquitin-specific-processing protease 7
USP14	Ubiquitin-specific-processing protease 14
USP20	Ubiquitin-specific-processing protease 20

Abbreviation	Explanation
USP35	Ubiquitin-specific-processing protease 35
USP53	Ubiquitin-specific-processing protease 53
UV	Ultraviolet
UV-DDB	Ultraviolet-damaged DNA binding protein
UVSSA	UV-stimulated scaffold protein A
VCAM-1	Vascular cell adhesion molecule 1
VEGF	Vascular endothelial growth factor
WES	Whole-exome sequencing
WGS	Whole-genome sequencing
WT	Wild type
XAB2	XPA-binding protein 2
XPCC	Xeroderma pigmentosum complementation group C
XRCC	X-ray repair cross-complementing protein

2. Introduction

2.1. DNA damage response and repair

2.1.1. DNA damage

In each mammalian cell division, billions of nucleotides have to be accurately copied in order to retain genomic integrity (1,2). All living cells are however continuously exposed to DNA damaging agents that can cause mistakes in DNA replication (2). Both exogenous and endogenous agents can lead to DNA damage, with the generation of approximately 10^5 lesions each day in mammalian genomes (1). Failure to copy DNA correctly during replication or a high frequency of replication errors will result in genomic changes in daughter cells (1–3). Changes in DNA through replication error can include gene amplifications, mutations leading to a change in gene function and deletions or rearrangements of chromosome segments (2–4). Accumulation of genomic alterations can potentially lead to unregulated cell growth and survival, deviations in cell cycle control and cancers (3,4).

2.1.2. Cell cycle checkpoints

Multiple cell cycle checkpoints exist to prevent the accumulation of replication errors and genomic instability during cell replication (5,6). Cell cycle arrest at these checkpoints allows time to facilitate cell survival via repair of DNA damage or programmed cell death via apoptosis (1,7,8). Normal cells have the capacity to arrest in G1, S, or G2 phase of the cell cycle, allowing multiple time points for repair of potentially lethal DNA damage prior to DNA replication or mitosis (5,8). Cells halt progression to the next part of the cell cycle until the previous phase has been successfully completed (9). Figure 2.1 summarises the cell cycle checkpoints.

At any given time, most normal cells will be in the gap/growth G1/G0 phases of the cell cycle, therefore cell cycle arrest at the G1/S checkpoint allows cellular repair prior to entering DNA replication (5,10). The S phase checkpoint arrests DNA replication to manage unrepaired DNA damage or repair DNA damage obtained from collapsed replication forks (8). The G2/M checkpoint allows time to repair DNA double strand breaks before cells enter mitosis and undergo cell division (8).

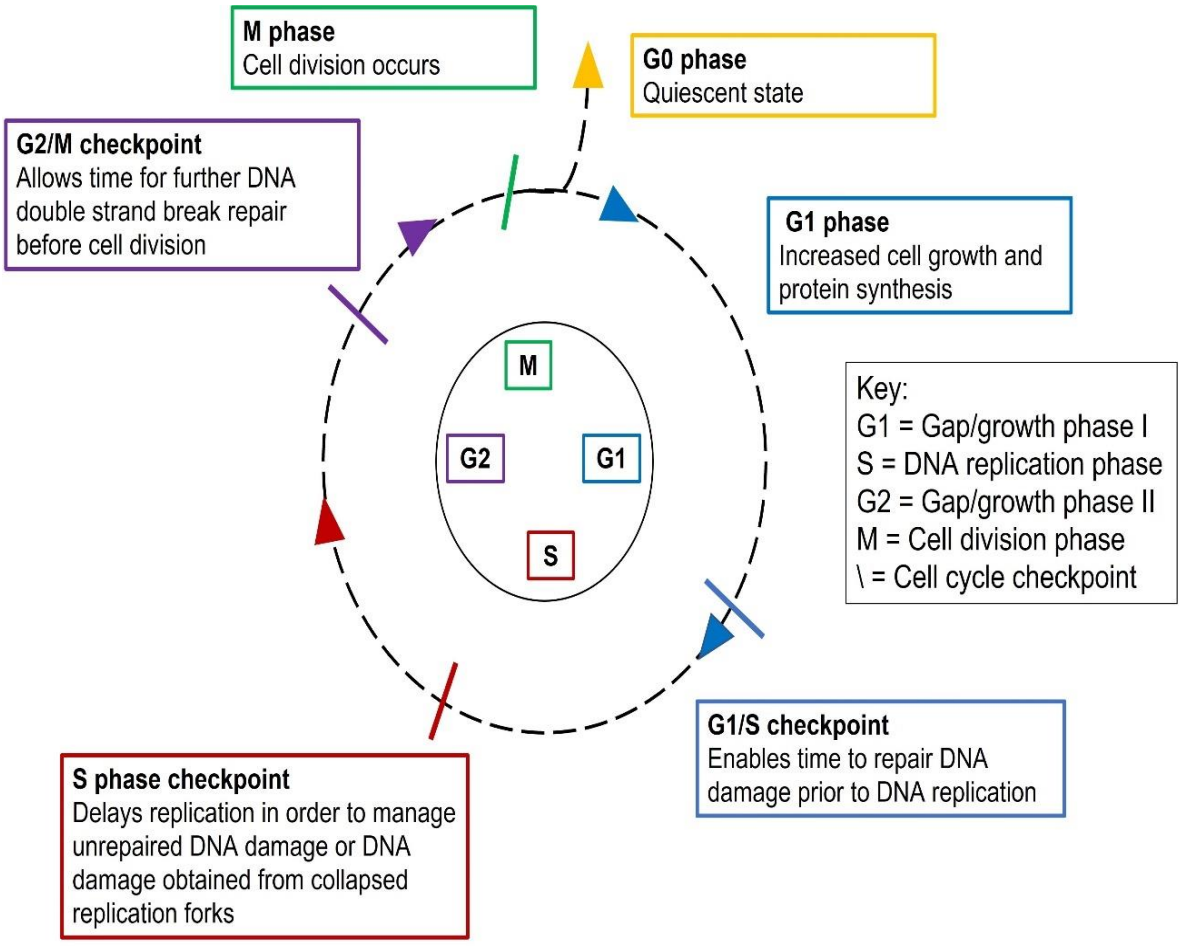

Figure 2.1. Cell cycle checkpoints. Adapted from O'Connor MJ, 2015 (148). Summary of the stages of the cell cycle leading to cell division. To maintain genome integrity, cell cycle checkpoints are in place. During cell cycle checkpoints, the cell cycle can be stalled to allow for DNA damage removal or repair before cell cycle progression occurs. The G0 phase, M phase and G1 phase are shown and described. The roles of the G1/S checkpoint, the S phase checkpoint and the G2/M checkpoint within the cell cycle are summarised.

2.1.3. Normal cell replication

Replication of DNA occurs only once during the cell cycle as shown in Figure 2.2. The initiation of replication is controlled via the replicative DNA helicase minichromosome maintenance complex 2–7 (MCM2–7) (1,11). During the G1 phase, the licensing process is initiated when 2 MCM2-7 complexes are loaded at replication origins and are activated exclusively during the subsequent S phase (1,12). The presence of the origin recognition complex (ORC), cell division cycle 6 (CDC6) and chromatin licensing and DNA replication factor 1 (CDT1) are also required to form the pre-replicative complex (11). An excess of pre-replicative complexes are present in cells but only a selected subset are used to initiate replication (13).

Origin firing is the activation of licenced origins and is triggered by cyclin-dependent kinase (CDK) and CDK-like kinase activity (1). This process depends on the stable association of CDC45 and the DNA replication complex GINS as well as other factors such as MCM10 which bind to DNA polymerase α (pol-α) (14). Re-replication is prevented by increased CDK activity and a blockade of MCM2-7 reloading outside of the G1 phase (1).

Replication fork progression is initiated by the CDC45–MCM2–7–GINS helicase which unwinds DNA (1). Synthesis of new DNA molecules is initiated by the Pol-α primer complex which contains DNA primase and polymerase subunits along with replication factor C (RFC) and proliferating cell nuclear antigen (PCNA)(1). The leading strand is extended by Pol-ε and lagging strand by Pol-δ (1,11). A further key component of fork progression is the Claspin–TIMELESS–TIMELESS- interacting protein (TIPIN) complex, which coordinates DNA unwinding (1,15).

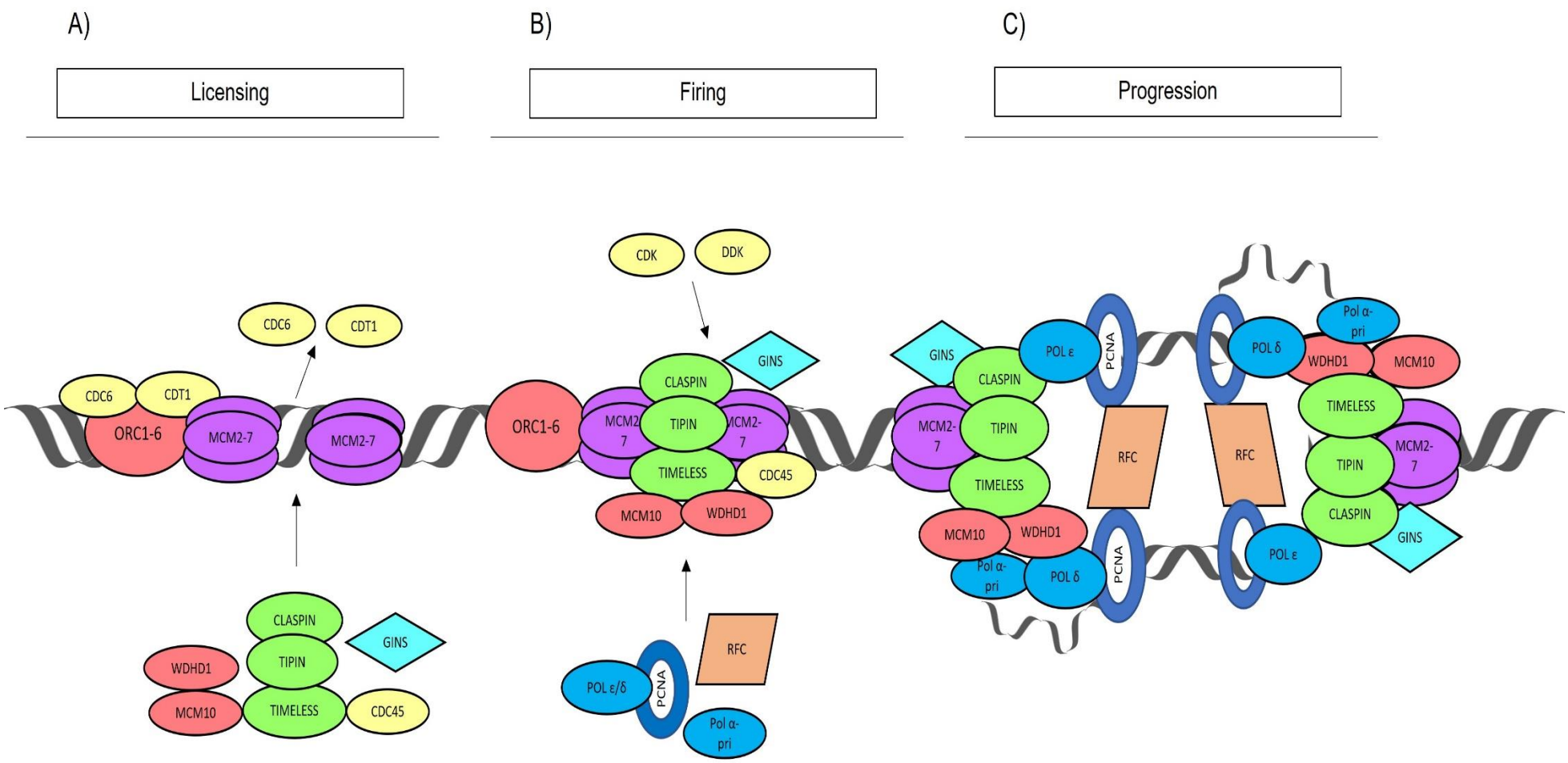

Figure 2.2. Principles of DNA replication. Adapted from Gaillard H et al., 2015 (1). DNA replication occurs once during each cell cycle. Replication is initiated by the DNA helicase minichromosome maintenance complex 2-7 (MCM2-7) which is loaded to the replication origins in G1 phase and activated in S phase. A) Licensing is the loading of 2 MCM-2 helicases at the replication origins. This requires the origin recognition complex (ORC) and the activity of cell division cycle 6 (CDC6) ATPase and chromatin and DNA licensing and DNA replication factor (CDT1) protein to form the pre-replicative complex. CDT1 and CDC6 are subsequently released when the pre-replicative complex is formed. B) Origin firing is triggered by cyclin dependent kinase (CDK) and CDK-like kinase with associated subunit (CDC7-DBF4). A stable association of CDC45 and the DNA replication complex GINS, which binds to DNA polymerase-α (pol-α), are required for origin firing to occur. At each fired origin, 2 sister replication forks separate from the origin by the activity of the CDC45-MCM2-7-GINS complex. C) Replication fork progression and DNA synthesis is initiated by the pol-α complex which contains DNA primase and polymerase subunits along with replication factor C (RFC) and proliferating cell nuclear antigen (PCNA). The Claspin-TIMELESS-TIPIN complex coordinates DNA unwinding with new DNA synthesis.

2.1.4. Mechanisms of DNA damage

DNA damage can be categorised as originating from either exogenous or endogenous sources (1,2,6,16–19). Exogenous DNA damage occurs from a range of environmental sources, chemical and physical insults causing damage to DNA (2,4,20) and are shown in Figure 2.3. Most endogenous DNA damage is due to DNA reacting in hydrolytic and oxidative reactions with water and reactive oxygen species (ROS) naturally present within cells (2,4,20).

Examples of exogenous DNA damage

Ultraviolet radiation

Ultraviolet (UV) radiation from the sun is a leading cause of skin cancers and can cause a range of insults to DNA (2,21). UV radiation can lead to direct excitation and instability of DNA and also cause indirect damage via photosensitising nearby molecules (2,22). UV damage, particularly from UVB radiation and the broader spectrum UVC, can cause pyrimidine dimers within DNA. This leads to distortion of the DNA helix and replication stress (2,23,24). UVA radiation damages DNA by the formation of DNA adducts and DNA strand breakages (2,22). UV radiation across all spectrums can also lead to DNA crosslinks linking between the two strands of the DNA double helix (2,24).

Ionising radiation

Ionising radiation (IR) consisting of alpha, gamma, beta rays and X-rays is present in the environment in several different forms. This ranges from soil and rocks to medical diagnostic purposes and radiotherapy treatment (2,25). IR can damage DNA directly by the formation of both single and double strand breaks (26). IR can also indirectly trigger DNA damage by the formation of DNA reactive free radicals which leads to the formation of base lesions (2,26,27).

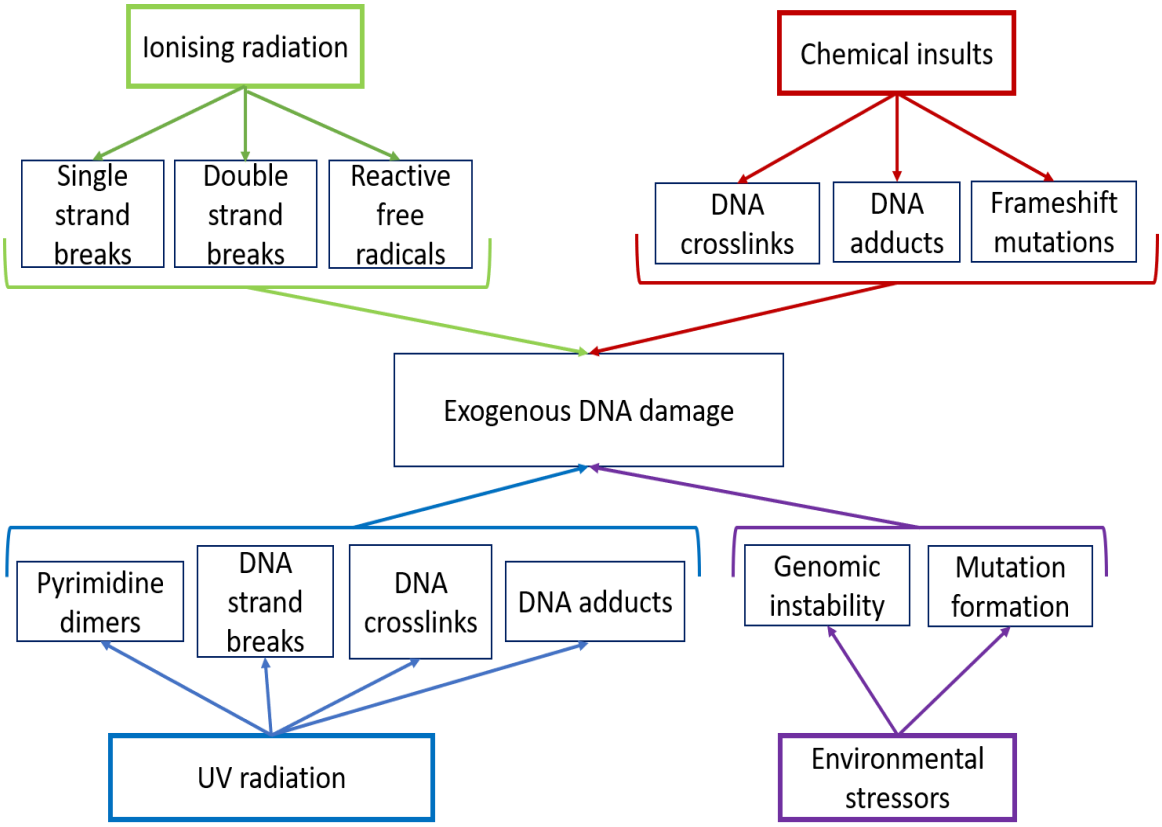

Figure 2.3. Examples of exogenous DNA damage. Summary diagram displaying how endogenous DNA damage can be obtained from ionising radiation, chemical insults, environmental stressors and UV radiation and examples of the type of DNA damage caused by each insult.

Chemical insults

Alkylating agents are found in tobacco smoke, in the industrial setting and are also used as chemotherapy agents (2). Such agents have an increased affinity for nucleophilic base ring nitrogens. This can lead to adducted DNA bases and both interstrand and intrastrand crosslinks which block the metabolic activity of DNA (2). Aromatic amines are also found in cigarette smoke, from fuel burning and industrial dyes (21,28). When activated by the P450 monooxygenase system, aromatic amines are converted into alkylating agents with carcinogenic properties (22). This can subsequently lead to DNA base substitutions and frameshift mutations leading to DNA damage (2,22). Poly-aromatic hydrocarbons are carbon compounds associated with carcinogenesis. Sources include incomplete burning of fossil fuels and cigarette smoke (2,28). Breakdown of these products leads to reactive intermediates which can cause DNA damage, including DNA adducts (28).

Environmental stressors

Environmental stressors such as extreme heat or cold and hypoxia can also lead to DNA damage (2,29,30). These stresses can lead to the formation of mutations at tri-nuclear repeats which generate cellular genomic instability (2).

Examples of endogenous DNA damage

Reactive Oxygen Species

The most common form of DNA damage is from the formation of Reactive Oxygen Species (ROS) (1,2). These are continuously formed as part of normal cellular biochemical and metabolic processes (20,31). At low levels ROS are important in redox reactions and as part of the immunological response, but at higher levels ROS can cause DNA damage. ROS can therefore can be linked to disease states including heart disease and cancers (2,32). ROS can lead to DNA base damage by adding to DNA double bonds, reaction with hydrogen atoms, creation of multiple single strand breaks and modifications to sugar structures (4,20,33).

Replication errors

Cell replication requires coordination of sequencing pathways and enzymes such as DNA polymerases to copy DNA accurately (1,32,34). Despite this, the process is error prone and can lead to thousands of base deletions, insertions and substitutions with each cycle (32,35). If unrepaired, this can lead to a shift in the reading frame and a potential change in protein (2,35). Topoisomerase enzymes can also cause DNA breaks when relaxing DNA strands for replication to occur. Normally strands are also re-ligated by topoisomerase enzymes to resolve the DNA helix (36,37) . Errors in this process could lead to mismatch of base alignment and destabilisation of DNA (2,36).

Base deamination

Base deamination provides another source of DNA mutation. This involves the loss of amine groups leading to a change in DNA bases. This occurs more commonly at the site of single strand breaks during active replication and transcription and can lead to faults in translated proteins (2,38). In addition, abasic sites can be formed when bonds between nitrogen and sugar groups in DNA are cleaved. These sites are unstable and readily convert to single strand DNA breaks (39).

DNA methylation reactions occur as part of normal cellular reactions but can also be a further source of DNA damage. Abnormal base pairing with other residues can lead to reactions such as erroneous mismatch repair and cytotoxicity (38,39). A summary of the potential causes of endogenous DNA damage is shown in Figure 2.4.

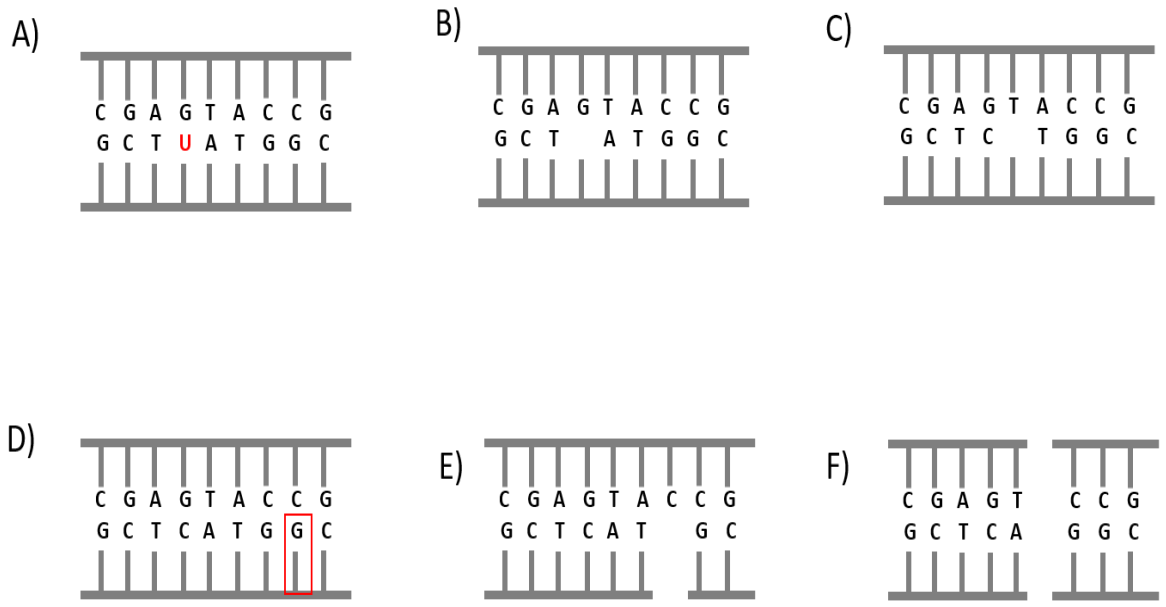

Figure 2.4. Examples of endogenous DNA damage. Adapted from Tubbs A and Nussenzweig A, 2017 (32). A) Cytosine deamination. Loss of amine groups can lead to base changes. B) Depyrimidination – loss of cytosine or thymine bases and C) Depurination. Loss of guanine or adenine bases are common mutations that can lead to base substitution if repaired incorrectly. D) Reactive oxygen species leading to modification of base structure and DNA breaks. E) Single strand DNA breaks and F) Double strand DNA breaks can occur from DNA insults and during DNA repair processes.

2.1.5. Replication stress and genomic instability

Genomic instability is the increased propensity for genomic errors or a dysregulation of cell cycle and is considered to be one of the enabling characteristics of cancer (2–4,40). Replication stress is characterised by the stalling of replication forks and slowing of new DNA synthesis leading to a disruption in cell cycle activity (1). High levels of unregulated DNA damage will lead to increased replication stress, which is a key cause of genome instability (41). The mechanisms leading to replication stress are discussed in this section and summarised in Figure 2.5 (42).

Licensed origin scarcity

Deregulated origin activation can lead to licensed origin scarcity during the S phase of the cell cycle (1). This can result from the partial depletion of the MCM2-7 complex, which is normally present in abundance. The reduced level of MCM2-7 prevents correct origin firing during S phase and will mean that replication cannot be completed before the transition to mitosis (1,43). This can lead to chromosome instability at fragile sites (43). A decrease in nucleotide supply or a reduction in other replisome proteins can also reduce the efficiency of replication thus leading to slow replication fork progression and increased DNA instability (44).

Repetitive elements

Some areas of the chromosome are more prone to DNA gaps and breaks when exposed to DNA damage. These fragile sites are characterised by trinucleotide repeats, usually CGG, CAG, GAA, and GCN (1,45). These sites are also prone to forming hairpins that can provide additional replication stress by inhibiting the progression of replication forks, leading to DNA breaks (1). There is a strong association with the presence of fragile sites and oncogene induced replication stress, including amplifications and mutations in tumour growth promoting genes such as *MYC and RAS* (44,46).

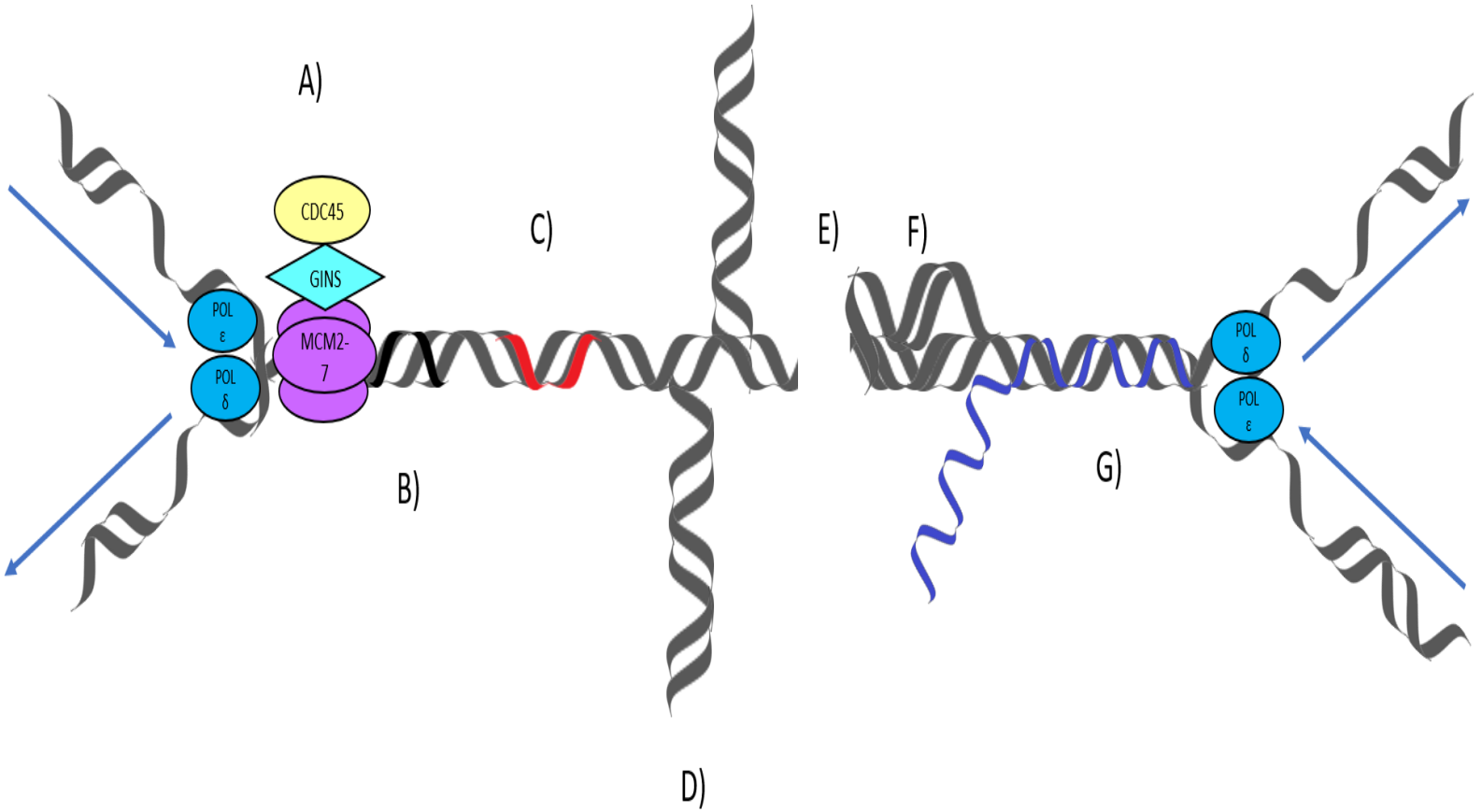

Figure 2.5. Mechanisms of replication stress. Adapted from Petropoulos M et al., 2019 (42). A) Replication-transcription collision. B) Formation of interstrand crosslinks (demonstrated with black interstrand links). C) DNA insults such as base nucleotide changes and deletions which change DNA structure (demonstrated with structural changes highlighted in red). D) Formation of secondary structures in the DNA such as hybridisations and R loops. E) Damage such as obtained with insults such as ionising radiation leading to double strand DNA breaks (demonstrated by a gap in DNA). F) Unscheduled replication from increased origin firing (shown with abnormal area of replication). G) Hybridisation of DNA and RNA which can promote single strand breaks (highlighted in blue as RNA hybridisation).

Interstrand crosslinks

Interstrand crosslinks (ICLs) are potentially toxic lesions which prevent DNA strands from being able to separate. The potential to cause damage to cancer cells with ICLs is exploited with the use of chemotherapeutic agents, in particular with alkylating agents and platinum chemotherapy (47,48). Covalent crosslinks occur at the site of DNA damage between both strands of the double helix leading to blockage of RNA and DNA polymerases (49). This subsequently can lead to double helix distortion and the disruption of DNA transcription and replication (48,49). If unrepaired, there is an increased potential for chromosomal deletions and DNA breaks (48).

Replication-transcription collisions

Transcription and replication sites tend to have an increased rate of errors as the two processes use the same template concomitantly (1,44). The coding DNA strand is single stranded during transcription and more unstable than the template strand. Damaged bases may therefore may not be repaired efficiently (44). Additionally, during transcription, positive or negative supercoiling can occur behind an elongating RNA polymerase. This can lead to single-stranded DNA breaks (50). The single stranded coding DNA strand may hybridise with the newly generated RNA, forming displaced areas of single stranded DNA known as R loops (1,50). Supercoiling and the accumulation of R loops can stall replication forks and lead to collisions between concurrent sites of transcription and replication, again leading to increased DNA breaks and DNA damage accumulation (1,44,50).

Unscheduled replication

Unscheduled replication is when the replication origin firing frequency is altered, leading to either replication occurring more than once during the cell cycle or an increase in origin firing in the S phase of the cell cycle (1). Re-replication is caused by an upregulation of CDT1 and CDC6 and this can be stimulated by oncogene upregulation (1,51). Re-replication also leads to replication fork slowing, although it is not clear if this is due to increased collisions or due to increased DNA breaks (1,51). Unscheduled replication is often seen in early malignant lesions and can be driven by an upregulation in oncogene expression, such as *CCNE1, c-MYC and RAS* (1,44,51).

2.1.6. DNA repair mechanisms

DNA repair pathways are selected and activated according to the type of DNA lesion acquired. These pathways remove and repair most DNA lesions that would otherwise generate mutation or errors in cellular metabolic processes which could lead to enhanced replication stress. These pathways can work independently but also cross-link with other DNA repair mechanisms in order to facilitate repair or cell death (19,52,53). Figure 2.6 shows these mechanisms of DNA repair in more detail (54).

Mismatch repair pathway

The DNA mismatch repair (MMR) pathway is the process of resolving single base mutations and small insertion/deletion loops formed by DNA polymerase (55–57). MMR is involved in the repair of DNA damage caused by replication errors along with damage from alkylating agents, chemotherapy agents such as Cisplatin, UV light and environmental agents involved in the formation of DNA adducts (58). MMR proteins are additionally involved in the activation of cell cycle checkpoints and apoptosis pathways in response to DNA damage (57). The mechanisms behind mismatch repair are not fully understood but it is well established that loss of mismatch repair or inherited mutations in MMR genes can lead to a predisposition to cancer as shown in Lynch syndrome (57–59).

Base excision repair

Modification or loss of bases from small endogenous sources, such as unavoidable hydrolysis, alkylation and oxidation, are repaired by base excision repair (BER) (38,60). This DNA repair process normally takes place during the G1 stage of the cell cycle (2). The pathway is divided into short patch BER (single nucleotide replacement and the predominant repair pathway) or long patch BER, where between 2 and 13 nucleotides are replaced. The subtype of BER selected is dependent on the nature of the 5‘ and 3‘ ends at the site of DNA damage (61).

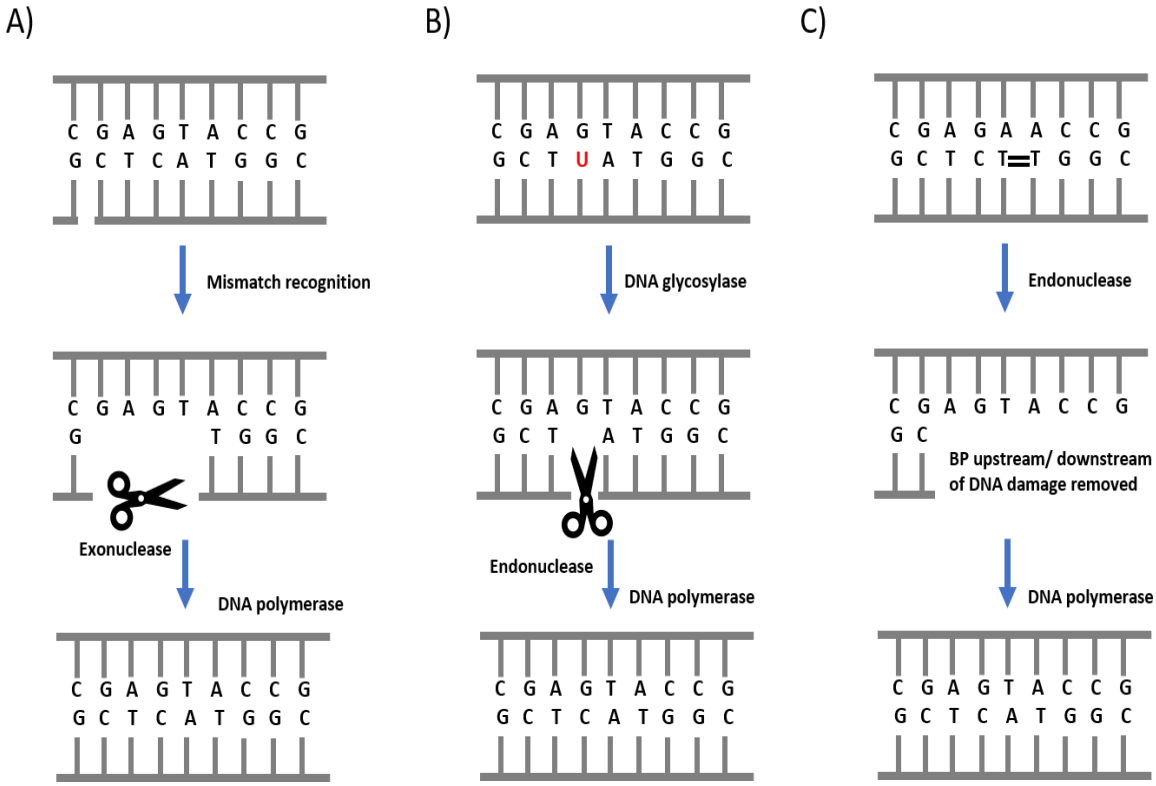

Figure 2.6. Mechanisms of DNA repair. Figure adapted from Nordicbiosite.com (54). A) Mismatch repair - this process repairs single base mutations and simple insertions and deletions. B) Base excision repair. Single base lesions are recognised by DNA glycosylase enzymes and repaired with excision and DNA polymerase repair. C) Nucleotide excision repair. Lesions such as pyrimidine dimers are detected and bases upstream and downstream of the lesion are removed before DNA polymerase repair of DNA sequence.

During BER, chromatin remodelling initially occurs at the site of DNA damage. Lesions are recognised by a series of DNA glycosylase enzymes (2,31,60). These DNA glycosylase enzymes excise damaged bases and cleave the phosphodiester backbone of the damaged base. A blocking residue remains attached to the deoxyribose upstream of the excised base, which is removed by either AP endonuclease 1 (APE1) or polynucleotide kinase phosphatase (PNKP), a 3' DNA phosphatase and 5' DNA kinase, depending on the modifications required for repair (31,61,62).

Base removal by a DNA glycosylase generates an abasic or apurinic/apyrimidinic site (AP site) in DNA (63). For short patch repair, this site is a substrate for APE1, which cleaves the DNA backbone 5' to the AP site, generating a 3'-hydroxyl and a 5'-2-deoxyribose-5'-phosphate (5'-dRP) (2,63). Gap repair is coordinated by the 5'-dRP lyase activity of DNA polymerase β (Pol-β) (gap tailoring), followed by filling the single nucleotide gap by Pol-β and ligation by either DNA ligase 1 (LIG1) or a complex of DNA ligase 3 (LIG3) and the scaffold protein X-ray repair cross-complementing protein 1 (XRCC1) (2,31).

For long patch repair up to 13 nucleotides are replaced by Pol δ or Pol ε and gap repair is completed by LIG1. Poly(ADP-ribose) polymerase 1 (PARP1) and XRCC1 facilitate repair by recruiting necessary repair enzymes and providing the scaffold for both short patch and long patch BER (61). The negative charge of the ADP-ribose polymers to the site of the break is necessary for the recruitment of XRCC, which subsequently recruits PNPK and DNA polymerase, and facilitates the loosening of chromatin to allow repair (61). BER protects against cancer, ageing and neurodegeneration and can take place both in the nucleus and in mitochondria (2,62).

Nucleotide excision repair

Nucleotide excision repair (NER) manages DNA helix-distorting lesions that interfere with base pairing and generally obstruct normal replication including bulky pyrimidine dimers, DNA adducts and crosslinks (63,64). NER is managed down 2 separate pathways – one that scans the global genome for distortions in the helix and a second that monitors transcription related damage (64). During the global genome NER (GGNER) pathway, a complex formed between the UV-damaged DNA binding protein (UV-DDB) and the GGNER specific DDB2 initiate damage recognition (63). DDB2 binds to and causes a kink in damaged DNA to facilitate xeroderma pigmentosum complementation group C (XPC) binding (33,65). XPC, which is complexed with hRAD23B and centrin 2 (CETN2), causes structural changes to the DNA and the recruitment of transcription initiation factor IIH (TFIIH) (33,65). Defects in the GGNER can lead to an increased development of cancers, as demonstrated in the skin cancer predisposing condition xeroderma pigmentosum (33).

Transcription coupled NER (TCNER) is initiated by lesion stalled RNA polymerase II (RNAPII), an enzyme which synthesises mRNA and microRNA (2). RNA polymerases can be blocked by bulky adducts, platinum induced intrastrand crosslinks and aromatic hydrocarbons, by discontinuities in the DNA template strand such as nicks and abasic sites, and by replication site collisions (65). Defects in the TCNER can lead to severe neurodevelopmental disorders such as Cockayne syndrome (33). Stalled RNAPII leads to the recruitment of TCNER-specific Cockayne syndrome proteins Cockayne syndrome WD repeat protein A (CSA) and Cockayne syndrome protein B (CSB). CSA and CSB are required for further assembly of a TCNER complex. This includes several TCNER-specific proteins, such as UV-stimulated scaffold protein A (UVSSA), ubiquitin-specific-processing protease 7 (USP7), XPA-binding protein 2 (XAB2) and high mobility group nucleosome-binding domain-containing protein 1 (HMGN1) (33,65). The TCNER is localised to the site of DNA damage due to the stalling of RNAPII, leading to exposure of the lesion site and recruitment of TFIIH (2,33,65). Both the GGNER pathway and the TCNER pathway converge at this stage to remove and repair the damage from the transcribed strand (2,33).

Interstrand crosslink repair

Interstrand crosslinks (ICL) are generated by chemotherapeutic crosslinking agents such as Cisplatin, nitrogen mustard and alkylating agents (2). ICL repair is initiated when replication forks are stalled triggering the activation of DNA repair pathways. This involves the coordination of multiple DNA repair mechanisms, including NER and homologous recombination and occurs in the S phase of the cell cycle (48). ICL repair is initiated by the chromatin loading of Fanconi anaemia (FA) pathway proteins as discussed later (66). The assembly of FA proteins and initiation of repair creates intermediate products, such as single strand and double strand breaks which are subsequently repaired by other repair mechanisms (2). Defects in FA family proteins lead to Fanconi anaemia, a condition associated with genomic instability and increased incidence of cancer (48).

Single strand break repair

Single strand breaks (SSB) are a commonly generated source of DNA damage. SSB are generated from a range of DNA insults, including the base excision repair process, damage from reactive oxidative species or from exposure to ionising radiation (2,55,67).

There is a marked overlap with the BER pathway and the latter stages of both SSB repair and BER converge into the same repair pathway (61). PARP1 and PARP2 act as molecular sensors of DNA damage from both single strand breaks and double strand breaks, which are recognised by two PARP1 zinc finger motifs. The activation of PARP1 and PARP2 and the subsequent synthesis of poly(ADP-ribose) (PAR) chains occur rapidly at the site of single strand DNA breaks (55,68). The PAR chains act as platforms to recruit additional DNA repair factors (55). X-ray repair cross-complementing protein 1 (XRCC1) is then recruited to the site of DNA damage through an interaction of its BRCA1 C-terminal (BRCT) domain BRCT1 with the PAR chains generated by PARP1 and PARP2 (68,69). As demonstrated in BER, XRCC1 then acts as a scaffold protein for the recruitment of Pol-β, LIG3 and end-processing factors, such as PNKP, to facilitate single strand break repair (68,69).

Single-strand breaks formed in association with trapped topoisomerase I involve the removal of topoisomerase I by tyrosyl-DNA phosphodiesterase 1 (TDP1), followed by activation of PNKP. Both TDP1 and PNKP rely on PARP1 and XRCC1 for their recruitment (61)

Double Strand Break Repair

Non homologous end joining

DNA double strand breaks (DSB) are the most dangerous DNA lesion as these can result in the loss of large chromosomal regions and catastrophic cell damage (70). For double strand break repair, two principal mechanisms are used: non-homologous end-joining (NHEJ) and homologous recombination (HR) (71). NHEJ is involved in the repair of DNA double strand breaks caused by both endogenous and exogenous toxic agents (55). NHEJ can occur throughout the cell cycle but predominantly occurs in the G1 phase (70–72).

DSBs are recognised by the Ku70-Ku80 complex that binds and activates the protein kinase, DNA-dependent protein kinase catalytic subunit (DNA-PKcs) (73). DNAPKcs undergoes autophosphorylation and activates the endonuclease Artemis, which cuts DNA substrates at boundaries between double and single stranded DNA (70,74). Nucleotide addition occurs via the activation of the βX family polymerases, Pol μ and Pol λ (74). These polymerases interact with Ku through their BRCT domains to coordinate a repair response (70). DNA ligation occurs via the interaction of XRCC4 and DNA ligase IV to complete DNA repair (70,75).

NHEJ is an adaptive process based on the site and complexity of the DSB, and the DNA ends can be acted upon by repair components multiple times. This variation may arise from the site of DNA damage and the configuration of the DNA ends requiring repair (74). During NHEJ, DNA is repaired by direct DNA blunt end joining without the use of a template and therefore can be prone to errors depending on the level of DNA modification at the DNA ends (70,71,74). The process of NHEJ is summarised in Figure 2.7.

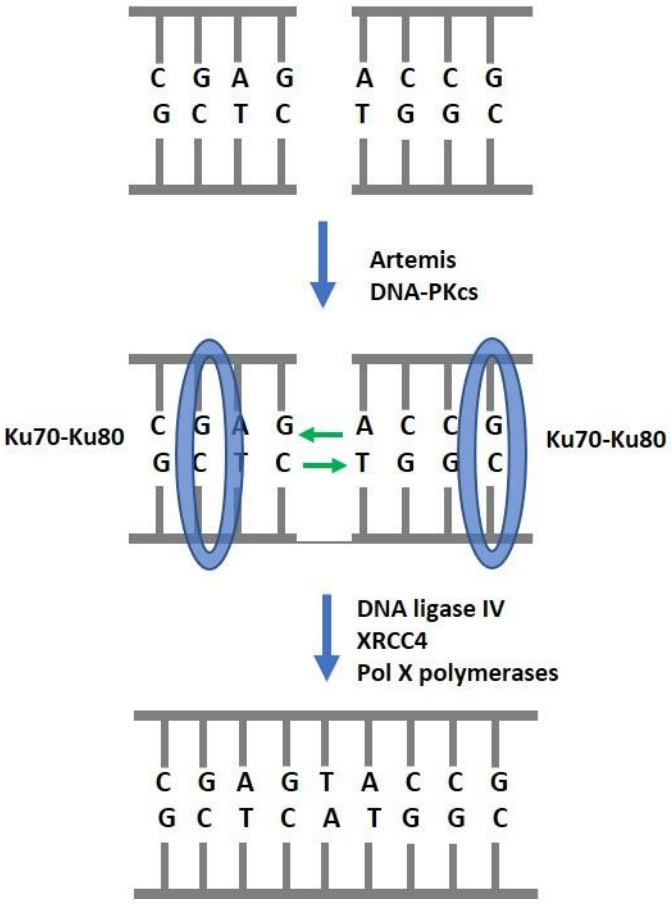

Figure 2.7. Non homologous end joining (NHEJ). Figure adapted from Nordicbiosite.com (54). Double stranded breaks are recognised by Ku70-Ku80. DNA-PKcs activate the endonuclease Artemis, which cuts DNA substrates at boundaries between single and double stranded DNA sites. Activation of DNA ligase IV, Pol X polymerases and XRCC4 leads to subsequent DNA repair.

Homologous recombination

Homologous recombination (HR) is another important mechanism for double strand break repair. HR preferentially occurs during S and G2 phases as the presence of sister chromatids are required (71). As the sister chromatid is identical to the damaged DNA strand, this repair mechanism restores the genetic configuration of the injured chromosome (76). HR is therefore thought to be more accurate than NHEJ (55,73). Spatial alignment, sequence pattern and physical cohesion of the two sister chromatids are thought to be contributory factors for selection of HR as the preferential repair mechanism rather than NHEJ (73). HR is summarised in Figure 2.8 (54).

During HR, a section of DNA around the site of DNA damage is resected and the correct DNA sequence on a homologous sister chromatid is used as the template for synthesising new DNA at the required site (72). Homologous repair is initiated by the generation of single stranded DNA breaks and this is promoted via proteins including replication protein A (RPA) and the MRE11-RAD50-NBS1 (MRN complex) (71). RAD51 is recruited and binds to single stranded DNA promoted by stimulation from the recombinant repair protein RAD52. This leads to the displacement of RPA coating the single strand DNA in order to initiate DNA repair (71,77,78).

Other proteins, including the breast cancer susceptibility proteins (BRCA) BRCA1 and BRCA2, co-localise with RAD51 and lead to a coordination of the components of DNA repair (71,72). BRCA1 is involved in the resection of double strand DNA breaks to generate 3' single strand DNA overhangs and also promoting the loading of RAD51 recombinase onto the single strand DNA (79). BRCA2 regulates RAD51 recombinase activity through direct interaction with several BRCA domains (76). BRCA2 also promotes the recruitment of RAD51 to the site of single strand DNA damage to initiate HR (76).

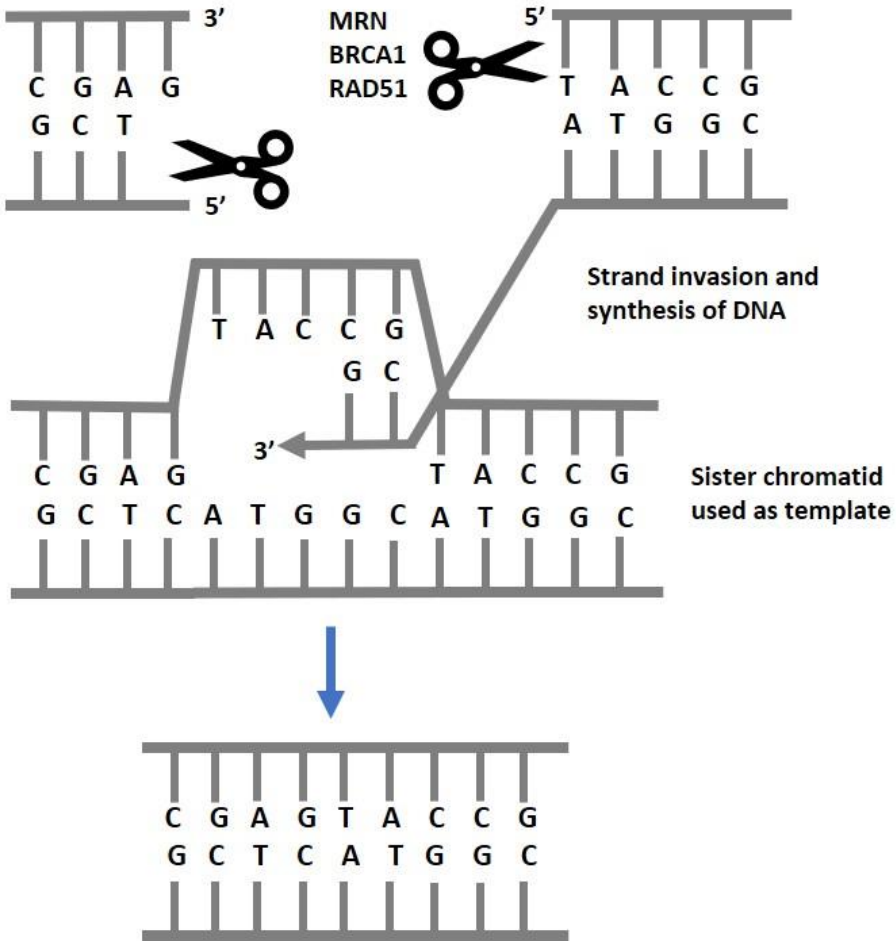

Figure 2.8. Homologous recombination (HR). Figure adapted from Nordicbiosite.com (54). During HR, sections of DNA around the site of DNA damage are resected and repaired with the use of a sister chromatid. This process occurs preferentially during S and G2 phases of the cell cycle. HR is considered to be a more accurate repair process than NHEJ.

The repair of double strand breaks involves the crossover of multiple DNA repair pathways. Homologous recombination is linked to the S and G2 checkpoint pathways discussed in Sections 2.1.7 and 2.1.9, with RPA being the initiation point of the ATR-CHK1 pathway and the MRN complex being key in the ATM/CHK2 pathway. HR is also used to reinitiate replication at stalled replication forks and is involved in the repair of interstrand crosslinks via the Fanconi anaemia pathway (71). Defects in the homologous repair pathway, such as BRCA1 and BRCA2 mutations, can lead to increased incidence of cancers, particularly breast and ovarian cancers (61,72,80).

In order to retain genomic integrity after DNA damage, cells have developed a complex network of DNA damage response (DDR) repair pathways as discussed in Section 2.1.1 (6,19). The role of the DDR pathways is to both activate cell cycle checkpoints which halt the cell cycle to allow time for cellular repair and also to directly facilitate DNA repair (19). Figure 2.9 shows a summary of the complex network of DDR pathways. The main pathways involved in DDR are the ATR/CHK1 pathway activated by single strand DNA breaks and the ATM/CHK2 pathway activated by double strand DNA breaks.

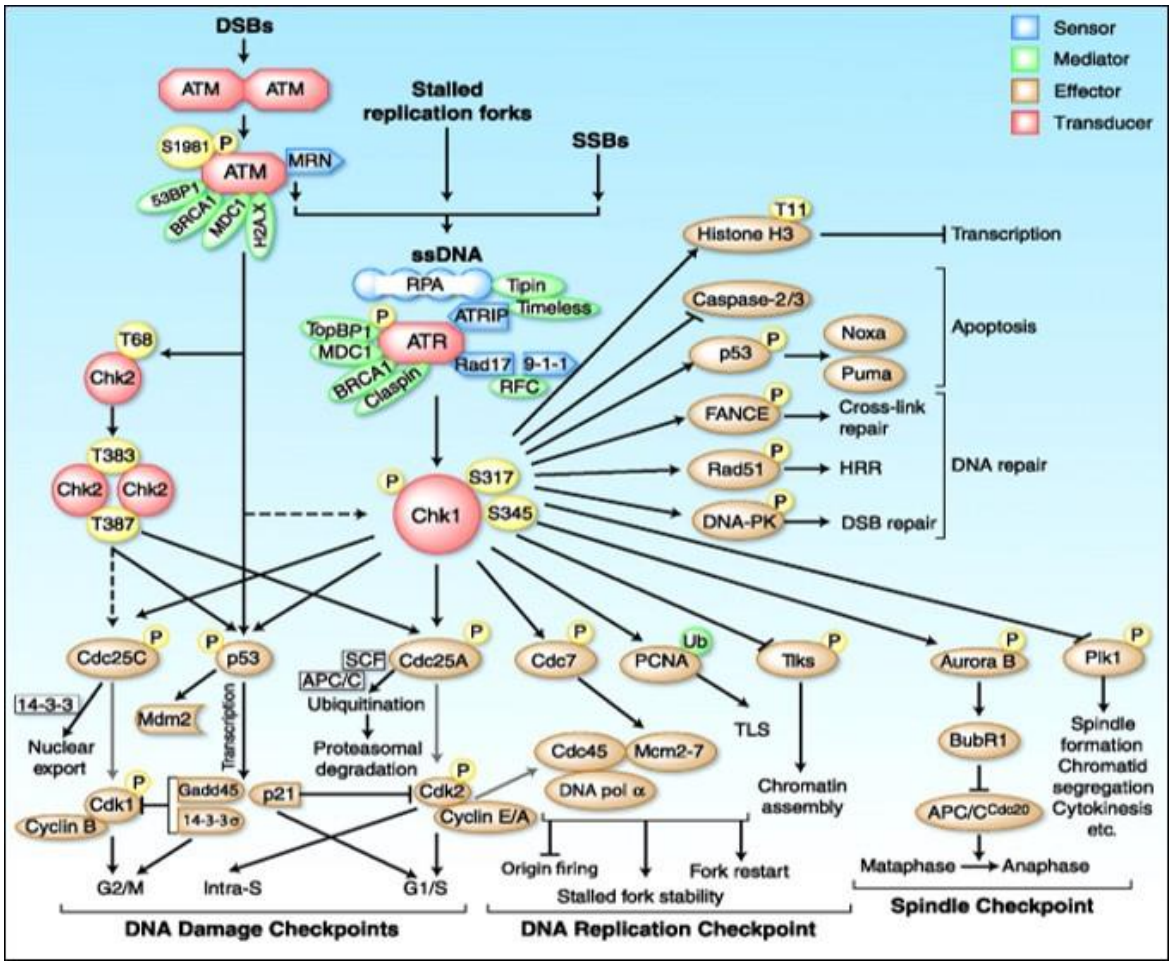

Figure 2.9. Summary of DNA damage repair pathways. Figure taken from Dai Y and Grant S, 2010 (92). This diagram summarises the complexity of the pathways involved in DNA damage repair and how pathways can interlink with each other. The roles of the DDR pathways are to activate cell cycle checkpoints and to allow repair of DNA damage.

2.1.7. The role of the ATR/CHK1 pathway

Ataxia-telangiectasia and Rad 3 related protein (ATR) is a PI3 kinase that regulates the pathway leading to the phosphorylation and activation of checkpoint protein 1 (CHK1) at the onset of single strand DNA breaks (18,81,82). This occurs after initial nucleotide excision repair, at stalled replication forks and the site of resected DNA double strand breaks (6). The ATR/CHK1 pathway is shown in Figure 2.10. RPA coats single stranded DNA which activates (ATR) and the co-factor ATR interacting protein (ATRIP) (82–84). RPA interaction with RAD17 also localises and loads RAD9, RAD1 and HUS1 to the site of DNA damage, which combine to form a heterotrimeric ring known as the 9-1-1 complex (17,81,84–86). The 9-1-1 complex subsequently recruits topoisomerase binding protein 1 (TOPBP1) (17,84,85).

Once ATR is activated and localised at the site of the DNA single strand break, ATR signals to coordinate cell checkpoint activation and DNA repair via multiple ATR substrates (6,83,87). The ATR/CHK1 pathway predominately exerts checkpoint control at the S and G2/M phases of the cell cycle (85,88,89). CHK1 is recruited to the site of DNA damage and activated by phosphorylation at Ser317 and Ser345 by ATR (86,90). Claspin becomes activated via the ATR dependent phosphorylation of RAD17 and acts as an adapter protein promoting the phosphorylation of CHK1 by ATR (18,90–92). Autophosphorylation of CHK1 on Ser296 occurs indicating an increase in catalytic activity (93). CHK1 is then released from chromatin, signalling the presence of DNA damage to downstream CHK1 targets within the nucleus. CHK1 release within the nucleus thought to be driven by CHK1 Ser345 phosphorylation (92,93).

Autophosphorylation of CHK1 on Ser296 is not required for CHK1 activation but is still an important marker of CHK1 activity. CHK1 Ser296 autophosphorylation has been shown to create a docking site for 14-3-3 in γ subtype-specific manner (93,94). CHK1 binding to 14-3-3γ then promotes a complex formation between CHK1 and Cdc25A, which induces Cdc25A-Ser76 phosphorylation. This leads to subsequent Cdc25A ubiquitinylation or degradation, which could modify cell cycle regulation (93,94).

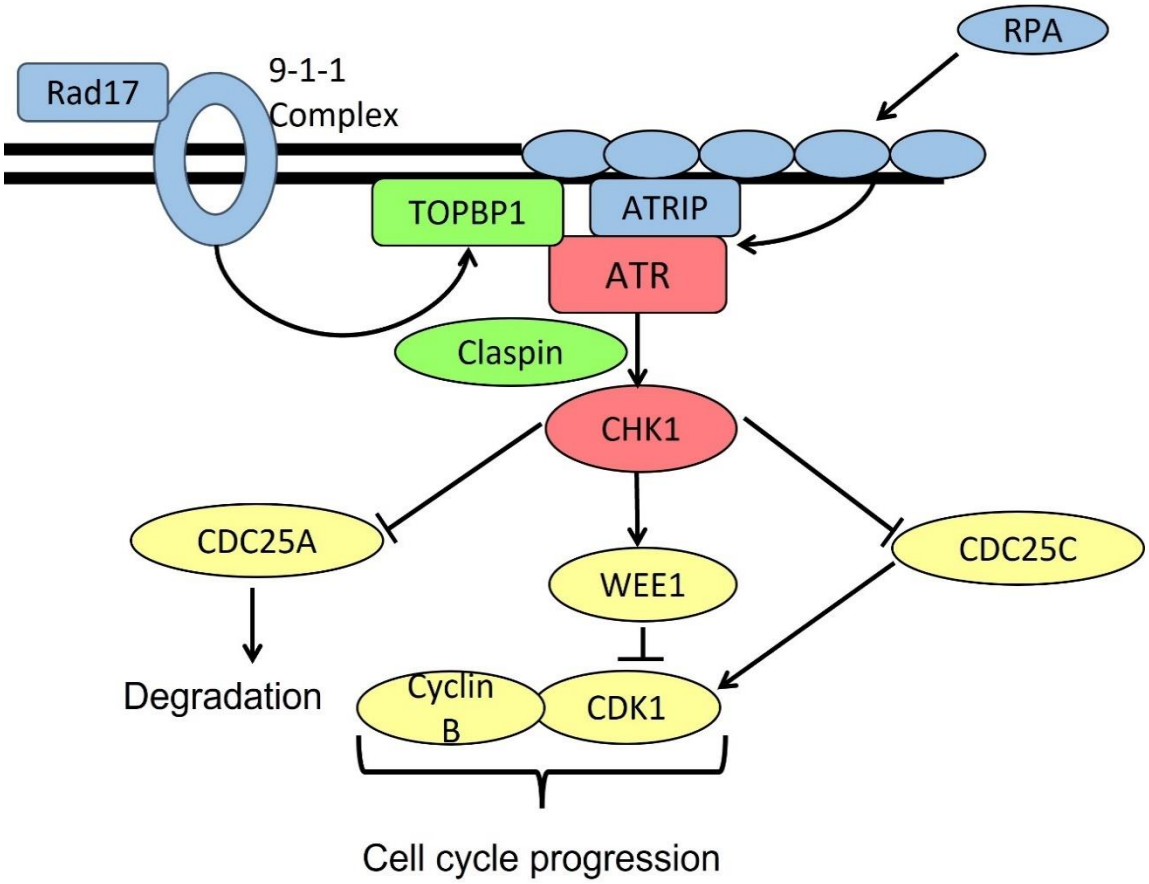

Figure 2.10. The ATR/CHK1 pathway. The ATR/CHK1 pathway predominately exerts checkpoint control at the S and G2/M phases of the cell cycle and is activated at the site of single strand breaks. RPA coats single stranded DNA activating ATR and ATRIP. RPA interaction with RAD17 also localises and loads the 9-1-1 complex to the site of DNA damage and TOPBP1 is subsequently recruited. Activated ATR then signals to coordinate cell checkpoint activation and DNA repair. CHK1 is recruited to the site of DNA damage and activated by phosphorylation at Ser317 and Ser345. Autophosphorylation of CHK1 on Ser296 is an indicator of CHK1 activity, but not required for activation. Activated CHK1 signals the presence of DNA damage to downstream CHK1 targets in order to stall cell cycle progression when appropriate.

S phase role of CHK1

The S phase DNA damage checkpoint downregulates DNA synthesis in response to cellular DNA damage accumulated during cell cycle S phase (95,96). CHK1 phosphorylation of cell division cycle 25A (CDC25A) triggers CDC25A degradation and leads to a decrease in cell division kinase 2 (CDK2) activity in S phase (19,95). This leads to a reduction in replication rate or a stalling of replication (86). CHK1 has also been seen to be active during an unperturbed S phase, suggesting a role in the surveillance of DNA replication under healthy conditions (89,90). Inhibition of CHK1 has been shown to lead to an increase in origin firing upstream of the CHK1 blockade (97). Cells subsequently accumulate incompletely duplicated DNA which can lead to 'mitotic catastrophe' and subsequent cell death (86).

ATR/CHK1 signalling in times of replication stress leads to reduced replication firing and a subsequent S phase cell cycle blockade. This reduces the rate of DNA replication to allow DNA repair (86). The mechanism behind this is not fully understood at this stage (6,86). These findings highlight the cellular dependency for the ATR/CHK1 pathway but also demonstrates that CHK1 under normal conditions plays a role in the regulation of origin firing.

Role of CHK1 in G2/M phases

The G2 DNA damage checkpoint ensures the maintenance of cell viability by stalling the progression into mitosis in cells with DNA damage (98). In the event of DNA damage during the G2 phase of the cell cycle, CHK1 phosphorylates the tyrosine kinase Wee1 (99,100). This leads to CDK1 phosphorylation at Tyr15 and prevents cells from entering mitosis (6). In addition, CHK1 phosphorylation of CDC25B at Ser323 during interphase prevents premature cell entry into mitosis by negatively regulating CDC25B at the centrosome (101).

Normally CDC25C activates CDK1 by dephosphorylation at the Tyr15 site to allow normal G2/M transition and therefore CHK1 acts to hold the cells at G2 in the event of damage and delay mitosis (99,100). Phosphorylation of CDC25C at Ser216 leads to the creation

of a binding site for 14-3-3 proteins, which leads to the exportation of CDC25C from the nucleus and thus further prevent CDK1 and cyclin B activation, thus halting mitosis (18,100,102,103).

CHK1 levels are regulated at different points of the cell cycle. For normal G2/M phase cell cycle progression to occur, CHK1 must be kept inactive. This can occur by the PLK1 dependent phosphorylation and degradation of the adaptor protein Claspin (86). CHK1 also cannot be activated at the point of mitotic entry (104). This is likely because DNA at this stage is double stranded and therefore the CHK1 recruitment proteins and activators such as RPA and ATR are not present (105). This mechanism is controlled by PKB/AKT although the mechanism behind this is not known (86,105). In addition, the increase in CDC25C activation and subsequent increase in CDK1 and cyclin B activity in late G2 also leads to a decrease in CHK1 activity. This is via phosphorylation of CHK1 at Ser 280/301 and prevents CHK1 activation by ATR (104). These restrictions of CHK1 in G2 allow cell cycle progression to mitosis.

2.1.8. Other roles of CHK1

Fanconi anaemia pathway

The Fanconi anaemia (FA) proteins are a family of proteins that form a pathway to repair DNA crosslinks (66). Eight of the FA proteins (FANCA, B, C, E, F, G, L, and M) form the FA core complex required for the monoubiquitination of FANCD2 and the subsequent assembly of FANCD2 nuclear foci (55,106). FANCD2 interacts with BRCA2/FANCD1 to facilitate the repair of interstrand crosslinks (106,107). FANCC, FANCE and FANCD1 form a complex together which is integral to enable crosslink repair (66).

The FANC/BRCA complex and FANC proteins additionally interact with other key DDR proteins, including BRCA1, ATM, the MRN complex and H2A histone family X (γH2AX) highlighting the complexity and interaction between different repair pathways (49,107–109). CHK1 directly phosphorylates FANCE at 2 sites, threonine 346 and serine 374, to facilitate cross link repair (106). Loss of CHK1 has been demonstrated to impair FANCD2 monoubiquitination. This again highlights the importance of CHK1 in the regulation of other cellular repair mechanisms (107).

AKT pathway

AKT/protein kinase B is another key cell cycle regulator that also interacts with CHK1 (110,111). A downstream effector of growth factor receptors and the PI3 Kinase (PI3K) pathway, AKT is activated by PDK1 at threonine 308 and by mTORC2 and DNA dependent protein kinase (DNAPK) at serine 473 (112). Activity of AKT is high at the G2/M phase of the cell cycle and can regulate cell cycle transition between G2 and M cell cycle phases (113). AKT activation can lead to the promotion of antiapoptotic activity and override G2 cell cycle arrest (113). In addition, enhanced AKT activity has been associated with resistance to chemotherapeutic agents (111).

DNAPK can directly phosphorylate AKT in the presence of DNA double strand breaks, indicating cross talk between multiple DNA damage and repair pathways (114). AKT can phosphorylate CHK1 at a different site on serine 280 which is in close proximity to serine 317 and serine 345 which are activated by ATR (110,113,115). Phosphorylation of CHK1

at this site by AKT inhibits CHK1 activation and prevents ATR activation on serine 345 (115). Location of BRCA1 to the site of DNA damage is impaired when AKT is activated which may lead to a reduction in CHK1 activation (110). Cells showing resistance post treatment CHK1 and PARP inhibitors in combination have been shown to have an amplification of AKT (116).

MK2 signalling

The p38MAPK/MK2 signalling complex is considered to be a stress response pathway activated by a variety of DNA damaging stimuli including UV radiation and reactive oxygen species (18,117). MK2 can directly phosphorylate CDC25B and CDC25C in response to genotoxic stress on the Ser323 14-3-3 binding site in CDC25B and also the Ser216 14-3-3 binding site on CDC25C (18). These sites are both also CDC25 phosphorylation targets for CHK1 and CHK2 (118). MK2 has a significant role in the phosphorylation of CDC25B and CDC25C in response to UV-induced DNA damage (18,118).

Downregulation of MK2 has been demonstrated to halt DNA damage induced G2/M and intra-S phase checkpoints (117–119). The P38/MAPK complex is thought to have an impact on cell cycle regulation both independently and via crosstalk with the ATM and ATR pathways (120–123).

2.1.9. The ATM/CHK2 pathway

The ATM/CHK2 pathway is involved in the repair of double strand DNA breaks (18,82,124–126). Ataxia-telangiectasia mutated protein (ATM) is a large molecular weight protein that crosslinks with many DNA damage response pathways (7). In response to DNA damage, ATM is recruited to the site of DNA damage by NBS1, part of the MRE11-RAD50-NBS1 (MRN) complex (124,127). p53 binding protein 1 (53BP1) and BRCA1 optimise the MRN complex-ATM link (128). ATM is also bound by MDC1 which is activated by the phosphorylation of histone H2AX at the site of DNA damage (129). The combination of the MRN complex and H2AX activation lead to the enhancement of ATM recruitment (18). Checkpoint kinase 2 (CHK2) activation is triggered by phosphorylation on Thr68 by ATM (18,130). This leads to subsequent CHK2 autophosphorylation on Thr383 and Thr387 (130). The ATM/CHK2 pathway is summarised in Figure 2.11

Like CHK1, CHK2 is a mediator to many downstream effectors. Activated CHK2 phosphorylates CDC25A leading to degradation and lack of CDK1/cyclin B activation (55,131). CHK2 also causes cell cycle arrest by phosphorylating the tumour suppressor p53 on Ser15 and Ser20 (132,133). This results in both p53 stabilisation and activation (133). p53 is a transcription factor which initiates the transcription of genes involved in DNA repair, cell cycle arrest and apoptosis (132,134,135). p53 also has a series of negative regulators, such as mouse double minute 2 (MDM2), a ubiquitin ligase that targets p53 for degradation (132,136,137). In response to DNA damage, p53 is phosphorylated by many kinases including ATR and CHK1 as well as ATM and CHK2, leading to cross-talk between the DNA damage response repair pathways (132). Phosphorylation of p53 by CHK2 and the other kinases listed blocks the interaction between p53 and MDM2 leading to accumulation of p53 (132,135). Active p53 promotes the transcription of CDKN1A, which encodes the CDK inhibitor p21, leading to p53-mediated G1 cell cycle arrest (137,138).

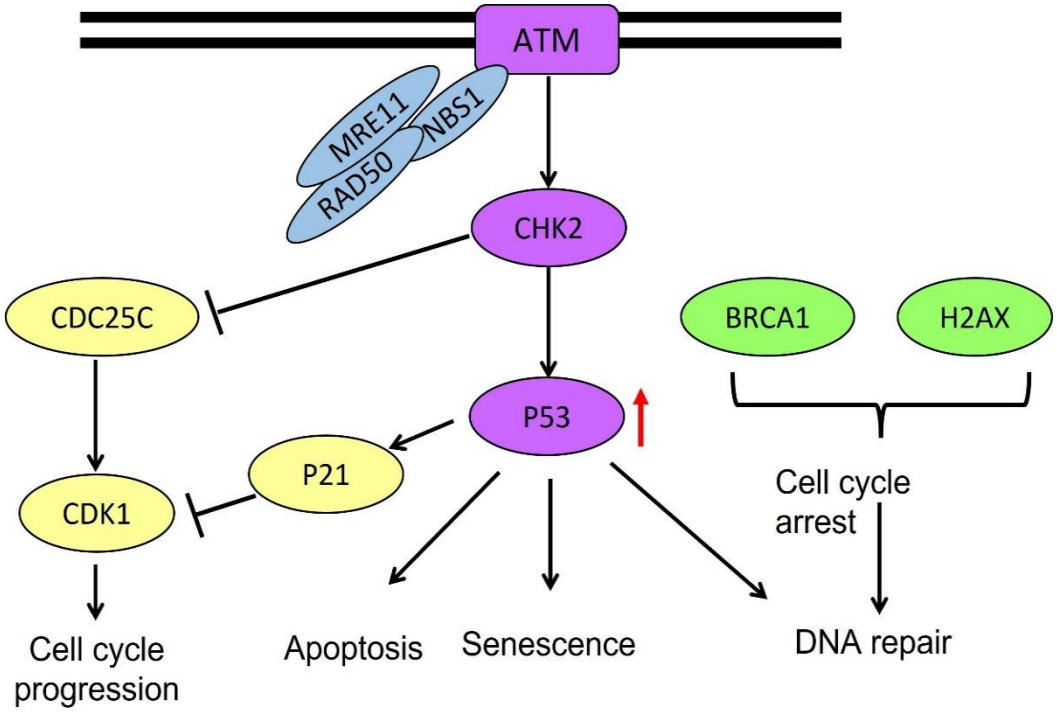

Figure 2.11. The ATM/CHK2 pathway. The ATM/CHK2 pathway is involved in the repair of double strand DNA breaks. In response to DNA damage, ATM is recruited by NBS1, part of the MRN complex. The combination of the MRN complex and H2AX activation leads to enhanced ATM recruitment. CHK2 activation is triggered by phosphorylation on Thr68 by ATM, leading to subsequent CHK2 autophosphorylation on Thr383 and Thr387. Like CHK1, CHK2 can act on many downstream effectors. Phosphorylation of p53 by both ATM and CHK2 lead to an activation of p53. CHK2 phosphorylates p53 on Ser15 and Ser20. p53 activation leads to activation of the CDK inhibitor p21, which mediates G1 checkpoint arrest.

CHK2 is also involved in G2/M phase cell cycle regulation. Similar to CHK1, CHK2 can also phosphorylate CDC25C downstream (138,139). CDC25C translocates to the cytoplasm via an interaction with 14-3-3 proteins (138,140). Once in the cytoplasm, CDC25C can no longer dephosphorylate and activate the cyclin B1/Cdk1 complex required for successful G2/M transition (138). The crossover between the ATR/CHK1 and the ATM/CHK2 pathways is shown in Figure 2.12.

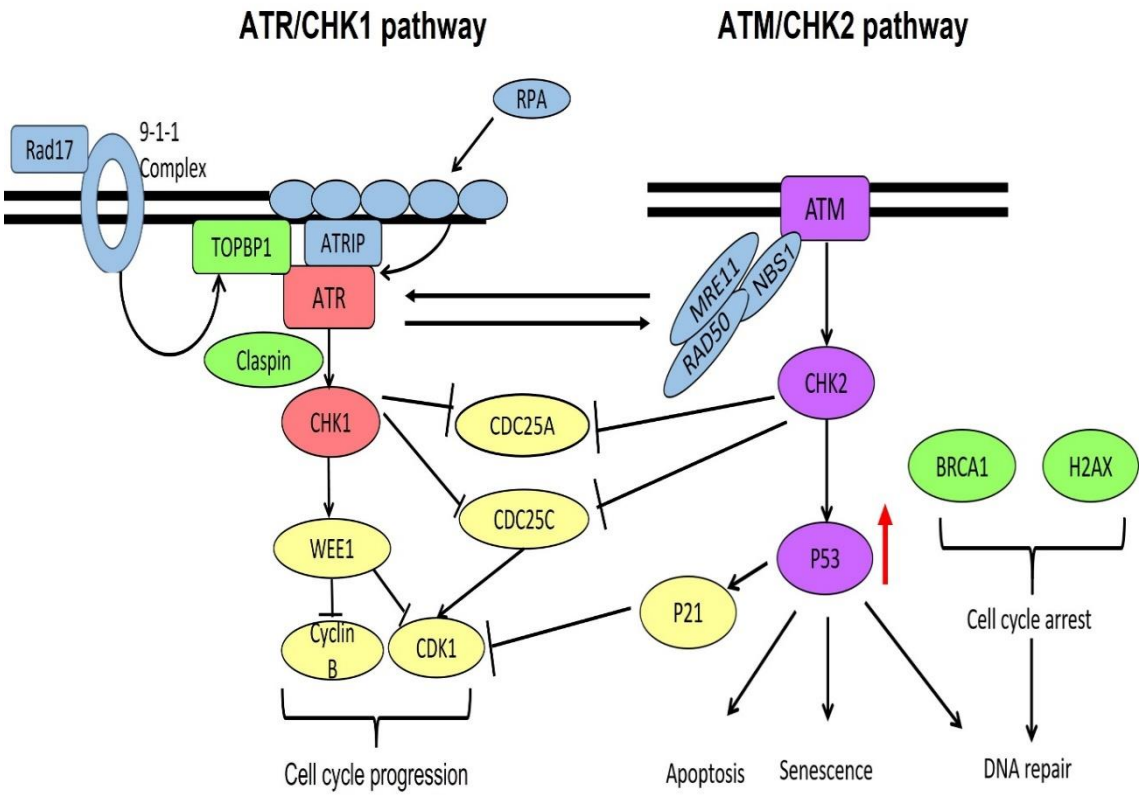

Figure 2.12. Interactions between the ATR/CHK1 and ATM/CHK2 pathways. There is significant crosstalk between the ATR/CHK1 and the ATM/CHK2 pathways to halt the cell cycle and allow cellular repair. Both CHK1 and CHK2 are mediators to many downstream effectors. Activated CHK1 and CHK2 phosphorylates CDC25A leading to degradation and lack of CDK1 activation. Like CHK1, CHK2 can also phosphorylate CDC25C downstream. CDC25C is translocated to the cytoplasm via an interaction with 14-3-3 proteins. Once in the cytoplasm, CDC25C can no longer dephosphorylate and activate the cyclin B1/Cdk1 complex required for successful G2/M transition. CHK1 can also be a direct target of ATM. ATR, CHK1, ATM and CHK2 can all phosphorylate and activate p53, leading to an impact on downstream effects.

2.1.10. Multiple roles of CHK2

CHK2 participates in DSB repair by phosphorylating the breast cancer susceptibility proteins, BRCA1 and BRCA2 (138,141,142). HR is then preferentially selected to repair DNA damage over NHEJ. Post DNA damage, CHK2 phosphorylation of BRCA1 facilitates the recruitment of RAD51 to the DNA lesion. This leads to the reduced action of MRE11, which is involved in the promotion of the NHEJ pathway (138,143). RAD51 subsequently promotes HR by promoting DNA strand invasion (55).

CHK2 also has been shown to have a role in base excision repair. CHK2 phosphorylates and activates the transcription factor forkhead box protein M1 (FoxM1) which subsequently stimulates the transcription of the genes encoding the BER factor XRCC1 and BRCA2 (144). The crossover between the different DNA checkpoints and repair pathways again highlights the complexity of the repair processes required to ensure DNA integrity is maintained. Table 2.1 compares the role of CHK1 and CHK2 in cell cycle control and DNA repair.

2.1.11. CHK1 in cancer

Genomic instability and DNA damage are recognised enabling characteristics of cancer (40). The activation of proto-oncogenes or inactivation of tumour suppressor genes can further accelerate tumour growth and progression (40,44). Mutations in the DDR can predispose to cancer and allow tumour proliferation despite significant DNA damage (71). Mutations in tumour suppressor genes such as *TP53* and *Rb* can lead to the dysregulation of cell cycle checkpoints including the ATM/CHK2 pathway, generating replication stress and genomic instability (145,146). In addition, replication stress can be further enhanced by increased expression of proto-oncogenes such as *RAS*, *cyclin E* and *MYC*, which can lead to increased origin firing and increased expression of CDK activity (82,147–151).

Table 2.1. Comparison of CHK1 and CHK2 function. Table summarising the main regulators and downstream effects of CHK1 and CHK2. There is crossover between the ATR/CHK1 pathway and the ATM/CHK2 pathway, however both CHK1 and CHK2 are known to have different downstream effects and interact with separate additional pathways.

Function	**CHK1**	**CHK2**
Cell cycle	S, G2/M	G1/S, G2/M
Activation	Single stranded DNA breaks	Double stranded DNA breaks
Main regulator	ATR	ATM
Main downstream targets	CDC25A, CDC25C, WEE1, CDK1, CDC2	CDC25A, CDC25C, p53, BRCA1, BRCA2
Crossover pathways	ATM/CHK2, FA pathways, PI3K/AKT, MK2	ATR/CHK1, Base excision repair

Cancer cells are highly mutagenic but still require some checkpoint regulation and intact DNA repair pathways to survive. Loss of the p53-driven G1 checkpoint as shown in Figure 2.13 can lead to a reliance on the ATR/CHK1 pathway to maintain replication and to facilitate cell repair (6,87). Deletions of *ATR* and *CHEK1* are embryonically lethal in animal models, highlighting the importance of this checkpoint pathway for survival (7,85,124). CHK1 mutations in cancers are rare and there are no known inherited *CHEK1* gene mutations which predispose to cancers in contrast to other checkpoint mediators including *TP53, CHEK2, ATM and BRCA1/2* (89,146).

Frameshift mutations of *CHEK1* have been shown in tumours with impaired mismatch repair, such as gastric, colorectal and endometrial cancers (41,85,152). An overexpression of CHK1 has also been demonstrated in small cell lung, nasopharyngeal and triple negative breast cancers (89,153–155). Many cancers do however have proto-oncogene upregulation in genes such as *RAS* or *MYC*, or a mutation in a tumour suppressor gene, such as *TP53* or *ATM.* Oncogene upregulation or mutation in tumour suppressor genes could lead to enhanced replication stress and an increased dependence on the ATR/CHK1 function for cell survival (19,146,148,151).

The development of drugs to inhibit CHK1 is therefore appealing to exploit tumour dependence on this pathway to promote irreparable tumour cell damage and cell death (19,87).

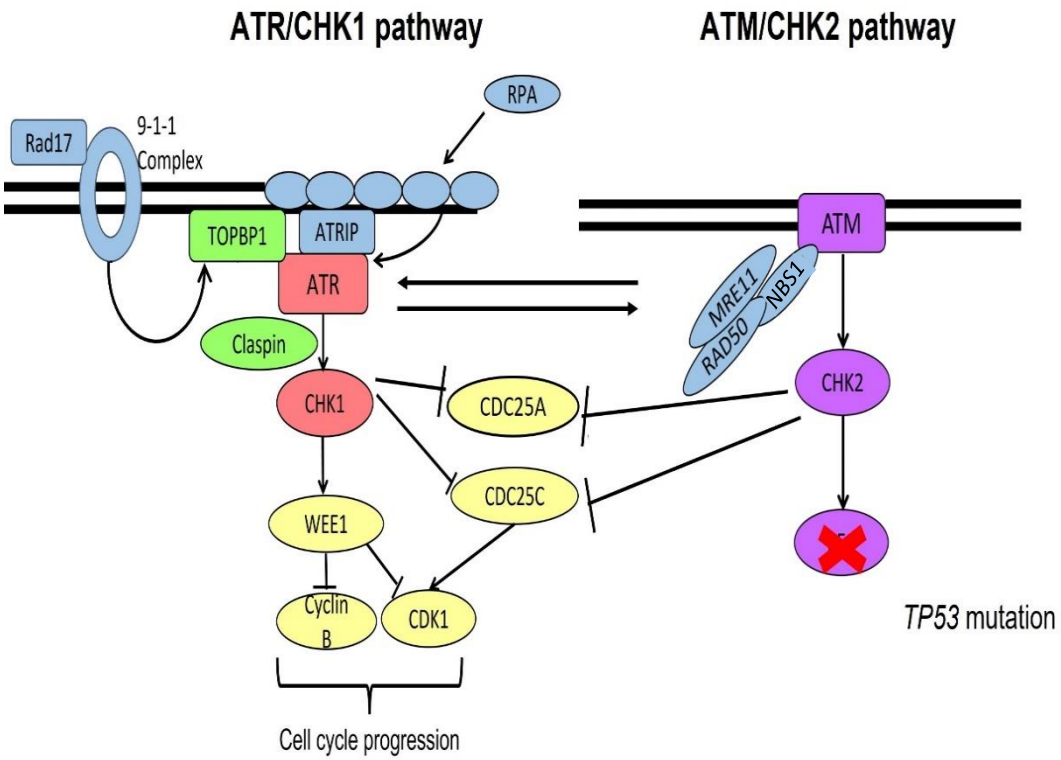

Figure 2.13. Dependence on ATR/CHK1 pathway in *TP53* mutant cancers. In cancers with *TP53* gene mutations, apoptosis cannot be driven by the activation of P21 and DNA repair downstream cannot be activated. Due to dysregulation of p53, cells become more genomically unstable with increased replication stress. This causes increased reliance on the ATR/CHK1 pathway for maintenance of cellular regulation and cell survival.

2.1.12. CHK1 as a potential therapeutic target

CHK1 inhibitors have been in development for many years and a summary of clinical trials to date is shown in Table 2.2 and ongoing clinical trials are shown in Table 2.3. Given the dependency of many cancers on the ATR/CHK1 pathway in cellular repair, CHK1 is an attractive therapeutic target (6,19,146,150).

Acting on the principles of 'synthetic lethality' as seen with PARP inhibitors (PARPi) and *BRCA1/BRCA2* mutations, cells that already have a loss of G1 checkpoint or proto-oncogene enhancement will have enhanced genomic instability (6,148). In theory this will make cells with enhanced genomic instability more sensitive to CHK1 inhibition, as this could lead to replication fork collapse and irreparable DNA damage (84,89,156). The proposed mechanism of CHK1i monotherapy is shown in Figure 2.14. In comparison to cells treated with PARP inhibitors, however, the cellular response to CHK1 inhibitors is likely to be more complex. This is because CHK1 has many roles and interactions within the DNA damage response pathways and there may be more complex compensatory signalling mechanisms in place.

Pre-clinical studies have shown success with CHK1 inhibition as a combination therapy with chemotherapy agents including Gemcitabine and Cisplatin (116,157–159). There is also evidence in pre-clinical studies for efficacy as a single agent in cancers driven by *MYC* and *RAS* (147). Initial CHK1 inhibitors were less specific and clinical trials had to be stopped due to significant side effects, including cardiac toxicity (151,160,161) and hyperglycaemia (162). More recently developed CHK1 inhibitors have been designed to be more specific to CHK1 (6,19).

Table 2.2. Completed CHK1 inhibitor trials to date. Drugs summarised with trial phase, cancer types included in the trial and the trial outcome. Drugs are also listed whether they were delivered as a monotherapy or in combination with other anticancer therapies.

Drug	Study	Phase	Additional drugs	Cancer types	Outcome	Ref
AZD7762	NCT00413686	I	Single agent/ with Gemcitabine	Advanced solid tumours	Completed	(163–166)
	NCT00473616	I	Single agent/ with Irinotecan	Advanced solid tumours	Terminated due to cardiotoxicity	(161)
	NCT00937664	I	Gemcitabine	Advanced solid tumours	Terminated due to cardiotoxicity	(167)
PF-00477736	NCT00437203	I	Gemcitabine	Advanced solid tumours	Terminated due to business reasons	(168)
MK8776/ SCH099776	NCT00779584	I	Single agent/with Gemcitabine	Advanced solid tumours/Lymphoma	Completed	(157)
	NCT00907517	I	Single agent/with Cytarabine	Acute leukaemia	Terminated – DLT of prolonged QT interval	(169)
	NCT01521299	I	Hydroxyurea	Advanced solid tumours	Withdrawn – insufficient patients	(170)
	NCT01870596	II	Cytarabine	Acute myeloid leukaemia	Completed	(171)
GDC-0575	NCT01564251	I/II	Gemcitabine	Solid tumours Lymphomas	Completed	(172)
Rabusertib/ LY2603618	NCT00415636	I	Pemetrexed	Solid tumours	Completed	(166,173,174)
	NCT00839332	I/II	Single agent/with Gemcitabine	Pancreatic cancer	Completed	(175)
	NCT00988858	I/II	Pemetrexed	Advanced non-small cell lung cancer	Completed	(176)
	NCT01139775	I/II	Pemetrexed/ Cisplatin	Non-small cell lung cancer	Completed	(177)

Drug	Study	Phase	Additional drugs	Cancer types	Outcome	Ref
	NCT01296568	I	Pemetrexed/ Gemcitabine	Advanced/Metastatic solid tumours	Completed	(166,178)
	NCT01341457	I	Gemcitabine	Advanced/Metastatic solid tumours	Completed	(166,179,180)
	NCT01358968	I	Desipramine/ Pemetrexed/ Gemcitabine	Advanced/Metastatic solid tumours	Completed	(19,166,181)
CCT245737/ SRA737	NCT02797964	I/II	Single agent	Solid tumours Lymphomas	Completed	(182)
	NCT02797977	I/II	Gemcitabine	Solid tumours Lymphomas	Completed	(183)
LY2603618 (Prexasertib)	NCT01115790	I/II	Single agent	Advanced/Metastatic solid tumours	Completed	(184)
	NCT02124148	I	Single agent/ Cisplatin/ Cetuximab/ G-CSF/ Pemetrexed/ Fluorouracil/ LY3023414/ Leucovorin	Advanced/Metastatic solid tumours	Completed	(185)
	NCT02203513	II	Single agent	High grade serous ovarian, triple negative breast cancer, metastatic castrate resistant prostate cancer, BRCA mutant breast or ovarian cancer	Active, not recruiting	(186,187)
	NCT02514603	I	Single agent	Advanced/Metastatic solid tumours	Completed	(188)
	NCT02555644	I	Cisplatin plus radiotherapy/ Cetuximab plus radiotherapy	Advanced Head and neck squamous cell cancer	Completed	(189)
	NCT02649764	I	Cytarabine and Fludarabine	Advanced AML/MDS	Active, not recruiting	(190)

Drug	Study	Phase	Additional drugs	Cancer types	Outcome	Ref
	NCT02735980	II	Single agent	Advanced small cell lung cancer	Completed	(191)
	NCT02778126	I	Single agent	Advanced/metastatic solid tumours	Completed	(192)
	NCT02808650	I	Single agent	Recurrent or refractory solid tumours in paediatric patients	Active, not recruiting	(193)
	NCT02860780	I	Ralimetanib	Advanced/metastatic solid tumours	Completed	(194)
	NCT02873975	II	Single agent	Cancers with HR deficiency/raised replication stress	Active, not recruiting	(195)
	NCT03057145	I	Olaparib	Advanced/metastatic solid tumours	Active, not recruiting	(196)
	NCT03414047	II	Single agent	Platinum resistant ovarian cancer	Active, not recruiting	(197)
	NCT03495323	I	LY3300054 (PDL1 inhibitor)	Advanced/metastatic solid tumours	Active, not recruiting	(198)
	NCT03735446	I	Mitoxantrone/ Carboplatin / Cytarabine	Relapsed or advanced AML/MDS	Terminated (Sponsor decision)	(199)

Table 2.3. Active CHK1i trials (as of April 2021). Clinical trials are currently recruiting for the CHK1 inhibitor Prexasertib within multiple primary tumour sites.

Drug	Study	Phase	Additional drugs	Cancer type	Status	Ref
LY2603618 (Prexasertib)	NCT04023669	I	Cyclophosphamide	Recurrent refractory/ progressive medulloblastoma in paediatric patients	Active and recruiting	(200)
	NCT04032080	II	LY3023414 (PI3K, DNA-PK and mTOR inhibitor)	Metastatic triple negative breast cancer	Active and recruiting	(201)
	NCT04095221	I/II	Irinotecan	Desmoplastic small round cell tumour and rhabdomyosarcoma	Active and recruiting	(202)

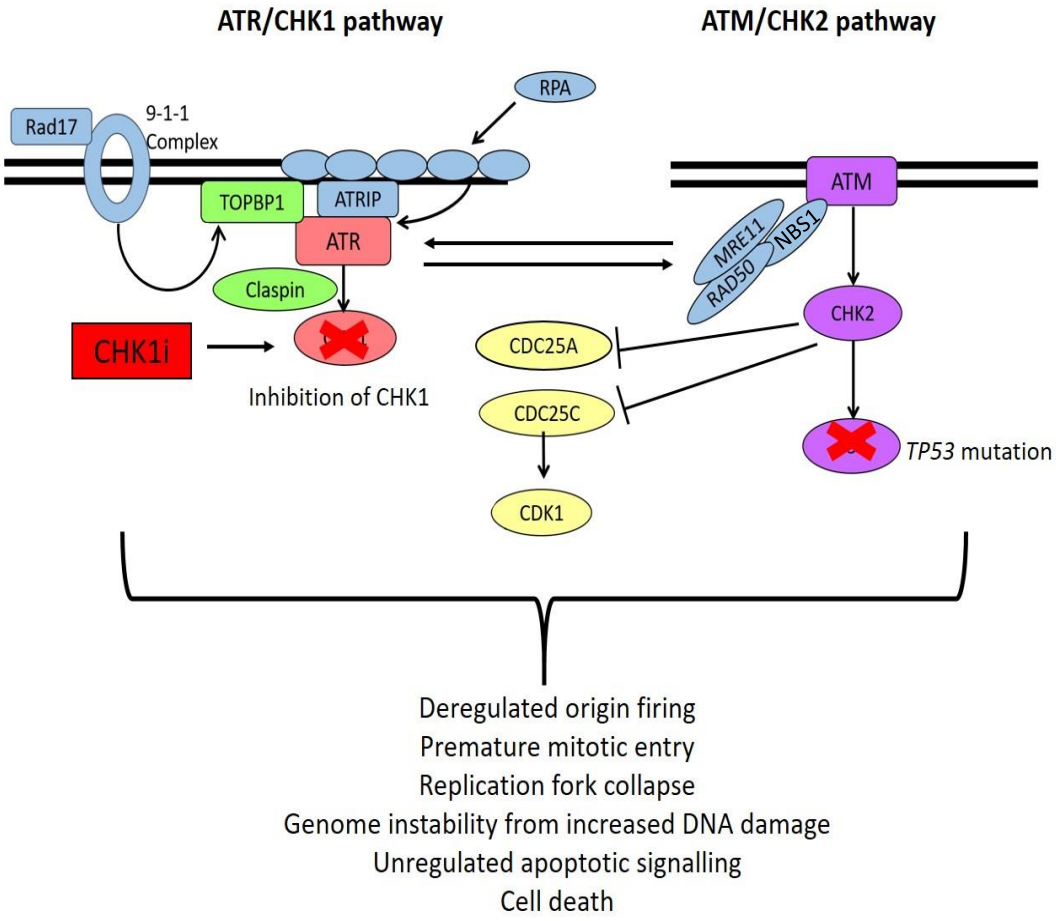

Figure 2.14. Proposed mechanism of CHK1i action as a single agent. In cancers already predisposed to genomic instability, for example tumours with *TP53* gene mutations, cells become reliant on the ATR/CHK1 pathway for regulation of genomic instability and cell survival. CHK1 inhibition will leave cells in these circumstances without checkpoint regulation and vulnerable to replication fork collapse.

2.1.13. Potential mechanisms of CHK1 inhibitor resistance

Previous CHK1 inhibitor studies have shown potential routes of drug resistance. A summary of some of these mechanisms is shown in Figure 2.15. A study examining the MK-8776 drug in cancer cell models has shown that cells responsive to this CHK1 inhibitor had an upregulation of CDK2 and cyclin A with an associated increase in double stranded DNA breaks (203). This study used multiple different cell lines from different tumour types, including prostate and colorectal cell lines (203). Drug sensitivity was associated with an increased accumulation of CDC25A (203). Cells in this study displaying drug resistance failed to dephosphorylate tyrosine 15 on CDK2 and therefore subsequently failed to activate CDK2 (203).

Treatment with the CHK1 inhibitor LY2603618 (Rabusertib) in head and neck cancer cell lines showed that sensitivity to the drug was dependent on CDK activity, highlighting CDK1 as significant in drug response. Increased CDK1 was indicative of reduced drug sensitivity (204). CDK1 has the potential to upregulate origin firing and overcome S phase replication stalling (204). CDK1 has also been shown to activate the MAPK/ERK pathway, which could potentially compensate for cell damage and enhance cell survival (204).

A study into BRCA wild type ovarian cancer using the CHK1 inhibitor Prexasertib has been published (205). This has shown that in both tumour biopsies and cell line models, resistance to Prexasertib is caused by a prolonged delay in the G2 phase of the cell cycle due to low CDK1/cyclin B activity (205). The cancer model in this study normally is dependent on the ATR/CHK1 pathway for cell survival due to the presence of a *TP53* mutation, but behaves differently to *BRCA* mutated ovarian cancers where PARP inhibition leads to synthetic lethality due to a fault in HR (205). This highlights mutation differences between the same tumour groups, which can lead to separate mutations indicating drug sensitivity or resistance.

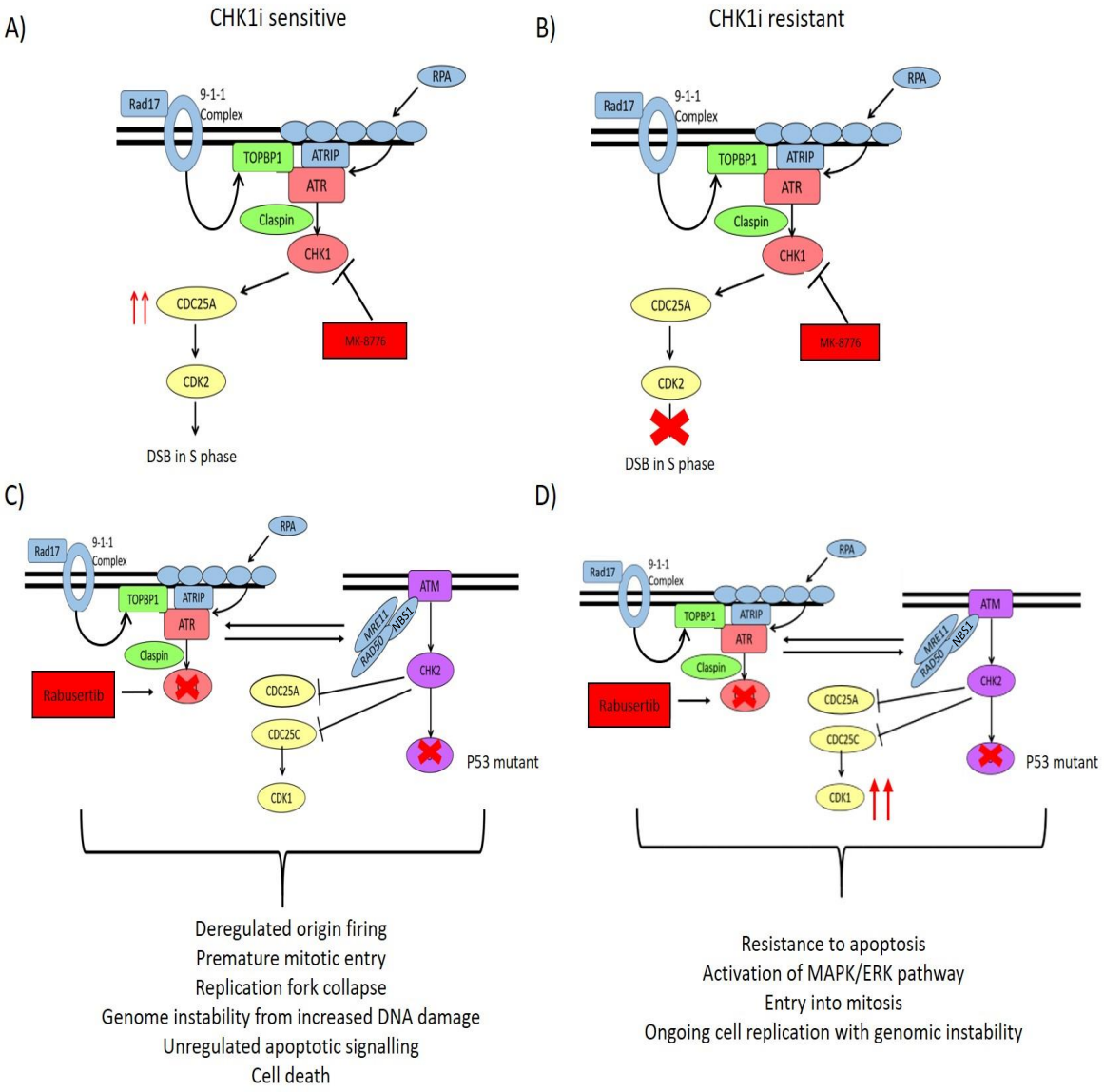

Figure 2.15. Further proposed mechanisms of CHK1i resistance. A) Shows the proposed mechanism of CHK1i sensitivity and B) proposed mechanism of CHK1i resistance for MK-8776. A) CHK1i sensitivity is dependent on CDC25A activation leading to further DNA damage and generation of double strand breaks. B) If CDC25A is not increased then cells can overcome CHK1i resistance. C) Shows the proposed mechanism of CHK1i sensitivity and D) the proposed mechanism of resistance to the CHK1i Rabusertib in an ATR/CHK1 dependent head and neck cancer cell line. C) CHK1i inhibition leads to increased apoptosis and deregulation of replication fork activity. D) In resistant cells, increased CDK1 expression can overcome S phase checkpoint regulation. This is associated with high levels of replication stress and activation of additional pathways such as MAPK/ERK.

Research into the CHK1 resistant mantle cell lymphoma cell line JEKO-1 response to the Chk1 inhibitor PF-00477736 showed that resistant cells had a shorter S phase and a reduced expression of cell cycle checkpoint proteins, including cyclin D1 (206). The gene transcripts of resistant cells in this study were investigated further. Upregulated genes were in cell survival pathways including MERK and NF-κB (206).

A recent study has also been published examining SRA737, the CHK1i used in the clinical trial described in this thesis (116,207). This was performed in ovarian cancer cell lines in combination with the PARP inhibitors Olaparib and Niraparib (116). In this study, sensitivity to the combination of CHK1i and PARPi was thought to be caused by an AMPK-dependent inactivation of ERK, AKT and NF-κB. Knockdown of either ATM or AMPKα lead to CHK1i drug resistance via ERK and AKT (116). It is difficult to ascertain if these changes are due to a response to one of the drugs in isolation, or both PARPi and CHK1i given in combination. This is because the data in this study was presented for both PARPi and CHK1i given in combination only.

Published data to date on CHK1 inhibitor resistance suggests that CHK1 inhibitor drug resistance involves alterations in cell cycle checkpoint control and/or upregulation of additional cell cycle survival pathways. Potential reasons for differences between drugs could be because of variations in mutation expression between cell lines examined, or contrasts between CHK1 inhibitors, with different CHK1 target and off target effects.

Previous unpublished work performed by the Perkins' lab has also shown that NF-κB mediators may have a role in CHK1 inhibitor resistance based on studies in cellular and animal models. The interactions between NF-κB and DNA damage will therefore be explored further within this thesis.

2.2. The NF-κB family of transcription factors

2.2.1. Introduction to the NF-κB pathway

The Nuclear Factor-κB (NF-κB) family of transcription factors play a critical role in the regulation of the cellular stress response including inflammation, immunological processes, cancer and cell survival pathways (208,209). The NF-κB response can be activated by a wide range of stimuli including immunoreceptors, cytokine and growth factors and genotoxic stress (210,211). Phosphorylation of NF-κB subunits can lead to either an enhancement or downregulation of target gene transcription depending on both the stimuli and the cellular context (208,211).

The NF-κB family consists of five members, NF-κB1/p50, NF-κB2/p52, RelA (p65), c-Rel, and RelB (212). All subunits share a Rel homology domain (RHD) which is responsible for DNA binding and dimerization (210,212). The NF-κB family subunits are shown in Figure 2.16. The transcription activation domain (TAD) required for the positive regulation of gene expression is present in RelA, c-Rel and RelB only (212). The additional family members, NF-κB1 and NF-κB2 have longer precursor proteins that can be cleaved during translation or via phosphorylation-induced partial proteolysis to their active DNA-binding forms of p50 and p52 (210).

NF-κB activation can provide a rapidly generated first line of defence against cellular stressors (210). Prior to induction, pre-synthesised NF-κB complexes are held in an inactive form in the cytoplasm by the inhibitor of NF-κB (IκB) proteins (209,212,213). These consist of IκBα, IκBβ and IκBε (210,212). In the presence of an inducing stimulus, phosphorylation of the IκBs by the IκB kinase (IKK) complex promotes their ubiquitylation and degradation leading to subsequent NF-κB localisation and activation within the nucleus (210,214). Strong activators of NF-κB such as TNF-α can cause rapid IκB breakdown in minutes highlighting the speed of acute cellular responses to stress (214). NF-κB1 and NF-κB2 also contain, in their C termini, the ankyrin repeat motifs that are found in the IκBs, which can mediate interaction with NF-κB subunits and which can themselves function as IκB proteins (210). NF-κB has 2 main routes of activation, the canonical and the non-canonical pathways.

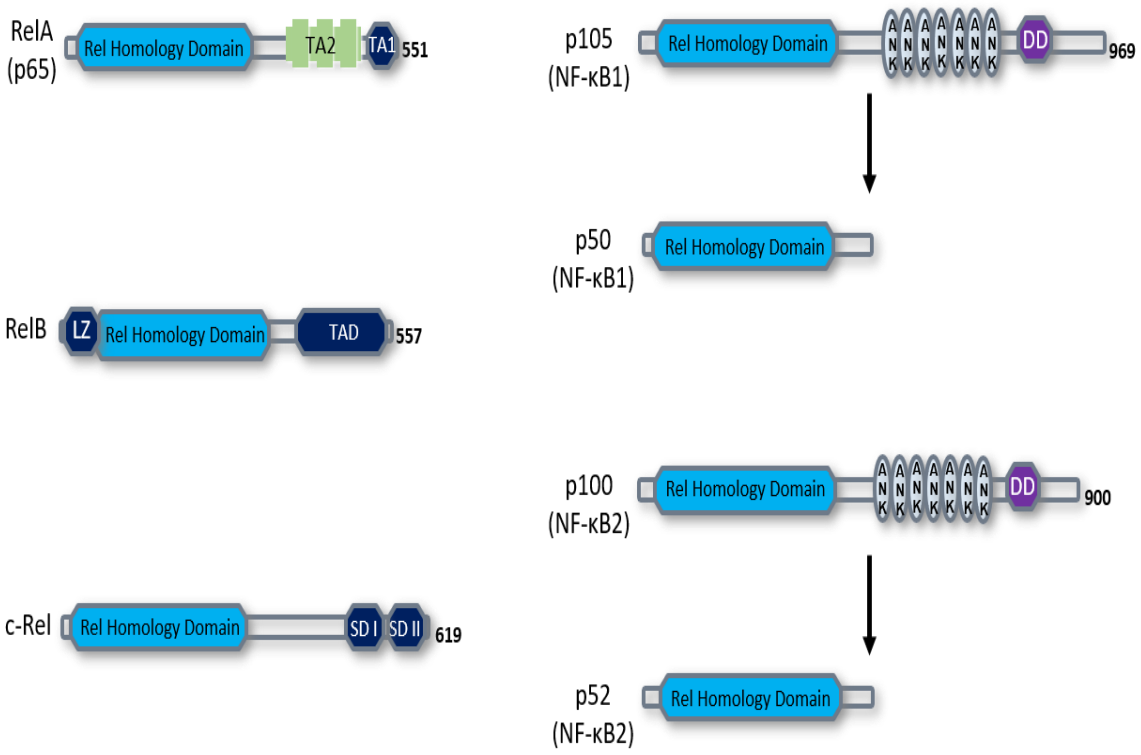

Figure 2.16. The NF-κB subunits. The mammalian NF-κB transcription factor consists of five proteins: p65 (RelA), RelB, c-Rel, p105/p50 (NF-κB1), and p100/p52 (NF-κB2). Figure shows RelA, RelB and c-Rel, plus the subunits for p105 and p50 (NF-κB1) and the subunits p100 and p52 (NF-κB2). The transcription factors can associate with each other to form distinct transcriptionally active homo- and heterodimeric complexes. They all share a conserved 300 amino acid long amino-terminal Rel homology domain (RHD). Sequences within the RHD are required for dimerization, binding of DNA, interaction with IκBs, and translocation to the nucleus. NF-κB1 and NF-κB2 have longer precursor proteins that can be cleaved during translation or via phosphorylation-induced partial proteolysis to their active DNA-binding forms of p50 and p52. NF-κB1 and NF-κB2 proteins additionally contain ankyrin repeats (ANK), similar to those found in IκBs, and therefore can also function as IκBs.

Canonical NF-κB pathway

The canonical NF-κB pathway is mediated by the scaffold protein NF-κB essential modulator (NEMO/IKKγ) and the IKKs IKKα and IKKβ (209). This pathway is typically activated by proinflammatory cytokines including IL-1 and TNF-α when a rapid response is required, for example with a viral infection (215). IKKα and IKKβ phosphorylate NF-κB-bound IκBs, leading to IκB ubiquitination and proteasomal degradation (209,216). Free IκBs are also degraded via a ubiquitin-independent proteasomal degradation pathway (209). The degradation of IκBs allows free NF-κB dimers containing a combination of RelA, c-Rel and p50 to translocate to the nucleus and therefore activate gene expression (209,217,218).

Non-canonical NF-κB pathway

The non-canonical pathway activates NF-κB in a NEMO-independent, but in a NF-κB inducing kinase (NIK) and IKKα-dependent manner (209,217). Activation of the non-canonical pathway are from signals that activate TNF receptors, such as RANKL and CD40 (209). Non-canonical NF-κB signalling controls a wide range of processes including B-cell survival and maturation, dendritic cell activation, and bone metabolism (219).

NIK, which is a kinase implicated in the phosphorylation of IKKα, has several roles in the non-canonical pathway. Upon receptor triggering, adaptor proteins from the TRAF family enable the recruitment of NIK. IKKα then targets p100, for phosphorylation and ubiquitination and leads to the limited proteolysis of its ankyrin-like C-terminus (215). This liberates a p52 subunit that forms a heterodimer with RelB. The p52:RelB dimer then subsequently localises to the nucleus and binds to DNA to activate transcription (209,215,217).

Active NIK/IKK1 complex also phosphorylates the p100 within IκBδ. This results in the partial degradation of the IκBδ complex and the release of bound NF-κB dimers for nuclear localisation and gene activation (209). A summary of both the canonical and non-canonical pathways is shown in Figure 2.17.

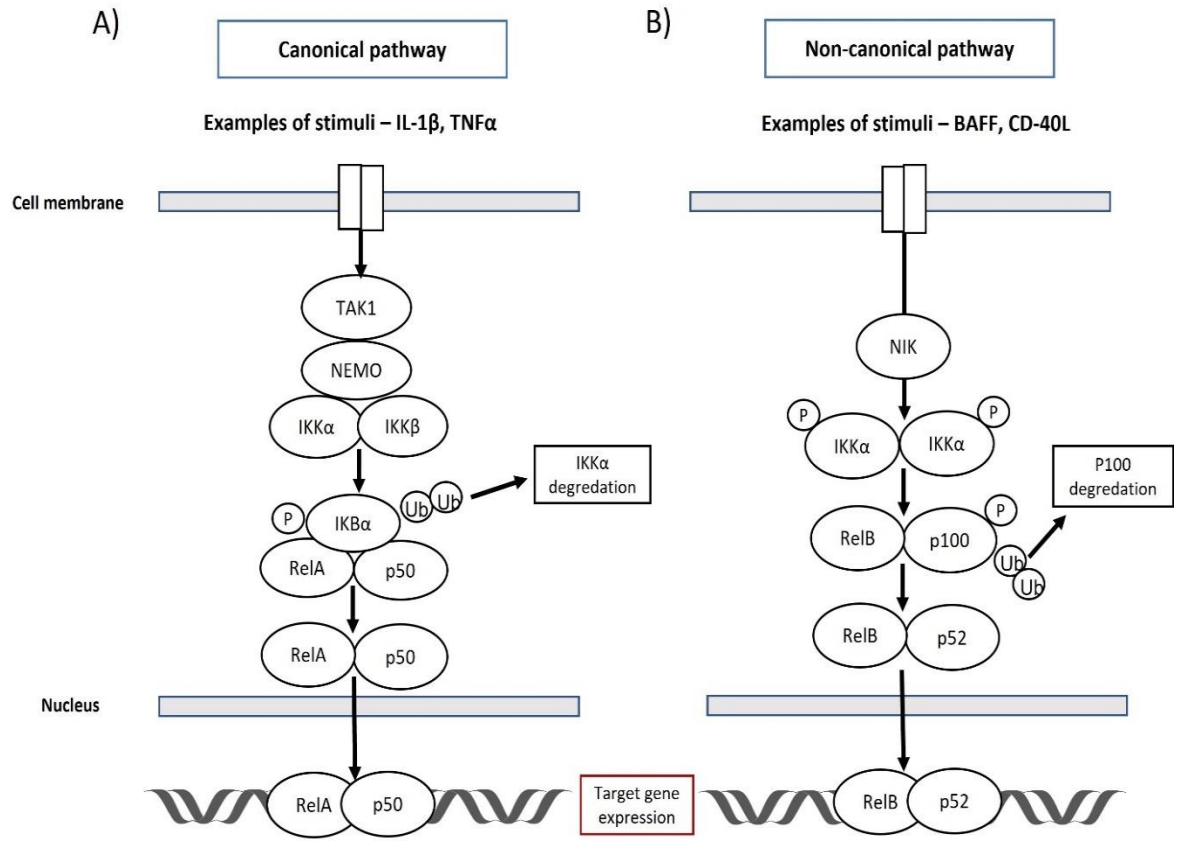

Figure 2.17. NF-κB signalling pathways. A) The canonical pathway is mediated by NEMO (IKKγ) and IKKα and IKKβ. This pathway is typically activated by proinflammatory cytokines when a rapid response is required. IKKα and IKKβ phosphorylate NF-κB-bound IκBs, leading to IκB ubiquitination and proteasomal degradation. This allows free NF-κB to translocate to the nucleus and activate gene expression. B) The non-canonical pathway requires activation in an NF-κB inducing kinase (NIK) and IKKα-dependent manner. This pathway is activated from signalling from receptors such as CD-40L. IKKα phosphorylates p100. This promotes NIK dependent processing of p100 into p52, which can form a dimer with RelB. The p52:RelB dimer localises to the nucleus and binds to DNA to activate transcription.

2.2.2. NF-κB and DNA damage

NF-κB plays an important role in the maintenance of routine cellular homeostasis and NF-κB activation is triggered early in the event of DNA damage. NF-κB signalling is triggered by many different cell pathway mediators, from pro-inflammatory signals to apoptotic signals (215,217). DNA damaging agents can directly activate NF-κB via IKK dependent complexes (217). The NF-κB pathways crosslink into other key DNA damage signalling pathways. ATM activates NF-κB by IKK protein interactions, leading to IKK degradation and RelA Ser 276 phosphorylation (217).

Activation of the IKK complex in a NEMO-dependent way leads to the phosphorylation of IkBα on serines 32 and 36, and its subsequent ubiquitination, similar to the classical NF-κB pathway (215). ATM also directly activates the NF-κB pathway by transporting from the nucleus to the cytosol. During this process, activated ATM binds to and phosphorylates Ser85 of IKKγ, triggering NF-κB ubiquitin-dependent nuclear translocation (220,221).

CHK1 can also directly trigger NF-κB signalling. Loss of CHK1 signalling in the presence of mutant p53 leads to the promotion of a caspase-2 apoptotic response in the presence of DNA damage. This is known as the CHK1 suppressed (CS) pathway (222). Persistently raised CHK1 levels in response to DNA damage in *TP53* mutant cells inhibits the CS-pathway and the activation of caspase-2. This also leads to the regulation of NF-κB activity and the induction of cell pro-survival mediators such as interleukin 6 (IL-6) and vascular endothelial growth factor (VEGF) (222).

2.2.3. The role of NF-κB in cancer

NF-κB has a complex role in cancer which can vary according to the stimulus and pathways activated (210). NF-κB signalling can therefore trigger both oncogene activation and tumour suppression depending on the activating circumstance (210). Multiple tumour suppressor genes such as *TP53, ARF* and *PTEN*, can regulate NF-κB by modulating NF-κB transcriptional activity. This subsequently suppresses the ability of NF-κB to express genes that promote tumour growth and survival (210,223,224).

NF-κB upregulation of cytokines, such as TNF-α and IL-6, and cellular adhesion genes can lead to increased inflammation and promote tissue damage and cell proliferation (210,225). NF-κB has been shown to promote inflammation in inflammatory bowel disease which can in turn lead to the development of colitis associated colorectal cancer (226). NF-κB1 has also shown to be protective against cell damage against known carcinogens, including alkylating agents in haematological malignancy (210,227). The response to DNA damage is very much dependent on the stimulus and the cellular environment as the same response was not demonstrated in response to ionising radiation (227).

Cell growth is a requirement for cancer proliferation and can be accelerated through abnormal activation of cell cycle regulation, or via the dysregulation of normal cell pathways and growth signals (228). NF-κB target genes which can regulate cell proliferation include *cyclin D1, cyclin E1 (CCNE1), CDK2*, and *c-MYC,* while growth signalling includes *interleukin 6 (IL6)* (228). Inhibition of NF-κB has been shown to halt cancer cell growth in multiple cancers, including breast cancer, melanoma and B-cell lymphoma (228–231).

NF-κB is known to regulate anti-apoptotic genes such as *BCL-XL* and *BCL2* and can lead to the promotion of cell survival by upregulation of these genes. This has been demonstrated in haematological malignancies, including B-cell lymphomas (225). NF-κB also indirectly prevents mitochondrially-mediated apoptosis via neutralisation of cell damage-initiating reactive oxygen species (228).

The formation of new blood vessels is crucial for tumour development and progression, and rapid tumour growth can quickly exceed existing blood supplies (228). Many of the signals which orchestrate angiogenesis are dependent on NF-κB signalling. The NF-κB-coordinated inflammatory cytokines TNFα, IL-1, and IL-6 can increase the expression of VEGF, which is one of the main regulators of new blood vessel growth (219,228). NF-κB can additionally promote a metabolic switch in cancer cells, from oxidative phosphorylation to glycolysis (the Warburg effect) by inducing the expression of glycolytic enzymes while also repressing mitochondrial gene expression (210,232). These metabolic changes can furthermore promote cancer growth and survival.

Late stage cancers often involve progression from localised to metastatic disease. Activation of the canonical NF-κB pathway has been implicated in epithelial-mesenchymal transition (EMT). This process is thought to promote tissue invasion and subsequently enhance metastatic potential (225,228). Activation of an EMT pattern involving genes such as *MMP2/9* encoding matrix metalloproteinases, *VCAM-1* encoding vascular adhesion molecule 1 and *ICAM-1* encoding intracellular adhesion molecule 1 was found to be dependent on NF-κB activation in a breast cancer model. Reversal of EMT in this cell model was stimulated by NF-κB inhibition (228,233). It has also been suggested that NF-κB may promote EMT and metastatic potential through transcriptional activation of TWIST, another EMT promoting transcription factor, in a study involving nasopharyngeal cancer cell lines (234).

The regulation of NF-κB in cells can depend on the functional status of key tumour suppressor genes and on oncogene expression (235). NF-κB and p53 can cause inhibition of each other by altering the regulation of gene expression of each other respectively (236). RelA competes with p53 for the transcriptional coactivator proteins p300 and CREB-binding protein (CBP) which potentially can alter the cellular balance between survival and apoptosis (210,236). p53 also can inhibit RelA mitochondrial localisation and subsequently prevent oxidative phosphorylation leading to a change in cellular metabolic regulation (237).

Mutations in the oncogene *KRAS* and mutations in the tumour suppressor gene *TP53* have been found in 20% to 25% of all cancers respectively. The rates of *KRAS* mutation are especially raised in pancreatic, colorectal, and lung cancers (235). *TP53* mutations are common in multiple cancers including ovarian and prostate cancers (238,239). Wild type p53 often suppresses NF-κB function as part of normal cell regulation. *TP53* mutation causes loss of NF-κB suppression, therefore upregulation of NF-κB can occur in cancers and lead to cancer proliferation (235). Mutation in *KRAS* has been shown to activate NF-κB in both cellular models and in mouse models of lung cancer (210,235,240,241). Some studies have shown this in conjunction with a *TP53* mutation (240), however other studies have demonstrated KRAS to activate NF-κB irrespective of p53 mutational status (241).

2.2.4. Claspin and the DNA damage response

Claspin is an adaptor protein which has an essential role in the ATR/CHK1 signalling pathway (242). Claspin mediates CHK1 phosphorylation and its subsequent activation by ATR in response to DNA damage (243,244). Claspin also plays a role in the surveillance of normal replication progression and may be associated with the regulation of origin firing (244–246). High levels of Claspin have been shown to increase the tolerance to replication stress in cancer (247). This stabilising role is structural, as Claspin forms a complex with TIMELESS and Tipin called the replication fork protection complex. This complex interacts with DNA polymerase ε and helicases during leading strand synthesis (247,248). This interaction with TIMELESS and TIPIN is thought to be independent of the ATR/CHK1 pathway but necessary for normal replication fork progression (246,247).

Expression of Claspin fluctuates at different stages of the cell cycle. Claspin levels are minimal in G0/G1 phases, at peak high levels during S/G2 phases and Claspin levels abruptly decrease at the onset of mitosis (243,249,250). Claspin degradation is tightly regulated via ubiquitination and is controlled by multiple ubiquitin ligases and deubiquitinases (244).

Regulation of Claspin is thought to be controlled in unperturbed cell cycles by the transcription factor E2F, however in the presence of DNA damage Claspin can also be regulated by the NF-κB pathway (244,251,252). This regulation of Claspin is dependent by change in IKK activity and can lead to both inhibitory and activating control of Claspin function (252). Data also suggests that depletion of RelB, c-Rel or p52 results in reduction of Claspin both at the protein and RNA levels, indicating that these NF-κB subunits also have an impact on Claspin regulation (223).

Degradation of Claspin is required for checkpoint recovery after cell cycle arrest (252,253). This leads to the deactivation of CHK1 to allow cell cycle re-entry once DNA damage has been repaired and replication can safely proceed (244). Claspin levels are therefore adapted depending on cell cycle stage, however CHK1 can phosphorylate and stabilise claspin to allow continued checkpoint activation. CHK1 inhibition therefore could lead to the destabilisation of claspin and a subsequent increased replication fork instability and replication stress (245).

2.2.5. Role of Claspin in cancer

To date, there have been multiple studies of Claspin in a range of cancers to see if there is an association between prognosis and Claspin expression (244). Studies in non-small cell lung cancer have shown that high levels of Claspin expression in early stage of the disease are a poor prognostic factor and often correlated with high disease activity (254). High Claspin expression has also been demonstrated in high grade renal carcinomas, gastric and ovarian clear cell carcinomas and thought to correlate with increased cancer proliferation (255–257). High levels of Claspin have also been demonstrated in viral associated cancers, for example HPV-associated cervical cancer (258). This could be due to an upregulation of CHK1 expression, leading to cell checkpoint activation and cellular repair and survival. It may also be possible that increased expression is demonstrated due to high cell turnover in high grade cancers with increased proliferation as more cells would be active.

Other studies have suggested that Claspin could act both as a tumour suppressor and an oncogene. Claspin has been shown to regulate BRCA1 phosphorylation on serine 1524, which is associated with CHK1 activation and promotion of cellular repair (234). However, it was also shown that cells with higher Claspin expression also had increased proliferation. There must be additional drivers of cell proliferation activated in these circumstances, as demonstrated in the cancers described, but the mechanisms behind this are not fully understood (234).

2.2.6. NF-κB regulation of Claspin

The NF-κB pathway has been shown to control the regulation of Claspin (252). The IKK-NF-κB pathway is activated by numerous cellular stresses including cytokines to stimulate the expression of target genes (259). IKK-NF-κB signalling is required to maintain normal levels of Claspin expression and disruption of IKK function has been shown to impair ATR mediated DNA repair following DNA damage (252).

The NF-κB subunit c-Rel has additionally been shown to directly activate transcription of Claspin. c-Rel can directly bind to the Claspin promoter and directly modulate Claspin RNA transcription (252). Recruitment of c-Rel to Claspin is dependent on IKKβ signalling but is independent of IKKα (252). This link between the ATR-Chk1 pathway and NF-κB signalling via Claspin is not fully understood, however it may link together complex cellular stress signals with the DNA damage response and repair in order to trigger cell survival or cell apoptosis (244,252).

2.2.7. NF-κB mouse models and CHK1 inhibition

The Perkins' lab have used mouse models to investigate CHK1 inhibitor response in B-cell lymphoma. The *Eμ-Myc* mouse is a transgenic model with upregulation of the oncogene *c-MYC*. This leads to the development of aggressive B-cell lymphomas (260). Previous work by the Perkins' lab has demonstrated that upon tumour development, this mouse model is highly sensitive to a 9-day treatment course of CHK1 inhibitor (CHK1i) monotherapy. This is demonstrated by a reduction in tumour bulk compared to vehicle treated controls (147). The CHK1 inhibitor used in this study was the tool compound CCT244747 and a precursor of SRA737, the CHK1 inhibitor used in the phase 1/2 clinical

trial discussed in this thesis in Section 2.4 (147,150). Similar outcomes were also demonstrated in the same mouse model using SRA737.

Additional work by the Perkins' lab has been conducted in NF-κB mouse models to assess CHK1i sensitivity. This work has shown that when the NF-κB *c-Rel -/-* mouse and NF-κB *RelA T505A* mutant mouse were crossed onto the Eμ-Myc mouse model, the resulting lymphomas were resistant to CHK1 inhibition (261). In the Eμ-Myc/*c-Rel -/-* and Eμ-Myc/*RelA T505A* models with tumour resistance, Claspin levels have been demonstrated to be low (261). The reason behind this low level of Claspin is unclear and in contrast to some of the other cancer models discussed which display high levels of Claspin in aggressive cancer models (254–256,258). The response of other DNA damage response pathway genes is also unknown in both the Eμ-Myc CHK1i sensitive and the CHK1i resistant Eμ-Myc/*c-Rel -/-* and Eμ-Myc/*RelA T505A* models.

This project will therefore further examine the expression of Claspin and other DNA damage response markers in both the CHK1i sensitive and NF-κB mutant CHK1i resistant mouse models to look for potential mechanisms of both CHK1i drug sensitivity and drug resistance.

2.3. Circulating cell free DNA

2.3.1. Introduction to circulating biomarkers

Over the last ten to fifteen years, treatment in cancer has moved from being tumour site specific to a more personalised and targeted approach. Alongside this, there has been a huge increase in the amount of research into the use and application of circulating cell free DNA (cfDNA) in cancer. The mutational profile of cancers can alter throughout the disease course in order to promote cell survival and metastatic potential (40,44). Different disease sites within the same patient can harbour different mutations as diversity increases within the sub-clone populations. This can lead to increased drug resistance as more mutations appear (262).

Moreover, for many disease sites, the traditional method of tissue biopsy can be challenging due to patient fitness and limited tumour accessibility. This can make it more difficult to capture mutational change on disease progression and treat cancers with targeted therapy (263). Hence, the capture of mutation changes over time in cancer from a minimally invasive blood sample is desirable and can in some cases be used to alter clinical management of tumours.

The technology available to assess circulating tumour biomarkers has also developed rapidly over the last decade and several different circulating biomarkers have been identified for clinical use (264). Circulating tumour cells (CTCs) can be identified within the circulation providing additional information from primary tumour sites (264–266). CTC numbers are normally very small and require complex technology to capture cells accurately (267). Micro RNA (miRNA) can also be detected as a circulatory biomarker. miRNA consists of small non-coding regions of RNA which have a role with gene transcription and regulation (264,266). miRNA expression can become unregulated in cancers making this ideal to track tumour related changes, however miRNA is difficult to extract because of small fragment size and due to miRNA attachment to lipids and proteins (266).

The most clinically used circulating biomarker is cfDNA. This is now used frequently in trials and in clinical practice for indications such as mutation detection and serial tumour monitoring (268–273). Further focus within this project will be on the use of cfDNA as a circulating tumour biomarker.

2.3.2. The origin of circulating cell free DNA

cfDNA consists of small DNA fragments present in the normal circulating bloodstream (274). These fragments are thought to be released from cell damage accrued during both necrosis and apoptosis (275–277). Normal physiological levels of cfDNA are low in healthy individuals but increased in pro-inflammatory conditions, including rheumatoid arthritis, sepsis and myocardial infarction (276–279). cfDNA fragments have an modal length of 166 base pairs but depending on nuclease activity fragments can be longer due to the inclusion of duplicate and triplicate sequences (280).

There is now established use of cfDNA testing in clinical practice. cfDNA is now used in pre-natal screening to detect foetal conditions including Downs syndrome and Edwards syndrome, as foetal cfDNA can be detected and distinguished from maternal DNA (281,282). The use of cfDNA has also been developed extensively both in clinical trials and in standard practice in cancer.

2.3.3. cfDNA and cancer

Circulating tumour DNA (ctDNA) is the fraction of cfDNA specifically from tumour origin (283). The overall tumour derived fraction of cfDNA is only a small proportion of the overall total cfDNA and can be less than 2% in total (262,284). There is more variation in fragment size in tumour derived cfDNA, from smaller fragments of approximately 90 base pairs to much longer fragments of up to 10,000 base pairs. This is thought to be due to the high cellular turnover of tumours and more fragments coming from necrosis rather than apoptosis therefore creating more irregularity in fragment size (280).

DNA is also thought to be actively released by cancer cells to promote metastatic transformation at distant sites (285,286). Evidence for this has been supported by findings in work performed in cancer cell lines (285). The presence of circulating tumour cells in the blood, and micro-metastatic deposits, such as in the bone marrow and liver, could also contribute to the release of ctDNA (266). Proposed mechanisms of cfDNA release are shown in Figure 2.18.

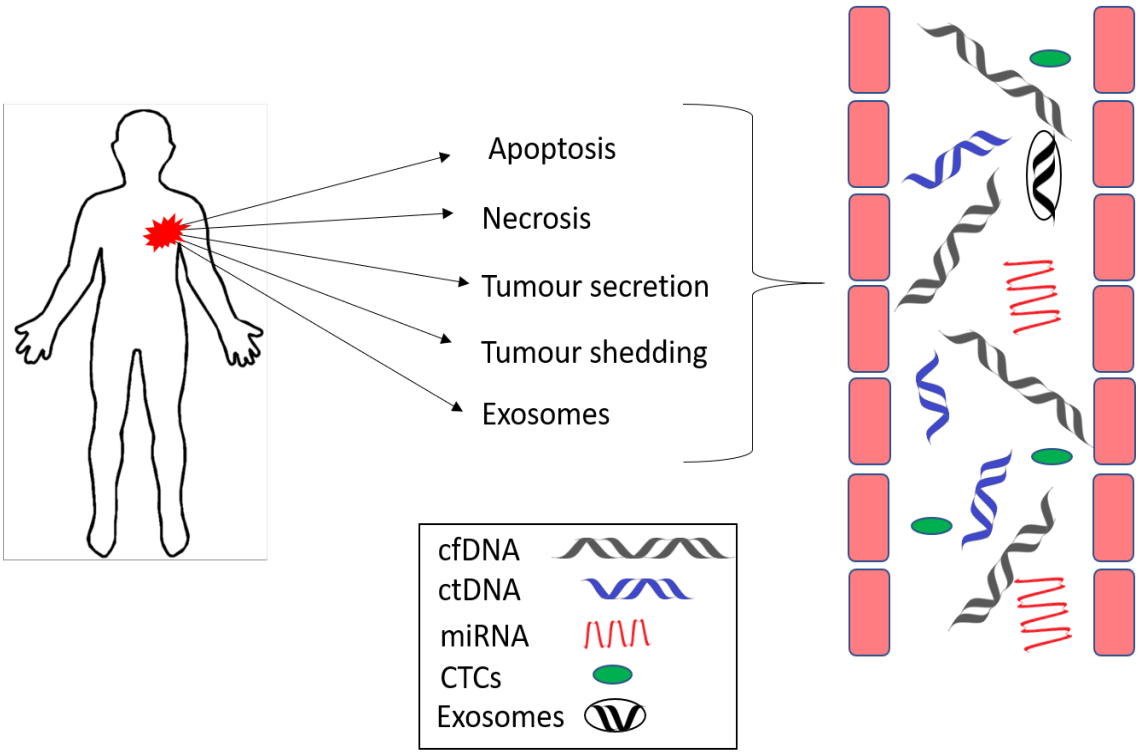

Figure 2.18. Proposed mechanisms of cfDNA release. Adapted from Johann DJ et al., 2018 (274). cfDNA is released by normal cells during apoptosis and during inflammatory processes, which can lead to necrosis. Additional circulating biomarkers include miRNA and CTCs. ctDNA is the proportion of cfDNA released directly from the tumour cells. In addition, some DNA can enter the circulation in exosomes during degradation. Tumours are also believed to directly release DNA to enhance metastatic potential.

The amount of cfDNA can vary according to tumour site. Some cancers, such as pancreatic, breast and melanoma have higher levels of cfDNA compared to low levels seen in renal and thyroid malignancies (287–289). The reasons for this are not clear but may be related in renal cancers to a rapid renal excretion of cfDNA (289). Low levels are seen in primary brain tumours and this is thought to be due to reduced cfDNA transfer across the blood-brain barrier (287).

Studies have demonstrated that cancer mutations can be detected in cfDNA and tests are now routinely used in clinical practice for some cancers including lung cancer. This has enabled a personalised treatment approach and a treatment shift from the primary cancer site to targeted tumour mutations where appropriate (270,290–293).

2.3.4. Utilisation of cfDNA testing in cancer

cfDNA is now regularly utilised in oncology both in the clinical practice and in early phase trials. This section discusses the use of cfDNA within these fields in more detail and how over the last few years this has revolutionised personalised medicine in oncology.

Mutation screening

Clinical trials in cancer have moved to screening patients for molecular targets or pathway mutations which make a drug response more likely. Prostate cancers commonly harbour mutations in the DNA damage response genes including *BRCA1* and *BRCA2*, *ATM* and *CHEK2* (294). Mutations in these genes make a response to targeted agents, such as PARP inhibitors more likely (294). cfDNA sampling and next generation sequencing panels targeted to look for DNA damage repair mutations can be used to identify patients who are more likely to have a response to the treatment (294). In addition, testing cfDNA after an interval of treatment can show some prognostic signs of response or resistance. This can be shown by either an increase or decrease in cfDNA or a change in the mutation profile within the cfDNA (294). The hope is that the appropriate use of biomarkers likely to indicate response or resistance to treatment will lead to increased drug response and more efficient drug development (264).

Diagnostic use

There is some scope to use cfDNA as a primary diagnostic tool in cancer. This could be useful in identifying mutation patterns in patients who have an unknown primary site of disease. In addition, biopsies of tumours may prove difficult to perform either due to patient fitness or tumour location. Numerous gene panels have been created to identify mutation patterns in patients or to look at mutations within a specific tumour site, such as lung cancer (295). One of the main challenges with using cfDNA as a diagnostic tool would be the variable amount of cfDNA in patients. The larger the gene panel, the greater the amount of patient cfDNA is required. In addition, some patients will have large quantities of cfDNA whereas some patients will have small amounts. Accounting for the correlation of disease burden and increasing amounts of cfDNA, use in early detection of disease may be difficult due to overall low cfDNA yield (295).

Outside of the clinical trial setting, there are commercial kits available, including Foundation 1 CDX liquid panel, that use large multigene panels to screen for common tumour mutations (296). The aim of performing these screening panels is to give a clue to tumour diagnosis or demonstrate evidence of targetable treatment mutations. Examples of patient groups who can benefit from such screening are patients with lung cancer or cholangiocarcinoma (297). Further tumour genetic profiling could be therapeutically useful as these tumours are difficult to biopsy but can have targetable and therefore treatable mutations (297).

Assessment of early cfDNA changes due to drug treatment

Clinical trials have incorporated cfDNA testing to gain more information about early tumour response to treatment. Samples can be taken to measure how cfDNA changes post drug treatment, with lower cfDNA levels indicating an early treatment response. cfDNA can be used in early drug development as a proof of mechanism to show that the intended genetic target has been reached and if it is responding to treatment (264). Use of cfDNA for this purpose can make drug development more efficient by recognition of early response and resistance markers and aid the selection of target patient groups based on mutation profile.

Tumour burden and treatment response

Determination of the response to cancer treatment is normally based on clinical review and imaging (295). Studies in metastatic breast cancer, colorectal cancer and melanoma have demonstrated that there is a correlation with a reduction in cfDNA levels in patients responding to therapy (273,298,299). In breast cancer patients, increase in tumour burden through cfDNA can be detected earlier in comparison to CT imaging and circulating tumour cells (300). This presents the possibility of being able to detect progressive disease at a much earlier stage.

In patients receiving immunotherapy treatment for melanoma, there can be uncertainty as to whether progression on CT imaging demonstrates true disease progression or pseudoprogression from an immune response (298). A rise in cfDNA levels in association with progression on imaging may be able to give more certainty into distinguishing true disease progression (298).

cfDNA mutational profiles have been tracked throughout treatment courses to assess if specific tumour clones present at the start of treatment respond differently to therapy (295). Whole-exome sequencing of samples taken from breast and lung patients at different stages of treatment have demonstrated increases in gene expression in genes conferring drug resistance, including *PIK3CA* in breast cancer and *EGFR* in lung cancer (295,301).

In current practice, patients commence new treatments when clinical or radiological disease progression is demonstrated. There is some debate as to whether therapeutic options should be explored on biochemical cfDNA relapse, however the benefit to this is unknown and both patient fitness and risk of the potential side effects need to be considered when making these treatment decisions (273,292).

Resistance tracking

cfDNA can be used to track the change in mutational profile of a cancer over time, including mutations that can confer treatment resistance. In lung adenocarcinoma, patients with an *EGFR* exon 19 or 21 mutation can be treated with targeted EGFR inhibitor treatment (302,303). In the event of acquired resistance, cfDNA sampling can be accessed in clinical practice to identify the *EGFR T790* mutation, which confers resistance to first line EGFR inhibitors, such as the reversible drugs Gefitinib and Erlotinib; and second generation EGFR inhibitors, including the irreversible drug Afatinib (304,305). When this mutation has been identified, patient treatment can be changed to the third generation EGFR inhibitor Osimertinib, which can work in the presence of an acquired *T790M* mutation (293,306). The identification of patients who will benefit from specific EGFR targeted treatments can improve patient outcomes. There will also be a reduction in morbidity from treatment toxicity in patients identified as being unlikely to respond to targeted therapies.

Further mutations that confer resistance to second line therapies, such as the *C797S* mutation have been subsequently identified in patient cfDNA samples (270). This has driven the development of new drugs in order to overcome this drug resistance and the generation of third line EGFR inhibitors to overcome further acquired mutations (306).

Studies in BRCA mutated ovarian, breast and prostate cancers have shown that cfDNA can identify changes in the *BRCA* genes which can lead to a repair of the initial homology-directed repair (HRD) defect (BRCA reversion) and resistance to PARP inhibitor treatment (307–309). These mutations are base substitutions or insertions/deletions which restore the reading frame of the gene generating functional BRCA proteins (307,308). cfDNA samples were compared both pre- and post PARP inhibitor in patients undergoing treatment and new reversion mutations were found in post treatment samples (307–309). Further studies in ovarian cancer with evidence of BRCA reversion have shown that the combination of a PARP inhibitor alongside other DNA damage pathway drugs including Wee1 inhibitors and ATR inhibitors may overcome PARP inhibitor resistance (310,311).

There are now large-scale prospective studies tracking genetic changes in individual tumour sites, for example, the TracerX studies in non-small cell lung cancer and renal clear cell cancer (290,312–314). These collect both circulating free DNA and biopsy samples from patient diagnosis until death to monitor tumour clonal change (314,315). The aim of such studies is to discover the evolutionary pattern of primary tumours and metastatic disease to aid the understanding of cancer evolution (314,315). Figure 2.19 summarises the use of cfDNA in cancer.

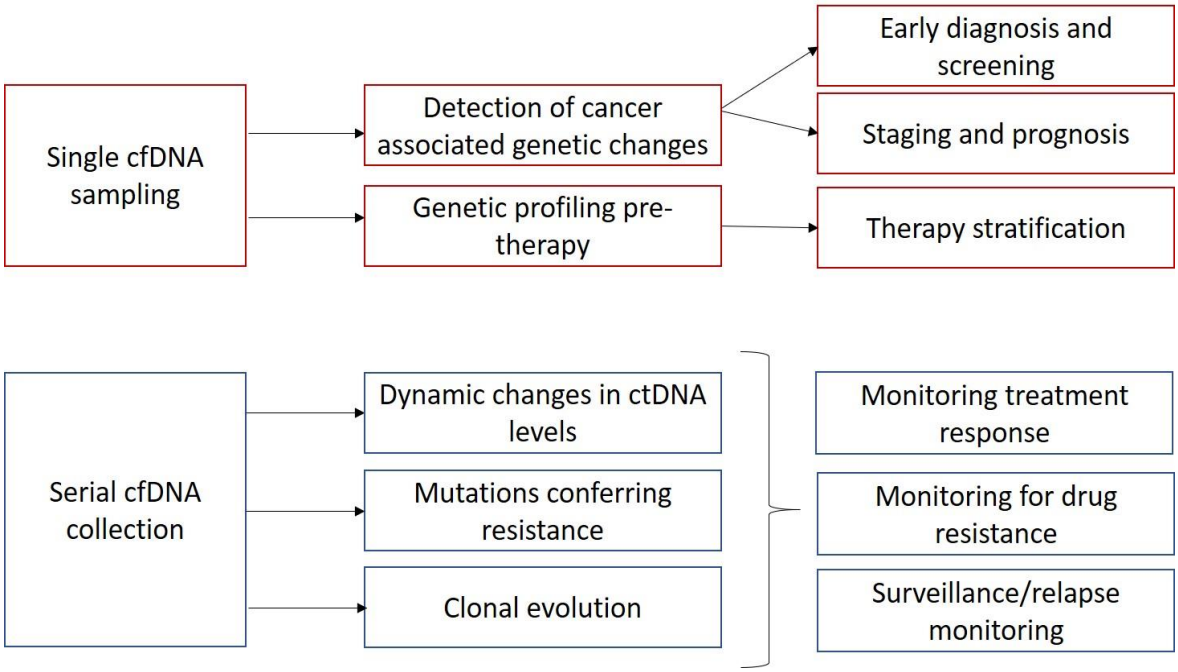

Figure 2.19. Use of cfDNA in cancer. Adapted from Bronkhorst AJ. et al., 2015 (345). Summary of how cfDNA can be utilised in cancer. Single samples and serial cfDNA samples are now in use in diagnosis, screening and management of cancers in a range of different categories.

2.3.5. *De novo* vs acquired resistance mechanisms to targeted cancer treatments

The development of targeted treatments has revolutionised the management of some cancers (316). These cancers include *EGFR* mutated lung adenocarcinomas, *BRAF* mutated melanomas and *BRCA* resistant ovarian cancers (270,314,316–320). The identification of the driving mutations and the development of a targeted treatment has helped to improve outcomes in these patient groups. Resistance to the targeted treatments however is at some point inevitable (316,321,322). The mechanism of drug resistance can either be primary (*de novo*) or acquired (316).

De novo drug resistance

Primary or *de novo* resistance is the lack of upfront treatment response to a drug. True primary resistance to a drug in a clearly defined and selective population for a targeted treatment is uncommon (316). Difficulty in identifying a molecular marker to indicate drug response may also contribute to *de novo* drug resistance as the patient selection group for likely responders may not be selective enough (316). *De novo* resistance can be caused by tumour mutation or patient related factors.

Examples of *de novo* resistance caused by tumour mutation include the presence of both an *EGFR* exon 19 mutation as well as an *EGFR T790M* mutation at diagnosis (321,323). This would confer resistance to first line therapies such as with Erlotinib and Gefitinib from the offset (316,323,324). Another example would be in gastrointestinal stromal tumours (GISTs). Tumours harbouring a *KIT* exon 9 or 11 mutation respond well to therapy with the multi kinase inhibitor Imatinib (325,326). In contrast to this, patients with wild type tumours without a *KIT* mutation do not respond well to Imatinib therapy (325,326).

Patient factors relating to *de novo* drug resistance can be altered by pharmacokinetic factors (316). This can include the absorption, distribution, metabolism and excretion of drugs and all of these factors can vary widely between patients (316). Drug distribution in patients of different body habitus and the renal clearance of a drug between different age groups are some examples of how patient factors can impact on the response to the same drug (327,328). Interactions between co-existing patient medications can

additionally change drug levels, for example via cytochrome P450 inhibitors and inducers which can impact on hepatic drug metabolism (316,328). Overcoming *de novo* resistance to a new drug is difficult and may require the development of an alternative drug, or delivering the drug in combination with an additional treatment (316).

Acquired drug resistance

Acquired drug resistance is the loss of response to a drug in patients who initially respond to treatment. The mechanisms behind acquired resistance are complex and can vary between patients and tumour types (316,321,328,329). This type of resistance normally leads to ongoing downstream cell pathway signalling despite the presence of treatment. Acquired drug resistance is inevitable with all cancer therapies and in all palliatively treated cancers that require sustained treatment courses (316). Changes in target mutation such as a second mutation can lead to this resistance mechanism. For example, this can be the acquirement of the *T790M* mutation in *EGFR* mutant lung cancer, or the development of a subsequent *C797S* mutation which alters response to the *T790M* targeted drug Osimertinib (270,324). Another example of acquired drug resistance is seen in patients with *BRCA* mutated ovarian cancers (307). Tumours with *BRCA* mutations have a defect in homologous recombination repair, however this mutation can be overcome and the protein become functional by subsequent additional mutations in the gene (330).

Tumours can develop an upregulation of alternative cell cycle pathways to bypass the pathway inhibited by a targeted agent. This has been demonstrated in *EGFR* lung adenocarcinoma, where tumours treated with EGFR inhibitors have subsequently developed *MET* amplifications (316,331,332). *BRAF* amplifications have also led to resistance with BRAF inhibitors in melanoma (286,318). Resistance to drug treatments can also be acquired through the histological transformation of the original tumour. For example, *EGFR* mutant lung cancers can transform from an adenocarcinoma to the more aggressive and rapidly growing neuroendocrine tumours which do not respond to the targeted agents (316,321,333).

There are several mechanisms that can be used to overcome acquired drug resistance. Drugs can be specifically designed to overcome the new acquired mutations, such as with the *T790M* mutations in *EGFR* mutated lung cancer and the development of Osimertinib (334,335). There have been suggestions in ovarian cancer to combine PARP inhibitors with other targeted treatments to keep tumour cells sensitive to the treatment (336). Drug therapies can also be given in combination to enhance DNA damage. The benefit of combined treatment has been demonstrated in *BRAF* mutant melanoma (319). Response rates to BRAF inhibitors are enhanced by the addition of MEK inhibitors which both reduces drug resistance and improves drug efficacy (319,337). BRAF and MEK inhibitors in combination also reduces drug toxicity by altering the off-target drug effects. Less patients develop cutaneous squamous cell cancers when taking combination therapy compared to BRAF inhibitors alone (338).

Drug resistance in cancer, whether *de novo* or acquired, provides an ongoing challenge in the management of disease control. The diversity between patients and tumours means that there is not necessarily a treatment to suit all cases, and it may be that treatment options upon drug resistance will have to be catered to the individual via further genomic tumour profiling. To do this, markers of response and resistance must be first identified to permit the tracking of the subsequent mutational changes.

2.3.6. Technologies used to assess cfDNA in cancer

The technology used to assess cfDNA has undergone rapid change over the last decade, enabling the detection of tumour specific mutations that can subsequently lead to targeted therapy. There are two main strategies of cfDNA mutation screening. The first method is using a targeted approach to pinpoint specific tumour mutations. This method involves a screening for a small number of mutations in a specific cancer (268). An example of this would be screening for the *EGFR* mutation in non-small cell lung cancer and subsequently looking for the presence of the T790M mutation on disease progression (293,317,322). The types of technology used may include qPCR, BEAMing and TAmSeq, which are discussed in more detail in Section 2.3.8 (268,339).

Targeted cfDNA testing can be an extremely sensitive and effective route of detection. Mutations can be detected with an allele frequency of 0.01% with high specificity (268). Given this high specificity, tests can be performed on samples with relatively low levels of cfDNA. An additional advantage is that using a selective mutation detection is more cost efficient as mass sequencing panels are expensive to both design and run (268,340). A disadvantage of this method of screening is that there needs to be some prior information about the primary tumour site to ensure that the cfDNA testing has been focused appropriately. There is also less scope to find novel mutations outside of the testing range (268).

The second route of cfDNA investigation involves the use of untargeted screening. This incorporates a genome-wide analysis for point mutations or copy number alterations using whole-genome sequencing or whole-exome sequencing (268,341). Examples of this include the commercial multigene cancer panels discussed previously.

Untargeted screening provides the ability to identify novel changes occurring during systemic therapy. Prior diagnostic information about the primary tumour genome is not required as a wider range of mutations can be simultaneously detected (268). This does however provide a distinct disadvantage as high concentrations of cfDNA are required for multigene panels for reliable detection of genome-wide changes (268,341). Although improving over time, untargeted ctDNA detection approaches have a much lower sensitivity (in the region of 5%–10%) in comparison to targeted approaches (268,341).

2.3.7. cfDNA collection and potential variables

The concentration of sample cfDNA can be affected by various preanalytical factors. These include the blood collection, the processing of serum and plasma, the time interval between collection and the initial centrifugation, and the storage conditions (342–345). A summary of these variables is shown in Figure 2.20.

Blood collection

Choice of medium – serum or plasma

cfDNA has been extracted in studies from both the plasma and serum components of blood. Both plasma and serum are liquids derived from full blood that has undergone different biochemical processing after collection of blood samples (346). Serum is obtained from blood that has coagulated whereas plasma contains clotting agents, and is collected with the use of anticoagulants such as EDTA or heparin to prevent clotting (346). Multiple studies have demonstrated that cfDNA is more abundant in serum samples compared to plasma samples (345,347,348). On further evaluation, it has been shown that serum samples also demonstrate more variability between patients (349). Raised levels of DNA in serum samples may be due to the presence of genomic DNA contamination (349,350).

Studies have shown that sample clotting within the collection tube can lead to the lysis of leukocytes and hematopoietic cells which can further increase DNA levels (343,345,351). DNA fragment length in serum has been shown to be significantly greater in comparison to plasma samples, which additionally supports the greater presence of genomic DNA in serum samples (345). Given that plasma samples have shown less variability and overall lower levels of cellular contamination in comparison to serum samples, plasma would appear to be the medium of choice for cfDNA analysis (345).

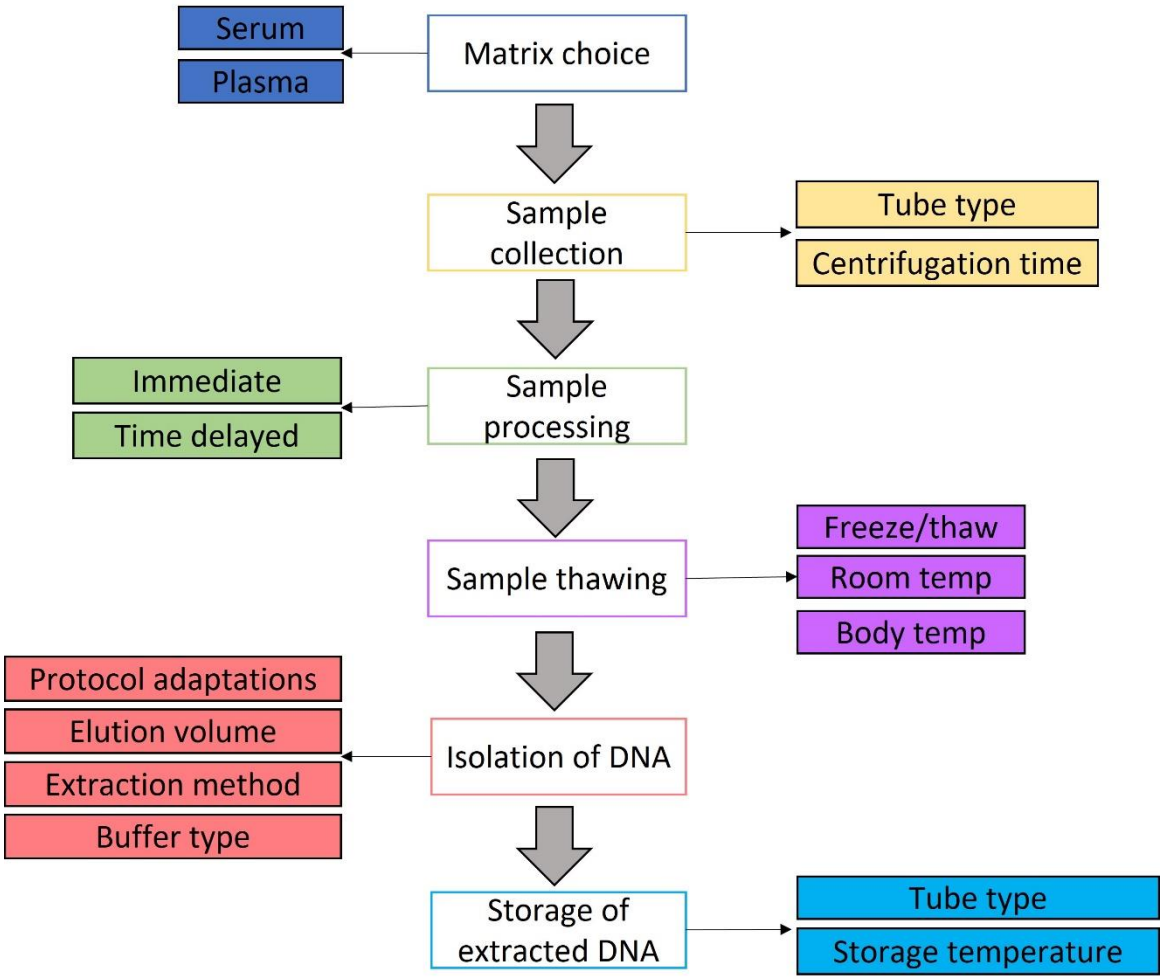

Figure 2.20. Preanalytical variables of cfDNA extraction. Adapted from Bronkhorst AJ et al., 2015 (345). This diagram shows stages of sample extraction and processing that can cause changes in cfDNA quantity and quality and areas which can cause this to change.

Sample processing and storage conditions

cfDNA concentrations increase over time between venepuncture and sample processing and this can affect the overall concentration of cfDNA (342,345). The length of time post-collection in which cfDNA concentration can be affected is still debatable (342,345). Some reports have demonstrated a significant increase in cfDNA levels within 4 hours of sample collection whereas others have shown no significant change within 24 hours of storage (342–344,352).

Sample storage temperature may additionally affect cfDNA concentration, however most studies have demonstrated that this is not a significant factor (345). There is also evidence that repeated freezing and thawing of plasma samples leads to fragmented DNA, but freeze/thaw cycles do not have a significant impact on extracted cfDNA samples (343). In general, swift sample processing is recommended prior to cfDNA analysis to limit any potential time related changes.

cfDNA isolation methods

cfDNA isolation methods in the literature vary and include a range of DNA isolation kits (345,353). The QIAamp Circulating Nucleic Acid Kit (QIAGEN) has been reported to be the most widely used commercial kit in more recent literature and this kit has also been shown to provide the highest cfDNA yield (350,354). There are also multiple methods of cfDNA quantification documented. The most commonly used method in studies has been shown to be qPCR (345), however the use of fluorometry is quick and cost effective for testing samples (350). Good correlation between qPCR and fluorometry methods has been demonstrated with similar levels of ctDNA shown, but less correlation when using UV spectrophotometry methods, such as via Nanodrop (350).

Biological challenges with cfDNA

Low cfDNA abundance

The overall quantity of cfDNA in the circulation is small. In healthy individuals this is usually 5–10 ng/ml of plasma (342,345). The quantity of cfDNA in cancer patients may increase by up to 50 times the normal range, however the amount of ctDNA within a cfDNA sample is still likely to be small (295). In most early-stage cancers, the level of ctDNA may be similar to healthy individuals making it more challenging to detect and monitor (297,342).

Tumour heterogeneity may impact on the mutation allele frequency within the sample. This can make the identification of targeted genes masked within a large background of normal cfDNA more difficult (297,342). Technological advances in library preparation and next generation sequencing have improved the overall sensitivity of ctDNA detection and quantification but the likelihood of a low ctDNA yield from samples has to be taken into consideration (267,297,342).

High fragmentation of cfDNA

cfDNA in itself is highly fragmented with large variability in fragment sizes (342). The wide variability in fragment size is secondary to the multiple mechanisms of cellular cfDNA release (280). cfDNA in healthy individuals mainly results from cellular apoptosis. This process produces small fragments that are generally uniform in length and on average are around 185–200 base pairs (342,355,356). In contrast, cellular necrosis and autophagy, which are the common mechanisms of cell death from tumours, produce DNA fragments more variable in size due to random and untargeted digestion of DNA (280,342).

DNA fragmentation additionally reduces the number of analysable DNA copies which can make DNA amplification and sequencing more challenging (357). Many of the technologies associated with the analysis of cfDNA, such as PCR based methods and next generation sequencing, can only assess fragments within a limited size range (272,358).

Low stability of cfDNA

cfDNA has a short circulating half-life and is rapidly cleared via the kidneys, liver and spleen (275,359). The half-life has been measured to be approximately 4–30 minutes in duration (359). The clearance of cfDNA can be influenced by multiple factors, such as drugs, the performing function of clearance organs and DNAse enzyme activity and the presence of inflammation (275,342). The different forms of circulating DNA based on the mechanism of release, for example from necrosis and from exosomes, can also exhibit different levels of stability (342,360).

2.3.8. Methods of cfDNA detection

PCR based methods

The simplest cfDNA detection methods use polymerase chain reaction (PCR). Real time PCR methods, such as Quantitative PCR (qPCR), can be used to detect and quantify single mutations within a reaction using specific primers (268). PCR-based methods have low DNA requirements and can be an efficient method to detect point mutations in patients with an already identified primary cancer (348). PCR methods are also cheap in comparison to other sequencing techniques, such as digital drop PCR and next generation sequencing, and PCR is relatively easy to perform. There is however a low sensitivity for mutations of 1%–2% frequency. This could make detection difficult in patients with early stage disease with low levels of cfDNA (348).

Digital PCR

Digital PCR is used to detect point mutations in cfDNA at low allele fractions (268). This technique includes droplet-based methods such as droplet digital PCR (ddPCR) and BEAMing (beads, emulsions, amplification, and magnetics) (268). ddPCR was developed to provide high precision and quantification of the copy number variation of target DNA, for example for quantification of somatic mutations (268,361). The ddPCR method uses a water and oil based emulsion to disperse the DNA sample into thousands to millions of droplets (268). Each droplet subsequently contains a single mutated or non-mutated DNA strand. These can be distinguished by flow cytometry using fluorescent probes (268).

The main advantage of using ddPCR is that it provides a high sensitivity in mutation detection. The technique is also a relatively inexpensive technique for the use of absolute copy number quantification (268). The disadvantages of using ddPCR are that only previously known gene variants can be screened and that only a limited number of variants can be investigated per reaction (268).

BEAMing is another digital PCR method which incorporates several techniques used to improve specificity and sensitivity of mutation detection by PCR (272). Firstly, the cfDNA is PCR amplified using primers that introduce sequence tags into the amplified DNA.

Amplicons are then combined with streptavidin coated magnetic beads which are coated with nested primers, and emulsified. Each drop in the subsequent emulsion contains on average one bead and one DNA fragment (272). PCR of the emulsion is then performed and this results in clonal amplification of each template located on the surface of the beads (272). The DNA beads are magnetically purified and the DNA on the beads is hybridised with oligos complementary to a sequence adjacent to the nucleotide region of interest (272). Fluorescently labelled dideoxynucleoside bases are used to discriminate droplets containing wild type or mutant sequences alleles by flow cytometry (268).

BEAMing is again a highly sensitive and specific technique, however the method is complicated to perform and time consuming to gain results (268,272). This method is also expensive to perform, which can limit its use in routine clinical work (268).

Next generation sequencing

Next generation sequencing (NGS), also known as massively parallel sequencing, has developed into an efficient method for sequencing DNA. NGS platforms allow hundreds of genes to be sequenced at the same time without requiring prior knowledge of cancer mutations (268,362). NGS is based on the analysis of millions of short DNA sequences, followed by sequence alignment to a reference genome (268).

Targeted panels

Many sequencing technologies incorporate NGS in the design of targeted gene panels. Tagged-Amplicon deep sequencing (TAm-seq) involves using site-specific primers with universal tails to build a more complex detection library (348,363). The process of TAm-Seq uses multiple PCR steps. To reduce sampling errors, the primers are first bound to a template during a preamplification step to amplify the original DNA (363,364). This is then followed by a second PCR where individual templates undergo amplification (363). This approach provided the opportunity to quantify DNA mutations at multiple sites in each patient and was initially used for the detection of *TP53* mutations in ovarian and breast cancers (363).

The safe sequencing system (Safe-SeqS) involves the addition of a unique identifier, or molecular barcode, to each template. Post DNA amplification, if a mutation does not appear in most of the templates with the same unique identifier sequences, it is likely to be erroneous (364). Safe-SeqS reduces sequencing errors by at least 70-fold, which improves confidence when calling rare variants (364,365). In addition, this method has a sensitivity as high as 98% for the detection of tumour mutations (299,364,365).

CAncer Personalized Profiling by deep sequencing (CAPP-Seq) uses a combination of ligation and library capture methods (272,364). A library panel is designed from the genomic regions of mutations commonly found in the population of interest. Custom oligonucleotides are then created to allow the hybridisation and capture of gene variants from prepared cfDNA samples (272,364). The types of mutations identified using this method are broad and may include indels, single base substitutions, large deletions and mutations which lead to a structural change (272).

The CAPP-Seq method has a high degree of accuracy and can be performed with as little as 7ng total quantity of ctDNA (272,364). Another advantage is that this method can be performed on samples without prior knowledge of cfDNA mutations (272). This method can be expensive as it requires custom oligonucleotide generation. The library preparation steps can additionally be time-consuming (272). There is also the potential to miss potential regions of interest as the panel generated remains selective.

Whole-genome sequencing and whole-exome sequencing

In addition to targeted sequencing, NGS can be applied to an untargeted panel to analyse genome-wide DNA variations. Whole-genome sequencing (WGS) is used to acquire the complete genomic profile of tumour DNA, including point mutations, indels, gene rearrangements and copy number variations (364). Although WGS provides extensive information, it is expensive and overall less sensitive than targeted methods (364).

Whole-exome sequencing (WES) is an alternative method to WGS which involves only sequencing the exons. This makes the process less expensive but overall WES is still costly

and generates a large data set for analysis (364). Both WGS and WES require a high input sample volume (366). The proportion of cfDNA in blood is relatively small and the proportion of ctDNA even smaller. Therefore WGS and WES is not suitable for early cancer diagnoses or screening techniques, as cfDNA levels in these situations are likely to be low (364).

NGS overall has high sensitivity and specificity and allows the detection of hundreds of genes at the same time (348,367). This technique, however, still has a random error rate between 0.1% and 1% depending on the sequencing platform used. This rate of error can therefore make the detection of rare mutations in cfDNA more difficult to detect as they are likely to occur at a low frequency within a cfDNA sample and could be dismissed as erroneous readings (268,341).

NGS is much more expensive than PCR based methods and requires specific platform-based equipment in order to run (268). Use of NGS can generate high volumes of data. Analysis of this data can be complex and time consuming and requires the knowledge of skilled bioinformaticians. Data storage also needs to be considered as this can additionally be costly for large data sets. Table 2.4 shows a summary of different sequencing techniques and some of the advantages and disadvantages of each method.

2.3.9. cfDNA within this project

Patients participating in the SRA737 clinical trial monotherapy arm had blood samples collected at different time points during CHK1i treatment (207). Plasma was then spun from these samples for further cfDNA extraction. These cfDNA samples were used for exploratory purposes to see if mutations in genes linked to the DNA damage response can be detected during CHK1i treatment.

Table 2.4. Advantages and limitations of sequencing techniques. All technologies vary in sensitivity and specificity, costs and cfDNA volume required. Larger volumes of data generated generally take more time to analyse and are more costly, however more data can be obtained with NGS compared to other methods.

Sequencing Technology	Examples	Number of targets	Advantages of technology	Limitations of technology	Reference
Digital PCR	ddPCR BEAMing	1-3 1-20	High sensitivity Small volume cfDNA required Relatively low cost	Known mutations only Limited variants Complex to perform	(268,361,368)
Real time PCR	Quantitative PCR	1	Inexpensive Rapid results Small volume cfDNA required	Known mutations only Limited variants Low sensitivity for low frequency mutations	(268,348)
Next generation sequencing	Deep sequencing TAm-Seq CAPP-Seq Safe-SeqS	Panel	High sensitivity and specificity Multiple genes Potential for WGS/WES	Need larger starting volume cfDNA Expensive Large volume of complex data generated	(299,348,363–365)

2.4. The SRA737 clinical trial

2.4.1. Trial outline

The SRA737 clinical trial was a phase 1/2 first-in-human trial of the SRA737 CHK1 inhibitor, clinical trials ref NCT02797964, which was open between June 2016 and December 2019 (207). The lead site for the trial was the Royal Marsden Hospital, London. The drug was initially developed in the ICR institute, London and initially known as CCT245737 (147). The drug has been tested in the phase 1 trial setting both as a monotherapy in solid tumours and lymphoma, and as a combination therapy in solid tumours alongside the antimetabolite chemotherapy Gemcitabine (207,369). Both studies then had an expansion cohort in the phase 2 trial setting based on patient tumour molecular profile and tumour site of origin (207,369).

The drug is highly selective and potent against CHK1 and has an IC_{50} of 30-220nM in cell lines (147). In addition, this drug was shown to enhance the potency of the chemotherapy agents Gemcitabine and the topoisomerase I inhibitor SN38 (147). In this study, we focus on the monotherapy arm of the trial only.

2.4.2. Monotherapy arm of trial

The monotherapy arm of the phase 1 SRA737 trial has been carried out in patients with advanced cancer in multiple different tumour sites and was carried out at multiple cancer centres as listed in Table 2.5 (207). The initial phase 1 part of the study was the dose escalation phase which was carried out in patients with solid cancers and lymphoma (182,207). This stage was to assess the safety profile of the drug. Patients were initially given a test dose during the screening stage 4-7 days before trial commencement as part of the safety assessment (207). Cohorts receiving each successive dose initially consisted of single patients. Subjects received escalating doses of SRA737 on a continuous daily dosing schedule in 28-day cycles (207). Adverse events were graded using the Common Terminology Criteria for Adverse Events (CTCAE) 4.03 (207,370). The CTCAE toxicity grading is summarised in Table 2.6.

Table 2.5. Cancer centres involved in SRA737 trial recruitment. The SRA737 monotherapy trial was a multicentre trial with recruitment in 15 cancer centres across the UK.

Cancer Centre	Location
Royal Marsden Hospital (lead site)	London
Velindre Cancer Centre	Cardiff
Western General Hospital	Edinburgh
Oxford University Hospitals	Oxford
University Hospitals of Leicester	Leicester
Freeman Hospital	Newcastle upon Tyne
The Christie Hospital	Manchester
University College Hospitals	London
Sarah Cannon Research Institute	London
Guys and St Thomas	London
The Beatson	Glasgow
Clatterbridge Cancer Centre	Wirral
Leeds Teaching Hospitals	Leeds
Sheffield Teaching Hospitals	Sheffield
Belfast City Hospital	Belfast

Table 2.6. Summary of CTCAE criteria toxicity. CTCAE criteria toxicity definitions listed as per version 4.03 as used in the clinical trial.

Grade of CTCAE Toxicity	Definition
1	Mild - asymptomatic or mild symptoms Clinical or diagnostic observations only, Intervention not required
2	Moderate – minimal, local or non-invasive intervention needed Limitations to daily activities
3	Severe or medically significant Requires hospitalisation or prolongation of hospital stay Disabling/limitations to daily activities
4	Life threatening consequences Urgent attention required
5	Death related to adverse event

Once an SRA737-related CTCAE Grade 2 toxicity was observed in a dose escalation cohort during Cycle 1, the cohort was expanded to between 3 to 6 subjects to further assess toxicity (207). Subsequent dose level cohorts followed a rolling 6 design until the maximum tolerated dose (MTD) was identified (182,207). The rolling 6 trial design allows the accrual of 2 to 6 patients concurrently onto a dose level. Recruitment is factored based on the patient numbers currently enrolled and evaluable, the number of patients that experience a dose-limiting toxicity and those that remain at risk of developing a dose-limiting toxicity (371,372). The clinical trial recruitment process is summarised in Figure 2.21.

2.4.3. Patient recruitment and selection

In the Cohort Expansion Phase 2 part of the trial, patients were recruited based on tumour sites known to have genomic alterations associated with increased replication stress. Subjects had one of the following primary cancer sites - prostate, colorectal, anal, high grade serous ovarian, non-small cell lung or squamous head and neck (207). These selected tumour sites were hypothesised to be more sensitive to CHK1 inhibitor treatment (207). The rationale behind tumour site selection is discussed below. A further summary of these findings is shown in Table 2.7.

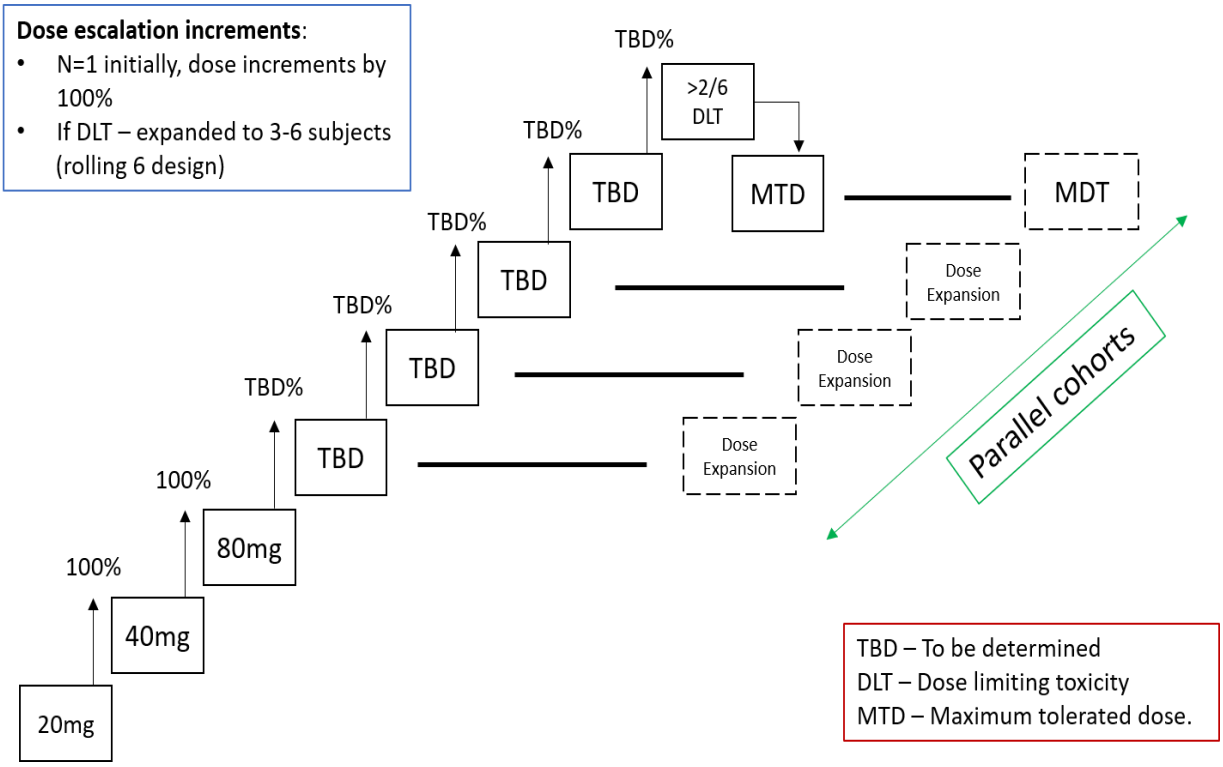

Figure 2.21. Schematic of drug dosing and patient recruitment in SRA737 monotherapy trial. Adapted from SRA737 trial protocol (Sierra Oncology). The trial initially recruited patients with an accelerated titration design. At each dose increment N=1 and the drug dose was escalated by 100%. When a drug related CTCAE Grade 2 toxicity or above toxicity was experienced, the trial cohort was extended to 3-6 subjects in that cohort and in subsequent cohorts following a rolling 6 design. If no further DLT was experienced, dose increments were adjusted by a trial cohort review process by approximately 25 to 75%. The dose expansion phase included patients selected based on tumour molecular profile and that group was run in parallel. If no slot was available in the dose expansion phase, the patients were enrolled in the expansion cohorts at a dose below. MTD was defined as the dose below where at least 2 of the 6 patients in the cohort experienced a dose limiting toxicity. This figure highlights that drug dosing between patients was variable and may have been sub-therapeutic for patients recruited at an early dose in the trial.

Table 2.7. Summary of tumour sites selected for phase 2 SRA737 trial expansion. These 6 tumour sites all commonly have mutations in oncogene drivers, tumour suppressor genes and key genes involved in DNA damage response function. Tumours with mutations in some of these genes have been predicted to have an enhanced response to CHK1 inhibitor treatment.

Cancer site	Common tumour mutations	DNA damage response pathway mutations	Reference
Prostate	Androgen receptor *RB1* *MYC*	*BRCA1* *BRCA2* *ATM* *TP53*	(238,373)
HGSOC	*MYC* *KRAS* *MLH1* *MSH2* *MSH6*	*TP53* *CCNE1* *BRCA1* *BRCA2*	(77,358,360, 362–364)
NSCLC	*EGFR* *ALK* *ROS1* *KRAS* *MYC* *CCNE1* *PD-L1* *CDKN2A*	*TP53* *ATR* *BRCA1* *BRCA2*	(365,366, 368–371,378)
Colorectal	*MLH1* *MSH2* *MSH6* *KRAS* *MYC*		(348,349, 352–356,379)

Cancer site	Common tumour mutations	DNA damage response pathway mutations	Reference
Head and neck squamous cell	*EGFR* *PD-L1* Previous HPV infection *CDKN2A* *MYC*	*TP53* *ATR* *BRCA*	(392–395)
Anal Squamous cell	*PIK3CA* *MYC* Previous HPV infection *AKT* *mTOR* *CDKN2A*	*TP53*	(396,397)

Prostate cancer

Most locally advanced prostate cancers are initially treated with and respond well to anti-androgen therapy. Disease which advances through anti-androgen therapy is classed as metastatic castrate resistant prostate cancer and studies on mutational profiles have been performed in advanced disease (238,373). *TP53* mutations are common and found in approximately 50% of cases (238). In addition, mutations in the tumour suppressor gene *RB1* and the oncogene *MYC* were found in 27% and 20% of samples respectively (238).

Additional genetic analysis of patients with advanced prostate cancer have shown that defects in DNA repair genes such as *BRCA1, BRCA2,* and *ATM* are found in 19.3% of cases (373). The combination of both mutations in DNA damage repair genes and alterations in tumour suppressor genes make castrate resistant prostate cancer prone to replication stress and a good candidate for CHK1 inhibitor therapy.

Colorectal cancer

The development of colorectal cancer can be associated with deficiencies in DNA mismatch repair (MMR). MMR is known to cause microsatellite instability (MSI). Approximately 15% of patients with colorectal cancer have MMR deficiency (385,386). These mutations can be both germline in association with genetic colorectal cancer syndromes such as hereditary non-polyposis colorectal cancer and Lynch Syndrome, or sporadic tumour mutations (386). The rate of MMR deficiency is approximately 90% in inherited colorectal cancer syndromes (398). Colorectal cancers that have high frequency microsatellite instability generally have a better prognosis and are more likely to respond to immunotherapy treatment (399). More than 300 different predisposing MMR gene mutations are known across the human MMR genes. These mutations mainly affect the MMR genes *MLH1, MSH2*, and *MSH6* (387).

Activating mutations or amplification of oncogenic drivers such as *KRAS* and *MYC* are also frequently present in colorectal cancer. Occurrence rates are up to 50% for *KRAS* and 20% for *MYC* (388–390). CHK1 inhibition in tumours with *RAS* and *MYC* mutations has

previously been shown to be successful (147,150,391). Mutations in mismatch repair along with oncogenic amplification of *KRAS* and *MYC* make colorectal cancers more prone to replication stress (1,147,390) and therefore potentially more likely to respond to CHK1 inhibition with SRA737.

High grade serous ovarian cancer

Mutations in genes associated with the DNA damage response are common in high grade serous ovarian cancer (HGSOC). *TP53* mutations have been reported as being present in 96% of tumour samples (374,400). In addition, the same study of over 400 samples found that mutations in oncogenes such as *MYC, KRAS* and *CCNE1* were present in at least 40% of samples analysed (374). The high rate of *TP53* mutations is suggestive of a defective G1/S checkpoint which could make HGSOC more susceptible to CHK1 inhibitor treatment (239,401). HGSOC, like colorectal cancer, is also associated with Lynch syndrome which is a cancer predisposing condition with defects in MMR (402).

Defects in homologous recombination repair are also frequently seen in ovarian cancer. *BRCA1* and *BRCA2* have been found to be mutated in between 13-15% of cases on genetic screening (375,376,400). This has changed the approach of ovarian cancer treatment over the last 10 years with PARP inhibitors now used in patients with *BRCA* mutations (377). The presence of *BRCA* mutations plus additional mutations in DNA damage response genes make HGSOC an ideal target for CHK1 inhibition.

Non-small cell lung cancer

Treatment advances have occurred over the last 10 years in non-small cell lung cancer (NSCLC). This has been with the introduction of targeted therapies for a small subset of patients. Patients with lung adenocarcinomas with *EGFR* mutations (378) and anaplastic lymphoma kinase (*ALK*) rearrangements (379) are now treated with EGFR inhibitors and ALK inhibitors respectively. There has also been the introduction of immunotherapy treatment using antagonist antibodies to programmed death receptor 1 (PD-1) and programmed death ligand 1 (PD-L1) (381,403). Unfortunately, even with these targeted therapies, most patients with NSCLC do not gain prolonged disease control (382).

Further studies have been performed to look for additional key genetic changes in NSCLC (383,384). The tumour suppressor genes, *TP53* and *CDKN2A*, have been found to be altered in 94% and 44% respectively of patient samples with squamous cell NSCLC in The Cancer Genome Atlas Project (TGCA) study (383). In addition, approximately 16% of these patients had activating mutations in key oncogenic drivers including *MYC*, *KRAS* and *CCNE1* (383). The DNA damage response gene *ATR* was amplified in 18-19% of patient samples, and mutations in *BRCA1* and *BRCA2* were mutated in approximately 6% of tumour samples (383).

Samples from patents with adenocarcinoma of the lung show generally lower yet still significant rates of mutations in key tumour suppressor genes and oncogenic drivers. *TP53* mutations have been found in approximately 47%, *CDKN2A* 24%, *MYC* 10%, and *ATR*, *BRCA1* and *BRCA2* mutations in less than 10% of tumour samples (384). *KRAS* mutations are relatively common and found in up to 35% of patients with lung adenocarcinomas (384). Alterations in major genes involved in the DNA damage pathways of interest make NSCLC a good candidate for CHK1 inhibition.

Squamous cell head and neck cancer

Squamous cell head and neck cancers have also benefitted from advances in targeted therapies. The EGFR inhibitor Cetuximab has been used in combination with platinum-based chemotherapy with favourable outcomes (392). Treatment with PD-1 targeted immunotherapy has also proven beneficial in patients as a second line therapy option (394). Treatment responses tend to be more favourable in human papillomavirus (HPV) associated cancers, however prognosis in recurrent disease remains poor (394,395).

Samples for head and neck cancer have also been screened in a TCGA study (393). A loss of function in the tumour suppressor genes *TP53* and *CDKN2A* was found in 50% of samples (393). Amplification of the oncogene *MYC* was found in approximately 13% of cases and less than 5% of samples had mutations in DNA damage response genes such as *ATR* and *BRCA* (393). The loss and amplification of key genes, plus alterations in DNA

damage pathway genes, imply that replication stress levels are high in squamous head and neck cancers again making this cancer group an attractive target for CHK1 inhibition.

Squamous cell cancer of anal canal

Squamous cell carcinoma of the anal canal is a rare malignancy of the gastrointestinal tract (396). There is no defined standard of care treatment for patients with relapsed disease and outcomes are poor (397). Entry into clinical trials is therefore considered early in relapsed disease to increase treatment options (397). As with squamous cell head and neck cancer, most of cases are linked to prior HPV infection (396,397). Mutations in *PIK3CA* and *TP53* mutations are most seen, with rates of both *TP53* and *CDKN2A* mutation being higher in the HPV negative cancers (396,397). Mutations in the *PI3K/AKT/mTOR* genes are seen in approximately two thirds of cases (397). Approximately 10% of tumours have been shown to have a *MYC* amplification (397). This cancer has gene mutations again associated with DNA damage repair pathways and its key regulators, making it a target for CHK1 inhibition.

Trial patient selection

Drug efficacy of SRA737 has previously been shown in mouse models of *MYC* driven lymphoma and *RAS* mutant lung cancers demonstrating drug benefit in models with high replication stress (132). Subjects therefore had to additionally have a confirmed tumour combination of mutations which were selected based on probability of CHK1 inhibitor response.

Mutations included:

- Oncogenic drivers such as *CCNE1* or *MYC*
- Genes involved in the DNA damage repair including *BRCA1, BRCA2, FANC* family genes, mismatch repair (MMR) mutations and/or high microsatellite instability.
- Tumour suppressor genes regulating G1 cell cycle progression/arrest including *TP53*, and *RAD50*.

- Positive human papilloma virus (HPV) status in patients with head and neck squamous cell cancer or anal squamous cell carcinoma.
- Indicators of replicative stress such as gain of function/amplification of *CHEK1*, *ATR* or other related genes.

Tumour genetics were determined using Next Generation Sequencing from biopsy samples (207). A summary of the tumour mutations used for patient selection is in Table 2.8.

Table 2.8. Gene selection criteria for SRA737 monotherapy in phase 2 expansion. Taken from SRA737 Trial Protocol (Sierra Oncology). Genes were selected as predicted to enhance sensitivity to CHK1 inhibitor treatment. Genes were grouped into 4 main categories. Tumour samples from patients were screened for these mutations to assess eligibility for the Dose Expansion part of the study.

Loss of function Missense/truncating mutation; deletion					**Gain of function Amplification; activating mutations**	
Tumour suppressor	*DNA damage repair*				*Replication stress*	*Oncogenic driver*
CDKN1A	*ATM*	*FANCF*	*MSH6*	*RAD51D*	*ATR*	*CCNE1*
CDKN1B	*BLM*	*FANCG*	*PALB2*	*RAD52*	*CHEK1*	*FBXW*
CDKN2A	*BRCA1*	*FANCI*	*PMS2*	*RAD54L*	Other	*KRAS*
CDKN2B	*BRCA2*	*FANCL*	*POLD1*	*RPA1*		*MYC*
CDCN2C	*CHEK2*	*FANCM*	*POLE*	*SETD2*		*MYCN*
RB1	*FANCA*	*MLH1*	*RAD50*	*SMARCA4*		Other
TP53	*FANCC*	*MLH3*	*RAD51*	*TP53BP1*		
MDM2	*FANCD2*	*MSH2*	*RAD51B*	*XRCC2*		
Other	*FANCE*	*MSH3*	*RAD51C*	*XRCC3*		
				Other		

2.4.4. Overall aims of the SRA737 monotherapy trial

The primary aims of the trial were:

- To establish the safety profile of SRA737. This was done by monitoring and recording safety parameters, accounting for the seriousness and severity of adverse events.
- To assess the maximum tolerated dose (MTD). This dose was calculated at the highest dose at which ≤33% of patients had a dose limiting toxicity in a cohort of up to 6 patients.
- To assess the recommended phase 2 dose of SRA737.
- To assess the objective response rate of SRA737. This was from time of first dose until the date of disease progression or date of death measured up to 32 months (207).

The pharmacokinetic profile of SRA737 was also measured during the trial. This was done by measuring plasma levels of the drug to determine drug bioavailability, drug concentration at a given time, drug half-life and excretion patterns (207).

This drug was delivered in a first in human trial, therefore the drug tolerance and subsequent response was not known. There will be patients who will have not responded to CHK1 inhibitor therapy. This is due to the diversity between patients and the variation in tumour development in different cancers. Patients had also received multiple different previous anti-cancer treatments which would vary according to their primary diagnosis.

Patients in the expansion phase had been selected based on tumour mutational profile but the mechanisms behind drug response and resistance were unclear at the offset. Exploratory cfDNA samples were taken from patients receiving SRA737 during this trial to see if mutations in genes linked to the DNA damage response could be detected during CHK1i treatment.

2.4.5. Collection of cfDNA samples

Blood samples were taken from patients at 3 different time points of the study as shown in Figure 2.22. Sample collection was performed nationally at multiple recruitment centres as listed in Table 2.5. All blood samples were spun twice and the plasma extracted. Samples were stored centrally before transporting to Newcastle University.

The first study point was during the screening stage (D-7 to D-4) and taken prior to patients having the first test dose of the CHK1 inhibitor. The second time point was on treatment cycle 3 day 1 (C3D1) when patients attended for clinical review. The final time point was when the patients were at the end of study (EOS), when treatment was discontinued. The final EOS sample was taken within 2 weeks of the cessation of treatment. Treatment was stopped due to patient drug intolerance, drug toxicity or evidence of disease progression.

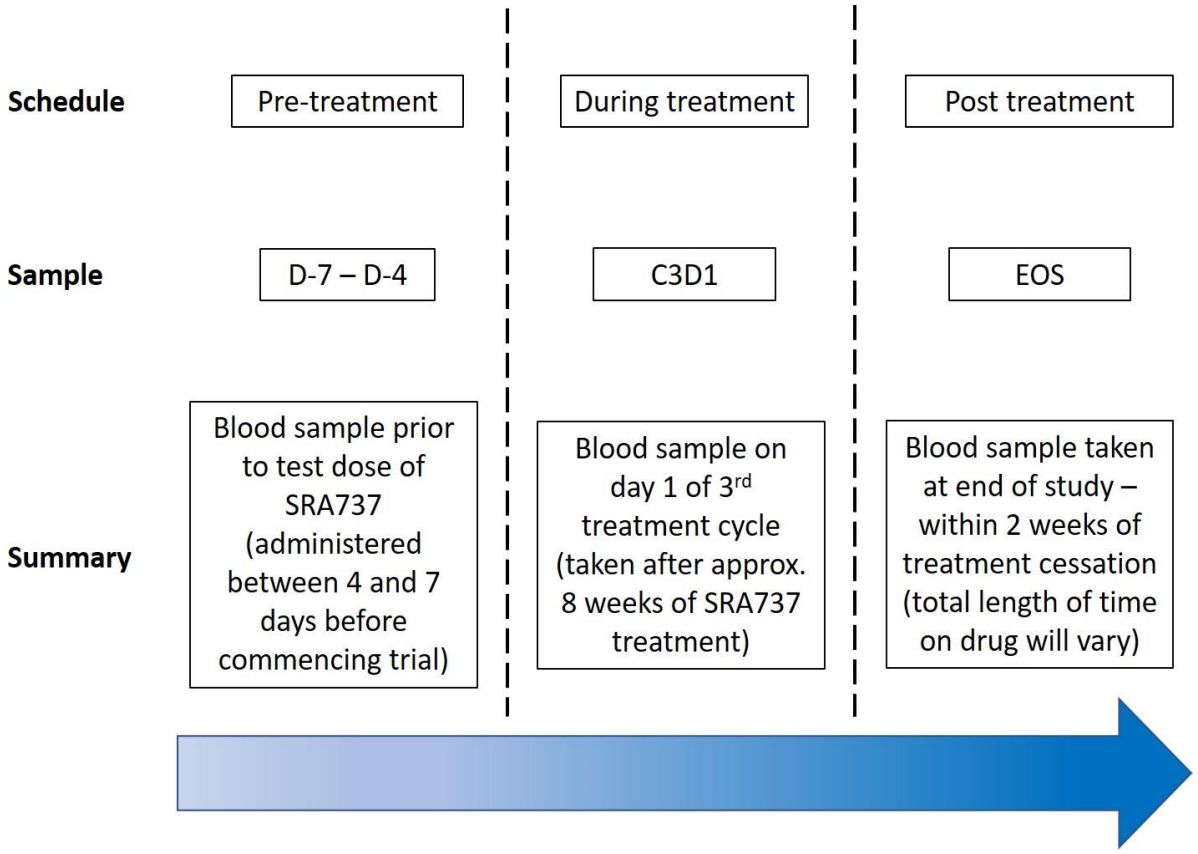

Figure 2.22. Schematic of cfDNA collection time points from SRA737 trial. Summary of when blood samples were taken for cfDNA analysis. 3 samples were planned in each patient - pre, during and post SRA737 treatment.

2.4.6. Challenges of cfDNA samples in early phase trials

There are several challenges and caveats associated with early phase clinical trials. For example, all patients included in the study had a sample taken pre-treatment (D-7 to -4) but not all patients had subsequent samples submitted. In early phase trials, patient populations already have advanced cancers and patients will have exhausted previous standard of care treatments, therefore they may drop out due to disease progression prior to or during their cycle 3 (C3D1) review visit. Patients could additionally be too unwell to attend for an end of study (EOS) review due to disease progression.

The patient population in early phase trials is diverse and patients have a range of different primary cancers, and this provides challenges. Both the primary cancer and subsequent chemotherapies received will have changed the mutational drive of each patient's cancer. Therefore, it may be difficult within a diverse population to isolate common patterns of initial mutations plus patterns of change within cfDNA samples.

In addition, in early phase trials, patients could be on a range of different treatment doses of the study drug. This is because the primary focus of any phase 1 clinical trial is always the safety of the drug in patients. Therefore, patients early in the study may not gain the same potential benefit as patients enlisted later in the trial, so this needs to be considered when looking at patterns of drug resistance and drug sensitivity. Alterations in mutational status may not be related to drug exposure if patients received a sub-therapeutic dose.

2.5. Overall aim

The overarching aim of this thesis was to begin to uncover mechanisms of both *de novo* and acquired resistance to CHK1 inhibitors used for the treatment of cancer. In order to investigate this, this project utilised three distinct but complementary model systems:

1) Transgenic mouse models established within the Perkins' laboratory and that had demonstrated *de novo* resistance to the CHK1 inhibitor, CCT244747. Samples from these animals were used to determine changes in gene expression in tumours that either responded to or were resistant to CHK1 inhibitor treatment.

2) U2OS Osteosarcoma cell line models, which were generated within the Perkins' lab during this thesis as a model of acquired resistance to the CHK1 inhibitor CCT244747 and utilised to determine mechanisms of CHK1 inhibitor sensitivity and resistance.

3) The extraction of cfDNA from patients treated with the SRA737 CHK1 inhibitor clinical trial, to determine whether mutations in key genes associated with the replication stress pathway could be detected in patient samples following exposure to SRA737, and to determine whether this could confer resistance to therapy.

The rationale behind using these strands was to help to identify clearly measurable markers of response or resistance to CHK1 inhibitor monotherapy that could inform the future clinical selection of patients.

3. Materials and methods

3.1. Ethics

3.1.1. Animal ethics

All animal experiments were approved by Newcastle University's Animal Welfare and Ethical Review Board. All procedures were carried out under project and personal licences approved by the Secretary of State for the Home Office, under the United Kingdom's 1986 Animal Act (Scientific Procedures) (404). Animals were bred in the Comparative Biology Centre, Newcastle University animal unit, according to the Federation of European Laboratory Animal Science Associations (FELASA) Guidelines (405). All mice used in these experiments were in the C57BL/6 background and mice were designated to an experimental group dependent on their strain, no blinding was undertaken during analysis. All animal work carried out as part of this thesis was undertaken by Dr. Jill Hunter.

3.1.2. Human ethics

Blood samples were taken from 2 ethically approved protocols run according to standards of Good Clinical Practice.

The first was a Phase 1 monotherapy study of SRA737 (NCT number 02797964). Lead site was the Royal Marsden Hospital, London. Samples were collected from: Royal Marsden Hospital, London; Velindre Cancer Centre, Cardiff; Western General Hospital, Edinburgh; Oxford University Hospitals, Oxford; University Hospitals of Leicester, Leicester; Freeman Hospital, Newcastle Upon Tyne; The Christie, Manchester; University College Hospitals, London; Sarah Cannon Research Institute, London; Guys and St Thomas, London; The Beatson West of Scotland Cancer Care, Glasgow; The Clatterbridge Cancer Centre, Wirral; Leeds Teaching Hospitals, Leeds; Sheffield Teaching Hospitals, Sheffield and Belfast City Hospital, Belfast. Samples were obtained from 18/07/2016 to 14/08/2018 following ethical review by the London - Surrey Borders Research Ethics Committee (Ethics number 16/LO/0423).

The second was the PROSPECT-NE study, with samples collected from patients waiting for consideration of early clinical trials at Newcastle upon Tyne Hospitals NHS Trust from 14/09/2017 to 02/11/2019 following ethical review by the North-East - Newcastle & North Tyneside Research Ethics Committee (Ethics number 17/NE/0208).

3.2. Animal models

3.2.1. Eμ-Myc mouse model

Eμ-Myc transgenic mice develop aggressive diffuse large B-cell lymphoma with a median onset of between the ages of three and six months but they exhibit the hallmarks of MYC overexpression by 4 weeks (406). Overexpression of *MYC* in this mouse model leads to increased pre-B cell proliferation up to 5 times normal. Mature B cells are reduced in number, but demonstrate increased cellular activity (406). The Eμ-Myc mouse model subsequently develops lymphoma of B-cell lineage as described above. These mice were purchased from The Jackson Laboratory (Maine, USA) and the line was maintained by crossing Eμ-Myc male mice with WT females.

3.2.2. Eμ-Myc /*c-Rel -/-* mouse model

Eμ-Myc/*c-Rel +/-* offspring were generated by mating *c-Rel -/-* female mice (a kind gift from Prof. Fiona Oakley, Newcastle University) with Eμ-Myc male mice. Eμ-Myc/*c-Rel -/-* mice were then generated by crossing Eμ-Myc/*c-Rel +/-* males with *c-Rel -/-* female mice. Eμ-Myc/*c-Rel -/-* mice have a significantly shorter overall survival (median survival 79 days) than Eμ-Myc mice (median survival 115 days) (261).

3.2.3. Eμ-Myc/*RelA T505A* mouse model

Eμ-Myc/*RelA T505A* transgenic mice were generated by Taconic Artemis (Cologne, Germany) using C57Bl/6 ES cells. All mice were maintained on a pure C57BL/6 background (407).

3.3. mRNA analysis

3.3.1. Harvesting cells for mRNA extracts

Total RNA was extracted according to the manufacturer's protocol (PeqLab peqGOLD Total RNA, #123014). mRNA generated from a 10cm plate was eluted into 50µl of nuclease-free water. RNA was stored at -80^{o}C.

3.3.2. Tumour extraction of mRNA

Tumour samples originated from Eµ-Myc, Eµ-Myc/*c-Rel -/-* and Eµ-Myc/*RelA T505A* mice treated with the CCT244747 CHK1 inhibitor for 8 hours. Tumours were added to bead tubes (Precellys; # P000918-LYSK0-A) with 400µl of RLT buffer (QIAGEN, #79216) with 1% (v/v) β-mercaptoethanol (Sigma; # M3148). Samples were homogenised using a Precellys tissue homogeniser set at 6500 rpm for 3 cycles of 10 seconds. The tissue supernatant was left to settle before transfer to QIA Shredder columns (QIAGEN; #79656). The beads were washed with a further 300µl of RLT buffer mix to enhance RNA yield and the supernatant was added to the shredder columns. Samples were centrifuged for 2 minutes at 14000 x g. RNA was then extracted using the RNeasy Kit (QIAGEN; #74136) according to manufacturer's protocol.

3.3.3. Analysis of mRNA concentration

RNA concentration was analysed using a NanoDrop 2000c spectrophotometer (Thermo Scientific). Nuclease-free H_2O was used as blank. The 260nm/280nm ratio was calculated to determine nucleic acid purity value compared to contaminants (acceptable ratios were 1.8-2.2).

3.3.4. Reverse transcription

Reverse transcription was performed using the QuantiTect Reverse Transcription Kit; #205310, following the manufacturer's protocol. 500ng to 1µg total RNA were used for the sample preparation and all samples in the same set were prepared to the same concentration. cDNA samples were diluted 1 in 10 in nuclease-free water prior to use.

3.3.5. Primer design and validation

Primers for real-time quantitative polymerase chain reaction (qPCR) were designed using NCBI Primer Blast and synthesised by Eurogentec. Some primer sets were purchased from QIAGEN (QuantiTect primer assays). See Table 3.1 for mouse primers and Table 3.2 for human primers. Prior to use, all primers were validated, see Table 3.3 for conditions. *RPL13A* was selected as reference gene, as this can be used at any temperature and does not change with drug treatment or genotype.

Table 3.1. Murine primer conditions. Primer sequences as designed or QuantiTect catalogue numbers and optimum cycling conditions for qPCR determined by temperature gradient.

Gene name	Primer sequence/order number **(Murine)**		Cycling temperature (°C)
	Forward	Reverse	
RPL13A	CCTTTTCCTTCCGTTTCTCC	CCCTCCACCCTATGACAAGA	Suitable at any temperature
ATM	GGAAACCCTGCTGACCATTG	CTCATCAAGACACGCTCAGC	59
ATR	AAAGGAGCTTCGCCAGTGTA	TGCAGTAGAGCGGCAATATG	55
ATRIP	CACCGAAGCATGTTCTCCACAATT	AAACGAAGCATGTTCTCCACAATTC	55
BACH2	QT01057147		58
BAX	QT100102536		57
BCL2	QT00149254		60
BCLXL	QT00149254		57
BID	QT00145061		58
CCND1	CTGACAACTCTATCCGGCCC	TTGCGGATGGTCTGCTTGTT	60
CCNE1	CCCCACTTCCCGTCTTGAAT	TTCGCACACCTCCATTAGCC	60
CDC25A	QT01058778		58
CDK1	GCTGTGGTACCGATCTCCAG	TTCTGGCCACACTTCGTTGT	60
CDK2	GCGACCTCCTCCCAATATCG	GTCTGATCTCTTTCCCCAACTCT	56
CDK4	TGTCTGTGCTACTTCCCGAAC	TCAGGTCCCGGTGAACAATG	59
CDKN1A	QT01752562		61
CHEK2	CTCGGCTTACCACAGAGGAG	CACACACAGACAGGCGTTTT	60
CHK1	TCGAACGTGGACAAACTGGT	CTCGAAGGTCTCTTTCAGGCA	58
CLSPN	QT00154609		59
CYCLIN A2	GTCATTGGCACAACAGACTGG	AGTGTCTCTGGTGGGTTGAG	60
GAPDH1	GCTACACTGAGGACCAGGTTG	GCCCCTCCTGTTATTATGGGG	Suitable at any temperature
GAPDH2	GCTACACTGAGGACCAGGTTG	GCCCCTCCTGTTATTATGGGG	Suitable at any temperature
LIG4	ATTCCTGGGACCACTCTCCT	CTGAATCGGACACCCAACTT	59
LIMA1	QT00126854		58
MDM2	QT00113722		57
microRNA 18S	TGACGGAAGGGCACCACCAG	CACCACCACCCACGGAATCG	55
MOT heatshock Protein 9	GGTGCAGTGGTTGTTATT	ACCACAGAAGGGGTAGTT	Suitable at any temperature
MRE11A	TTCAGGACAGCAGTGAGGA	TCCGATGATGTGTGGAAGCT	59

Gene name	Primer sequence/order number **(Murine)**		Cycling temperature (°C)
	Forward	Reverse	
NBS1	GGCAACCATGATGATCCCAC	TAAGCCGTACAGAGCGAGTT	59
NBS1	TTCAGGACAGCAGTGAGGAG	TCCGATGATGTGGTGGAAGCT	59
RAD17	CAAGGAGGATCAAGCTTTCG	TCAGGGCTTCCATTTTCAAC	55
RAD50	AGGTGCTAGCGTCTCTCATG	TCCACTACTCAGATCGCCC	59
TOPBP1	AACCAGAGCCTCCAGTAGCA	TTTTCTGTGCGTCTCCTCCT	60
TRP53	AGAGACCGCCGTACAGAAGA	CTGTAGCATGGGCATCCTTT	60
USP1	QT00177352		55

Table 3.2. Human primer conditions. Primer sequences as designed or QuantiTect catalogue numbers and optimum cycling conditions for qPCR were determined by temperature gradient.

Gene name	Primer sequence/order number **(Human)**		Cycling temperature (°C)
	Forward	Reverse	
RPL13A	CCTGGAGGAGAAGAGGAAAGAG A	TTGAGGACCTCTGTGTATTTGTCAA	Suitable at any temperature
ACTIN	CTGGGAGTGGGTGGAGGC	TCAACTGGTCTCAAGTCAGTG	58
ATM	TTCCTCAAGACTTTGGCTGTCA	GGCTCCTTTCGGATGATGGA	56
ATR	GAGCACTGATCTTCAGACAAC	TCCCCTAAACATTCCCCAC	58
ATRIP	CTTCATGATGCACTGCGTGG	AGTCCGTCACATCAGGAAGC	55
BAX	QT00031192		58
BCLXL	QT00236712		55
CDC25A	CAACCTGACCGTCACTATGGA	TGACTCGGAGGAGCCCATTC	56
CDK1	GGTCAAGTGGTAGCCATGAAA	TGGAATCCTGCATAAGCACA	58
CDK2	GTTGTGTACAAAGCCAGAAAC	ATCTCTCGGATGGCAGTA	58
CDK4	AGAGTGTGAGAGTCCCCAATG	CAAACACCAGGGTTACCTTG	56
CHEK1	TGGCTTGGCAACAGTATTTCG	CATGGCAATTCTCCAGCGAG	60
CLSPN	GGTTTTGTGTGGCTTGCTCC	GCCTTGAAGCAGCGTTTCTG	58
CYCLIN A2	CGCTGGCGGTACTGAAGTC	GAGGAACGGTGACATGCTCAT	60
RAD17	TGCTCTGTCAGGGATGTTCTG	GCCACCAATAGCTTGGACCT	56
RAD50	GGCAGGTACGTCAGACACAA	TCTTTCGGCTATCCAAGGCT	58
SLUG	GAGCATTTGCAGACAGGTCA	ACAGCAGCCAGATTCCTCAT	58
TOPBP1	CTCTTTCTGCCAGCCCTCAA	GGGCAAGAAATCACAGGAAG	55
TP53	QT00233646		56
USP1	QT00008568		55

Table 3.3. PCR master mix used for temperature gradient testing and troubleshooting (volume for one reaction).

	Supplier	**Eurogentec Primers (μl/well)**	**QuantiTect Primers (μl/well)**
cDNA (mouse/human)		5	5
GoTaq Buffer (5x stock)	Promega	4	4
$MgCl_2$ (25mM)	Promega	3	3
dNTPs (2mM)	Life Technologies	2.5	2.5
GoTaq (5 unit/μl)	Promega	0.2	0.2
Nuclease free dH_20	Promega	4.8	4.8
Primer mix (10μM)		0.5	0.5

Agarose gel electrophoresis was used for temperature gradient analysis of primer sets and to troubleshoot real-time quantitative PCRs. 2% (w/v) agarose gel (Life Technologies; # 16500500) were prepared in 1x tris-acetate-EDTA (TAE) buffer (40mM Tris, 20mM Glacial Acetic Acid, 1mM EDTA pH8). The solution was heated until boiling using a microwave checked at 30 second intervals (Panasonic Genius). After a brief period of cooling, 2µl of SYBR safe (ThermoFisher; #S33102) were added to 100µl of gel to allow visualisation of DNA.

DNA samples were mixed with prepared PCR as per Table 3.3. 20µl of master mix were loaded per well. 5µl of 100 base-pair ladder (Invitrogen; #10488) were used in the first lane of the gel. Gels were then run at 140V (HU13 System) until the dye front almost reached the edge of the gel. Bands were visualised using a Fujifilm LAS-4000 (Fujifilm) using the automatic setting.

3.3.6. Real Time – Quantitative Polymerase Chain Reaction

For each reaction, 5µl of the diluted cDNA were added to 15µl of master mix, see Table 3.4 for conditions.

Real-time quantitative PCR was carried out using the SYBR green method using QIAGEN Rotor-Gene Q with the following settings: initial hold for 10 minutes at 95^{o}C, then cycles of 95^{o}C for 30 seconds, X^{o}C for 30 seconds (optimal cycling temperature between 55^{o}C and 60°C) and 72^{o}C for 30 seconds for a total of 40 cycles. Readings were taken after the annealing step of each cycle. A final 10-minute gradual increase in temperature was performed from 60^{o}C to 95^{o}C to produce a melt curve. DNA-free controls prepared with nuclease-free water were used for each primer per run. Each reaction was carried out in duplicate with the reference gene *RPL13A* also prepared in duplicate.

Following completion, the melt curve was analysed for double products or unusual curves and outliers were excluded. Threshold values were set at 0.1 across all runs, ensuring that the exponential increase phase of the reaction was consistently measured. Ct values were exported to Excel for further analysis.

Table 3.4. qPCR master mix for Eurogentec and QuantiTect Primer Assays. Volumes listed are for one reaction.

	Supplier	**Eurogentec Primers (μl/well)**	**QuantiTect Primers (μl/well)**
GoTaq Buffer (5x stock)	Promega	4	4
$MgCl_2$ (25mM)	Promega	3	3
dNTPs (2mM)	Life Technologies	2.5	2.5
SYBR Green (1:200 DMSO)	Sigma	0.2	0.2
GoTaq (5 unit/μl)	Promega	0.2	0.2
Nuclease free dH_20	Promega	4.6	3.1
Primer mix (10μM)		0.5	2

3.3.7. Data analysis and statistics

Data were normalised using the 2-ΔCT method (R = 2–[ΔCP sample – ΔCP control]) (408) using the gene *RPL13A* as reference. Graphs were plotted using GraphPad Prism and statistically analysed as described per each individual figure.

Raw Ct values were also stored in Excel and plotted using GraphPad Prism to ensure that the reference gene was not moving (data not shown) and to demonstrate that this method of analysis was not skewing the data presented in its final form.

3.3.8. Preparation of samples for RNA-seq

RNA was extracted according to the manufacturer's protocol as described previously (Section 3.3.1 for human tissues and Section 3.3.2 for mouse tissues). Sample quality was analysed using Biorupter (Agilent 6000 Nano kit, #5067-1511) or TapeStation automated electrophoresis (Agilent; #5067-5576 RNA ScreenTape, #5067-5578 Agilent RNA ScreenTape ladder, #5067-5577 RNA ScreenTape buffer) following manufacturer's instructions to assess sample RNA integrity number (RIN) score and RNA quantity. Sample RIN score was required to be greater than 6 and starting amount of RNA of at least 2000ng. Samples were diluted using RNA and nuclease free water to a final concentration between 30 and 50ng/µl.

3.3.9. RNA-seq analysis

Samples were run using the Illumina platform by Leigh Taylor at the Genomics Core Facility at Newcastle University. Bioinformatic analysis was performed by Peter Leary, Newcastle University Bioinformatics Centre. Validation of genes of interest was performed by Dr. Jill Hunter and Nicola Hannaway using qPCR as per Section 3.3.6 or via western blot protein analysis as per Section 3.8.2.

3.4. Mammalian cell culture

3.4.1. Cell lines

All cell lines used in this study were obtained from ATCC. Most experiments were performed using U2OS cells, a highly used immortalised cell line originally derived from a tibia osteosarcoma of a 15-year-old female. They have an epithelial adherent cell morphology and are moderately differentiated. This cell line was selected for use as they are sensitive to CHK1 inhibition as discussed with Michelle Garrett, University of Kent. I also confirmed this in preliminary work. U2OS cells are also highly transfectable, therefore this cell line was selected with the potential to modify drug response.

Other experiments were performed using PC3, SW620 and HCT15 cell lines. PC3 cells are a highly immortalised cell line originally derived from bone metastases from a prostate cancer of a 62-year-old male. This cell line was selected for use as they are highly resistant to CHK1 inhibition, this was re-confirmed with preliminary studies. This cell line is also highly transfectable.

SW620 cells are derived from a Dukes C colorectal adenocarcinoma from a 51-year-old male. HCT15 cells also originate from a colorectal cancer from a male, age unknown. These cell lines were selected given the inclusion of colorectal cancers in the expansion phase of the SRA737 study and to assess CHK1i drug response in these cell lines (409).

3.4.2. Passage of immortalised cell lines

U2OS cells were cultured in Dulbecco's modified Eagle's medium (DMEM) (LONZA; #3235) supplemented with 10% (v/v) sterile-filtered foetal bovine serum (FBS) (Gibco; #10270), 5mM penicillin and streptomycin and 5mM L-glutamine (LONZA; #7779). Cells were kept at 37^{o}C in a humidified incubator with 5% CO_2/21% O_2.

PC3 cells were cultured in RPMI 1640 medium (LONZA; #BE12-167F) supplemented with 10% (v/v) sterile-filtered FBS (Gibco; #10270), 5 mM penicillin and streptomycin, 5mM L-glutamine (LONZA; #7779) and 12.5 mM HEPES (Scientific Laboratory Supplies, # LZBE12-709F). Cells were kept at 37^{o}C in a humidified incubator with 5% CO_2/21% O_2.

SW620 cells were cultured in DMEM (LONZA; #3235) supplemented with 10% (v/v) sterile-filtered FBS (Gibco; #10270), 5mM penicillin and streptomycin and 5mM L-glutamine (LONZA; #7779). Cells were kept at 37^{o}C in a humidified incubator with 5% CO_2/21% O_2.

HCT15 cells were cultured in RPMI 1640 medium (LONZA; #BE12-167F) supplemented with 10% (v/v) sterile-filtered FBS (Gibco; #10270), 5mM penicillin and streptomycin and 5mM L-glutamine (LONZA; #7779). Cells were kept at 37^{o}C in a humidified incubator with 5% CO_2/21% O_2.

For passage, cells were washed once with room temperature phosphate buffered saline (PBS) (LONZA; #3053) and dissociated from their surface using 1x trypsin (LONZA; #1366) at 37^{o}C for no more than 10 minutes. Trypsin was inactivated via the addition of fresh DMEM or RPMI and cells were re-suspended into a single cell suspension and split by a dilution factor of 1:6. Cells were predominantly grown in T75 flasks, however T150 flasks and 10cm plates were also used. Cells were not grown beyond 80% confluence and were split at 70% confluence. Efforts were made to keep cell passage number under 30 as cancer cell lines with a high mutation load can become more genomically unstable with increasing passage number.

3.4.3. Freezing, storage and thawing of cell lines

Cells were washed once in PBS (LONZA; #3053) and dissociated from their surface using 1x trypsin (LONZA; #1366) at 37^{o}C for no more than 10 minutes. Trypsin was inactivated through addition of fresh DMEM media (LONZA; #3235) and cells were resuspended into a single cell suspension before being centrifuged at 400 x g for 5 minutes to pellet the cells. Supernatant was then carefully removed, and the cells were resuspended in 90% (v/v) FBS and 10% (v/v) dimethyl sulfoxide (DMSO) (Sigma-Aldrich; #D2650). 1ml of this cell suspension was then aliquoted into cryovials. Cells were frozen slowly and stored at -80^{o}C.

To thaw cells, cryovials were removed from storage and stored on dry ice until required. Cryovials were placed in a 37^{o}C water bath to quickly thaw the cells. The contents of the cryovial were transferred into a pre-prepared flask containing the appropriate growth media. Plates were stored in the incubator overnight. After 16h of incubation, media was replaced with fresh growth media to remove any DMSO. Cells were then checked regularly to ensure healthy growth before passage was carried out. Early passages were split at a lower ratio of 1:2 to 1:4 depending on the rate of cellular growth.

3.5. Experimental treatments of mammalian cells

3.5.1. Treatment with CHK1 inhibitors

U2OS, PC3, HCT15 or SW620 cells were seeded at 6x10^{5} cells per 10cm^{2} plate and left overnight. Cells were then treated for 24 hours with the CHK1 inhibitor CCT244747. This CHK1 inhibitor is a tool compound related to the SRA737 CHK1 inhibitor currently in phase 1/2 clinical trial. Cells were treated at either 1µM or 5µM dose. For harvesting, the media was removed and cells were washed in PBS and scraped into a fresh microcentrifuge tube. Samples were spun at 500 x g for 5 minutes at 4^{o}C and PBS was removed. The cell pellets were then extracted for either protein as per Section 3.6.2 or RNA as per Section 3.3.1.

3.5.2. Generation of isogenic cell lines

U2OS cells were cultured in DMEM media with increasing doses of the CHK1 inhibitor CCT244747 starting at 0.1µM to a maximum concentration of 5µM. Surviving cells from each concentration were monitored and the dose was increased when confluency level hit 50%. Surviving cells were then cultured in DMEM media and used for further studies. With each cell line generated, a control sample of U2OS WT cells cultured in DMEM media alone was also grown from the same starting cells.

3.6. Harvesting cells and tumour samples for protein extracts

3.6.1. Tissue whole protein extraction

Tissue samples were kept on dry ice until required. Samples were homogenised in bead tubes with 300µl of Phosphosafe (Merck Millipore; #71296) using a Precellys tissue homogeniser set at 6500 rpm for 3 cycles of 10 seconds. Samples were transferred to 1.5ml tubes. The bead tubes were washed with an additional 200µl of Phosphosafe. Samples were left at room temperature for 5 minutes, then centrifuged at 4^{o}C at 14000 x g for 10 minutes, according to manufacturer's instructions. Supernatant (protein fraction) was transferred to fresh tubes.

3.6.2. Cell whole protein extraction

After treatments, cell culture plates were placed on ice and cells were scraped into the media using a sterile plastic scraper. This cell suspension was transferred to a 10ml conical tube on ice and suspensions were centrifuged at 400 x g for 5 minutes at 4°C. The media supernatant was aspirated. Pellets were resuspended in 1ml cold PBS and transferred to Eppendorf tubes. These were then centrifuged at 1500 x g for 10 minutes at 4°C. Phosphosafe was then added to the cell extract at double the pellet volume. Samples were incubated at room temperature for 5 minutes, then centrifuged at 14000 x g for 10 minutes at 4^{o}C. Samples were flash frozen on dry ice and stored at -80^{o}C before use.

3.7. Determining the protein concentration of lysates

The Bicinchoninic acid (BCA) assay is a copper-based colourimetric assay used for protein quantification (410). BCA works via the initial formation of a Cu^{2+}–protein complex followed by reduction of the Cu^{2+} to Cu^{+} leading to a colour change from green to purple (410). The total amount of Cu^{2+} reduced is proportional to the amount of protein present in solution (410).

Protein concentrations of lysates were determined by a Pierce™ BCA assay (Thermo Scientific #23225) according to the manufacturer's instructions and analysed using the POLARstar Omega plate reader (BMG LABTECH). BSA was used to produce a standard curve alongside the protein samples. Protein samples were prepared to appropriate concentrations for resolving proteins of interest. Equal amounts of protein (10-20µg per gel) were mixed with 2 x Laemmli loading buffer (BioRAD #1610737) supplemented with β-mercaptoethanol and water and heated to 95°C for 10 minutes.

3.8. Protein analysis

3.8.1. SDS-PAGE

Precast Criterion™ 4-20% gradient gels (BioRAD #3450034) were used for sodium dodecyl sulphate (SDS)-polyacrylamide gel electrophoresis (SDS-PAGE). Gels were loaded into the tank and combs were removed. 100mls of 10 x TGS buffer (BioRAD #1610732) were diluted with 900mls water and the tank was filled with prepared buffer to the appropriate fill line. 15µl of samples were loaded into the wells and 10µl of PageRuler Protein Ladder (ThermoFisher #26616) were loaded into lane 1 and 5µl were loaded into the last well. Gels were run at 90V for 10 minutes and then 100V for approximately 150 minutes or until the dye front reached the bottom of the gel.

3.8.2. Western blot

Following SDS-PAGE, proteins were transferred onto polyvinylidene difluoride (PVDF) membrane (Immobilon-P; #IPVH00010). Membranes were activated in methanol for 15 seconds and water for 2 minutes. 1 x transfer buffer was prepared (10% (v/v) 10 x TG buffer (BioRAD #1610734), 20% (v/v) methanol and water) and used to fill the transfer tank. An ice pack was used in the tank to keep the tank cool. Proteins were transferred at 100V by wet transfer (BioRAD) for 1 hour with 1 layer of blotting paper to protect the gels and membranes. Membranes were blocked in 5% (w/v) non-fat dry milk/TBS-T (10mM Tris pH 7.4, 150mM NaCl, 0.01% (v/v) Tween) for 1 hour at room temperature, washed 3 times in TBS-T for 5 minutes, and then incubated with primary antibodies overnight at 4^{o}C. See Table 3.5 for antibodies used.

After primary antibody incubation, membranes were removed, and antibody solutions were stored at -20^{o}C for future use. Membranes were washed in TBS-T 1 x prior to incubation for 1 hour at room temperature in appropriate horseradish peroxidase (HRP)-tagged secondary antibody as listed in Table 3.6. Cells were washed 3x in TBS-T for 10 minutes before being exposed to Pierce^{TM} Enhanced Chemiluminescence (ECL) Western Blotting Substrate (ThermoFisher; #32106) following the manufacturer's protocol. Membranes were developed on auto-radiography film using an automatic x-ray film processor (Xograph Compact X4). Exposure times varied depending on signal strength.

Table 3.5. Primary antibodies used for western blotting.

Antibody	Manufacturer	Catalogue number	Target	MW (kDa)	Dilution	Dilutant (in TBST 1x)	Incubation time
AKT	Cell Signaling	9272	αRabbit	60	1:500	5% BSA	Overnight
AMPKα1	Cell Signaling	2795	αRabbit	60	1:500	5% BSA	Overnight
BCLXL	Cell Signaling	2764	αRabbit	30	1:1000	5% BSA	Overnight
CDC25A	ProteinTech	550311AP	αRabbit	59	1:1000	5% BSA	Overnight
CDK2	ProteinTech	101221AP	αRabbit	33	1:1000	5% BSA	Overnight
CHK1	Cell Signaling	2360	αMouse	56	1:1000	5% BSA	Overnight
CLSPN	Moravian	N/A	αRabbit	~ 150	1:1000	5% milk	Overnight
Cyclin A2	ProteinTech	182021AP	αRabbit	48-52	1:1000	5% BSA	Overnight
Cyclin D1	Cell Signaling	2922	αRabbit	36	1:1000	5% BSA	Overnight
GSK3β	Cell Signaling	9315	αRabbit	46	1:500	5% BSA	Overnight
H2AX	Cell Signaling	7631	αRabbit	15	1:1000	5% BSA	Overnight
pAKT (s473)	Cell Signaling	4060	αRabbit	60	1:500	5% BSA	36 hours
pAMPKα (Thr172)	Cell Signaling	2535	αRabbit	62	1:500	5% BSA	Overnight
PARP	Cell Signaling	9542	αRabbit	89, 116	1:1000	5% BSA	Overnight
pCHK1 (S345)	Cell Signaling	2348	αRabbit	56	1:1000	5% BSA	Overnight
pGSK3β (S9)	Cell Signaling	9336	αRabbit	46	1:500	5% BSA	Overnight
pGSK3β (y216)	Abcam	Ab75745	αRabbit	46	1:500	5% BSA	Overnight
RAD17	Santa Cruz	SC-5613	αRabbit	77	1:500	5% BSA	Overnight
RAD51AP1	ProteinTech	1122551AP	αRabbit	38	1:1000	5% BSA	Overnight
USP1	ProteinTech	143461AP	αRabbit	110	1:1000	5% BSA	Overnight
USP14	ProteinTech	145171AP	αRabbit	60	1:1000	5% BSA	Overnight
WDR48	ProteinTech	165031P	αRabbit	70	1:500	5% BSA	Overnight
ZAP-70	ProteinTech	155921AP	αRabbit	70	1:1000	5% BSA	Overnight
βActin	Sigma	A5441	αMouse	42	1:10000	5% BSA	Overnight
γH2AX	Cell Signaling	2577	αRabbit	15	1:1000	5% BSA	Overnight

Table 3.6. Secondary antibodies used in western blotting.

Antibody	Manufacturer	Catalogue number	Raised in	Dilution	Dilutant (In TBST 1x)	Incubation time
Anti-Mouse IgG HRP linked	Cell Signaling	7076	Rabbit	1:4000	5% BSA	2 hours
Anti-Rabbit	Sigma	A6154-1ML	Goat	1:4000	5%BSA	2 hours
Anti-Rabbit IgG HRP linked	Cell Signaling	7074	Goat	1:4000	5% BSA	2 hours

3.9. Preparation of samples for proteomic analysis

Samples selected for proteomic analysis were from acute 8 hour Eμ-Myc and Eμ-Myc/*c-Rel -/-* mouse studies. Selection was based on the results of our western blots showing the greatest selected protein changes at 8 hours after single dose of the CCT244747 CHK1 inhibitor. The sample preparation was done by Dr. Amy Campbell at the University of Liverpool. Validation of proteins of interest was performed by western blot as described in Section 3.8.2 by Nicola Hannaway and subsequently by Dr. Jill Hunter at Newcastle University.

3.10. Cell survival

3.10.1. PrestoBlue assay

The PrestoBlue assay measures cell viability by using the reducing power of living cells to determine proliferation. This resazurin based assay turns from blue to red in colour and highly fluorescent, therefore increased fluorescence is indicative of more living cells after drug treatment (411).

U2OS, PC3, SW620 or HCT15 cells were plated out in 96-well plates at 10 x 10^5 cells/well with 100μl of media. Plates were treated with the appropriate dose of small molecule inhibitor and incubated at 37°C. PrestoBlue assays were performed following the manufacturer's protocol. Absorbance was recorded at 570nm after a 60 minute incubation of cells with the PrestoBlue reagent (ThermoFisher, #A13262) and transfer of the reagent to black plates to reduce background fluorescence. Gain was set at 50% from the well containing the lowest cell number. This was done to alter the voltage signal to the detector to prevent signal saturation from the fluorescence (412). Cell viability was expressed as a percentage relative to media controls. Graphs and statistical analyses were carried out using Excel and GraphPad Prism as described.

3.10.2. Clonogenic assay

The clonogenic assay is a cell survival assay based on the ability of a single cell to grow into a colony of at least 50 cells (413,414). Untreated cells plated as a single-cell suspension at low densities will grow to form colonies in ~ 10–14 days (plating efficiencies

(PE) variable between cell lines) (414). PE is the ratio of colony number to the number of cells seeded. The number of colonies arising after cell treatment is called the surviving fraction (SF) (414).

U2OS cells were harvested and cells were counted. 2 x 10^5 cells were added to each well in a 6-well plate. Cells were incubated overnight at 37°C. Cells were treated with small molecule inhibitors at the required concentration for 24 hours. Cells were harvested by washing once with PBS and then by adding 0.5ml of trypsin x 1 to each well. Plates were incubated at 37°C until the cells detached. 1.5ml DMEM media were added to each well after cell detachment.

Cells in each well were counted using a haemocytometer and the volume required for a 1 x 10^4/ml ^{stock} was calculated for each well. Plates were set up per required cell number (500 or 1000 cells per well) from the stock volume and DMEM media was added to a total of 2ml per well.

Plates were examined every few days for colony formation. If colonies of a suitable size had formed, dishes were fixed, stained and counted. DMEM medium was removed from all plates with care not to disturb colonies. Carnoy's fixative (components – 75% (v/v) methanol, 25% (v/v) acetic acid) was added to cover each well and left for 5 minutes. The Carnoy's fixative was decanted from the plate and placed back into the stock solution for re-use. 0.4% (w/v) crystal violet (Sigma; #C0775) was added to cover each well and left for 15 minutes to visualise the colonies. The crystal violet solution was decanted back into the stock solution for re-use. Plates were washed with tap water to remove excess dye. Plates were left to dry at room temperature and review later.

Plates were scanned and imaged using the FujiLas 300 imaging system to compare colony coverage. Cells were counted by hand by Dr. Jill Hunter using a clicker and a pen to mark the cells already scored.

3.11. Plasma cfDNA Preparation

3.11.1. Plasma cfDNA extraction (QIAGEN)

The QIAamp Circulating Nucleic Acid kit (QIAGEN #55114) was used for cfDNA extraction and all buffers and extraction columns described in this section were included in the kit unless stated otherwise. The cfDNA extraction protocol used in this thesis using the QIAamp Circulating Nucleic Acid kit protocol was used to generate NICR SOP 433. A water bath was pre-heated to 60°C and a heating block was pre-set at 57°C. Plasma samples were defrosted at room temperature and centrifuged at 1000 x g for 10 minutes to remove traces of lymphocytes. Proteinase K (Sigma-Aldrich # P4850-5ML) was pipetted into a 50ml centrifuge tube (protocol adjusted per starting volume of plasma). Table 3.7 shows the volumes of reagents used according to plasma volume.

The starting volume of plasma was added to the 50ml tube containing Proteinase K. Buffer ACL (lysis buffer) as per Table 3.7 was added to each 50ml tube. Tubes were mixed by pulse-vortexing for 30 seconds. Tubes were immediately incubated in a 60°C water bath for 30 minutes. Following incubation, tubes were placed back on the lab bench and the caps were unscrewed. Buffer ACB (binding buffer) as per Table 3.7 was added to the lysates in the tubes. Tube caps were closed and tubes were mixed thoroughly by pulse-vortexing for 15 seconds. The lysate–buffer ACB mixtures were incubated for 5 minutes on ice.

The QIAamp Mini Columns were connected into the VacConnector on the QIAvac 24 Plus vacuum manifold (QIAGEN; #19413). 20ml tube extenders (labelled with appropriate sample numbers) were inserted into the open QIAamp Mini Columns. The collection tubes were retained for use later.

The lysate–buffer ACB mixture was pipetted into the tube extender of the QIAamp Mini Column. The vacuum pump was switched on. When all lysates had been drawn through the columns completely, the vacuum pump was switched off and the pressure was released to 0 mbar by removing one of the white luer plugs. The luer plug was then re-inserted. The 20ml tube extender was then discarded.

Table 3.7. Buffer volumes used for cfDNA extraction. Buffers used for cfDNA extraction were from the QIAamp Circulating Nucleic Acid kit (QIAGEN #55114). Buffer volumes were adjusted according to the starting volume of plasma in each sample.

Plasma starting volume (mls)	Proteinase K	ACL lysis buffer	ACB binding buffer	AVE buffer
1	100µl	0.8ml	1.8ml	50µl
2	200µl	1.6ml	3.6ml	100µl
3	300µl	2.4ml	5.4ml	150µl

600µl of wash buffer ACW1 were added to the QIAamp Mini Columns. The lids of the columns were left open, and the vacuum pump was switched on. After all of buffer ACW1 had been drawn through the QIAamp Mini Column, the vacuum pump was switched off and the pressure was released to 0 mbar by removing one of the white luer plugs. The luer plug was re-inserted.

750µl of wash buffer ACW2 were added to the QIAamp Mini Columns. The lids of the columns were left open, and the vacuum pump was switched on. After all of buffer ACW2 had been drawn through the QIAamp Mini Column, the vacuum pump was switched off and the pressure was released to 0 mbar by removing one of the white luer plugs. The luer plug was re-inserted.

750µl of 100% ethanol were added to the QIAamp Mini Columns. The lids of the columns were left open, and the vacuum pump was switched on. After all of the ethanol had been drawn through the QIAamp Mini Columns, the vacuum pump was switched off and the pressure released to 0 mbar by removing one of the white luer plugs. The luer plug was re-inserted.

The lids of the QIAamp Mini Columns were closed. All mini columns were removed from the vacuum manifold, and the VacConnector was discarded. The QIAamp Mini Columns were placed in clean 2ml collection tubes (saved from earlier), and samples were centrifuged at 20000 x g for 3 minutes.

The QIAamp Mini Columns were placed into new 2ml collection tubes. The lids of the columns were opened, and the columns were incubated at 56°C for 10 minutes in order to dry the membrane completely.

The QIAamp Mini Columns were placed in clean 1.5ml DNA LoBind micro-centrifuge Eppendorf tubes (Sigma Alrdrich #Z666548) and the 2ml collection tubes from the drying stage were discarded. Buffer AVE as per Table 3.7 was applied to the centre of the QIAamp Mini Column membranes. The lids of the columns were closed and samples were

incubated at room temperature for 3 minutes. Samples were centrifuged in a micro-centrifuge at 20000 x g for 1 minute to elute the DNA.

A pipette was used to take up the eluate (flow-through) and the eluate was again added directly onto the centre of the QIAamp Mini Column membrane. The lids of the columns were closed and samples were incubated at room temperature for another 3 minutes. Samples were centrifuged in a micro-centrifuge at 20000 x g for 1 minute to elute the DNA. Samples were labelled according to the initial sample label and the DNA was stored at -20°C until required.

3.11.2. Qubit fluorometric testing

The Qubit fluorometer is a DNA quantification device that measures the fluorescence intensity of fluorescent dye binding to double-stranded DNA (415). The Qubit assay can be used for checking DNA quality before next-generation sequencing (415).

Samples were assessed using the Qubit dsDNA HS Assay Kits (ThermoFisher; # Q32854). All reagents discussed in this section are from this kit. Qubit dsDNA HS buffer and Qubit dsDNA HS dye reagent were prepared by mixing at the ratio 200:1.

200µl total volume were prepared per Qubit tube. 2 standards (Qubit dsDNA HS standard 1 and 2) were prepared as 190µl buffer: dye solution and 10µl Qubit dsDNA HS standard solution. cfDNA samples were then prepared as 199µl buffer:dye solution and 1µl cfDNA sample. Samples were vortexed for 5 seconds and left to stand at room temperature for 10 minutes. Standards and samples were analysed using the Invitrogen™ Qubit™ 3.0 Fluorometer (ThermoFisher).

3.11.3. TapeStation analysis of samples (Agilent)

The Agilent TapeStation system is an automated gel electrophoresis system used to calculate sample quality control (size, quantity and integrity) of DNA and RNA samples (416).

The protocol described in the text is used for HS D1000 ScreenTapes. See Table 3.8 for the details and reagent volumes for all other ScreenTape protocols used in this study. Reagents were left to equilibrate at room temperature for 30 minutes. cfDNA samples were defrosted at room temperature and stored on ice. Samples and reagents were vortex mixed before use. Ladder solution was prepared by mixing 2µl sample buffer with 2µl D1000 Ladder. Samples were prepared by mixing 2µl D1000 sample buffer with 2µl DNA sample. Samples were spun down, then vortexed using the IKA vortexer and adaptor at 2000 rpm for 1 minute. Samples were spun down to position samples at the bottom of the tube.

Samples were loaded into the 2200 TapeStation instrument. Samples were labelled as required on the 2200 TapeStation Controller Software and run as per the HS D1000 programme.

Table 3.8. TapeStation protocols for HS D1000, HS D5000 and Genomic DNA ScreenTapes. The protocols vary in the amount of reagent and sample used. Key: (T) ScreenTape, (L) ladder, (B) buffer.

ScreenTape used	Catalogue numbers	Buffer volume (µl)	Ladder volume (µl)	Sample volume (µl)
HS D1000	5067-5584 (T) 5067-5587(L) 5067-5603 (B)	2	2	2
HS D5000	5067-5592 (T) 5067-5594 (L) 5067-5593 (B)	2	2	2
Genomic DNA	5067-5365 (T) 5067-5366 (L+B)	10	1	1

3.11.4. Vacuum spin

Samples were defrosted on ice. Samples were transferred to Eppendorf Lo-Bind microcentrifuge tubes (Sigma Alrdrich #Z666548) and vacuum spun using the Savant SPD131DDA SpeedVac Concentrator (ThermoFisher) on medium heat and automatic setting. Samples were reviewed at 30 minute intervals to check sample volume, aiming for a final volume of less than 50µl. Samples were analysed using TapeStation HS D1000 ScreenTapes (Agilent) to calculate fragment length and cfDNA quantity.

3.11.5. Library preparation of cfDNA samples (Illumina)

The protocol was followed for the Illumina Trusight 170 kit (Illumina, # 20028821) as per the manufacturer's instructions. All reagents in this section were used from the Illumina Trusight 170 kit and used as per manufacturer's instructions unless stated otherwise. An Illumina Nextera Rapid capture custom enrichment kit was custom made for the project to enable the investigation of genes of interest.

Modifications to the protocol were made in order to add unique molecular identifier (UMI adapters) as recommended by Illumina. UMIs were custom built into the Illumina Nextera Rapid capture custom enrichment kit. The library preparation of cfDNA was done by Raf Hussain at the Genomics Core Facility, Newcastle University and library preparation was assisted by Nicola Hannaway.

3.11.6. End repair and A-tailing

This process converts the overhangs from the cfDNA fragments into blunt ends. The addition of A-tails to the 3' end of the DNA prevents the DNA fragments from ligating to each other during the library preparation. 30ng of cfDNA were prepared to a volume of 50µl with TE buffer. cfDNA samples were brought to room temperature and a 96 well plate was labelled accordingly with sample details. cfDNA samples were mixed and placed on ice. A master mix of End Repair A-tailing Enzyme Mix 1 (ERA1-A) and End Repair A-tailing Buffer 1 (ERA1-B) was prepared according to the manufacturer's instructions. 10µl of the ERA1 master mix were added to each sample. The plate was microsealed and

shaken for 2 minutes. The plate was incubated at 30°C for 30 minutes, then 72°C for 20 minutes. The plate was then rested on ice for 5 minutes.

3.11.7. Ligation of adaptors

During this stage adaptors are added to the ends of the cfDNA fragments. Unique molecular identifiers (UMI) are added to give a unique marker to individual patient samples during sequencing. 60µl of Adapter Ligation Buffer 1 (ALB1) reagent were added to each well in the 96 well plate. 5µl of DNA Ligase 3 (LIG3) were added to each well. The UMI adaptor mix was vortexed for 10 seconds and 10µl of the UMI adaptor mix were added to each well. The plate was sealed and mixed then incubated at room temperature for 30 minutes. 5µl of stop ligation mix (ST2) were added to the wells and the plate was microsealed and vortexed for 2 minutes.

3.11.8. Ligation clean-up

This process uses sample purification beads to clean the cfDNA products and remove impurities. 112µl of sample purification beads were added to each well. The plate was sealed and vortexed for 2 minutes, then incubated at room temperature for 5 minutes.

To wash, samples were placed on a magnetic plate for 10 minutes. The supernatant was discarded from the wells. Samples were removed from the magnetic stand and washed with freshly prepared 80% (v/v) ethanol. Samples were returned to the magnetic stand and the supernatant was discarded. The wash step was repeated twice.

To elute, the plate was removed from the magnetic stand. 27.5µl of resuspension buffer were added to each well. The plate was sealed and mixed for 2 minutes, then incubated at room temperature for 2 minutes. The plate was placed on a magnetic stand for 2 minutes and 25µl of each eluate were transferred to a corresponding well on a fresh 96 well plate.

3.11.9. Index polymerase chain reaction

During this stage, cfDNA fragments are amplified using primers that add index sequences. This allows sample multiplexing during the sequencing process. Individual index primer numbers (1-16) were assigned to each sample and documented. 5µl of the designated index primer were added to each well. 20µl of enhanced PCR mix (EPM) were added to each well. The plate was sealed and vortexed for 2 minutes.

The PCR was run in a thermocycler as follows:

Settings:
- Lid temperature 100°C, reaction volume 50µl
- 15 cycles of 98°C for 10 seconds, 60°C for 30 seconds, 72°C for 30 seconds and 72°C for 5 minutes.
- Thermocycler held at 10°C on completion.

3.11.10. First hybridisation

At this stage, a selected pool of oligos is hybridised with the cfDNA libraries. The custom oligos designed from our gene panel were used rather than standard rapid capture Trusight 170 oligos. 20µl of each DNA library were added to a new plate labelled HYB1. The central wells on the plate were used to minimise evaporation during the PCR reaction. 15µl of target capture buffer 1 (TCB1) were added to each well. 10µl of target capture additives 1 (TCA1) were added to each well. 5µl of custom oligo mix (1.25µl oligo and 3.75µl resuspension buffer) were added, as the oligos were prepared at a higher concentration than the standard kit oligo mix. The plate was sealed and vortexed.

The plate was placed on the thermocycler and the HYB1 program listed below was run (1 cycle only).

Settings:
- 95°C for 10 minutes
- 95°C for 2.5 minutes
- 85°C for 2.5 minutes
- 75°C for 2.5minutes
- 65°C for 2.5minutes
- Temperature held at 57°C for hybridisation overnight (18 hours total)

3.11.11. First capture

During this process, streptavidin magnetic beads (SMB) were used to capture probes hybridised to targeted regions of interest. Wash steps are to remove any products with non-specific binding. The enriched library is then eluted from the beads prior to a second hybridisation.

Binding step

150µl of streptavidin magnetic beads were added to pre-labelled sample 1.5ml tubes. Then 50µl from each library preparation were added to the appropriate tube. Tubes were sealed and vortexed and samples were incubated at 57°C for 25 minutes, shaking intermittently to stop the beads settling. Samples were placed on a magnetic stand for 2 minutes and the supernatant was removed.

The tubes were removed from the magnetic stand. 200µl of enhanced enrichment wash 2 (EEW2) were added to each well. Samples were pipette mixed five times, then sealed and vortexed. Samples were incubated at 57°C for 5 minutes, then placed on a magnetic stand for 2 minutes. Whilst remaining on the magnetic stand, samples were pipetted to remove and discard the supernatant. The wash step was repeated twice, performing 3 washes in total.

Elution step

The reagents enrichment elution 2 (EE2) and 2NNaOH (HP3) were combined to form an elution mix – for 16 samples, 456µl of EE2 and 24µl of HP3 were mixed. Samples were vortexed for 2 minutes.

17µl of the elution mix were added to each bead pellet. The samples were vortexed for 2 minutes to mix. All samples were placed on the magnetic stand for 2 minutes. 15µl of each eluate were transferred to a new plate (ELU1 – using the middle wells again to reduce evaporation as further PCR was required). 5µl of elution target buffer 2 (ET2) were added to each eluate. The plate was microsealed and vortexed for 2 minutes.

3.11.12. Second hybridisation

A second hybridisation step increases the specificity of targeted cfDNA regions. 15µl of TCB1 and 10µl of TCA1 were added to each well. Custom oligos were diluted (1.25µl custom oligos and 3.75µl resuspension buffer) and 5µl of the diluted custom oligos were added to each sample well. Samples were run on the pre-programmed HYB2 program on PCR for 2 hours (recommended hybridisation time of 1.5 to 4 hours). This was the same program as the HYB1 program (for 1 cycle only).

Settings:
- 95°C for 10 minutes
- 95°C for 2.5 minutes
- 85°C for 2.5 minutes
- 75°C for 2.5 minutes
- 65°C for 2.5 minutes
- Temperature held at 57°C for 1.5 hours

3.11.13. Second capture

Binding step

The ELU1 plate was removed from the thermocycler. 150µl of streptavadin magnetic beads (SMB) were added to each pre-labelled sample tube. 50µl of each library from the ELU1 plate were added to the corresponding sample tube. Samples were vortexed and incubated at 57°C for 25 minutes.

Samples were placed on a magnetic stand for 2 minutes. Whilst on the magnetic stand, a pipette was used to remove and discard the supernatant from each well.

Wash step

Samples were removed from the magnetic stand. 200µl of resuspension buffer were added to each well. Samples were mixed with a pipette and placed on a magnetic stand for 2 minutes. A pipette was used to carefully remove and discard the supernatant.

Elution step

An EE2+HP3 Elution mix was prepared and mixed – 456µl of EE2 and 24µl of EE3 were used for 16 samples. The samples were removed from the magnetic stand. 22µl of the EE2+HP3 Elution mix were added to each sample pellet. Samples were vortexed for 2 minutes, then placed on a magnetic stand for 2 minutes. 20µl of eluate from each sample tube were transferred into the corresponding well of a new plate labelled ELU2. 5µl of ET2 were added to each eluate in the ELU2 plate. The plate was vortexed for 2 minutes.

3.11.14. Amplification of enriched library

5µl of PCR Primer cocktail 3 (PPC3) were added to each well of the ELU2 plate. 20µl of EPM were added to each well. The plate was vortexed for 2 minutes. The ELU2 plate was placed on a thermocycler and samples were run on the following PCR program stored as EL-PCR (run for 1 cycle only).

Settings:
- Preheated lid at 100°C
- 98°C for 30 seconds
- 18 cycles of: 98°C for 10 seconds, 60°C for 30 seconds, 72°C for 30 seconds, 72°C for 5 minutes
- Held at 10°C on completion.

3.11.15. Clean-up of enriched library

Bind step

This step uses sample purification beads (SPB) to purify the enriched library from unwanted reaction components. A new 96 well plate was pre-labelled as BIND2. The ELU2 plate was removed from the thermocycler. 110µl of SPB were added to each well of the BIND2 plate. 50µl of each library from the ELU2 plate were transferred to the corresponding well of the BIND2 plate. The plate was vortexed for 2 minutes and incubated at room temperature for 5 minutes.

Wash step

The BIND2 plate was placed on a magnetic stand for 5 minutes. All supernatant from each well was removed and discarded. 200µl of fresh 80% (v/v) ethanol were added to each well for 30 seconds, then removed and discarded. The wash step was repeated. All residual supernatant was removed from each well.

Elution step

The BIND2 plate was removed from the magnetic stand. 32µl of resuspension buffer were added to each well. The plate was mixed and vortexed for 2 minutes. Samples were incubated at room temperature for 2 minutes, then the plate was placed on a magnetic stand for 2 minutes. 30µl of each eluate were transferred from the BIND2 plate to the corresponding well on a new plate labelled PL.

3.12. Next generation sequencing

3.12.1. Next generation sequencing preparation

Next generation sequencing preparation was performed by Raf Hussain at the Genomics Core Facility at Newcastle University.

3.12.2. Quantification of enriched library

Libraries were first reviewed using the TapeStation with HS D5000 ScreenTape and reagents as discussed in Section 3.11.3. This allowed the visualisation of fragment peaks with the samples to check that libraries appeared similar in peak distribution. Samples were also quantified using Qubit as discussed in Section 3.11.2 in duplicate prior to normalisation to ensure consistency.

3.12.3. Normalisation of library

This process ensures that the samples are uniform in quantity before libraries are pooled for next generation sequencing. The samples were diluted to match the concentration of the lowest value with PCR grade H20.

3.12.4. Next generation sequencing methods

Library pools were prepared by Raf Hussain and run on the NextSeq 500 sequencer (Illumina) using the NextSeq 500/550 High Output kit (Illumina, #20024906) as per the manufacturer's protocol. Samples were run for 75 cycles with paired end reads and dual indexing performed.

3.13. Analysis of next generation sequencing data

Dr. Iglika Ivanova from the Perkins' lab worked with Dr. Peter Leary at Newcastle University Bioinformatics Support Unit (BSU) to develop an analysis pipeline where variant calling could be made with high confidence. This was coordinated via the use of Mutect2 analysis software. This method is discussed extensively in Section 6.11.

4. Results 1: What happens to mouse models of B-cell lymphoma in response to CHK1i monotherapy?

4.1. Introduction to chapter

The Eμ-Myc mouse is a transgenic model with translocation of the oncogene *c-MYC* onto the IgH enhancer in B cells which leads to the development of aggressive B-cell lymphomas (260). This is a good mouse model to use to study the effects of CHK1 inhibition as there is oncogene-induced replication stress driven by MYC (150,390,417,418). Previous work by the Perkins' lab has demonstrated that upon tumour development, when implanted into WT mice, Eμ-Myc tumours are sensitive to a 9-day treatment course of CHK1 inhibitor (CHK1i) monotherapy. This leads to a reduction in tumour bulk compared to vehicle treated controls (147). The drug used in this study was the tool compound CCT244747 and a precursor of SRA737, the CHK1i currently in phase 1/2 clinical trial (147,150).

Additional unpublished work by the Perkins' lab has shown that when the NF-κB *c-Rel -/-* mouse and the NF-κB *RelA T505A* mutant mouse were crossed onto the Eμ-Myc model, the resulting lymphomas in these mice are resistant to CHK1 inhibition. Moreover, both the Eμ-Myc/*c-Rel -/-* and Eμ-Myc/*RelA T505A* mutant mice have been found to have low levels of Claspin mRNA and protein. This also correlated with an earlier onset of lymphoma in both the Eμ-Myc/*c-Rel -/-* and Eμ-Myc/*RelA T505A* models.

Claspin is an adaptor protein in the DDR and has an important role in the ATR/CHK1 signalling pathway (242). Claspin plays a role in the surveillance of normal replication (245) and mediates phosphorylation of CHK1 and its subsequent activation by ATR in response to DNA damage and replication stress (243). In addition, Claspin degradation is required for checkpoint recovery after cell cycle arrest (253). CHK1 can phosphorylate and stabilise Claspin to allow continued checkpoint activation, therefore CHK1 inhibition and subsequent destabilisation of Claspin could lead to enhanced replication stress and cell death (245). The mechanism behind the change of Claspin expression is currently

unclear, but it could mean that CHK1 inhibitor resistant cells also downregulate other ATR/CHK1 pathway mediators to prevent cell death.

We also do not know if the previous results seen after 9 days of CHK1 inhibitor are a true reflection of a treatment response. I will therefore also examine the acute response to CHK1 inhibition after a single dose of CHK1 inhibitor to how this will impact on the gene and protein expression of DNA damage response markers.

This chapter will further investigate changes in DNA damage response gene expression in the CHK1i sensitive Eμ-Myc mouse model. Genes with significant changes in expression and a correlation with treatment response in tissue will also be investigated in the CHK1i resistant Eμ-Myc/*c-Rel -/-* mouse model. The presence of DDR gene expression changes between the two mouse models could provide valuable information about the markers of treatment response and resistance to CHK1i. Efficacy with the clinical compound SRA737 has already been shown in the Eμ-Myc WT model (147), therefore my work in this chapter has the potential to enhance the understanding of CHK1i sensitivity.

4.2. Chapter aims and hypotheses

Research aim 1 - To analyse changes in DNA damage response pathway gene expression in sensitive and resistant transgenic models in response to CHK1i.

- Hypothesis - DNA damage response mechanisms will be upregulated in sensitive models in response to CHK1 inhibition.

- Hypothesis - There will be differences in the regulation of DNA damage response pathway gene expression between sensitive and resistant mouse models.

Research aim 2 - To analyse for acute changes in DNA damage response pathway gene expression in mouse models in response to CHK1 inhibitor treatment.

- Hypothesis - DNA damage response gene expression will be upregulated post CHK1 inhibitor treatment.

- Hypothesis - There will be differences shown in DNA damage gene expression between the 8, 24 and 48 hour time points after a single dose of CHK1 inhibitor treatment.

Research aim 3 - To investigate statistically significant genes of interest at the protein level.

- Hypothesis - Protein expression will correlate with changes in DNA damage response gene expression.

4.3. Inguinal lymph node weight decreases following 9 days of CHK1 inhibitor treatment in the Eμ-Myc mouse model

Data and subsequent inguinal lymph node tissue samples from the previously published Eμ-Myc study were obtained from Dr. J Hunter (147). The Eμ-Myc mouse model is a model of B-cell lymphoma driven by overexpression of *c-MYC*. The Eμ-Myc mouse responds to CHK1 inhibitor treatment with a reduction of tumour burden. This mouse was used in these studies as it is a good model for oncogene induced replication stress. In addition, other MYC-driven mouse models and cell models of neuroblastoma have shown efficacy with the CCT244747 CHK1 inhibitor in pre-clinical development and also the SRA737 CHK1 inhibitor treatment during early drug development (150,419).

Cells from Eμ-Myc tumours were re-implanted into multiple synergistic recipient mice. Lymphoma was allowed to develop in the WT mice before commencing treatment with 100mg/kg CCT244747 once daily orally for 9 days (Figure 4.1A). Mice were culled 24 hours after the last dose of CHK1 inhibitor treatment.

Inguinal lymph node weight decreased following CHK1i treatment in the Eμ-Myc mouse model following 9 days of CHK1 inhibitor treatment (Control 0.0029 ±0.00026; CHK1i treated 0.0013±0.00021; p=0.0002. Shown in Figure 4.1B. This shows that these mice have responded to treatment with the CCT244747 CHK1 inhibitor.

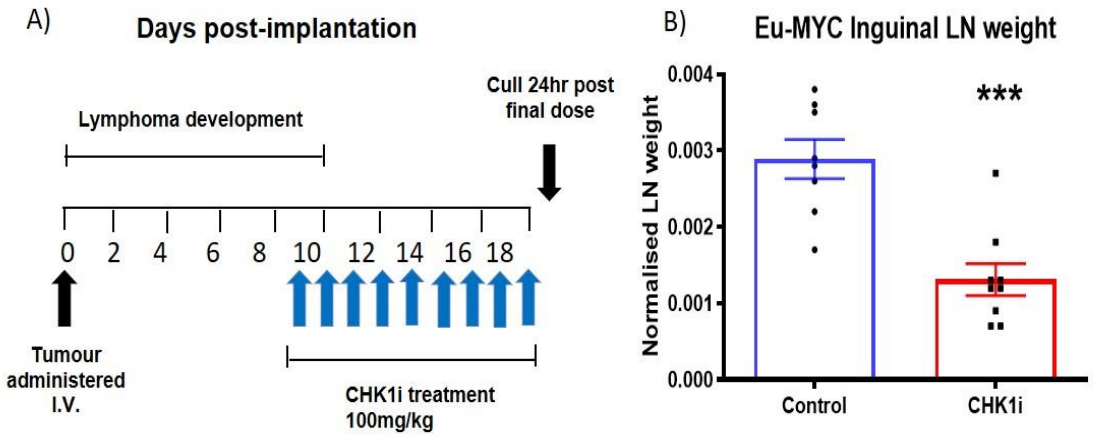

Figure 4.1. Eμ-Myc mice respond to treatment with the CCT244747 CHK1 inhibitor. Data obtained from Dr. Jill Hunter. WT mice were re-implanted with tumours from the Eμ-Myc mouse model and lymphoma allowed to develop. Mice were then treated with 100mg/kg CCT244747 once daily orally for 9 days. A) Schematic showing CHK1i treatment. B) Inguinal lymph node weight in vehicle treated mice compared to CHK1i treated mice. Graph shows mean ±SEM. An unpaired Student's t-test was performed (p=0.0002).

4.4. DNA damage response gene expression increases in inguinal lymph node of the Eμ-Myc mouse model

To investigate the DDR response in the Eμ-Myc mouse model, RNA was extracted from the inguinal lymph nodes from both CHK1i-treated and vehicle control treated mice from the previously listed study as per 3.3.2. after 9 days of CHK1 inhibitor therapy. qPCR was performed using *RPL13A* as the reference gene. Genes tested included genes from the ATR/CHK1 pathway, the ATM/CHK2 pathway and a selection of non-homologous repair and apoptotic pathways (Table 4.1). This was to assess the response of the DDR response genes in a model responsive to CHK1 inhibitor therapy. The drug used was CCT244747, the laboratory compound related to the SRA737 trial drug.

Overall, the CHK1i treated mice showed a large increase in DDR expression showing activation of DDR pathways. This was most prominently seen with genes associated with the ATR/CHK1 pathway upstream of CHK1 and the ATM/CHK2 pathways, but also with genes associated with transcription and cytoskeleton regulation. There has, however, been a general increase in gene expression in both positive and negative regulators of the cell cycle.

The greatest fold changes in gene expression were seen in *RAD50* (x5.3), *ATR* (x5.1) and *ATM* (x4.9). Statistically significant expression changes were also shown in *TOPBP1*, *RAD17, CLASPN* (gene for Claspin protein), *CHEK1* (gene for CHK1 protein) and *ATRIP* from the ATR/CHK1 pathway and *TP53* (gene for p53 protein), *NBS1, MDM2*, *CHEK2* (gene for CHK2 protein) and *MRE11* from the ATM/CHK2 pathway. This could indicate that after CHK1 inhibition, the ATR/CHK1 pathway is upregulated upstream of CHK1 to try and halt the cell cycle and allow for cell repair. The increase in *CLSPN* expression after CHK1i treatment correlates with previous evidence from the NDP lab that this is increased in the CHK1 inhibitor responsive Eμ-Myc model.

Table 4.1. Summary of DDR gene expression following CHK1i treatment. Tissue from the Eμ-Myc mouse model inguinal lymph nodes was extracted after 9 days of CCT244747 CHK1 inhibitor treatment compared to vehicle control treated mice and real time qPCR was performed on genes associated with the ATR/CHK1 and ATM/CHK2 pathways along with genes that regulate apoptosis pathways. NS = not significant.

Gene	Direction change	Fold change	p value	Gene pathway	Reference
RAD50	Increase	5.3	0.0217	ATM/CHK2	(15,49,108)
ATR	Increase	5.1	0.0065	ATR/CHK1	(6,82,420,421)
ATM	Increase	4.9	0.0071	ATM/CHK2	(82,124,179)
LIMA1	Increase	4.5	0.0092	Cytoskeleton regulation	(422,423)
RAD17	Increase	4.1	0.0045	ATR/CHK1	(82,424,425)
CDC25A	Increase	3.9	0.0031	ATR/CHK1	(123,131,426)
BACH2	Increase	3.8	0.0186	Transcription regulation	(204,427)
CLSPN	Increase	3.6	0.0186	ATR/CHK1	(179,244,428)
NBS1	Increase	3.2	0.0032	ATM/CHK2	(49,108,429)
Bcl-xL	Increase	3.1	0.0054	Anti-apoptotic, can impair p53 function	(116,430)
TOPBP1	Increase	2.7	0.0474	ATR/CHK1	(97,431)
TP53	Increase	2.6	0.0187	ATM/CHK2; master regulator gene	(82,146,151)
CYCLIN A2	Increase	2.6	0.0077	Controls G1/S and G2/M Complexes with CDK1 and CDK2	(179,432,433)
CHEK1	Increase	2.3	0.0007	ATR/CHK1	(6,9,82,87)
BID	Increase	2.1	0.0109	Pro-apoptosis	(434)
CDK2	Increase	2.1	0.0014	ATR/CHK1 – G1/S cell cycle progression	(132,179,435)
MDM2	Increase	2.1	0.0095	ATM/CHK2	(44,137,436)
ATRIP	Increase	1.9	0.0083	ATR/CHK1	(425,431,437)
MRE11	Increase	1.8	0.0107	ATM/CHK2	(49,108)
CHEK2	Increase	1.7	0.0037	ATM/CHK2	(18,131,143)
BAX	NS	1.8	0.0632	Apoptosis regulated by p53	(434,438)
CCND1	NS	1.7	0.0591	Downstream regulatory subunit of CDK4 and CDK6	(329,439)

Gene	Direction change	Fold change	p value	Gene pathway	Reference
CDKN1A	NS	1.7	0.0629	Downstream regulator CDKs – CDK2	(46,440)
CDK4	Increase	1.6	0.0023	G1/S cell cycle progression	(204)
LIG4	NS	1.6	0.3669	DNA repair through NHEJ	(74,432)
CDKN2A	NS	1.5	0.0858	Can cause cell cycle arrest; Downstream regulator CDKs – CDK4 &CDK6	(46,276,397)
CCNE1	NS	1.4	0.065	Downstream regulator of CDK2	(179,436,441)
CDK1	NS	1.1	0.179	ATM/CHK2 – G2/M cell cycle progression	(132,432,442)

The upregulation of the ATM/CHK2 pathway is interesting as this indicates that cells are attempting to repair damage using other mechanisms. This could also indicate that the drug is working leading to enhanced DNA damage and an increase in double stranded DNA breaks leading to activation of ATM and CHK2.

Downstream of CHK1, there is also an increase demonstrated in *CYCLIN A2*, *CDK2* and *CDC25A* expression. This could be secondary to the inhibition of CHK1 leading to a failure to halt cell cycle regulation (426,435,443). This would be more indicative of a drug response leading to further DNA damage by keeping these genes upregulated in response to treatment. This could also represent a cell survival mechanism as the cells could be evading cellular repair and apoptosis.

LIMA1 is associated with the regulation of the cytoskeleton (422,423) and this was also markedly elevated in CHK1i treated mice compared to vehicle controls (X 4.5-fold change). This could mean that structural changes have occurred in the responsive cells indicating enhanced DNA damage. Conversely, this could indicate that surviving cells have adapted structurally in order to survive drug treatment. *BACH2* is a regulator of transcription (427) and was increased x 3.8-fold. This could again indicate that gene expression changes after 9 days have been established and again that the cells have adapted to the CHK1 inhibitor treatment to allow survival.

A mixed picture was demonstrated by markers of apoptosis. The pro-apoptotic gene BID was raised which could indicate an increase in cell death secondary to treatment. This is however contrasted by a high expression of the anti-apoptotic gene *BCL-XL* which indicates that after 9 days, some of the cells may have adapted to survive drug challenge.

Figure 4.2 shows results for genes with the largest change shown for *ATR*, *ATM*, *RAD17* and *RAD50*. As discussed, after 9 days of CHK1i therapy it is difficult to establish if the change seen is an ongoing response to the CHK1i, or a surviving population of cells that do not respond to therapy. The increase of both anti- and pro-apoptotic genes could indicate a mixed population of responsive and resistant tumour cells. This could also be reflective of normal cellular behaviour as the gene expression changes between responsive vs non-responsive cell behaviour had not been determined in this population.

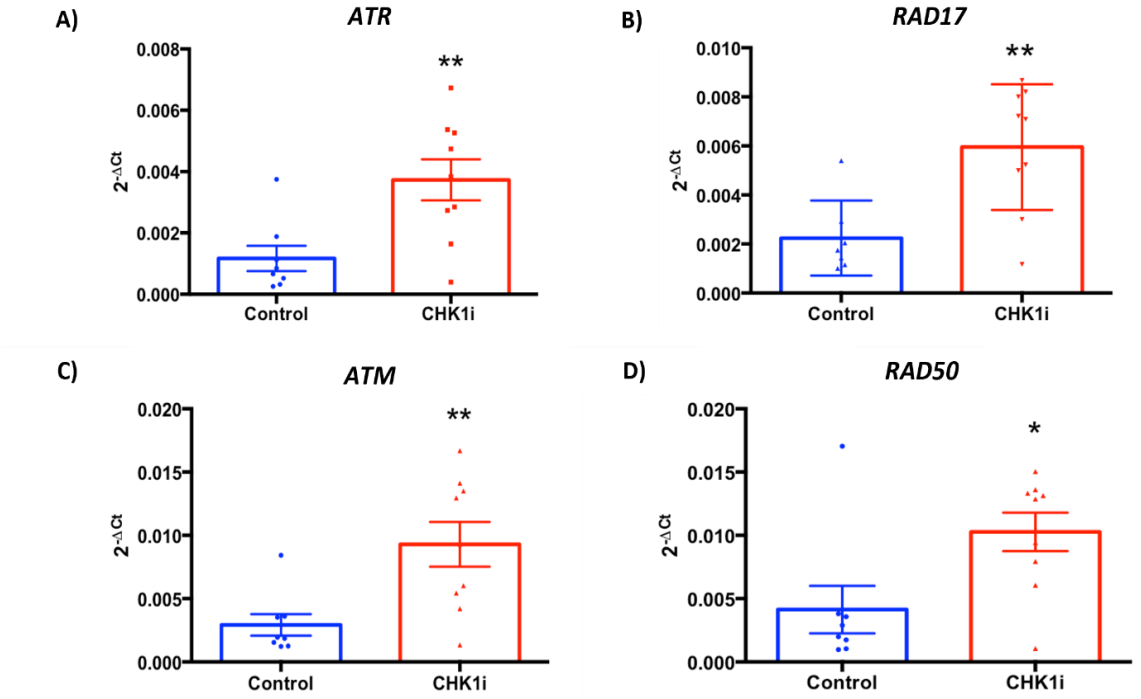

Figure 4.2. DDR genes upregulated in inguinal LN in Eμ-Myc mice following CHK1 inhibitor treatment. N=1. Genes with the greatest fold change response post 9 days treatment with CHK1 inhibitor. Data were normalised using the 2-ΔCT method (R = 2–[ΔCP sample – ΔCP control]) using the gene *RPL13A* as reference. Graphs show mean ± SEM. A) *ATR* (x5.1), B) *RAD17* (x4.1), C) *ATM* (x4.9) and D) *RAD50* (x 5.3). Statistical difference calculated using Student's t-test. ** = $p<0.01$; * = $p<0.05$.

Although the overall trend in treated mice showed an increase in DDR expression, not all genes tested showed a significant response. The *RPL13A* ribosomal protein selected as the reference gene did not change with CHK1 inhibitor treatment (data not shown), therefore this indicated that this was a good reference gene selection (444).

In addition, there was no significant change in the genes *CCND1, CCNE1, CDKN1A, CDKN2A, BAX* and *LIG4*. *CCND1, CCNE1 CDKN1A* and *CDKN2A* regulate CDKs leading to cell cycle arrest (46,393,440,441). If there is no upregulation of these genes in response to DNA damage caused by CHK1 inhibition, this could lead to a failure to halt the cell cycle. This could again be indicative of a response pattern to the CHK1 inhibitor. *BAX* is associated with p53-regulated apoptosis (434). It could indicate that the cells are undergoing apoptosis via a different pathway, but this could also mean that this is not increased to allow cell survival. *LIG4* is associated with DNA repair by non-homologous end joining (70,74). This could indicate that the cellular repair is driven predominantly by homologous repair and this would fit with the increase in expression with genes associated with the ATR/CHK1 and ATM/CHK2 pathways.

Identifying genes that do not change in the Eμ-Myc mice after 9 days of CHK1i treatment demonstrated that changes seen are likely to be a true effect on the pathways rather than a non-specific effect on gene expression. Figure 4.3 shows some examples of genes that did not change with CHK1 inhibitor treatment. Gene expression may not be fully reflective of protein expression, however, and that is why protein expression in these mice was also investigated.

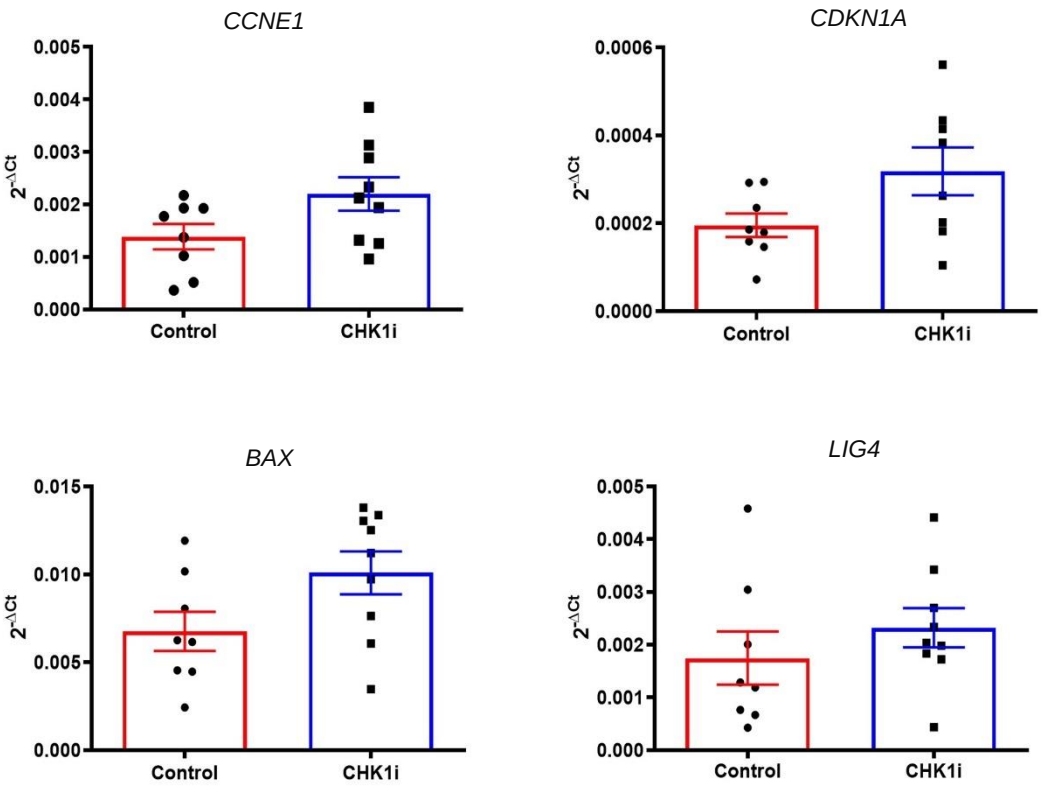

Figure 4.3. An increase in gene expression is not universally demonstrated in the Eμ-Myc model mouse. N=1. Data were normalised using the 2-ΔCT method (R = 2–[ΔCP sample – ΔCP control]) using the gene *RPL13A* as reference. Trends still show a general increase in gene expression; however, no statistically significant fold change was demonstrated in these genes. Graphs show mean ± SEM. A) *CCNE1* (x1.4), B) *CDKN1A* (x1.7), C) *BAX* (x1.8) and D) *LIG4* (x 1.6). Statistical difference calculated using Student's t-test. ** = p<0.01; * = p<0.05.

4.5. DDR gene expression correlates with LN weight in sensitive mice after 9 days CHK1i treatment

To further investigate whether the gene expression changes seen were a consequence of the effectiveness of CHK1 inhibitor treatment on lymphoma growth, I performed a more in depth statistical analysis. The aim of this was to determine whether there was an association between CHK1i treated Eμ-Myc mice and their corresponding inguinal lymph node weights after treatment, the latter being a marker for the effectiveness of the drug treatment. Spearman's r correlation was calculated for each of the genes that I had performed qPCR on using the 2-ΔCT values (as discussed in Section 3.3.7) alongside normalised inguinal lymph node weights. Correlation was performed on vehicle treated control treated and CHK1i treated mice separately. 8 vehicle treated control mice and 9 CHK1 inhibitor treated Eμ-Myc mice were analysed.

Genes were grouped into four main groups based on correlation pattern, and this is shown in Table 4.2. The first group highlighted in orange, shows a significant negative correlation with both the control treated and CHK1i treated mice. The second group highlighted in green shows a significant negative correlation with CHK1i treatment only. The group highlighted in blue shows significant correlation with the control group only. The final highlighted group in purple shows no statistically significant correlation pattern.

A negative correlation between gene expression and inguinal lymph node weight in treated mice was shown for *ATR, NBS1, CDKN1A, TOPBP1, TP53, ATM, CHEK1, BACH2, CDKN2A* and *Bcl-xL*. *ATR*, *TOPBP1*, *CHEK1* and *CDKN2A* are all associated with the ATR/CHK1 pathway and *NBS1*, *TP53* and *ATM* are part of the ATM/CHK2 pathway. *BACH2* is involved in the transcriptional regulation of B cells.

Table 4.2. Spearman's r correlation of DDR genes with LN weight. Genes are grouped by correlation results. Yellow = significant correlation with control and CHK1. Green = Significant correlation with CHK1i only indicating that as LN weights decreased, gene expression increased. Blue = significant correlation with control only. Purple = no correlation seen. NS= not significant. (p value <0.05 taken as statistically significant).

Gene	CHK1 i			
	-		+	
	r	p value	r	p value
ATR	-0.7857	0.0279	-0.7005	0.0418
NBS1	-0.8095	0.0218	-0.7591	0.0337
CDKN2A	-0.7381	0.0458	-0.8271	0.0086
CHEK1	-0.8095	0.0218	-0.6992	0.0408
ATM	-0.7143	NS	-0.8946	0.0022
TOPBP1	-0.6667	NS	-0.8018	0.0128
TP53	-0.6071	NS	-0.9429	0.0167
Bcl-xL	-0.5714	NS	-0.8608	0.0047
BACH2	-0.5238	NS	-0.7849	0.0162
CHEK2	-0.9286	0.0067	-0.6583	NS
RAD50	-0.7619	0.0368	-0.4811	NS
MDM2	-0.8333	0.0154	-0.5908	NS
MRE11	-0.7381	0.0458	-0.5940	NS
RAD17	-0.7857	0.048	-0.6330	NS
BID	-0.8982	0.005	-0.4338	NS
CYCLINA2	-0.7857	0.0279	-0.6060	NS
CLSPN	-0.7857	0.0279	-0.5739	NS
CDK4	-0.4286	NS	0.0337	NS
CDK2	-0.6905	NS	-0.1857	NS
CDK1	-0.6905	NS	-0.4217	NS
CCNE1	-0.5714	NS	-0.1857	NS
ATRIP	0	NS	-0.5127	NS
CCND1	-0.6667	NS	-0.3207	NS
BAX	-0.4762	NS	-0.6414	NS
CDC25A	-0.6190	NS	-0.6498	NS
LIG4	-0.6667	NS	-0.3545	NS
LIMA1	-0.6905	NS	-0.6667	NS
CDKN1A	-0.2162	NS	-0.3758	NS

The group highlighted in green in Table 4.2 shows that for *ATM*, *TOPBP1*, *TP53*, *Bcl-xl* and *BACH2*, there is no correlation pre-treatment and a negative correlation after CHK1i treatment. This indicates that as tumour weight decreased, the expression of these genes was demonstrated to increase. This could indicate that the loss of CHK1 pathway activity may have led cells to induce gene transcription of other genes, such as *ATM* and *TP53* to induce compensatory signalling pathways.

In contrast, *CHEK2, RAD50, MDM2, MRE11, RAD17, BID, CDK1, CYCLINA2* and *CLSPN* negatively correlate with lymph node weight pre-treatment but are not correlated after CHK1i treatment (Table 4.2). There appears to be a change of these genes following CHK1i treatment; as the genes that are negatively correlated in the untreated mice are no longer significantly correlated in CHK1i treated mice. This may reflect a dysregulation of these genes after treatment with CHK1i.

MRE11 and RAD50 are involved in the recruitment of ATM along with NBS1 as part of the MRN complex (124,127). In contrast to *MRE11* and *RAD50*, there has been a negative correlation demonstrated in both control and CHK1i mice for *NBS1*. *CHEK2* has also shown a loss of correlation after CHK1i treatment. Activated CHK2 phosphorylates CDC25A leading to degradation and lack of CDK1/cyclin B activation (55,131). CHK2 also causes cell cycle arrest by phosphorylating the tumour suppressor p53 on Ser15 and Ser20 (132,133). Loss of cell cyclin and p53 regulation could potentially lead to increased cell damage with CHK1i exposure.

ATR and TOPBP1 are upstream of CHK1 in the ATR/CHK1 pathway and have been shown to be upregulated in response to CHK1 inhibition (Table 4.1). *ATR* and *CHEK1* are negatively correlated with both untreated and CHK1i treated mice, indicating that gene expression levels increase with a decrease in inguinal lymph node weight. This could be indicative of the importance of their role in cell cycle control. CHK1 inhibition is known to increase DNA damage and lead to an increase in ATR recruitment to sites of damage (90). *RAD17* and *CLSPN* are genes also involved in ATR/CHK1 pathway activation pathway

(18,90,91), however the same correlation pattern is not seen in these genes after the CHK1i treatment.

BACH2 is also negatively correlated in CHK1i treated mice. BACH2 is a lymphoid-specific transcription factor with a role in B-cell development (427). Given that gene expression levels of *BACH2* increase with CHK1i treatment, this could be indicating an attempt to increase B-cell regulation when there is drug enhanced B-cell stress.

TOPBP1 is negatively correlated with CHK1i treated mice only (Table 4.2). TOPBP1 is required for effective ATR activation (52), therefore an increase of *TOPBP1* expression with CHK1i treatment is likely due to an attempt by the cells to cope with CHK1 inhibition and the associated increase in ATR I have observed. The increased gene expression of *ATM* and *TP53* (Table 4.1) are likely to be due to enhanced genomic instability and an increase in double strand DNA breaks due to CHK1 inhibition and an inability to repair single stranded DNA breaks (90).

CDKN2A is capable of inducing cell cycle arrest in G1 and S phases and interacts with p53 (417,445). The protein can also act as a downstream inhibitor of cyclin dependent kinases (CDKs) including CDK4 and CDK6 (44,417). The negative correlation of increased gene expression with reduced lymph node weight (Table 4.2) might suggest that the CHK1i treated cells are undergoing cell cycle arrest as a means to attempt to repair the DNA damage caused by CHK1 inhibition, or for the cell to ultimately decide it cannot cope with anymore genomic instability, and it will die. It would now be useful to further investigate the downstream gene expression of CDKs and see if changes in expression also correlate with a reduction in inguinal LN weight or whether levels of expression are reduced due to CHK1 blockade.

The proteins Bcl-xL and p53 are both involved in the regulation of apoptosis (210). A negative correlation of these genes with inguinal lymph node weight in responsive tissue (Table 4.2) could be indicating different patterns within cells. The change in *TP53* could imply that apoptosis is occurring in the CHK1i tumour cells. This demonstrates that the

CHK1i is causing some degree of tumour death in the Eμ-Myc model and this response correlates with a reduction in tumour bulk. Bcl-xL however is anti-apoptotic; therefore, cells may be adapting in order to survive and escape. This could be a consequence of a mixed population of cells both sensitive and resistant to CHK1i treatment. *BAX* and *LIG4* also showed no significant change in gene expression (Table 4.1). *BAX* is also a pro-apoptotic gene (434), but it may be that this gene is not associated with DNA damage repair upon CHK1 inhibition.

ATRIP shows no correlation between untreated or CHK1 inhibited lymph node samples (Table 4.2). ATRIP is upstream of CHK1, it could be that as a co-factor of ATR (87,160) the downstream impact on tissue change is not regulated by this gene. CDK2 and CDK4 are downstream from CHK1 and have low gene expression levels in the tissue as determined by qPCR as well has showing no correlation with inguinal lymph node weight (there is no demonstrated association with gene expression and the inguinal lymph node weight). Therefore, these genes may not be activated in these CHK1i treated mice.

CDC25A and *CDK1* are genes involved in the regulation of the downstream cell cycle kinases of CHK1 (93,94,446) and do not show any correlation with LN weight. There is also a lack of correlation with the downstream effectors of CHK2, including the genes *cyclin A2* and *CDK2*. Dysregulation of these downstream regulators could be due to an effective CHK1 block by the CHK1i. Changes in CDK and cell cyclin regulation could lead to increased genomic instability and cell damage. It could be simply also that expression of these genes is not altered with CHK1i treatment.

Examples of correlation patterns between inguinal lymph node weight and gene expression are shown in Figure 4.4. This displays linear regressions and Spearman's correlations for *ATR*, *ATM*, *RAD50* and *RAD17*. These genes were selected as they had the highest initial fold change in gene expression. *ATR*, *ATM, RAD17* and *RAD50* subsequently have been shown to have a negative correlation, but the findings were not statistically significant for *RAD50* and *RAD17*.

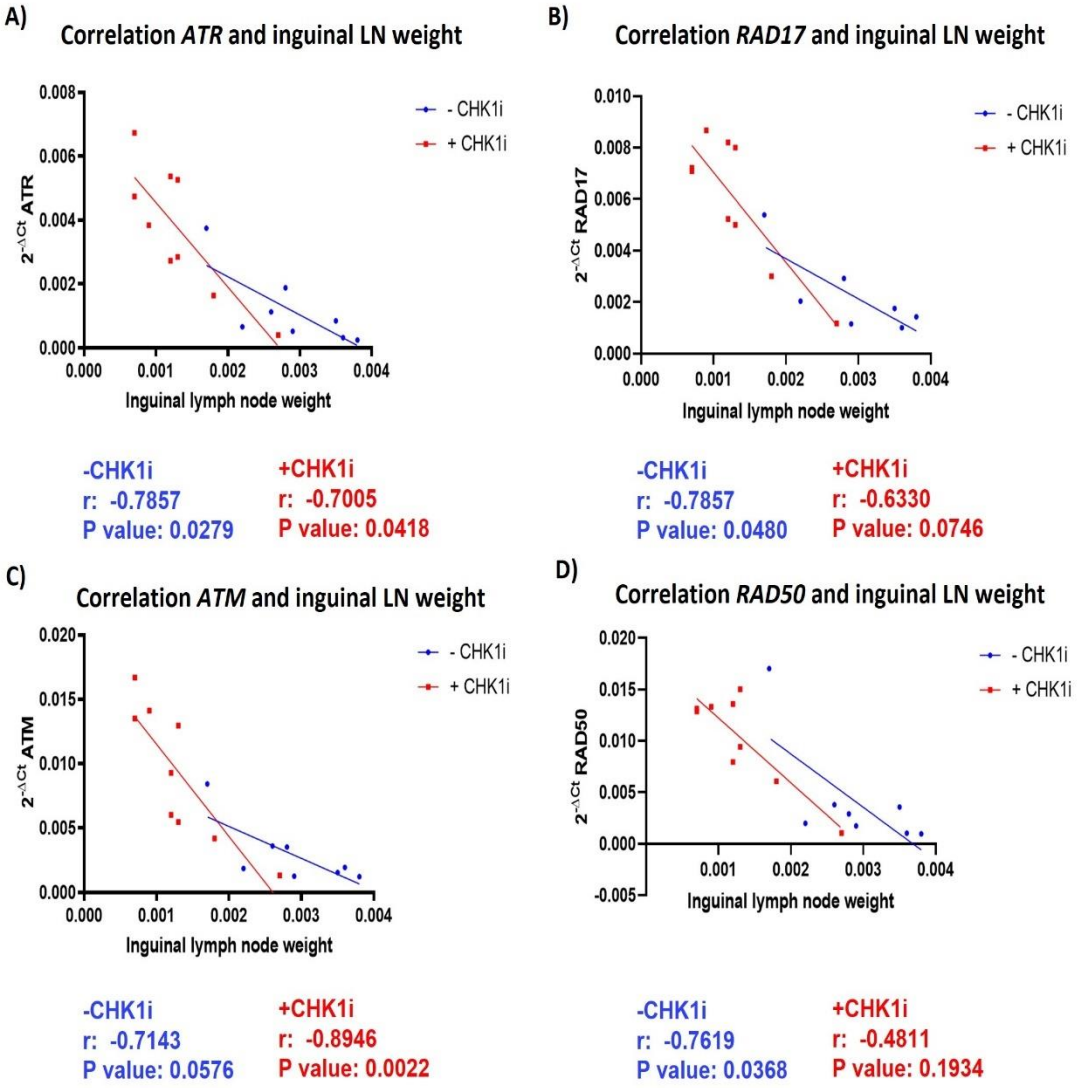

Figure 4.4. DDR gene expression is not universally positively correlated with a decrease in inguinal lymph node weight in the Eμ-Myc mouse model. Graphs show linear regression and Spearman's r correlation for A) *ATR*, B) *RAD17*, C) *ATM* and D) *RAD50*. *ATR* and *ATM* subsequently have been shown to increase with a reduction in inguinal lymph node weight. A similar pattern is shown for *RAD17* and *RAD50* but the correlation is not statistically significant in the context of CHK1 treatment. (p value <0.05 taken as statistically significant).

4.6. Inguinal lymph node DDR gene expression does not increase in Eμ-Myc/*c-Rel -/-* mice in comparison to the Eμ-Myc model

Given the DDR gene expression changes in WT Eμ-Myc mice, I wanted to determine whether similar changes were occurring in the resistant Eμ-Myc/*c-Rel -/-* mice. Therefore, qPCR was performed on inguinal lymph nodes using the same primers as used in the Eμ-Myc model. Table 4.3 lists the genes tested in the Eμ-Myc/*c-Rel -/-* mice. These mice were also treated with 9 days of the CCT244747 CHK1i as shown in Figure 4.5. These mice had previously been demonstrated to show low Claspin levels (Dr. J Hunter, pre-published), therefore I wanted to see if related DDR genes were also lower in the resistant model.

In striking contrast to the Eμ-Myc CHK1i responsive model, no statistically different change was seen in gene expression between the vehicle control treated and CHK1i treated Eμ-Myc/*c-Rel -/-* mice. Table 4.3 and Figure 4.6 show that in genes that showed a significant change in gene expression in the sensitive Eμ-Myc mice, such as *ATM*, *ATR*, *CLSPN* and *CHEK1*, there is no significant change. This is the same for both the control and CHK1i treated Eμ-Myc/*c-Rel -/-* mice. This could be that the homologous repair pathways of ATR/CHK1 and ATM/CHK2 are not activated in these mouse groups in response to CHK1i treatment. It could also be that these genes are suppressed in these mice and therefore little change is seen between groups – this could also explain the previously demonstrated low levels of *CLSPN* in the Eμ-Myc/*c-Rel -/-* model.

Genes that did not show a significant change in expression or fold change in the Eμ-Myc mice, such as *CDK2*, *CCND1*, *CYCLIN A2* and CDK4 were also assessed in the Eμ-Myc/*c-Rel -/-* mice. This was to see if, conversely, these genes had increased expression after treatment compared to the Eμ-Myc model. Again, no difference was demonstrated.

Table 4.3. Summary of DDR gene expression in the Eμ-Myc/*c-Rel -/-* mouse model following CHK1i treatment. Tissue from the Eμ-Myc/*c-Rel -/-* mouse model inguinal lymph nodes was extracted after 9 days of CCT244747 CHK1 inhibitor treatment compared to vehicle control treated mice. Real time qPCR was performed on genes associated with the ATR/CHK1 and ATM/CHK2 pathways along with genes that regulate apoptosis pathways. In contrast to the CHK1i responsive Eμ-Myc mice, there are no significant fold changes seen (p value <0.05 taken as statistically significant).

Gene	Direction change	Fold change	p value	Gene pathway	Reference
ATM	Decrease	0.8	0.793	ATM/CHK2	(82,124,179)
ATR	No change	1.1	0.2218	ATR/CHK1	(6,82,420,421)
CCND1	Decrease	0.6	0.9586	Downstream regulatory subunit of CDK4 and CDK6	(329,439)
CCNE1	Decrease	0.9	0.6139	Downstream regulator of CDK2	(179,436,441)
CDK2	No change	1.0	0.7853	ATR/CHK1 – G1/S cell cycle progression	(132,179,435)
CDK4	No change	1.5	0.4268	G1/S cell cycle progression	(204)
CHEK1	No change	1.0	0.6697	ATR/CHK1	(6,9,82,87)
CLSPN	Decrease	0.4	0.4269	ATR/CHK1	(179,244,428)
CYCLINA2	Decrease	0.9	0.6328	Controls G1/S and G2/M Complexes with CDK1 and CDK2	(179,432,433)

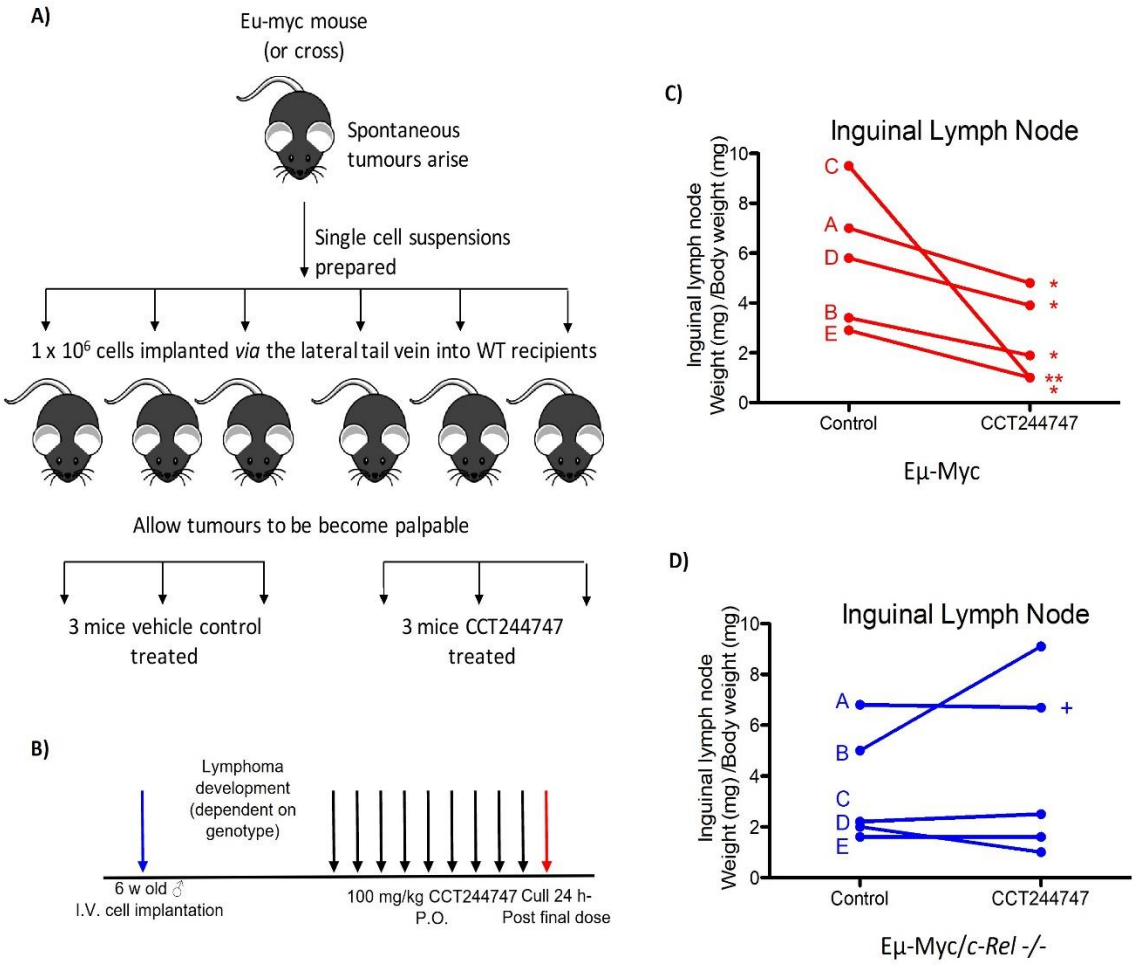

Figure 4.5. Schematic showing CHK1i treatment with the CCT244747 CHK1 inhibitor in the Eμ-Myc/*c-Rel -/-* model 9 day study. A) WT mice were re-implanted with tumours from the Eμ-Myc/*c-Rel -/-* mouse model and lymphoma allowed to develop. B) Mice were then treated with 100mg/kg CCT244747 or vehicle control once daily orally for 9 days. A, B C, D and E in the graphs shown in C) and D) indicate two matched mice implanted with the same tumours, one treated with vehicle control and one with CCT244747. C) Data indicating clinical response in inguinal lymph nodes of Eμ-Myc mice after 9 days of CHK1i treatment as already discussed, with a reduction in lymph node weight with CHK1i treatment. D) Data for the Eμ-Myc/*c-Rel -/-* mouse model showing no reduction of inguinal lymph node weight after 9 days of CHK1i treatment. This indicates resistance to the CHK1i CCT244747.

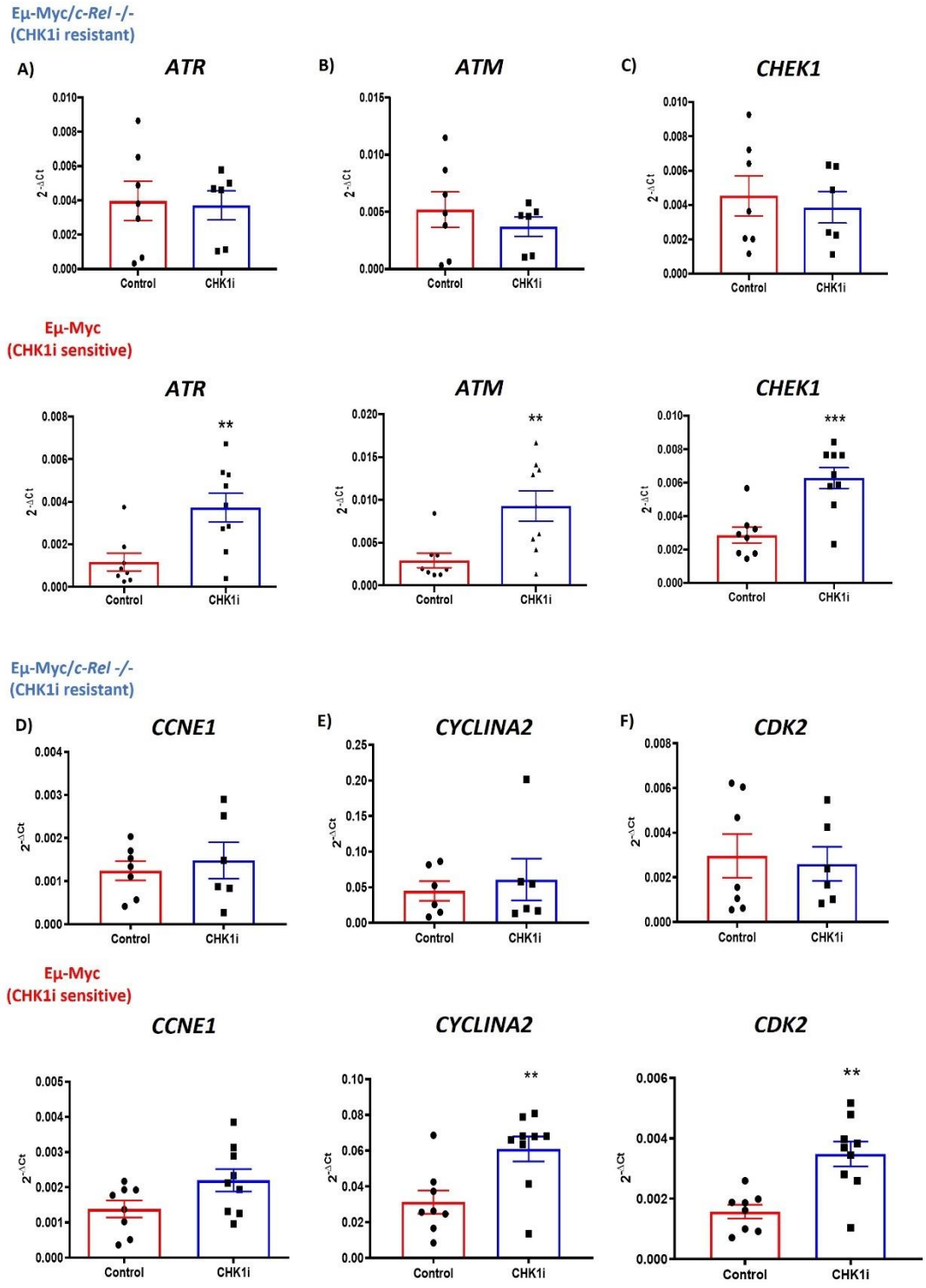

Figure 4.6. DDR expression does not increase in the Eμ-Myc/*c-Rel -/-* model following 9 days of CCT244747 CHK1 inhibitor treatment in contrast to gene expression changes shown in the Eμ-Myc model. N=1**.** Data were normalised using the 2-ΔCT method (R = 2–[ΔCP sample – ΔCP control]) using the gene *RPL13A* as reference. A) *ATR*; B) *ATM* and C) *CHEK1* shows a significant increase in gene expression post CHK1i treatment in the Eμ-Myc mice but not the Eμ-Myc/*c-Rel -/-* mice. D) *CCNE1*; E) *CYCLIN A2* and F) *CDK2* also do not show a significant increase in gene expression post CHK1i treatment for the Eμ-Myc/*c-Rel -/-* mouse model (note - CCNE1 not statistically significant for both Eμ-Myc and Eμ-Myc/*c-Rel -/-* mouse models). Statistical difference calculated using Student's t-test. ** = $p<0.01$; * = $p<0.05$.

4.7. No differences were demonstrated in DDR protein expression between the Eμ-Myc mouse model and Eμ-Myc/*c-Rel -/-* mouse model post 9 days of CHK1 inhibitor treatment

Given that changes in gene expression are not always reflective of changes shown at the protein level, we wanted to further examine what happens to protein expression in both the Eμ-Myc and Eμ-Myc/*c-Rel -/-* mice after 9 days of CHK1 inhibitor treatment. Therefore, western blot analysis was performed to check protein levels of key DDR genes in the same Eμ-Myc and Eμ-Myc/*c-Rel -/-* mice used for qPCR. Protein samples were obtained from lymph node tumours as were the samples for RNA analysis.

The protein targets selected were genes that showed a statistically significant change in gene expression after 9 days of CHK1 inhibitor therapy earlier in WT Eμ-Myc mice. Results are shown in Figure 4.7. Western blot data shows no clear differences in protein expression between the Eμ-Myc and the Eμ-Myc/*c-Rel -/-* mice. There are also no clear differences between the CHK1i and vehicle control treated mice.

There is some variation seen between mice even within the same groups, this could be due to natural background variation in response to the drug treatment, but also there could be differences in drug response in different mice. This could indicate that the changes in gene expression in the Eμ-Myc mice after 9 days of CHK1i treatment could be more reflective of a resistant cell population after treatment. Variation between mice could be an indication of tumour heterogeneity and an indication of tumours developing differently within individual mice as well. Therefore 9 days may be too long to capture the acute response to CHK1i treatment in both the CHK1i sensitive Eμ-Myc mouse and the CHK1i resistant Eμ-Myc/*c-Rel -/-* mouse.

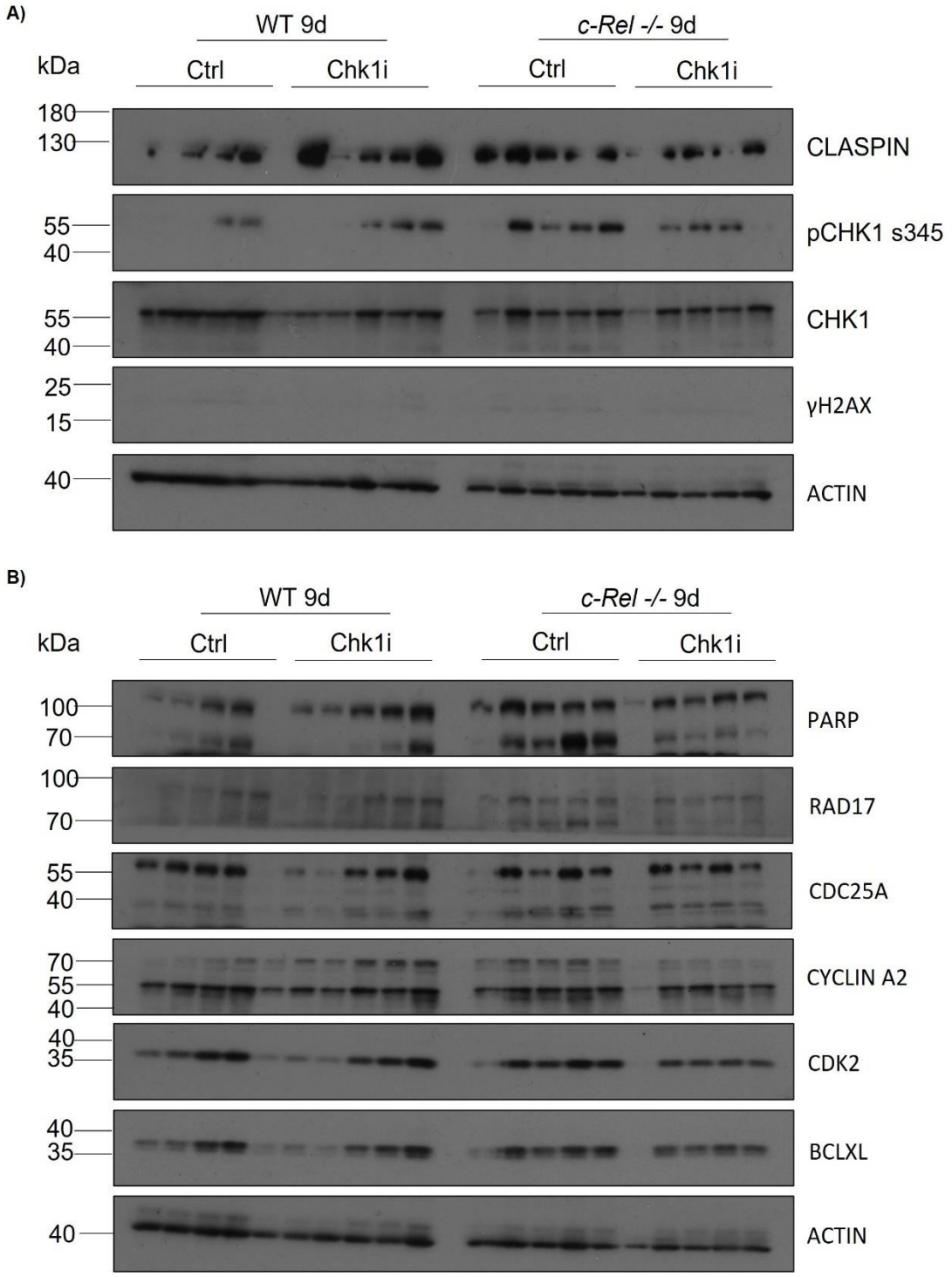

Figure 4.7. No differences are seen in DDR protein expression between the Eμ-Myc and Eμ-Myc/*c-Rel -/-* mouse models after 9 days of CHK1i treatment. N=1. Eμ-Myc mice labelled as WT. 5 Eμ-Myc mice and 5 Eμ-Myc/*c-Rel -/-* mice were treated with CCT244747 (100 mg/kg orally) daily for 9 days before harvest and 5 of each with vehicle control. A) Western blot data shows no clear differences in protein expression between the Eμ-Myc and the Eμ-Myc/*c-Rel -/-* mouse and for Claspin, phosphorylated and total CHK1 and γH2AX. B) Western blot data in the same grouped mice for PARP, RAD17, CDC25A, CYCLIN A2, CDK2 and BcL-xL, again showing no clear differences. There are also no clear differences between CHK1i and vehicle control treated mice.

4.8. Inguinal lymph node DDR expression in the CHK1i sensitive Eμ-Myc mouse model does not differ at 8 hours, 24 hours and 48 hours after single treatment of CHK1 inhibitor

9 days of CHK1i treatment has shown marked changes in DDR gene expression in the CHK1i sensitive Eμ-Myc mouse but no significant difference in the CHK1i resistant Eμ-Myc/*c-Rel -/-* mouse. No changes however are shown in protein expression. This could be that 9 days of treatment is too long to assess drug response and may be more a reflection of surviving resistant cells.

Taking this into account, we wanted to assess what would happen in an acute model and whether both gene expression changes and protein expression changes would be shown. Therefore, a preliminary study with the CHK1i sensitive Eμ-Myc mice was set up. 9 mice were treated with a single dose of the of CCT244747 CHK1 inhibitor (100mg/kg orally) and 9 treated with vehicle control and culled at 8, 24 or 48 hours post treatment. The 3 time points were selected in order to compare and select the optimal time point for looking at the acute CHK1 inhibitor response after a single dose of CHK1i treatment. A schematic of the acute mouse model preliminary study is shown in Figure 4.8.

qPCR was performed on DDR genes as previously performed in Section 4.6. No changes were seen in the DDR response between the 3 time points. Results between the 3 time points are demonstrated in Figure 4.9 for ATM and ATR, 2 of the genes with the biggest change in gene expression in the Eμ-Myc mouse after 9 days of CHK1i treatment. This could be because the time points are too early to cause a change in transcriptional response. This could also be that a single dose of CHK1i treatment does not cause a sustained change in gene expression and that prolonged exposure to the drug is required for this to occur.

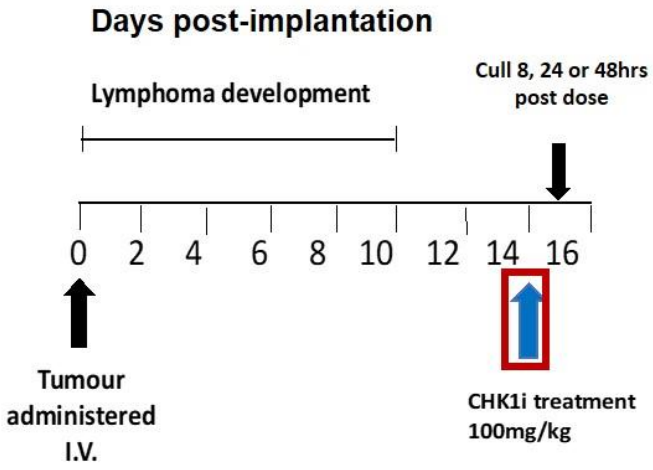

Figure 4.8. Schematic showing CHK1i treatment with the CCT244747 CHK1 inhibitor in the preliminary acute Eμ-Myc model study. WT mice were re-implanted with tumours from the Eμ-Myc mouse model and lymphoma allowed to develop. Mice were then treated with a single dose of 100mg/kg oral CCT244747 or vehicle control. Mice were then culled at either 8, 24 or 48 hours post CHK1i treatment.

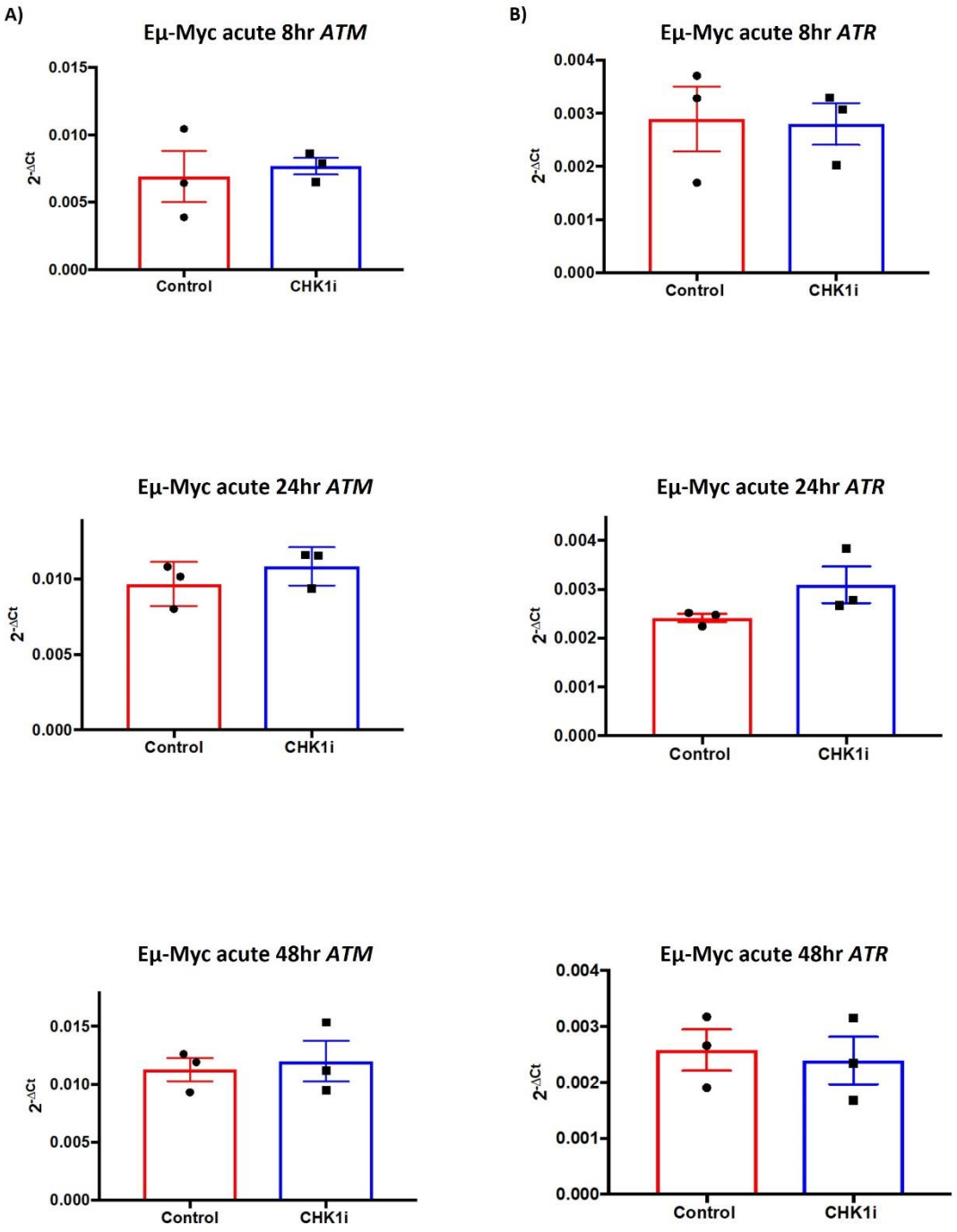

Figure 4.9. There is no change in DDR gene expression after single dose CCT244747 CHK1 inhibitor treatment at 8, 24 and 48 hours in the acute Eμ-Myc mouse model. N=1. Data were normalised using the 2-ΔCT method (R = 2–[ΔCP sample – ΔCP control]) using the gene *RPL13A* as reference. 9 Eμ-Myc mice were treated with CCT244747 (100 mg/kg orally), and 9 with vehicle control, for a single dose. Mice were harvested at either 8, 24 or 48 hours post treatment. Representative trends in A) ATM and B) ATR shown these genes have shown increased expression in the 9 day CHK1i treated Eμ-Myc mice. No differences were seen in the selective gene expression between control and CHK1i treated mice in all 3 time groups. Statistical difference calculated using Student's t-test. ** = $p<0.01$; * = $p<0.05$.

4.9. An increase in phosphorylation signalling demonstrating an increase in ATR activity and DNA damage in response to a single dose of CHK1 inhibitor is present in the CHK1i sensitive Eμ-Myc mouse model 8 hours post treatment, but not sustained at 24 and 48 hours post treatment

No increase in gene expression was demonstrated in selected DDR genes by qPCR at 8 hours, 24 hours or 48 hours post single dose of CHK1i treatment in the acute Eμ-Myc study. It was possible that this was too early for a signalling response change. We wanted to additionally assess if there was a change in protein expression at these time points after a single drug treatment, therefore this was assessed by western blot for the same mice. Protein samples were extracted from lymph nodes from mice in the study.

A striking increase in CHK1 phosphorylation was demonstrated at 8 hours after CHK1 inhibition, with an accompanying increase in γH2AX. This is shown in Figure 4.10. This could be because initially ATR is trying to force the upregulation of CHK1 activity due to an increase in genomic instability and DNA damage. This has been seen in other studies in other animal models after the CCT244747 CHK1 inhibitor treatment (150).

PARP cleavage also appears to be increased 8 hours after treatment. This may also be a consequence of cells attempting to maintain genomic stability after DNA damage. These increases in phosphorylation and DDR activation were not sustained at 24 and 48 hours. This could be that the single dose is not enough to sustain a longer-term DDR upregulation. Figure 4.10 shows the results for the 3 time points and the predominant changes 8 hours after single dose CHK1i treatment.

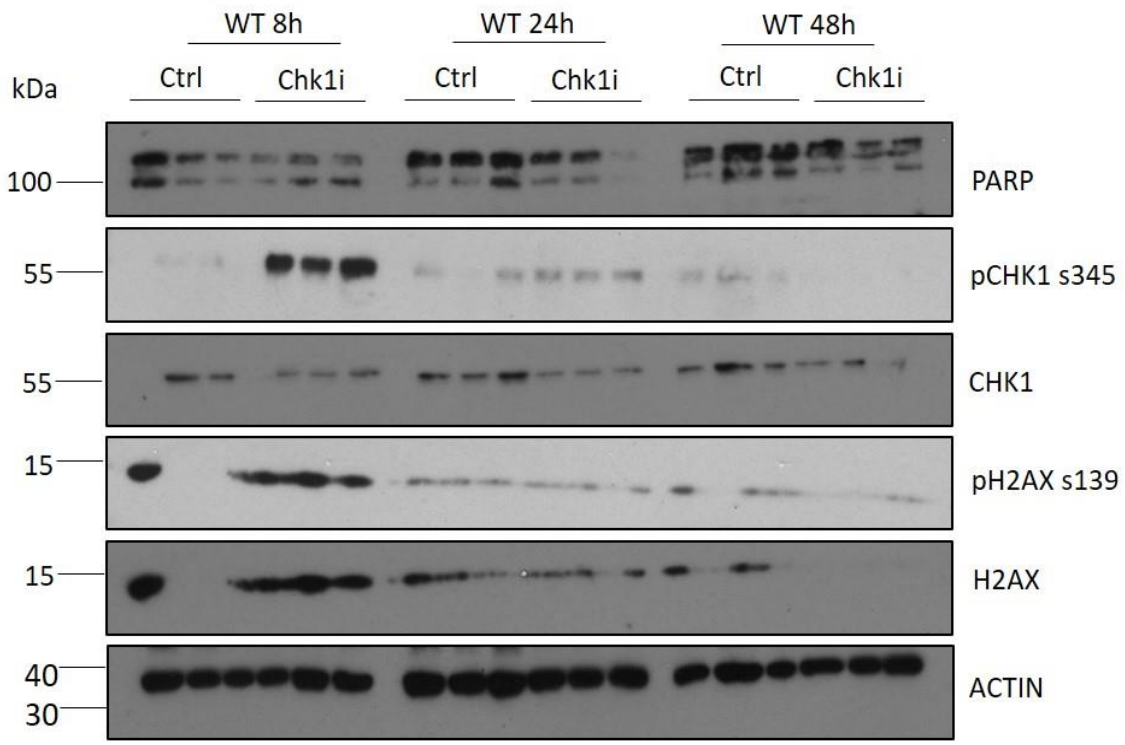

Figure 4.10. Protein expression changes after single dose CCT244747 CHK1 inhibitor treatment are demonstrated in the Eμ-Myc mice after 8 hours, but not sustained at 24 and 48 hours. N=1. 3 Eμ-Myc mice in each group were treated with CCT244747 (100 mg/kg orally), and 3 with vehicle control, for a single dose and harvested at either 8, 24 or 48 hours post treatment. Western blot data shows an increase in pCHK1 (Ser345) and an increase in γH2AX (Ser139) and H2AX expression 8 hours after single dose CHK1i treatment. Total CHK1 levels have decreased in the CHK1i treated mice, indicating altered target stability. PARP cleavage is increased at 8 hours in comparison to the other time points.

4.10. Eμ-Myc/*c-Rel -/-* mice downregulate expression of DDR genes in response to CHK1i treatment

Due to the large response at 8 hours post single dose CCT244747, further experiments were performed with single dose CHK1i treatment in Eμ-Myc, Eμ-Myc/*c-Rel -/-* and Eμ-Myc/*RelA T505A* mouse models at the 8 hour time point. Western blot analysis was performed to further examine the acute differences in DDR gene and protein expression between the CHK1i responsive Eμ-Myc mice and the CHK1i resistant Eμ-Myc/*c-Rel -/-* and Eμ-Myc/*RelA T505A* models.

A schematic of experimental set up for the acute CHK1i study is shown in Figure 4.11. Mice were grouped based on initial genotype and tumour re-implantation, with 3 vehicle control treated and 3 CHK1i in each group (total of 6 vehicle control and 6 CHK1i in each category).

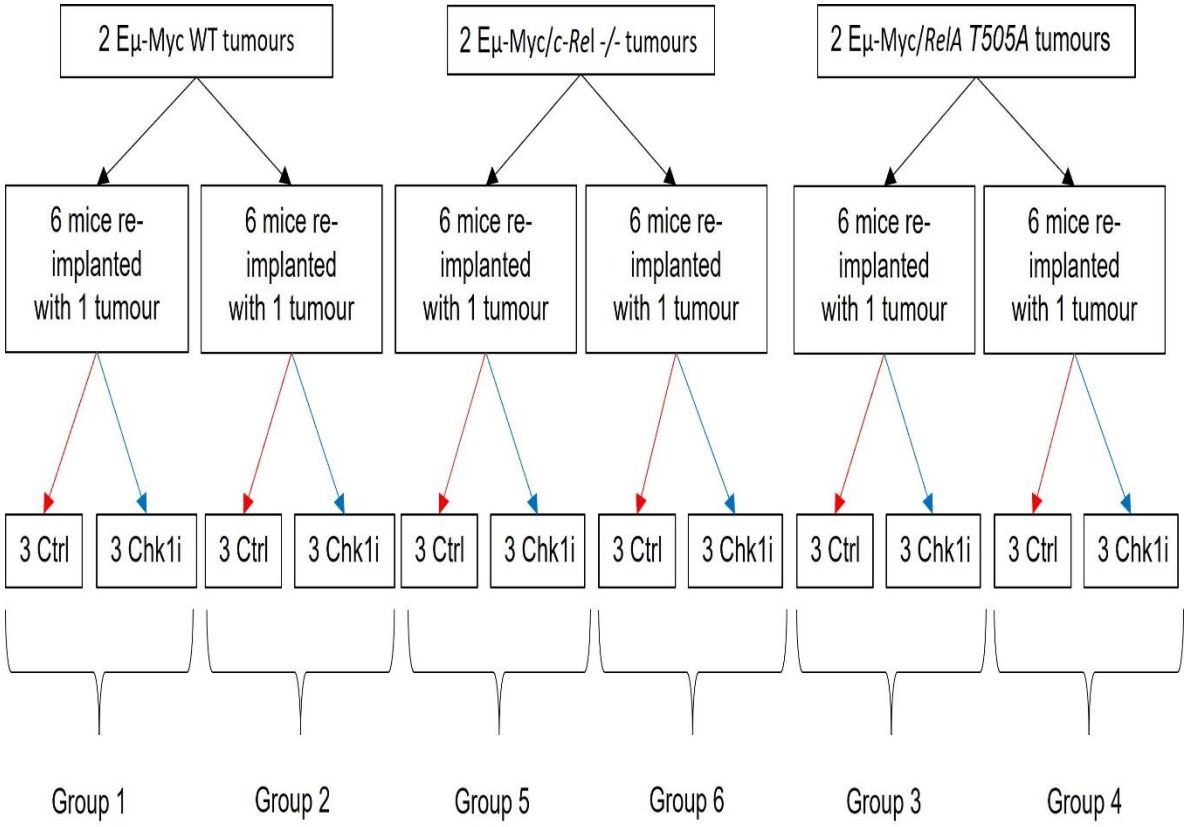

Figure 4.11. Schematic to show set up of acute CHK1i treatment models. Eμ-Myc (WT), Eμ-Myc/*c-Rel -/-* and Eμ-Myc/*RelA T505A* tumours were re-implanted into WT mice and lymphoma developed. Mice were treated with a single dose of CCT244747 (100 mg/kg orally) or vehicle control and culled 8 hours after treatment. Groups 1 and 2 are Eμ-Myc WT, groups 3 and 4 are Eμ-Myc/*RelA T505A* and groups 5 and 6 are Eμ-Myc/*c-Rel -/-* mice.

The results are shown in Figure 4.12. The CHK1i sensitive Eμ-Myc WT mice show protein expression levels for phosphorylated CHK1 and H2AX similar to the previous results shown in Figure 4.9 with an increase in expression after CHK1i treatment. PARP cleavage appears to be stabilised. Total CHK1 is reduced indicating a response to CHK1i treatment. These results suggest an upregulation of ATR to attempt to repair DNA damage and an overall increase in DNA damage leading to double stranded DNA breaks. There are no clear changes in CDK2 expression present. There is some variation between individual mice and the different tumours as shown between Figure 4.12A and 4.12B, but similar overall trends are displayed.

In striking contrast, the CHK1i resistant Eμ-Myc/*c-Rel -/-* completely downregulate their DNA damage response. Baseline levels of Claspin, PARP, both phosphorylated and total CHK1, CDK2 and phosphorylated H2AX are all lower in the Eμ-Myc/*c-Rel -/-* mice. There is an additional failure to increase the expression of these DNA damage response proteins after CHK1i treatment as shown in the Eμ-Myc WT model. This correlates with previous Perkins' lab findings of a loss of CLSPN expression in the Eμ-Myc/*c-Rel -/-* mouse models, however this DDR pathway appears to be impacted with a global downregulation of protein expression. This downregulation of the DDR response could be significant in cell survival and CHK1i drug resistance. If the drug target, CHK1, is absent in the Eμ-Myc/*c-Rel -/-* mouse model, this may explain why the mouse are CHK1i resistant to CHK1 inhibition.

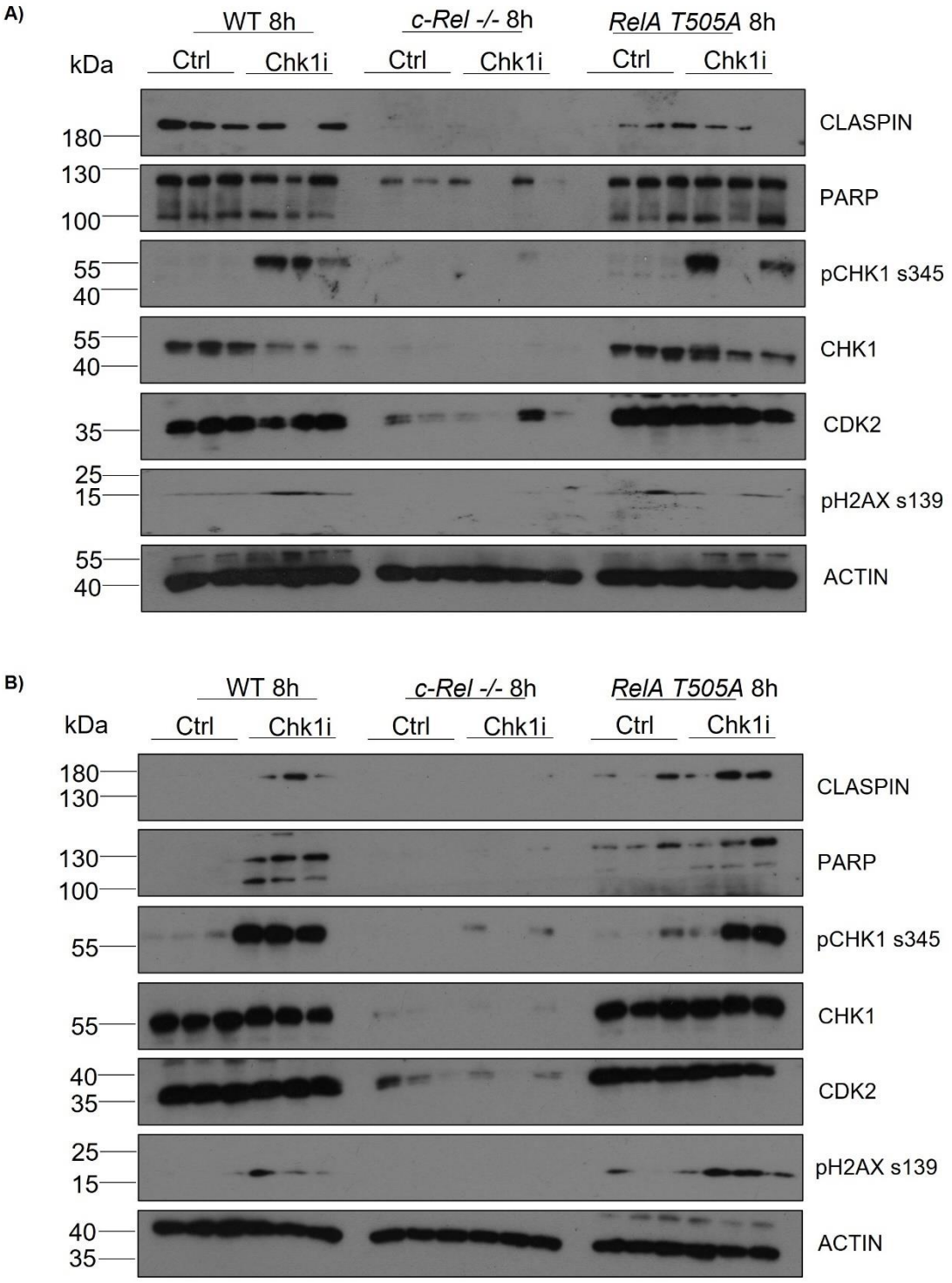

Figure 4.12. Eμ-Myc/*c-Rel -/-* mice do not upregulate protein expression of DDR genes in response to CHK1i treatment. N=1. 6 Eμ-Myc WT mice (sets 1 and 2), 6 Eμ-Myc/*c-Rel -/-* mice (sets 5 and 6) and 6 Eμ-Myc/*RelA T505A* mice (sets 3 and 4) were treated with CCT244747 (100 mg/kg orally), and 6 in each group with vehicle control, for a single dose and harvested at 8 hours post treatment. A) shows mouse sets 1,3 and 5 and B) shows mice sets 2, 4 and 6. Differences are most pronounced in the Eμ-Myc/*c-Rel -/-* mice, with no DDR upregulation seen after CHK1i therapy for Claspin, PARP, and γH2AX. Pre-treatment levels of total CHK1 and CDK2 are also downregulated in the Eμ-Myc/*c-Rel -/-* mice. There is some heterogeneity in protein expression in CHK1i treated Eμ-Myc and Eμ-Myc/*RelA T505A* mice, however both mice sets show an increase in pCHK1 S345 expression and an overall increase in pH2AX S139 expression after CHK1i treatment (this is shown in Eμ-Myc/*RelA T505A* set 4 but not in set 3). Total CHK1 levels reduce with CHK1i treatment in Eμ-Myc set 1 but not in set 2.

Eμ-Myc/*RelA T505A* mice are also resistant to CHK1 inhibition, however there are differences shown in protein expression in comparison to the Eμ-Myc/*c-Rel -/-* mice. There seems to be no difference in CHK1, H2AX and CDK2 levels in this mouse group. In the first CHK1i treated group of Eμ-Myc/*RelA T505A* mice there does not appear to be a change in CHK1 in response to treatment. Claspin appears to be lower in the Eμ-Myc/*RelA T505A* mice compared to Eμ-Myc WT but again there is variation between the mice. There are no clear changes in PARP between treated and untreated mouse groups.

Overall, the Eμ-Myc/*RelA T505A* mice seem to be able to respond to CHK1 inhibition differently again in contrast to the Eμ-Myc WT and Eμ-Myc/*c-Rel -/-* models. The Eμ-Myc/*RelA T505A* mice are also resistant to the CCT244747 CHK1 inhibitor but appear to develop drug resistance in a different way to the Eμ-Myc/*c-Rel -/-* model.

4.11. RNA-seq analysis of the acute Eμ-Myc WT mouse models at 8 hours show very little change in gene transcription after CHK1i treatment

To further investigate transcriptional changes 8 hours post treatment in the CHK1 inhibitor sensitive Eμ-Myc and the CHK1i resistant Eμ-Myc/*c-Rel -/-* and Eμ-Myc/*RelA T505A* mouse models, RNA-seq was performed. This was done to see if perhaps any other pathways involved in the DNA damage response were being differentially regulated in response to CHK1 inhibitor treatment in the various experimental groups, and also to capture whether there were any intrinsic difference between the different genotypes in terms of their transcriptomic profile.

RNA was extracted according to the manufacturer's protocol as described previously (Section 3.3.2 for mouse tissues). After quality assessment using the TapeStation, the RNA samples were run using the Illumina platform by Leigh Taylor at the Genomics Core Facility at Newcastle University.

RNA-seq data was analysed by Peter Leary at the Newcastle University Bioinformatics Support Unit (BSU). Gene expression changes between Eμ-Myc WT control and CHK1i treated mice 8 hours post CHKi1 single dose treatment are shown in Table 4.4.

Table 4.4. RNA-seq data for gene changes shown between the acute Eμ-Myc WT control and CHK1i treated mice 8 hours post dose. This table shows all significant gene changes between the two mouse groups. This demonstrates that there were not many transcriptional changes seen between control and treated mice after a single dose of treatment and at this time point. (logFC shows calculation for log fold change, p<0.05 taken as significant adjusted P value). Summaries of gene function have been described in this table alongside the data.

Gene	Gene full name	logFC	Adjusted P value	Gene function	Reference
Esm1	*Endothelial cell-signalling molecule 1*	-0.711236561	0.039222682	Cell survival, migration and EMT	(447,448)
Supt3	*Suppressor of Ty 3 homolog*	-0.38225412	0.046437539	Cell proliferation and resistance to apoptosis	(449)
Vat1	*Vesicle amine transport protein 1*	0.391107849	0.01114098	Vesicular transport, mitochondrial fusion Phospholipid transport and cell migration	(450)
Pld3	*Phospholipase D family member 3*	0.422924968	0.042563989	Cell survival, growth and migration	(451)
Neurl3	*Neuralised E3 ubiquitin protein ligase 3*	0.460752568	0.031881387	Inflammatory response Enables ubiquitin protein ligase activity	(452)
Gas6	*Growth arrest-specific protein 6*	0.527275369	0.039222682	Cell proliferation, survival and migration	(453,454)
Slc30a1	*Solute carrier family 30 member 1*	0.596743199	0.022712666	Modulation of zinc transportation	(455)
Slc7a8	*Solute carrier family 7 member 8*	0.597998301	0.009197544	Transport of amino acids	(456)

Gene	Gene full name	logFC	Adjusted P value	Gene function	Reference
Hist3h2a	*Histone cluster 3 H2A*	0.613168446	0.003439054	Gene expression DNA damage regulation	(109,457)
Tsc22d1	*TSC22 domain family member 1*	0.634404018	0.022712666	Transcriptional repressor Acts on the C-type natriuretic peptide (CNP) promoter	(458)
Rasgef1b	*RasGEF domain family member 1B*	0.664719985	0.022712666	Cell proliferation and survival	(459)
Msantd2	*Myb/SANT DNA binding domain containing 2*	0.829963543	0.023788944	Protein coding gene, function unknown	(460)
Cd4	*T-cell surface glycoprotein CD4*	0.850478722	0.0042644	Regulator of immune response	(461–463)
Fam234a	*Family with sequence similarity 234 member A*	0.952577539	0.022712666	Protein coding gene, function unknown	(464)
Fads6	*Fatty acid desaturase 6*	0.961208608	0.046466435	Fatty acid metabolism Cell growth and proliferation	(465)

Gene	Gene full name	logFC	Adjusted P value	Gene function	Reference
Pou6f1	*POU class 6 homeobox 1*	0.986354532	0.022712666	Enables DNA-binding transcription repressor activity RNA polymerase II-specific and sequence-specific double-stranded DNA binding activity	(466)
Gpr171	*G protein-coupled receptor 171*	1.003370582	0.01114098	Cell proliferation Suppression of T cell activation	(467,468)
Hist1h2bc	*H2B clustered histone 4*	1.020508537	5.66E-04	Transcription regulation	(469))
Adgrg1	*Adhesion G protein-coupled receptor G1*	1.070278348	0.031881387	Cell migration, proliferation and invasion	(470,471)
Hist1h1c	*Histone cluster 1 H1 family member C*	1.096268594	0.004264513	Compaction of chromatin	(472)
Gm42653	*piR-42653-001*	1.14433723	0.022712666	RNA gene, function unknown	(473)

Data was analysed in more detail beyond the time point of this thesis. Overall, very little transcriptional change was seen between the control and CHK1i treated mice. In addition, no significant changes were demonstrated in genes associated with the ATR/CHK1 and the ATM/CHK2 pathways. This data supports my findings shown earlier in Section 4.8.

The genes in Table 4.4 do show some trends. There are genes associated with cell proliferation and migration, such as *Esm1*, *Supt3*, *Gas6* and *Adgrg1* (447,449,453,454,471). This could be indicative of genes upregulated to enhance cell survival after drug treatment. There are also genes associated with intracellular transport of ions and amino acids such as *Slc30a1* and *Slc7a8* (455,456). There are also genes involved in lymphocyte regulation including the T-cell regulatory gene *Cd4* and the G protein coupled receptor *Gpr171* (462,468). The cancer in this mouse model is a B-cell lymphoma, therefore this may impact the regulation of T-lymphocytes as part of the inflammatory response. There are genes upregulated which are associated with histone regulation, including *Hist1h1c* and *Hist1h2bc* (457,469). This could be indicative of increased DNA damage with drug treatment and correlates with increased H2AX expression as demonstrated in Figures 4.10 and 4.12 post CHK1i treatment. Some of the upregulated genes do not have an established known function, such as *Msantd2* (460).

Given that there are only a small number of genes upregulated in the Eμ-Myc mouse at this acute treatment stage, these data suggest that the majority of effects at this early time point after CHK1 inhibitor treatment are post-transcriptional. I will discuss further in the proteomic analysis of these samples (Section 4.15).

4.12. RNA-seq analysis of the acute Eμ-Myc mouse models at 8 hours show differences between the Eμ-Myc CHK1i sensitive model and the Eμ-Myc/*c-Rel -/-* CHK1i resistant model in genes associated with the ATR/CHK1 pathway

RNA-seq data was further interrogated to see if differences were evident in gene expression between the Eμ-Myc mouse models at the basal level without CHK1i treatment. The final analysis was performed after this thesis was submitted by Dr. Peter Leary and Dr. Megan Hasson at the Newcastle BSU, using DESeq2 for differential gene expression (474). Previous analysis (Section 4.11) had shown that there were very little transcriptional differences shown in the CHK1i sensitive Eμ-Myc mouse model post treatment.

Functional profiling of the genes whose mRNA expression varied between the Eμ-Myc WT and Eμ-Myc/*c-Rel -/-* mouse groups was undertaken. Interestingly, this revealed 36 genes associated with 'Activation of ATR in response to replication stress' (REAC:R-HSA-176187). 32 of the 36 genes were shown to be downregulated in the acute *c-Rel -/-* Eμ-Myc mouse models. This included *CHEK1* and *CLSPN* transcript levels, which were later validated by Dr. Jill Hunter using qPCR. *CLSPN* has previously been shown *in vitro* to be a *c-Rel* target gene (252) and therefore a reduction in *CLSPN* level could be associated with the *c-Rel* knockdown status, as *CLSPN* transcription is dependent on *c-Rel*. The Perkins' lab has already previously demonstrated that the *CLSPN* transcript levels are decreased in the *c-Rel -/-* mice which is in keeping with findings from this study.

There was still far fewer gene changes demonstrated in the RNA-seq data compared to the subsequent proteomics data, which supports that most changes seen between the mouse models are post transcriptional changes. Table 4.5 shows the gene changes shown between the Eμ-Myc CHK1i sensitive model and the Eμ-Myc/*c-Rel -/-* CHK1i resistant model in the ATR/CHK1 pathway associated genes. The downregulation of the ATR/CHK1 pathway demonstrated in the RNA-seq data supports my findings shown in this chapter for the Eμ-Myc/*c-Rel -/-* mouse model. The downregulation of the ATR/CHK1 pathway in this mouse model could be a mechanism of CHK1i resistance.

Table 4.5. RNA-seq data for gene changes shown between the acute Eμ-Myc WT CHK1i and the Eμ-Myc/*c-Rel -/-* CHK1i treated mice 8 hours post dose. Table produced by Dr. Jill Hunter. This table summarises changes in the ATR/CHK1 pathway associated genes between the CHK1i sensitive and resistant mouse groups. 32 of the 36 genes showing variation between these mouse models show a downregulation in the Eμ-Myc/*c-Rel -/-* mouse model. ($p<0.05$ taken as significant adjusted P value).

ATR pathway genes	Fold change log2	Adjusted p value
CDC25C	-2.70	1.36403E-16
CHEK1	-2.20	6.594E-13
MCM10	-2.17	2.28421E-10
CDC6	-2.11	9.66523E-12
CLSPN	-2.00	8.45403E-12
CDC45	-1.92	6.48256E-14
MCM6	-1.73	2.11556E-13
MCM3	-1.66	8.28725E-13
MCM5	-1.65	3.58692E-12
RFC4	-1.63	4.52474E-12
MCM7	-1.60	1.56684E-13
MCM2	-1.59	8.19789E-11
CDC7	-1.53	2.68592E-15
ORC2	-1.46	1.51114E-17
MCM4	-1.40	1.23948E-12
DBF4	-1.36	4.71863E-14
ORC6	-1.36	5.89705E-13
ORC1	-1.30	0.00853
MCM8	-1.28	8.84119E-11
CDC25A	-1.19	3.67803E-12
RFC5	-1.17	1.51509E-10
RPA3	-1.16	1.54334E-09
RPA2	-1.15	1.13117E-10
RFC3	-1.09	8.4964E-11
CDK2	-1.00	2.59781E-17
HUS1	-0.98	7.83871E-08
RFC2	-0.91	3.52178E-13
ORC5	-0.76	1.11968E-14
ORC4	-0.69	3.98262E-07
RPA1	-0.65	4.74165E-10
RAD1	-0.64	1.81826E-09
ATR	-0.59	1.24476E-08

4.13. RNA-seq analysis of the acute Eμ-Myc mouse models at 8 hours show a downregulation of the deubiquitinase encoding genes *USP1* and *USP14* in the Eμ-Myc/*c-Rel -/-* mouse model

Given the downregulation of the ATR/CHK1 pathway at 8 hours post CHK1i dose in the Eμ-Myc/*c-Rel -/-* mouse model, further analysis of the RNA-seq data from these mouse models was performed. This data identified that the deubiquitinases (DUBs) *ubiquitin specific peptidase 1* (*USP1*) and *ubiquitin specific peptidase 14* (*USP14*) were downregulated by approximately 2 fold at the mRNA level in the Eμ-Myc/*c-Rel -/-* samples in comparison to the Eμ-Myc WT samples as shown in Figure 4.13. DUBs are a family of proteases that cleave ubiquitin markers from proteins prior to proteosomal degradation (475,476).

USP1 has been shown to play a role in stabilising members of the DDR, including FANCD2 as removing K48 polyubiquitination prevents subsequent K48 targeted degradation (475,477,478). It has also been suggested that USP1 can directly act as a DUB for CHK1 by preventing proteosomal degradation (479). USP14 is raised in many cancers, including prostate and breast cancers, and has been shown to have an impact on DNA double strand break regulation by negatively regulating NHEJ and promoting HR repair (480–483). These DUBs could both be influential towards CHK1i resistance in the Eμ-Myc/*c-Rel -/-* mouse model. Both *USP1* and *USP14* have both potential direct influence on the DDR and further investigation is required. The downregulation of *USP1* could be significant because a direct mechanism of CHK1 stabilisation may have been removed.

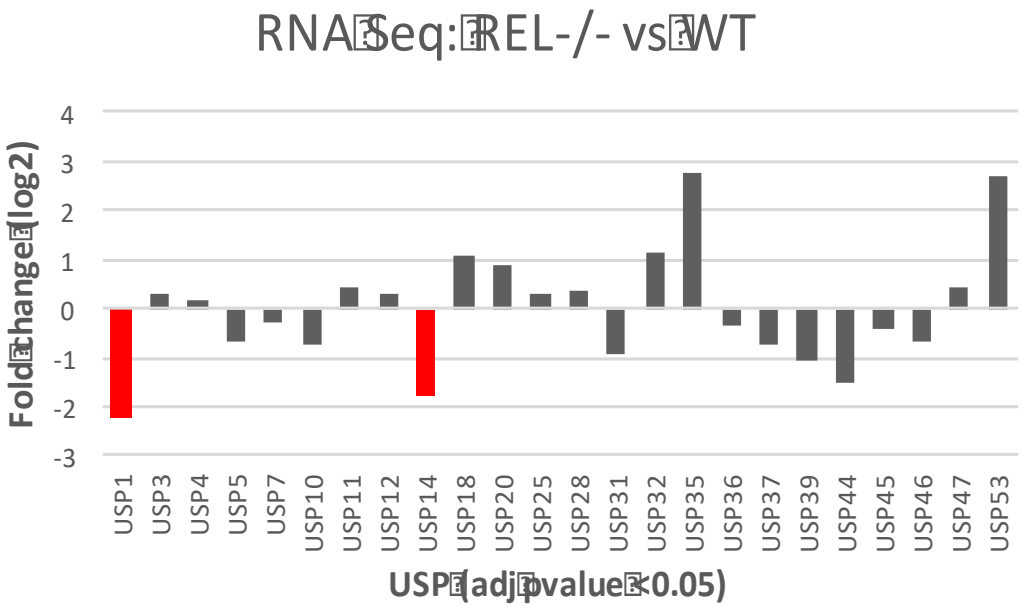

Figure 4.13. RNA-seq data has shown a downregulation of *USP1* and *USP14* in Eμ-Myc/*c-Rel -/-* compared to Eμ-Myc WT mice. Graph produced by Prof. N Perkins. The expression of the deubiquitinase encoding genes *USP1* and *USP14*, highlighted in red, was found to be significantly lower in Eμ-Myc/*c-Rel -/-* mice. This could impact on CHK1 stability and requires further investigation. There is also an upregulation of *USP53* and *USP35* in this mouse model, which again could impact on cell proliferation and survival.

There were also upregulatory changes seen in DUBs as shown in Figure 4.13. Further investigation of these DUBS was not performed due to time constraints for this thesis. There was an increase in *ubiquitin specific peptidase 53* (*USP53*) in the Eμ-Myc/*c-Rel -/-* mouse model. *USP53* has been shown to regulate apoptosis and glycolysis through the AKT pathway. Low levels have been seen to be protective against apoptosis in lung adenocarcinoma cell and tumour models (484).

USP53 has also been shown to have an important role in the metastatic potential of renal cell carcinoma cell models. USP53 expression was negatively correlated with tumour progression, therefore higher levels of USP53 are associated with less progression (485). NF-κB related genes, including *RelA* and *RelB*, were shown to be downregulated with *USP53* overexpression in cell models of renal cell carcinoma. USP53 has been shown to lead to the inactivation of the NF-κB pathway by reducing the ubiquitination of IκBα. This subsequently led to less tumour proliferation in these models (485). Therefore, a high level of *USP53* in the Eμ-Myc/*c-Rel -/-* mice could show that *USP53* expression and the subsequent impact has been context dependent, as it appears to be upregulated in the CHK1i resistant mouse model.

There was also an upregulation of *ubiquitin specific peptidase 35* (*USP35*) expression in the Eμ-Myc/*c-Rel -/-* mouse model as shown in Figure 4.13. USP35 has also been shown in cellular models to inhibit cancer cell proliferation and have an inhibitory role in TNFα-induced NF-κB regulation (486). Higher levels of *USP35* (and *USP53*) would suggest being protective from cancer proliferation based on previous studies, so these studies appear to contradict what has been shown in the Eμ-Myc/*c-Rel -/-* CHK1i resistant mouse model. It could be that the regulation of the DUBs and NF-κB is context-dependent and also dependent on the synchronous regulation of alternative cell cycle pathways. More investigations are required to determine the mechanism behind the upregulation of *USP53* and *USP35* in the Eμ-Myc/*c-Rel -/-* mouse model.

4.14. Validation of changes seen in *USP1* in the acute Eμ-Myc WT, Eμ-Myc/*c-Rel -/-* and Eμ-Myc/*RelA T505A* mouse models

The RNA-seq data has shown that *USP1* levels are significantly downregulated by approximately 2 fold in the Eμ-Myc/*c-Rel -/-* mouse model compared to the Eμ-Myc WT mice. The ubiquitination enzyme USP1 is involved in the maintenance of total and phosphorylated levels of CHK1 in response to genotoxic stress (107). *USP1* depletion has been shown to stimulate DNA-binding protein 1-dependent degradation of phosphorylated CHK1. This can be both FANCD2 dependent and independent in origin (107). The downregulation of *USP1* in the Eμ-Myc/*c-Rel -/-* mice may therefore impact on the downregulation of the DNA damage response, including levels of *CHEK1*.

qPCR was performed to further assess the trancriptional differences in basal *USP1* levels between the Eμ-Myc WT, Eμ-Myc/*c-Rel -/-* and Eμ-Myc/*RelA T505A* mouse models. *RPL13A* was used as the reference gene. Results are shown in Figure 4.14. These findings further support that the *USP1* transcript levels are significantly reduced in tumours from Eμ-Myc/*c-Rel -/-* mice at baseline when compared with tumours from the Eμ-Myc WT mice. This again supports downregulation of *USP1* in addition to DNA damage response regulatory proteins in the Eμ-Myc/*c-Rel -/-* mouse model.

In addition, the *USP1* transcript levels appear to be overall lower than Eμ-Myc WT mice for the Eμ-Myc/*RelA T505A* group, but the levels are higher than the Eμ-Myc/*c-Rel -/-* group. More work is required to look at the mechanisms of Eμ-Myc/*RelA T505A* CHK1i resistance, as this remains unclear at this stage.

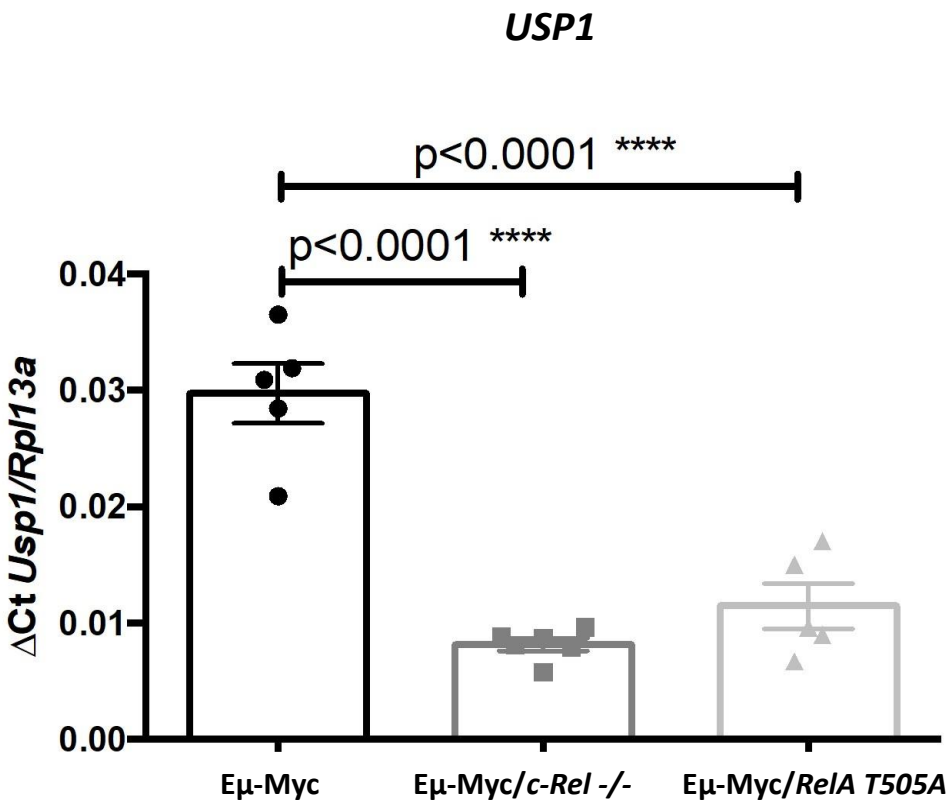

Figure 4.14. qPCR validation of RNA-seq analysis for basal *USP1* in the acute Eμ-Myc WT, Eμ-Myc/*c-Rel -/-* and Eμ-Myc/*RelA T505A* mouse models. N=1. Data were normalised using the 2-ΔCT method (R = 2–[ΔCP sample – ΔCP control]) using the gene *RPL13A* as reference. Relative *USP1* transcript levels are significantly reduced in tumours from Eμ-Myc/*c-Rel -/-* when compared with Eμ-Myc WT. *USP1* transcript levels appear to be lower than Eμ-Myc WT mice for the Eμ-Myc/*RelA T505A* group but higher than the Eμ-Myc/*c-Rel -/-* group. Data represents mean ± SEM, each point is an individual mouse. p** <0.01, p***<0.001 (Unpaired student's t-test).

Western blot analysis was performed to examine levels of USP1 in the acute Eμ-Myc WT, Eμ-Myc/*c-Rel -/-* and Eμ-Myc/*RelA T505A* mice. Results are shown in Figure 4.15. In Eμ-Myc WT and Eμ-Myc/*RelA T505A* mice, USP1 is depicted by a double band. This is because, when active, USP1 autocleaves itself in preparation for its subsequent downregulation. The lower of the 2 bands is indicative of the autocleaved, inactivated USP1 (487). USP1 levels vary between mice in the Eμ-Myc WT and Eμ-Myc*/RelA T505A* groups but do not appear to be downregulated with CHK1i treatment.

By contrast, levels of USP1 are dramatically depleted in the Eμ-Myc/*c-Rel -/-* group at baseline and remain low after CHK1i treatment. This would correlate with the previous findings shown with loss of CHK pathway proteins, as if USP1 is not present, CHK1 may not be protected from degradation.

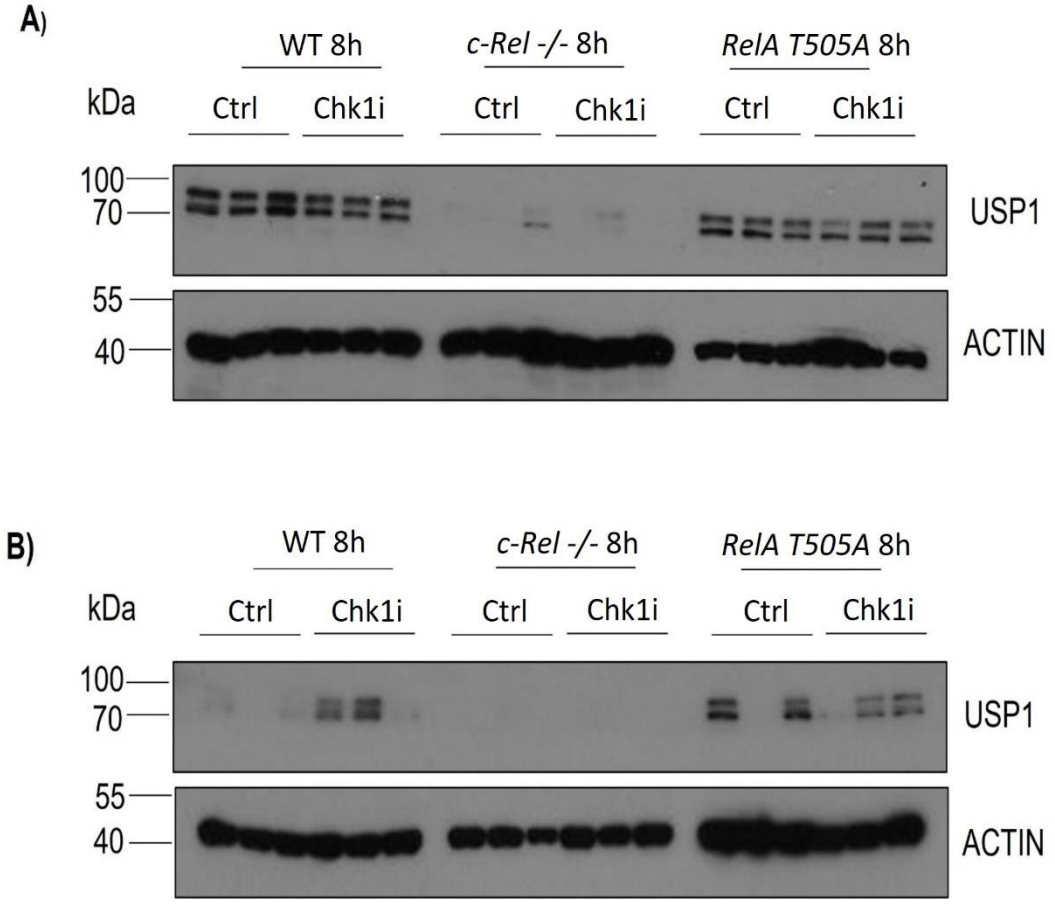

Figure 4.15. USP1 results in Acute Eμ-Myc WT, Eμ-Myc/*c-Rel -/-* and Eμ-Myc/*RelA T505A* mutant mice. Western blots showing USP1 in Eμ-Myc WT, *c-Rel -/-* and *RelA T505A* mutant models harvested 8 hours after a single dose of CCT244747 CHK1 inhibitor. N=1. Mice were treated with a single dose of 100mg/kg oral CCT244747 or vehicle control. Each blot shows results for 3 control treated and 3 CHK1i treated in each group in two separate sets of mice. A) and B) show different mouse sets: A) Results for Eμ-Myc WT set 1, Eμ-Myc/*c-Rel -/-* set 5 and Eμ-Myc/*RelA T505A* set 3. B) Results for Eμ-Myc WT set 2, Eμ-Myc/*c-Rel -/-* set 6 and Eμ-Myc/*RelA T505A* set 4. Levels of USP1 are strikingly lower in the Eμ-Myc/*c-Rel -/-* mice in comparison to the other groups, although there does appear to be heterogeneity in USP1 for the Eμ-Myc WT and Eμ-Myc/*RelA T505A* mice both pre- and post CHK1 inhibition.

4.15. Proteomics analysis of the acute Eμ-Myc mouse models at 8 hours show differences between the Eμ-Myc WT lymphomas and the Eμ-Myc/*c-Rel -/-* lymphomas

The data in Section 4.11 showed very few differences in gene expression in the acute Eμ-Myc WT and Eμ-Myc/*c-Rel -/-* mouse groups post CHK1i treatment. These findings, and the alterations in protein expression seen in Figure 4.10 and 4.12, suggest that the changes leading to CHK1i sensitivity or CHK1i resistance were post transcriptional in nature.

In order to further investigate post transcriptional changes in the Eμ-Myc WT and the Eμ-Myc/*c-Rel -/-* mouse models, samples from the acute 8 hour single dose study were selected for total and phosphoproteomic analysis. This was performed at the University of Liverpool in collaboration with Prof. Claire Eyers and Dr. Amy Campbell.

Analysis of this data showed a large number of CCT244747 effects in the Eμ-Myc WT lymphomas. A total of 622 proteins and 625 phosphopeptides exhibited a significant upregulation or downregulation (P-value ≤0.05). Figure 4.16 shows volcano plots displaying the differences between Eμ-Myc WT control and Eμ-Myc WT CHK1i treated samples. These findings indicate that there are many post-transcriptional changes after CHK1i treatment in the Eμ-Myc WT CHK1i sensitive mouse model.

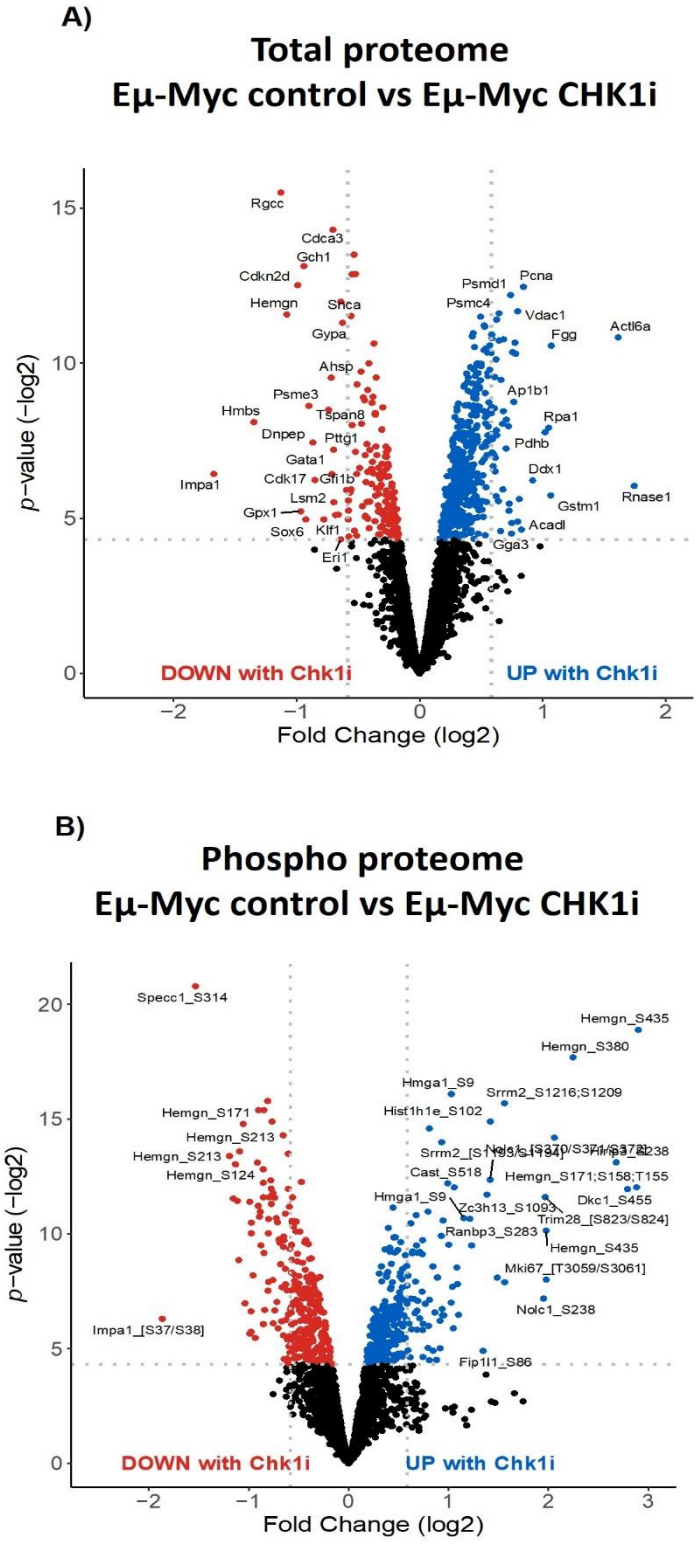

Figure 4.16. Total proteome and phosphoproteome data for the acute Eμ-Myc WT control vs CHK1i treated samples. Figure produced by Dr. J Hunter. Volcano plots showing total proteome and phosphoproteome changes 8 hours post a single dose of CHK1i treatment. Mice were treated with a single dose of 100mg/kg oral CCT244747 or vehicle control. A total of 622 proteins and 625 phosphopeptides exhibited a significant upregulation or downregulation in the Eμ-Myc WT mice after CHK1i treatment. This indicates that there are many post transcriptional effects in this CHK1i sensitive mouse model after CCT244747 treatment (P-value ≤0.05).

STRING analysis (488) of the phosphoproteomic data from Eμ-Myc WT lymphomas was performed by Prof. Neil Perkins. Results revealed a cluster of CHK1 associated proteins where phosphorylation was downregulated after CCT244747 treatment as shown in Figure 4.17. This data has shown that CHK1 has been targeted by the CHK1i CCT244747 *in vivo* and suggests that there are very few off target effects.

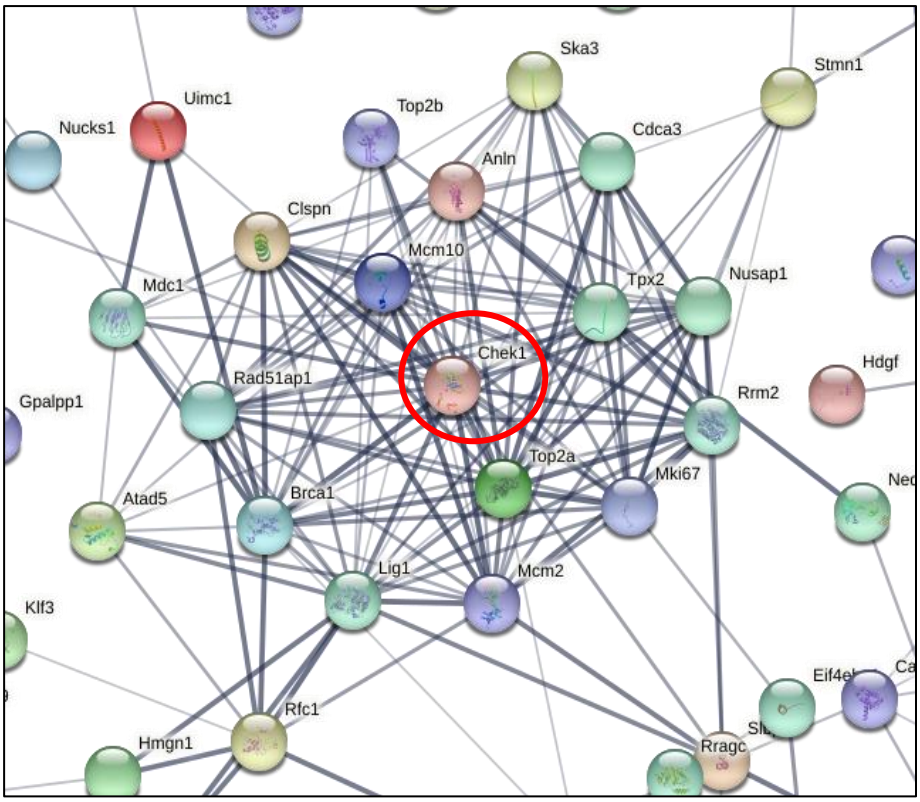

Figure 4.17. STRING analysis of phosphoproteomic data of CHK1i treated Eμ-Myc WT mice has shown a cluster of associated downregulated proteins. STRING analysis from (https://string-db.org/) and diagram produced by Prof. N Perkins. The cluster around CHK1 itself (highlighted with red circle) in response to treatment suggests that the CHK1i CCT244747 is reaching its target with minimal off-target effects. Line thickness in the analysis represents the degree of confidence in the prediction of the protein interactions. The different colours are used as a visual aid only, to identify which node goes with which description in list of input proteins and interactors below the network.

The proteomics data for the CHK1i resistant Eμ-Myc/*c-Rel -/-* mouse model was reviewed to look for evidence of compensatory cell signalling pathways. Data was analysed by Dr. Amy Campbell and Prof. Neil Perkins. Activation of compensatory signalling pathways is a major contributing factor in acquired resistance to kinase inhibitors (286,331,332). The activation of such pathways normally correlates with the tumour cell having bypassed the need for the drug target.

The proteomics data has revealed that Eμ-Myc/*c-Rel -/-* mouse lymphomas had substantially altered their cell signalling pathways, with a high level of both downregulated and upregulated phosphopeptides compared to the Eμ-Myc WT mice. Data showing the overlap between the upregulated phosphosites and total proteome between the Eμ-Myc and the Eμ-Myc/*c-Rel -/-* mouse models are displayed in Figure 4.18. Analysis of the phospho- and total proteomic data in the Eμ-Myc/*c-Rel -/-* mouse models without CHK1i treatment compared to wild type controls showed 517 upregulated phosphopeptides, representing 480 unique phosphopeptides which correlated to 297 unique phosphosites, together with 624 upregulated proteins ($p<0.05$).

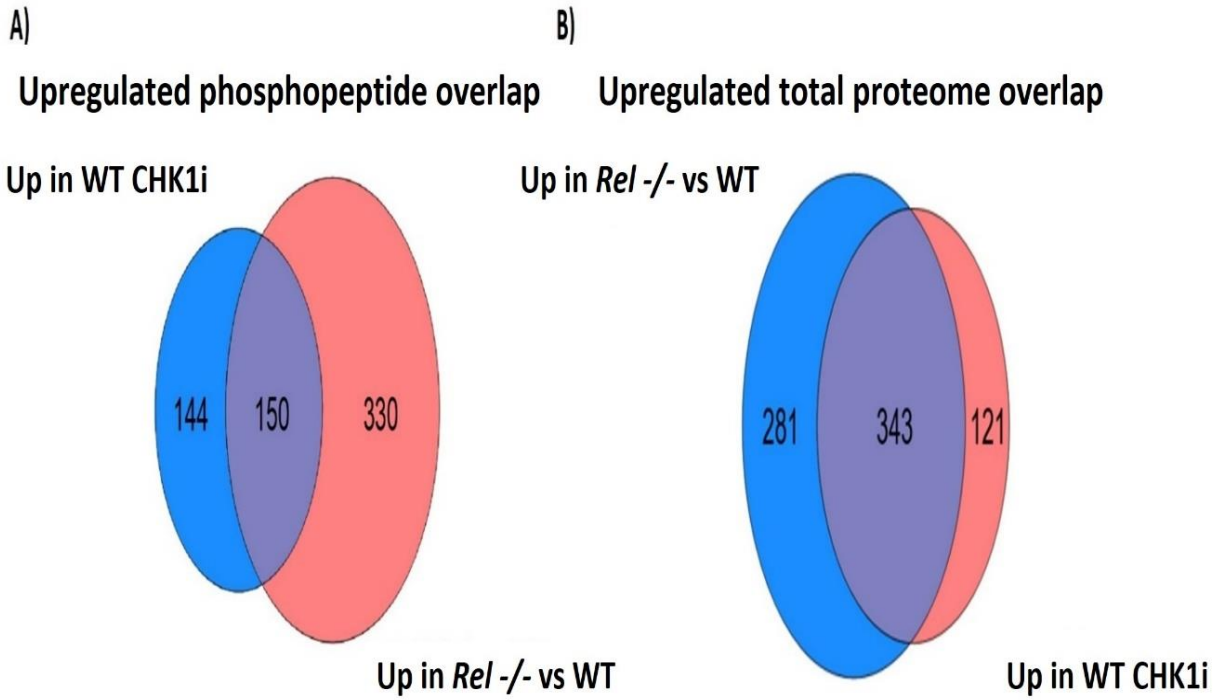

Figure 4.18. Summary of the upregulation of phosphopeptides and upregulation of total proteome between the Eμ-Myc WT and Eμ-Myc/*c-Rel -/-* mouse models. Data analysis performed by Dr. Jill Hunter. Analysis of the A) phosphopeptide and B) total proteomic data revealed 517 upregulated phosphopeptides ($p<0.05$), representing 480 unique phosphopeptides correlating to 297 unique phosphosites (at a ptmRS score ≥0.998), together with 624 upregulated proteins ($p<0.05$) in untreated Eμ-Myc/*c-Rel -/-* mice compared to WT controls. Of the 294 unique phosphopeptides and 464 proteins elevated in WT Eμ-Myc lymphomas in response to the CHK1i CCT244747, 51% and 74% respectively were also upregulated in Eμ-Myc/*c-Rel -/-* mice without treatment. However, the magnitude of the increases seen in the CHK1i treated Eμ-Myc WT mice was lower in both cases than that seen constitutively in Eμ-Myc/*c-Rel -/-* lymphomas.

In mice treated with the CCT244747 CHK1 inhibitor, 294 unique phosphopeptides and 464 proteins were elevated in wild type Eμ-Myc lymphomas. 51% of these phosphopeptides and 74% of these proteins were also upregulated in Eμ-Myc/*c-Rel -/-* cells without treatment. The magnitude of the increases seen in the treated wild type cells, however, was lower in both cases than what was shown in the Eμ-Myc/*c-Rel -/-* lymphomas.

These results demonstrated that Eμ-Myc/*c-Rel -/-* lymphomas have an intrinsic defect in CHK1 kinase signalling, which is comparable to the effect of inhibiting CHK1 in WT Eμ-Myc mice. The proteomics data again shows that the ATR/CHK1 pathway is downregulated in the Eμ-Myc/*c-Rel -/-* mice. This supports my findings shown in Section 4.9 and Section 4.10.

Figure 4.19 shows volcano plots for the total proteomics and phosphoproteomics data in the Eμ-Myc/*c-Rel -/-* mice. In comparison to the Eμ-Myc mice, there are hardly any changes after CHK1i treatment in this CHK1i resistant mouse model.

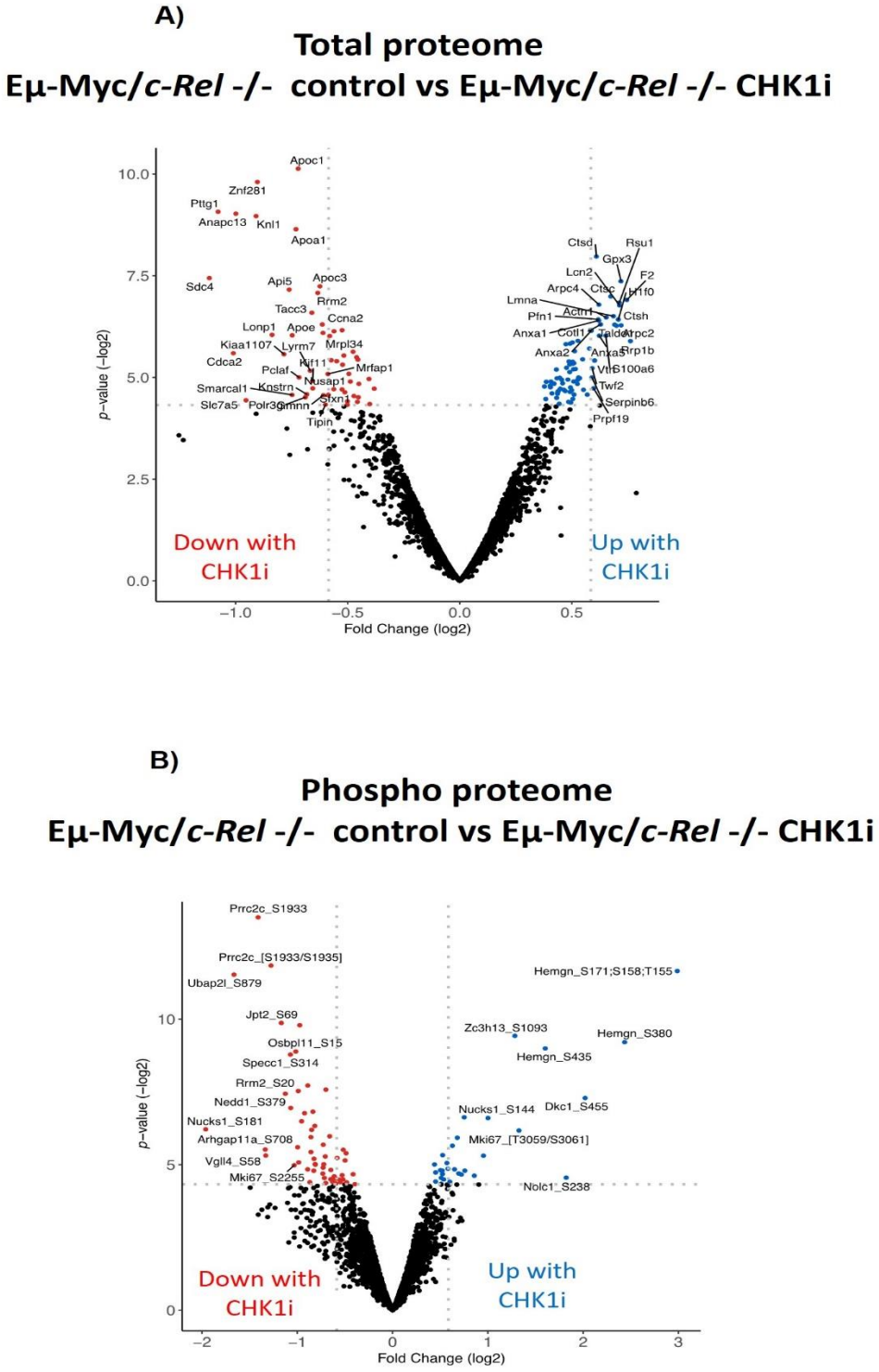

Figure 4.19. Total proteome and phosphoproteome data for the acute Eμ-Myc/*c-Rel* -/- control vs Eμ-Myc/*c-Rel* -/- CHK1i treated samples. Figure produced by Dr. J Hunter. Volcano plots showing total proteome and phosphoproteome changes 8 hours post a single dose of CHK1i treatment. Mice were treated with a single dose of 100mg/kg oral CCT244747 or vehicle control. In comparison to the CHK1i sensitive Eμ-Myc WT model, there are less changes demonstrated in the CHK1i resistant Eμ-Myc/*c-Rel* -/- mouse model.

4.16. Pathways associated with AKT1, ERK1, JNK1 and p38 are upregulated in the Eμ-Myc/*c-Rel -/-* lymphomas in comparison to the Eμ-Myc WT lymphomas

STRING analysis was used to reveal information about the activity of compensatory cell signalling pathways in Eμ-Myc/*c-Rel -/-* lymphomas versus WT cells. Clusters of linked proteins associated with the following signalling pathways, AKT1, ERK1, JNK1 and p38 MAPK, were all found to be upregulated. A summary of these proteins are shown in Table 4.6. There is some overlap shown in the table indicating potential cross talk and shared targets between these pathways.

AKT is already known to interact with multiple DDR genes including *TOPBP1* and *ATM* and to have a regulatory role with CHK1 (110,115,489,490). The P38/MAPK complex has an impact on cell cycle regulation both independently as part of the Ras-Raf-MEK-ERK cell signalling pathway and via crosstalk with the ATM and ATR pathways (120–123). JNK1 forms part of an additional MAPK pathway, which also coordinates with CHK1 to inhibit mitotic entry during cell cycle arrest (491).

ERK1 is a serine/threonine kinase that forms part of the Ras-Raf-MEK-ERK signal transduction cascade (492,493). This cell signalling pathway participates in the regulation of a large variety of processes including cell adhesion, cell cycle progression, cell migration and survival, metabolism, proliferation, and transcription (492,493). Ras is a key downstream effector of EGFR, which is mutationally activated or overexpressed in a wide variety of human cancers, such as lung cancer as discussed previously (493–495).

AKT as part of the PI3K/AKT pathway, JNK1 and MAPK associated proteins are known to be linked to NF-κB signalling (219). P38 and related kinases such as ERK1 are linked to the activation of NF-κB signalling (496,497). NF-κB has been shown to antagonise JNK1 pro-apoptotic signalling during an inflammatory response (219,491,496,498). This again highlights that the role of NF-κB varies depending on the stimulus and the cellular environment.

Table 4.6. STRING links to proteins with upregulated phosphorylation in the Eμ-Myc/*c-Rel -/-* mouse model in comparison to the Eμ-Myc WT. Data taken from STRING analysis (https://string-db.org/) and diagram produced by Dr. J Hunter and Prof. N Perkins. Data from STRING analysis of the mouse models revealed clusters of linked proteins in this dataset suggesting increased activity of specific kinases in the Eμ-Myc/*c-Rel -/-* lymphomas. This included AKT1, ERK1, JNK1 and p38 MAPK.

AKT1	ERK (MAPK3)	JNK1 (MAPK8)	p38 MAPK (MAPK14)
Abi1	Abi1	Akt1s1	Arhgap27
Acaca	Akt1	Atn1	Bnip2
Acin1	Akt1s1	Bcl10	Cfl1
Akt1s1	Canx	Bin2	Fn1
Arhgap1	Cfl1	Canx	Foxo1
Bach2	Cic	Cfl1	Hdac1
Bcl10	Ep300	Dbnl	Hdac2
Canx	Fn1	Ep300	Hnrnpa1
Cast	Foxo1	Erbb2ip	Hnrnpk
Cfl1	Hdac1	Fn1	Hsp90aa1
Crtc2	Hdac2	Foxo1	Hsp90ab1
Dennd1b	Hnrnpk	Hdac1	Hspb1
Dnmt1	Hsp90aa1	Hdac2	Irf3
Dock2	Hsp90ab1	Hnrnpk	Lcp1
Edc3	Hspb1	Hsp90aa1	Mef2c
Eml4	Irf3	Hsp90ab1	Myc
Ep300	Lcp1	Hspb1	Ncoa3
Flna	Mef2c	Irf3	Nfatc2
Fn1	Myc	Lcp1	Nfkb1
Foxo1	Ncoa3	Map1b	Pea15a
Hdac1	Nes	Myc	Ptprc
Hdac2	Nfkb1	Ncoa3	Pxn
Hnrnpa1	Pea15a	Nfatc2	Slc9a1
Hsp90aa1	Ppp1r12a	Nfkb1	Spag9
Hsp90ab1	Ptges3	Palld	Vcl
Hspb1	Ptprc	Ptprc	Yap1
Irf3	Pxn	Pxn	
Iws1	Slc9a1	Spag9	
Lamtor1	Stub1	Sptan1	
Lbr	Tnfrsf13c	Vcl	
Lcp1	Vcl	Yap1	
Map1b	Yap1		
Mapk14			
Marcks			
Mef2c			

AKT1	ERK (MAPK3)	JNK1 (MAPK8)	p38 MAPK (MAPK14)
Myc			
Myh9			
Ncoa3			
Nes			
Nfatc2			
Nfkb1			
Npm1			
Ostf1			
Pa2g4			
Palld			
Pdcd4			
Pea15a			
Pml			
Ppig			
Ptprc			
Pxn			
Ranbp3			
Rbl1			
Rbm25			
Rplp0			
Rps3			
Slc9a1			
Slc9a3r1			
Srsf1			
Stk4			
Stub1			
Tfeb			
Tnfrsf13c			
Tns3			
Trp53bp1			
Usp7			
Usp8			
Vasp			
Vcl			
Yap1			
Zyx			

Both AKT and MAPK pathways crosslink with CHK1 and other DDR proteins and are therefore strong candidates for CHK1i resistance via upregulation of alternative cell survival pathways. Both pathways are aberrantly activated in a wide range of cancers and are attractive targets for cancer therapy, however the benefits of targeted therapies are often limited due to complex cross-talk between many regulatory cell pathways (499).

Due to time constraints, these pathways and potential resistance mechanisms have not been examined in detail in this thesis. Further ongoing work has been performed by the Perkins' lab in order to investigate this. Some preliminary work looking at some of the potential areas of interest, such as AKT and proteins related to MAPK, has been performed and is shown in Section 4.15.

4.17. Validation of changes seen in AKT and associated proteins between the acute Eμ-Myc WT, Eμ-Myc/*c-Rel -/-* and Eμ-Myc/*RelA T505A* mouse models

Time was limited in the context of this study but preliminary validation studies were initiated to further explore some of the key findings shown in RNA-seq and with the proteomics data.

To investigate if changes seen in the proteomics data of the acute Eμ-Myc WT and Eμ-Myc/*c-Rel -/-* were demonstrated at the protein level, western blot analysis was performed. Eμ-Myc/*RelA T505A* mouse models were also included here although not directly compared in the proteomics data. Protein samples originate from lymph node tumours as previously.

Proteins examined included AKT and its downstream pathway proteins, including AMPK and GSK3β. Figure 4.20 shows results for AMPK and GSK3β and Figure 4.21 shows results for AKT.

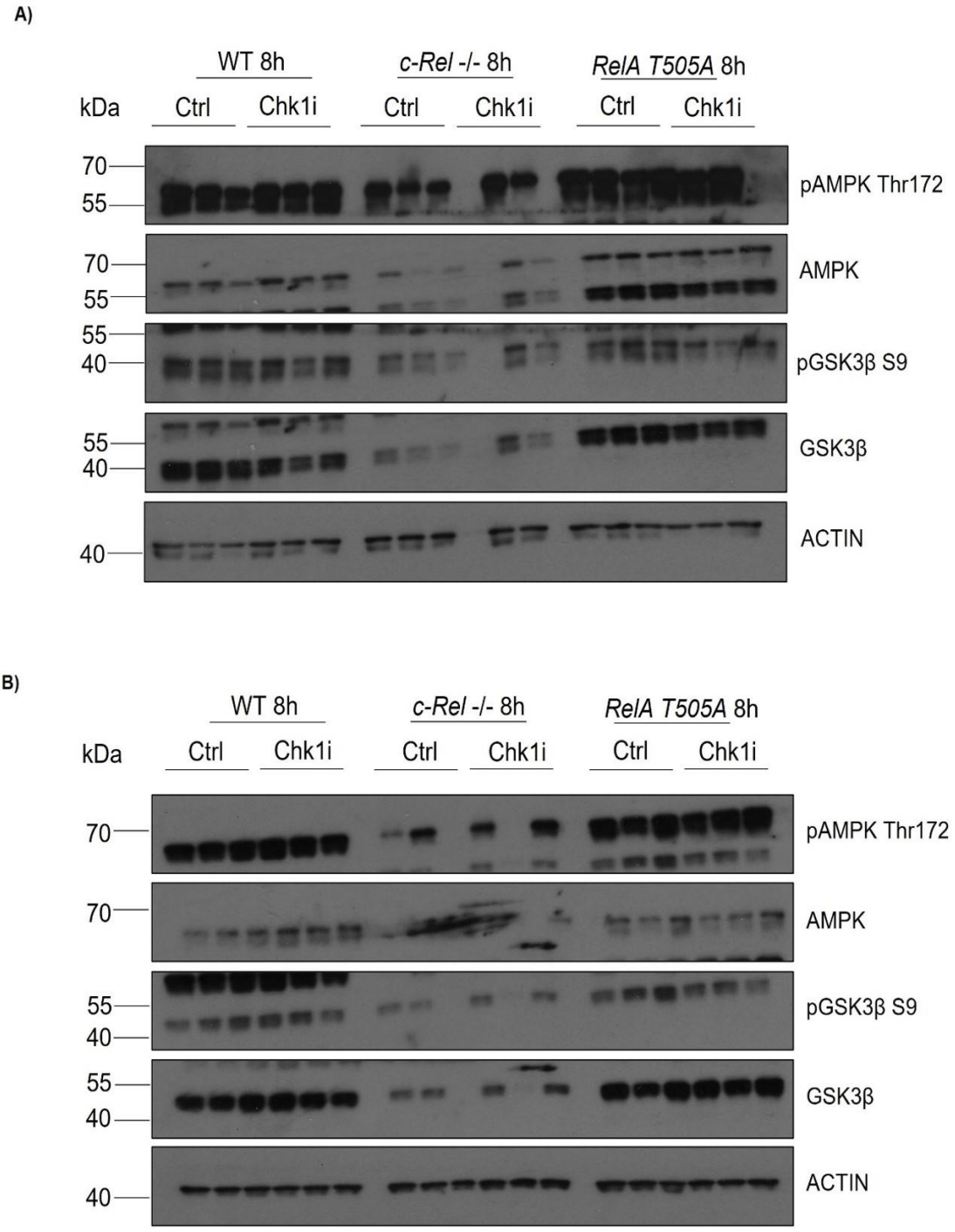

Figure 4.20. AMPK and GSK3β results in Acute Eμ-Myc WT, Eμ-Myc/*c-Rel -/-* and Eμ-Myc/*RelA T505A* mutant mice. Western blots showing AMPK and GSK3β in Eμ-Myc WT, Eμ-Myc/*c-Rel -/-* and Eμ-Myc/*RelA T505A* mutant models harvested 8 hours after a single dose of CCT244747 CHK1 inhibitor. N=1. Each blot shows results for 3 control treated and 3 CHK1i treated in each group in two separate sets of mice. A) and B) show different mouse sets – A) displays Eμ-Myc WT set 1, Eμ-Myc/*c-Rel -/-* set 5 and Eμ-Myc/*RelA T505A* set 3. Levels of pAMPK, AMPK, pGSK3β S9 and GSK3β are overall lower in the Eμ-Myc/*c-Rel -/-* mice but there is some variability seen between the individual mice. 1 CHK1i treated mouse sample cannot be analysed as the β ACTIN control has not shown therefore sample likely to be erroneous. B) Results for Eμ-Myc WT set 2, Eμ-Myc/*c-Rel -/-* set 6 and Eμ-Myc/*RelA T505A* set 4. As per A), levels are variable in the Eμ-Myc/*c-Rel -/-* mouse group with some showing downregulation of pAMPK, AMPK and pGSK3β S9 and GSK3β. Levels between Eμ-Myc WT and Eμ-Myc/*RelA T505A* mice appear to be similar in all groups.

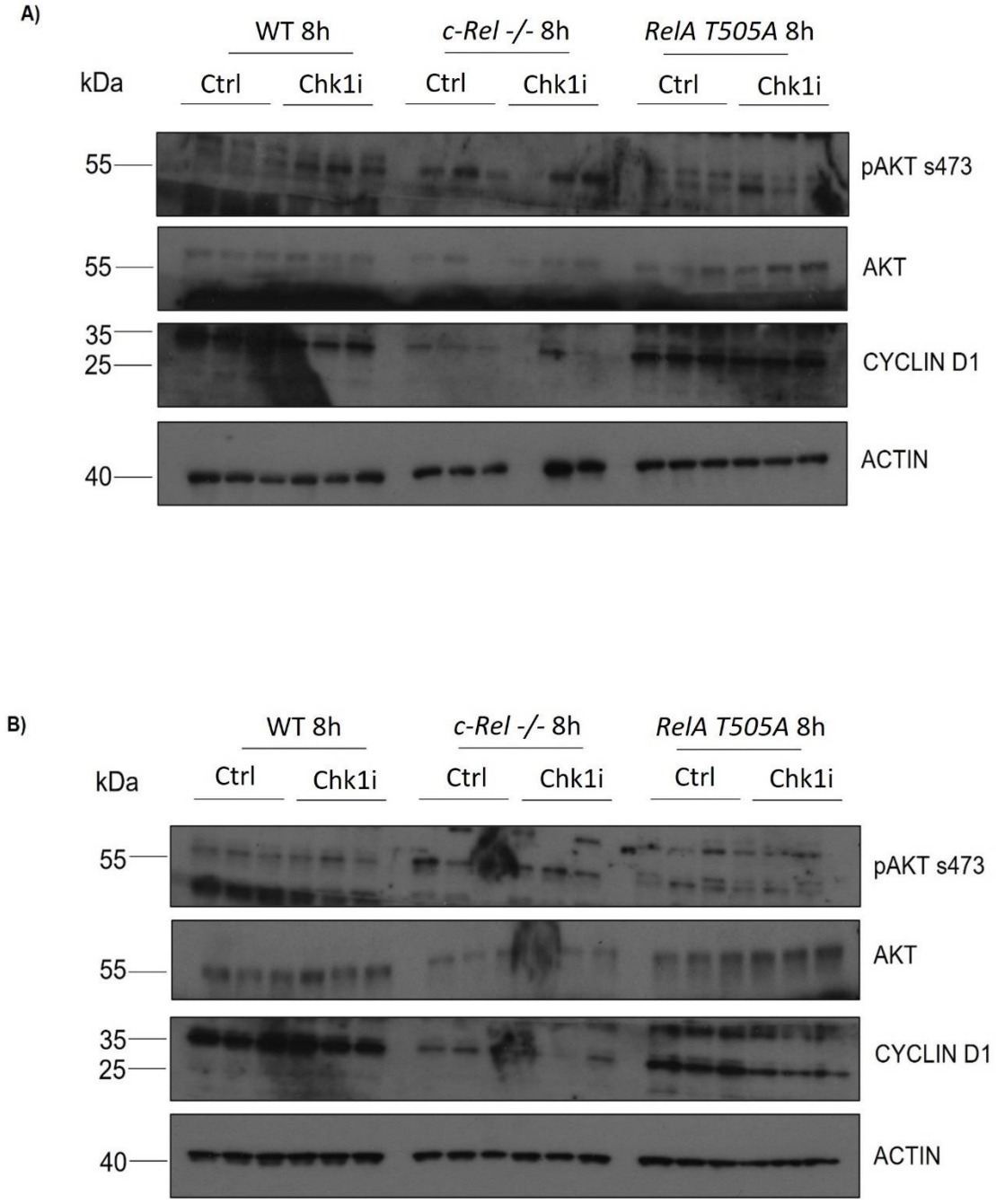

Figure 4.21. AKT and cyclin D1 results in Acute Eμ-Myc WT, Eμ-Myc/*c-Rel -/-* and Eμ-Myc/*RelA T505A* mutant mice. Western blots showing pAKT Ser473, AKT and cyclin D1 in Eμ-Myc WT, Eμ-Myc/*c-Rel -/-* and Eμ-Myc/*RelA T505A* mutant models harvested 8 hours after a single dose of CCT244747 CHK1 inhibitor. N=1. Each blot shows results for 3 control treated and 3 CHK1i treated in each group in two separate sets of mice. A) and B) show different mouse sets – A) displays Eμ-Myc WT set 1, Eμ-Myc/*c-Rel -/-* set 5 and Eμ-Myc/*RelA T505A* set 3. B) Displays results for Eμ-Myc WT set 2, Eμ-Myc/*c-Rel -/-* set 6 and Eμ-Myc/*RelA T505A* set 4**.** AKT levels overall are difficult to judge due to increased background signal in these blots. Levels of cyclin D1 appear to be lower in the Eμ-Myc/*c-Rel -/-* mutant mice. There are also multiple bands for the pAKT s473 blots, which could be indicative of non-specific binding for this antibody.

AKT signaling is activated by diverse stresses including hypoxia, metabolic stress, and oxidative stress (500). AMPK has been recognised as a regulator of the PI3K/AKT pathway in conditions of cellular stress including hypoxia (500). AMPK is activated by the growth factor EGF and phosphorylates S-Phase Kinase-Associated Protein 2 (Skp2) at Ser256. This promotes the integrity and E3 ligase activity of Skp2 SCF complex, leading to K63- linked ubiquitination and subsequent activation of AKT (500).

Figure 4.20 shows that levels of pAMPK, AMPK, pGSK3β S9 and GSK3β are generally lower in the CHK1i resistant Eμ-Myc/*c-Rel -/-* mice in comparison to the acute Eμ-Myc WT and Eμ-Myc/*RelA T505A* mice. A) shows 1 sample in the Eμ-Myc/*c-Rel -/-* category with a missing loading control, therefore this sample should be discounted. Within the other Eμ-Myc/*c-Rel -/-* mice in both A) and B) there appears to be some heterogeneity with pAMPK, AMPK, pGSK3β S9 and GSK3β levels. This could mean that whilst some mice display a downregulation of these pathways, other mice do not. This could also demonstrate that potential mechanisms of drug resistance can vary between mice and reflect what is shown in clinical practice. Overall, however, the GSK3β levels appear to increase in the Eμ-Myc/*c-Rel -/-* mice post CHK1i treatment.

Glycogen synthase kinase 3 (GSK3) is involved in the modulation of many metabolic processes, including protein and lipid synthesis, glucose and mitochondrial metabolism, as well as autophagy (501). GSK3 can have different functional roles depending on the cellular and signalling context (502,503). Phosphorylation of serine 9 in GSK3β causes the N-terminal tail of GSK3 to act as a pre-phosphorylated substrate and this has an inhibitory action (504). GSK3-mediated phosphorylation frequently leads to the inactivation and proteasomal degradation of its targets (501). Multiple signaling kinases feed into this site to increase the serine-phosphorylation of GSK3, including AKT, which can lead to a stimulation of glycogen synthesis in anabolic conditions (504). GSK3 can also phosphorylate AMPK to inhibit its catabolic activity (504,505).

Phosphorylated GSK3β appears to be lower in the Eμ-Myc/*RelA T505A* CHK1i treated mice in comparison to the control treated mice. pAMPK levels seem to increase in the WT mice post CHK1i treatment but these changes are not shown within the Eμ-Myc/*RelA T505A* mice post treatment and protein levels appear to be similar. Given that phosphorylation of GSK3β is inhibitory in nature, this could mean that GSK is more active in the metabolic regulation of the cell in the Eμ-Myc/*RelA T505A* mice. Phosphorylation of GSK3β in the Eμ-Myc WT mice could correlate with increased cellular stress and the requirement to modify other cell pathways in order to survive.

Other studies have shown that deprivation of glucose in cells activates AMPK. This causes phosphorylation of CHK1 on an alternative site at Ser280 leading to subsequent β-TrCP binding and ubiquitination for CHK1 degradation (500). It has been suggested that the AMPK-CHK1-β-TrCP axis plays an important role in the regulation of CHK1 in growth environments that favour tumourigenesis (506). This could be significant in the CHK1 resistant Eμ-Myc/*c-Rel -/-* mice as a reduction in CHK1 by degradation would aid cell survival in conditions of high cellular turnover and low levels of glucose.

Figure 4.21 shows pAKT Ser473, AKT and cyclin D1 for all mouse groups. Again, protein signal is seen in the Eμ-Myc/*c-Rel -/-* mice indicating that there is protein detectable in these samples despite lack of signal for the ATR/CHK1 pathway. pAKT Ser473 and AKT are difficult to assess due to poor quality blots and the presence of background signal.

Levels of cyclin D1 appear to be lower in the Eμ-Myc/*c-Rel -/-* CHK1i resistant mice. I have previously shown that levels of DNA damage proteins tested in the Eμ-Myc/*c-Rel -/-* mice have decreased. Therefore, a low level of cyclin D1 would correlate with the previous pattern shown in Figure 4.10 and Figure 4.12. Cyclin D1, with its binding partners CDK4 and CDK6, forms active complexes that promote cell cycle progression in the G1/S phase. This cell cycle checkpoint is normally highly regulated by CHK1. If this is downregulated, then this could correlate with a lower dependence on CHK1 for cell checkpoint regulation in this resistant mouse model. This correlates with the pattern previously seen with

downregulated cyclin D1 in resistant cell lines treated with the PF-00477736 CHK1 inhibitor in mantle cell lymphoma (206).

The quality of the western blots for AKT and pAKT, however, are not great and blots would have to be repeated to examine these proteins further. There are also multiple bands for the pAKT S473 blots, which could be indicative of non-specific binding for this antibody. Repeat analysis was not performed in this study due to time constraints. Further validation of this pathway would also be required, as upstream proteins such as PI3K have not been examined in this study.

ZAP-70 was also tested in these experiments as it has been shown to interact with the MAPK pathway in previous studies (507,508). ZAP-70 is a T cell antigen receptor (TCR) associated protein that when activated can impact on several signalling cascades (507). Over-expression of ZAP-70 is linked to chronic lymphocytic leukaemia and enhanced B-cell receptor signalling and cell survival (509,510). There is a recognised feedback loop involving p38 MAPK and ZAP-70 which can modify the T cell immunity response (508). MAPK is directly phosphorylated and activated by ZAP-70 downstream of the TCR, which in turn can also phosphorylate Thr293 in the interdomain B region of ZAP-70 (508).

The results for ZAP-70 are shown in Figure 4.22. ZAP-70 levels appear to increase in the Eμ-Myc WT group post treatment and reduce in both the Eμ-Myc/*c-Rel -/-* and Eμ-Myc/*RelA T505A* groups. A reduction of ZAP-70 in the context of raised MAPK activity in the Eμ-Myc/*c-Rel -/-* mice could indicate a change in cell regulatory pathways in the lymphoma, as you would expect levels to be elevated in a drug resistant cellular model. This is, however, highly complex, and the regulatory changes seen in these mouse models have shown crosslinking of multiple cell regulatory pathways. There are also several bands present for ZAP-70 and this could represent non-specific binding for this antibody. Therefore, more work would be needed to investigate these patterns of ZAP-70 expression further.

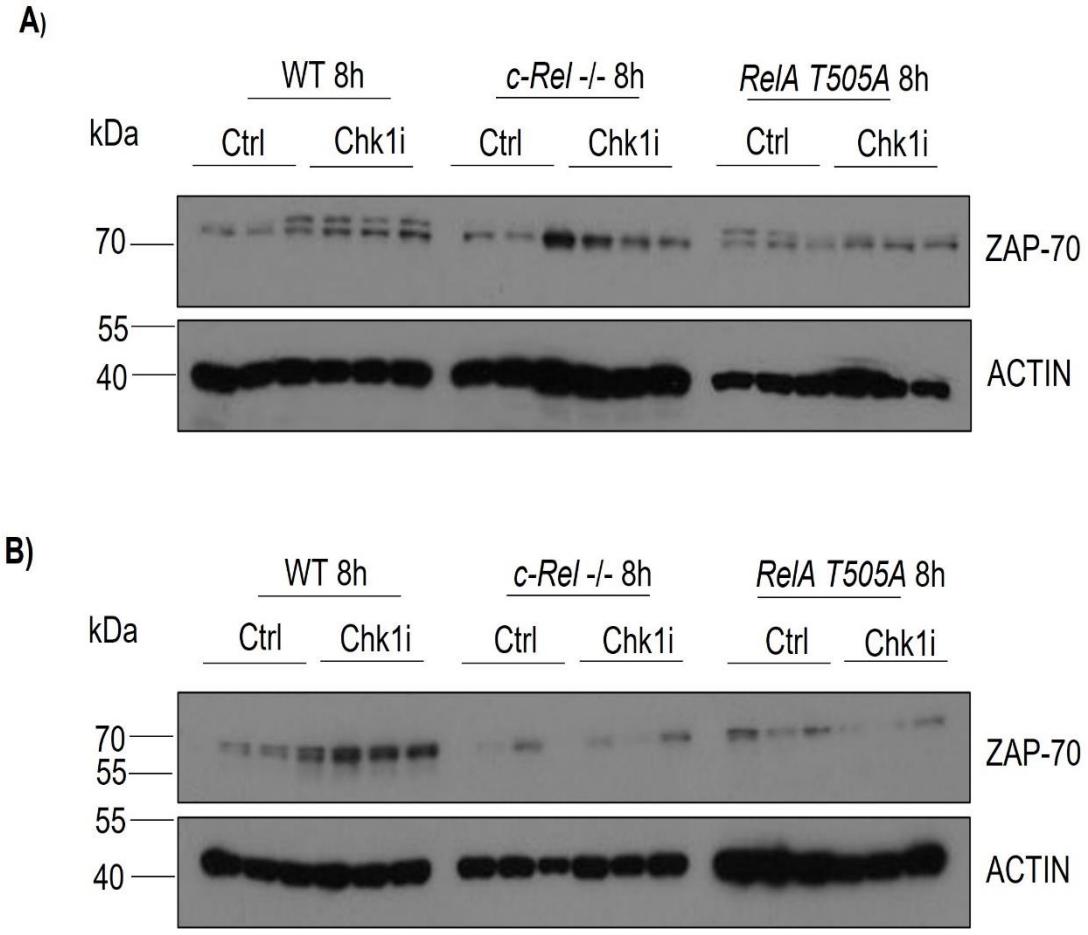

Figure 4.22. ZAP-70 results in Acute Eμ-Myc WT, Eμ-Myc/*c-Rel -/-* and Eμ-Myc/*RelA T505A* mutant mice. Western blots showing ZAP-70 in Eμ-Myc WT, Eμ-Myc/*c-Rel -/-* and Eμ-Myc/*RelA T505A* mutant models harvested 8 hours after a single dose of CCT244747 CHK1 inhibitor. N=1. Each blot shows results for 3 control treated and 3 CHK1i treated in each group in two separate sets of mice. A) and B) show different mouse sets: A) Results for Eμ-Myc WT set 1, Eμ-Myc/*c-Rel -/-* set 5 and Eμ-Myc/*RelA T505A* set 3. B) Results for Eμ-Myc WT set 2, Eμ-Myc/*c-Rel -/-* set 6 and Eμ-Myc/*RelA T505A* set 4. ZAP-70 levels appear to be less in both Eμ-Myc/*c-Rel -/-* and Eμ-Myc/*RelA T505A* mouse groups in response to treatment compared to the WT group. There are multiple bands for ZAP-70 in the western blots which could represent non-specific binding.

4.18. Chapter summary and discussion

I have further explored the DNA damage response in the CHK1i sensitive Eμ-Myc and CHK1i resistant Eμ-Myc/*c-Rel -/-* and Eμ-Myc/*RelA T505A* mouse models. I have shown that DDR gene expression is increased post CHK1 inhibitor after 9 days of CCT244747 treatment in the Eμ-Myc model, but in contrast this is not shown in the Eμ-Myc/*c-Rel -/-* model. No clear differences are demonstrated at the protein level in either mouse group after 9 days of treatment. The major caveat of the 9 day study is that it is difficult to establish if we are truly identifying sensitivity in the Eμ-Myc mice, or a response from the tumour cells that have evaded treatment thus far. This could also be a representation of normal gene expression in response to the CHK1i treatment. These results do not explain the lack of DDR upregulation in the Eμ-Myc/*c-Rel -/-* mice.

Differences in mRNA and protein stability could cause the variation in results between mRNA and protein. Changes in mRNA and protein can both occur quickly. The half-life for mRNA is short at approximately 10-20 hours, whereas proteins are more stable with a half-life of up to 48-72 hours (511). Therefore, changes in protein at 9 days may be more reflective of the CHK1i drug response after this time period. Changes in mRNA in this study could still be reflective of the mRNA response after 9 days of CHK1i therapy.

In order to further explore drug sensitivity, we developed a model examining the acute response to CCT244747 after a single dose. This showed very little change in gene expression across the board, or more specifically of genes associated with the DDR in the Eμ-Myc model after CHK1 inhibitor, even though these mice are sensitive to the compound. It could be possible that this is because this is not seen in the acute response to treatment, however 8 hours is more likely to be too short a time period for a transcriptional change. It could also be reflective of mRNA instability compared to protein, and changes may have resolved due to a short mRNA half-life (511).

My western blotting data and the large scale (phospho) proteomic analysis illustrated that there was a change in protein expression at 8 hours in the Eμ-Myc model with an increase

in the phosphorylation of CHK1 and H2AX. This demonstrates that the cells are attempting to upregulate ATR and that DNA damage is occurring in this responsive model.

More striking changes, however, were shown at the protein level in the resistant Eμ-Myc/*c-Rel -/-* mice, with a complete downregulation of the DDR. This could be the way that these tumour cells manage to survive CHK1i treatment, as less DNA damage is both recognised and generated. This may also explain why tumours grow more quickly in this mouse model as there is less regulation with cell cycle control. The Eμ-Myc/*RelA T505A* mice do upregulate the DDR in response to DNA damage but like the Eμ-Myc/*c-Rel -/-* mice are resistant to CHK1 inhibition. Therefore, it is likely that this mouse model has a different route of drug resistance.

CLSPN levels were low in the Eμ-Myc/*c-Rel -/-* model as demonstrated previously by the Perkins' lab, however other DDR genes were also downregulated in this model. Previous studies have shown that the NF-κB subunit *c-Rel* can regulate *CLSPN* transcription (252). Claspin normally mediates the phosphorylation and subsequent activation of CHK1 by ATR, therefore downregulation of Claspin could potentially lead to downregulation of downstream proteins such as CHK1 and ATR (252). The Eμ-Myc/*c-Rel -/-* is a knockout model of *c-Rel*, therefore this may have altered the mouse model's ability to regulate Claspin and may be a mechanism of drug resistance. This does not however account for the drug resistance shown in the Eμ-Myc/*RelA T505A* mouse which appears to have developed CHK1i resistance by a different mechanism.

There are many genes involved in cell cycle regulation and the DNA damage response and it could be that we have not identified the pathways involved in the mechanisms of drug sensitivity and drug resistance at this stage. Therefore, a more global investigation into gene expression was required to establish if we are identifying the correct genes involved in the drug response. The proteomics analysis showed that genes in the PI3K/AKT and MAPK pathways including *AKT1*, *ERK1*, *JNK1* and *p38 MAPK* were upregulated in the Eμ-Myc/*c-Rel -/-* mouse model. RNA-seq data showed that *USP1* and *USP14* were downregulated in this mouse model and that *USP53* and *USP35* were upregulated in this mouse model.

Preliminary validation work has shown that USP1 is downregulated in the Eμ-Myc/*c-Rel -/-* mice but there can be some heterogeneity between the Eμ-Myc WT mice at the protein level. The lack of USP1 could be a route of CHK1 pathway downregulation, as USP1 normally protects CHK1 from proteasomal degradation. A loss of USP1 in the Eμ-Myc/*c-Rel -/-* could be leading to CHK1 breakdown.

There could also be crosstalk between USP1 and AKT. USP1 has previously been reported to be a negative regulator of AKT. USP1 has been demonstrated in mouse muscle to act as a direct DUB for AKT, and USP1 depletion in mouse muscle increased Akt ubiquitination and subsequent glucose uptake during fasting (512). USP1 has also been shown to regulate AKT phosphorylation by modulating the stability of PH domain leucine-rich repeat protein phosphatase 1 (PHLPP1) in lung cancer cells (513). It would be therefore interesting to explore both USP1 and AKT in more detail in relation to the Eμ-Myc/*c-Rel -/-* mouse model.

AKT was difficult to identify clearly on the preliminary western blots and these experiments need to be repeated and blotting conditions improved in order to assess properly. No specific pathways were implicated in the Eμ-Myc/*RelA T505A* mouse model, making it difficult to establish a direct cause for drug resistance in this model.

Given the importance of CHK1 in cell survival, it may be difficult to identify one single pathway that is leading to a difference in response in these animal models. Indeed, we can see a difference in DDR regulation between the two drug resistant models used here. It may however provide us with an idea of the significant genes involved to allow further exploration of resistance mechanisms in response to CHK1i treatment.

Further suggested work

To further validate the findings of PIK3/AKT and MAPK upregulation and USP1 downregulation in the Eμ-Myc/*c-Rel* -/- CHK1i resistant mouse models, it would be useful to further explore protein expression in these mouse models at the 8-hour time point. This would involve the exploration of other parts of the pathway, such as PI3K upstream of AKT and to explore the role of GSK3β in cell survival. More time needs to be spent on the optimisation of the western blots to obtain good quality blots. Depending on outcomes, it would be useful to examine what happens in cellular knockout models of USP1, USP14, USP53, USP35 and AKT. This could be done through small interfering RNA (siRNA) from cells generated from the resistant mouse models.

To check if drug response is a single CHK1 inhibitor effect or a drug class effect in the Eμ-Myc CHK1i sensitive mice and the Eμ-Myc/*c-Rel -/-* and Eμ-Myc/*RelA T505A* CHK1i resistant mice, studies could be repeated in the mouse models using other CHK1i. This, however, must be balanced with the generation of further mice and use of animal models which takes time and is under strict regulation.

It would also be useful to explore what happens in the Eμ-Myc/*c-Rel -/-* drug resistant mice if drugs to block either PI3K or AKT in combination with the CHK1 inhibitor CCT244747. It may show that drugs given in combination can overcome the CHK1 inhibitor resistance by overcoming the CHK1i blockade provided by activation of these proteins. Drug toxicity in combination would have to be accounted for, as it may be that these type of drugs in combination are not tolerated well in animal models. Drugs in combination also have to be dosed differently due to potential increased toxicity and drug availability.

In this chapter I have shown some alterations in the Eμ-Myc/*c-Rel -/-* mouse model that correlate with CHK1i resistance. I have also recognised that the Eμ-Myc/*RelA T505A* mouse model has a different mechanism of drug resistance and that due to the importance of CHK1 and the DDR pathways in cell survival, there may be multiple mechanisms of CHK1i drug resistance.

In the next chapter I will explore what happens in a generated cell model with an acquired resistance to CHK1 inhibition and how this compares with the innate CHK1i resistance in the Eμ-Myc *c-Rel -/-* and Eμ-Myc/*RelA T505A* mouse models.

5. Results 2: What happens to global gene expression and the phosphoproteome in response to CHK1 inhibitor treatment in sensitive (and resistant) models?

5.1. Introduction to chapter

Previous data within this thesis (Chapter 4) has identified that Eμ-Myc/*c-Rel -/-* mouse lymphomas resistant to the CHK1i, CCT244747, exhibit downregulation of the ATR-CHK1 pathway. Potential mechanisms for this downregulation could be down to loss of the adaptor protein, Claspin, or loss of the deubiquitinases, USP1 and USP14. Proteomics data has also shown that alternative pathways could be upregulated, such as the PI3K/AKT pathway to potentially enhance cell survival. The Eμ-Myc/*c-Rel -/-* mouse model is a *de novo* model of drug resistance so no response is shown to the drug from the offset.

Drug resistance is a common issue in oncology as cancers can mutate or modify pathway responses through upregulation or downregulation in order to survive despite treatment with systemic therapy (311,430,514). This can be *de novo* in origin, as demonstrated in this mouse model, or resistance can also be acquired in response to mutational changes on systemic therapy (328,329). I therefore also wanted to determine whether similar mechanisms of CHK1i resistance could be generated in a cellular model of acquired drug resistance.

In clinical practice, there can be marked individual patient variation regarding sensitivity to anticancer therapies (515). Traditionally patients with the same primary tumour type would have all been treated with the same chemotherapeutic agents to variable effect (515,516). Over the last ten years, practice in oncology has been moving to a more personalised treatment approach. For some tumour types, patients are treated not by the tumour primary site but given targeted therapy based on the tumour mutational status (273,274). This means that the patients most likely to respond to the drug can be selected, but also patients likely to be non-responders can avoid lengthy treatments and side effects (233).

Previous CHK1i trials have shown that patients display different sensitivity to CHK1 inhibitors in combination with other treatments (138). The SRA737 monotherapy trial, as previously discussed, was recruiting patients most likely to respond to CHK1i treatment as a single therapeutic modality (264), but the mechanisms behind CHK1i resistance are still not known.

Utilising *in vitro* models to investigate the basic biology around CHK1i resistance mechanisms provide us with useful tools in order to study and manipulate the system. We have already explored CHK1 inhibitor resistance within the Eu-Myc mouse model displaying *de novo* CHK1i drug resistance. We have also created a cellular model of acquired CHK1i resistance. This chapter will therefore explore what happens to gene and protein expression within a generated CCT244747 drug resistant cellular model and further investigate potential mechanisms of drug resistance.

5.2. Chapter aims and hypothesis

Research aim - To develop and characterise *in vitro* models of acquired CHK1 inhibitor resistance and compare these with *in vivo de novo* models of resistance to CHK1 inhibitors.

Hypotheses

- Different cell line models will exhibit differential sensitivity to CHK1 inhibitor treatment.
- Cell lines resistant to CHK1i will have developed biochemical changes in key DDR pathway components to evade death by CHK1 inhibitors.

5.3. Determining a cell line system suitable for the development of a model of acquired resistance to CCT244747

In order to determine which cell line model to take forward and use to develop a model system for CHK1i resistance, I first wanted to assess CCT244747 CHK1i sensitivity in a number of cell line models. Cell lines chosen were lines commonly used in the Perkins' lab. Table 5.1 shows the cell lines, tissue of origin and key mutations present. All original cell lines in this project were obtained from ATCC and the summary information in Table 5.1 is from ATCC (409). U2OS, an osteosarcoma cell line, was selected as cells have an intact DNA damage pathway. This cell line can also be easily transfected and manipulated for investigation of DNA markers. This is important when assessing drug sensitivity vs drug resistance in matched models.

The prostate cancer cell line PC3 was selected as well as the colorectal cell lines SW620 and HCT15. These cell lines were selected due to the phase 2 expansion of the SRA737 CHK1i clinical trial in both prostate and colorectal cancers.

Table 5.1. Key mutations in cell lines used in preliminary studies to assess CHK1i sensitivity. The data detailing the cell mutations was obtained from ATCC resources. HCT15, SW620 and PC3 cell lines have mutations in key oncogenes such as *RAS* and *MYC*, and tumour suppressor genes, such as *TP53*. These cell lines also have mutations which can impact on DNA damage response function. The U2OS cell line does not have any proven mutations in these pathways.

Cell line	Tissue origin	Key mutations
U2OS	Osteosarcoma	Multiple chromosome re-arrangements
HCT15	Colorectal	*TP53*, *KRAS*, *CHEK2*, *FANCD2*, *MLH1*, *APC*
SW620	Colorectal	*c-MYC*, *KRAS*, *HRAS*, *NRAS*, *TP53*, *APC*
PC3	Prostate	*TP53*, 62 chromosomes

PrestoBlue cell viability assays were performed in U2OS, PC3, SW620 and HCT15 cell lines. This was performed as a preliminary study (N=1) to assess the cell viability following CHK1 inhibition. The cell lines were treated with a high dose of the CHK1i CCT244747 (2µM) and assessed at both the 24 hour and 48 hour time points. This was to ensure that the CHK1i killed the cells and to assess that a change in response could be detected using cell viability assays. Figure 5.1 shows that treatment with 2µM CCT244747 reduced cell viability in the U2OS, HCT15 and SW620 cells but there was no response in the PC3 cells.

Subsequent cell viability assays were performed with a titrating dose of the CHK1i CCT244747 from 0.1µM to 10µM. Cells were counted and seeded into 96 well plates. All cells were treated and exposed to drug for 24 and 48 hours before PrestoBlue evaluation was performed. Dose response curves of CCT244747 were generated and IC_{50} values calculated (Figure 5.2 and Table 5.2).

Figure 5.2 shows that cell viability was impacted with drug CHK1 treatment in U2OS and SW620 cells, and the PC3 cells were resistant to CHK1 inhibition, which is consistent with the initial findings (Figure 5.1). However, in this case, the HCT15 cell line did not respond to the CHK1 inhibitor. Table 5.2 shows a summary of IC_{50} values for all 4 of the cell lines treated with CHK1i. U2OS cells were sensitive to CHK1 inhibition (IC_{50} 1µM). SW620 cells showed a response at higher levels of CHK1i (IC_{50} 5µM), but HCT15 and PC3 cell lines were highly resistant to the drug (IC_{50} not calculable as curves could not be fitted).

A)

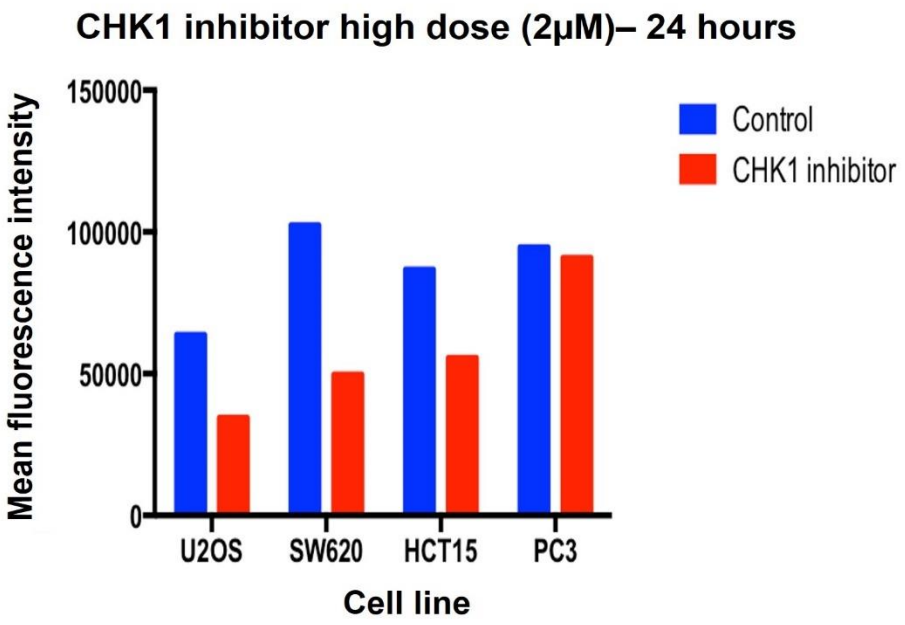

B)

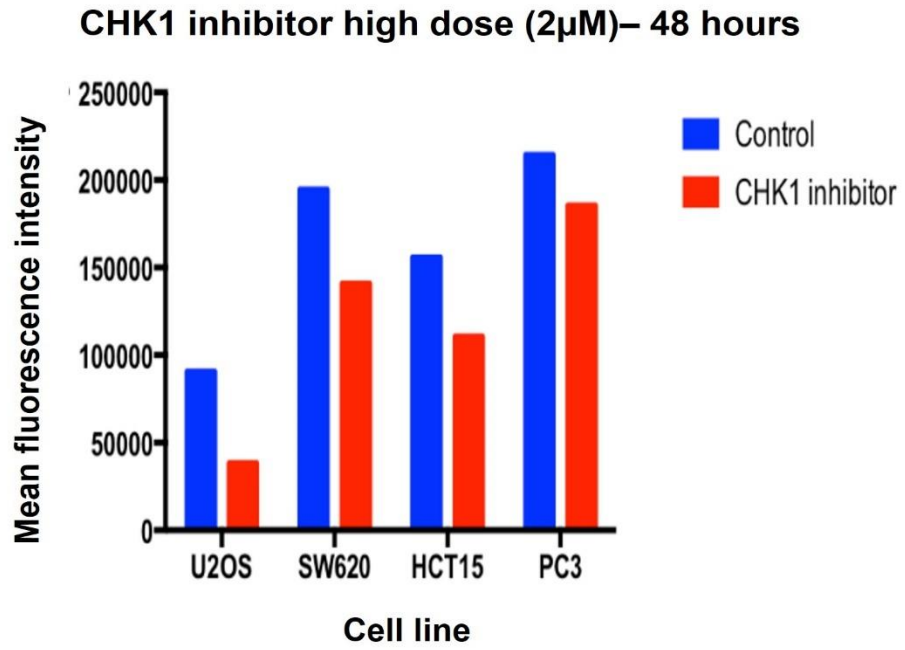

Figure 5.1. PrestoBlue cell viability assay can be used to assess cell number changes. N=1 for all cell lines. Absorbance was recorded at 570nm after a 60-minute incubation of cells with the PrestoBlue reagent. Gain was set at 50% from the well containing the lowest cell number. Cells were treated with high dose CCT244747 CHK1 inhibitor (2μM) for A) 24 and B) 48 hours to establish that a clear change in cell number after CHK1 inhibitor treatment could be detected. The figure shows from the reduction in mean fluorescence intensity that the greatest cell number changes were seen in the CHK1i sensitive U2OS cell line in comparison to the SW620, HCT15 and PC3 cell lines.

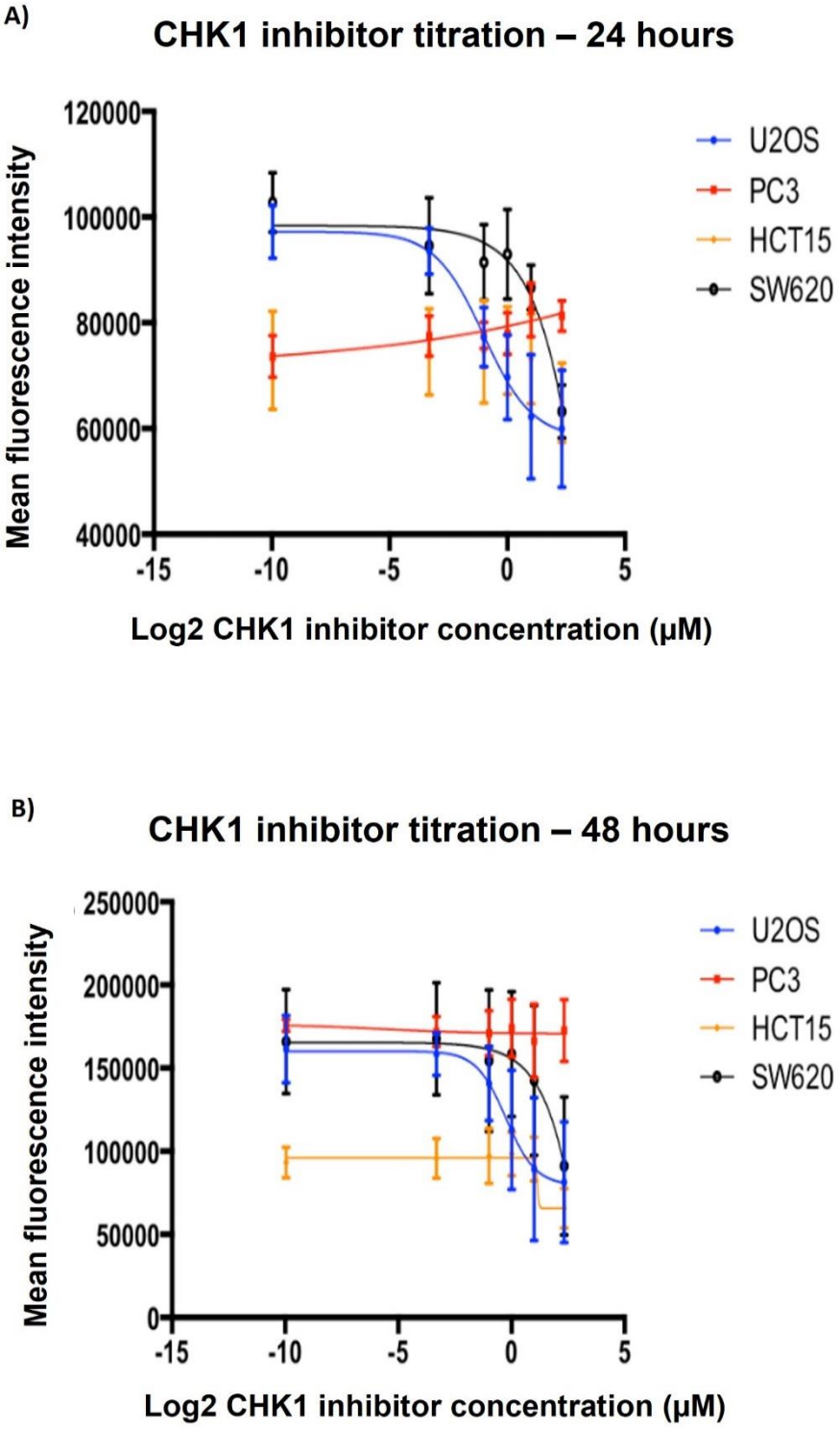

Figure 5.2. Different cell lines respond differently to the CHK1 inhibitor CCT244747. N=3 for all cell lines. Absorbance was recorded at 570nm after a 60-minute incubation of cells with the PrestoBlue reagent. Gain was set at 50% from the well containing the lowest cell number. A) CHK1 inhibitor titration at 24 hours and B) at 48 hours. Note that values at -10 are cells treated with vehicle control only. U2OS cells show the greatest reduction in mean fluorescence intensity indicating less viable cells as the CHK1i dose increased. There is very little change in mean fluorescence intensity in the PC3 and HCT15 cells indicating no clear change in cell viability. There is some change in mean fluorescence intensity in the SW620 cells at higher drug concentrations, however the change is less pronounced than in U2OS cells. Data presented as mean ± SEM. Curves are 4 parameter line fits using Graphpad Prism.

Table 5.2. IC_{50} values for preliminary cells treated with the CHK1 inhibitor CCT244747. U2OS cells showed sensitivity to treatment with CHK1i. SW620 cells also showed some drug sensitivity but more drug was required to initiate a change in cell viability. PC3 and HCT15 cells were resistant to CHK1i inhibition and IC_{50} values could not be calculated.

Cell line	IC_{50} for CCT244747 CHK1i treatment
U2OS	1μM
HCT15	*IC_{50} not calculable as curves could not be fitted*
SW620	5μM
PC3	*IC_{50} not calculable as curves could not be fitted*

Based on these pilot studies, the U2OS osteosarcoma cell line was selected for generation of CHK1i resistance. This cell line is sensitive to CHK1 inhibition and growth can be measured well, as shown in Figures 5.1 and 5.2. With regards to cell line characteristics, the U2OS cell line has multiple chromosome rearrangements (which could be an indicator of genetic instability) but it does not have a notable oncogenic driver such as a *RAS* or *MYC* mutation compared to other cell lines tested. SW620 cells showed some response to CHK1 inhibition, but this cell line is not as sensitive as the U2OS cell line. PC3 cells and HCT15 cells were highly resistant to CHK1 inhibiton. These cell lines would not be favourable for generating a resistant cell line as the CHK1i does not have any impact on cell growth at baseline and it is important to select a CHK1i sensitive line when generating a CHK1i resistant line for comparison of drug effects.

Table 5.1 shows that the PC3 cell line has 64 chromosomes, which could potentially lead to increased chromosomal instability. There is also a *TP53* mutation in the prostate cancer cell line. HCT15 cells also have a *TP53* mutation as well as multiple other potential oncogenic drivers, including *KRAS* and the mismatch repair protein mutation *MLH1*. The presence of a *TP53* mutation in these cell lines in theory would increase CHK1i sensitivity due to a possible increased dependence on CHK1 for survival, but this has not been demonstrated here. It is likely that the additional mutations in these cell lines are leading to drug resistance with upregulation of alternative cell survival pathways, as shown in the Eμ-Myc/*c-Rel -/-* mouse model in Chapter 4.

Table 5.1 shows that the SW620 cell line has a mutation in *c-MYC*, a gene upregulated and driving the lymphoma in the Eμ-Myc model which may explain drug sensitivity, however CHK1i response is not as pronounced as the U2OS cell line and the additional gene mutations such as *NRAS* may be impacting on drug sensitivity. This cell line also has a *TP53* mutation, but has some response to the drug, therefore the presence of a *TP53* mutation does not exclusively lead to CHK1i resistance.

The DNA damage response pathway in U2OS cells, including the ATR/CHK1 pathway, is also intact. This is a favourable baseline feature prior to introducing drug resistance. This cell line was also chosen as it is used frequently in the Perkins' lab and can be genetically manipulated through CRISPR Cas-9 modifications, which would be useful for potential follow up studies of resistance mechanisms.

5.4. Generation of CHK1i resistant U2OS cell lines

The CCT244747 drug resistant U2OS cell model was generated by Dr. Jill Hunter. Figure 5.3 shows a summary of how the CHK1i resistant U2OS model was generated. U2OS cells were cultured in DMEM media with increasing doses of the CHK1 inhibitor CCT244747 starting at 0.1μM to a maximum concentration of 5μM. Surviving cells from each concentration were monitored and the dose was increased when confluency level hit 50%. Surviving cells were then cultured in DMEM media and used for further studies.

With each cell population generated, a control sample of U2OS WT cells cultured in DMEM media was also grown from the same starting U2OS cells. These cells were treated with DMSO at the same time as the CHK1 resistant cell lines received CHK1i treatment in case of DMSO related toxicity. Four separate CHK1 inhibitor resistant U2OS cell lines were generated in total.

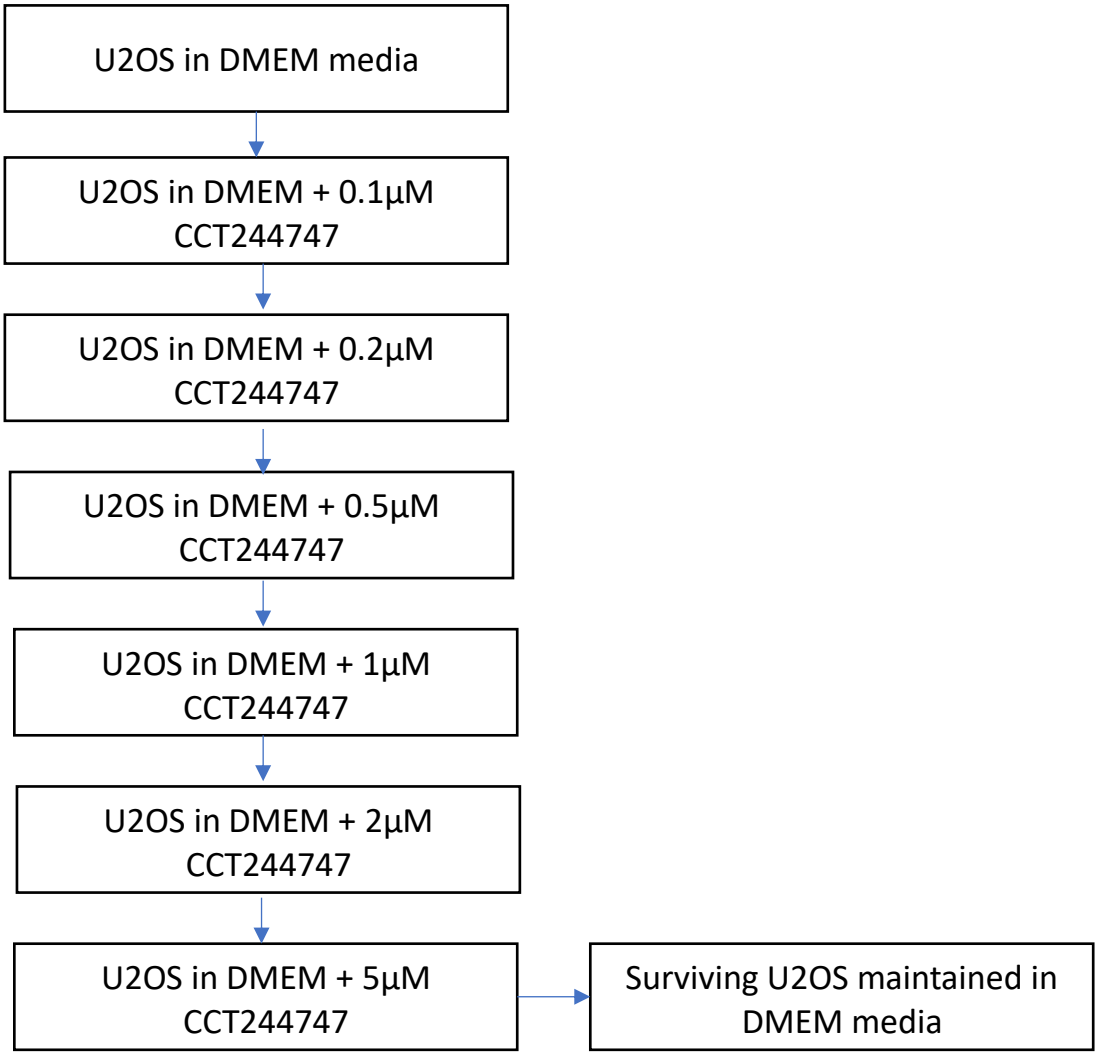

Figure 5.3. Generation of U2OS CHK1i resistant cell lines. U2OS cells were cultured in DMEM media with increasing doses of the CHK1 inhibitor CCT244747 starting at 0.1µM to a maximum concentration of 5µM. Surviving cells from each concentration were monitored and the dose was increased when confluency level hit 50%. Surviving cells were then cultured in DMEM media and used for further studies. With each cell line generated, a control sample of U2OS WT cells cultured in DMEM media alone was also grown from the same starting cells.

5.5. Resistance to the CHK1 inhibitor CCT244747 was confirmed in the generated U2OS CHK1i resistant cell lines using PrestoBlue growth assay and clonogenic cell viability assay studies

Once the resistant U2OS cell lines were established, I wanted to confirm resistance to CCT244747. This was done in both the CHK1i resistant (CR) U2OS and matched wild type (WT) U2OS cells using the cell viability, PrestoBlue assay.

Briefly, cells were dosed with the CCT244747 CHK1 inhibitor at incremental doses between 0.001 and 100μM for 24 hours. Previous data (Figure 5.2) had shown the IC_{50} of WT U2OS to be approximately 1μM. Dose response curves for the CHK1 inhibitor sensitivity between cell lines were generated. Results of the dose response curves are shown in Figure 5.4. This data is the mean of three independent experiments +/- the SEM. All WT U2OS cell lines showed a rapid drop in cell viability at 1μM dosing indicating cells were no longer viable at this dose. This is in keeping with the IC_{50} for the U2OS cell line. In contrast, the CR U2OS cell lines continue to show minimal change in cell viability until 10μM (x 10 the dose of the drug sensitive cell line).

At 10μM concentration of drug, there is likely to be an increased rate of off-target effects such as increased activity from other pathways and apoptosis from other routes. U2OS cells were unable to grow beyond 5μM of drug concentration when generating the resistant cell line. This again indicates that there is a reduction in drug tolerability at high drug concentration.

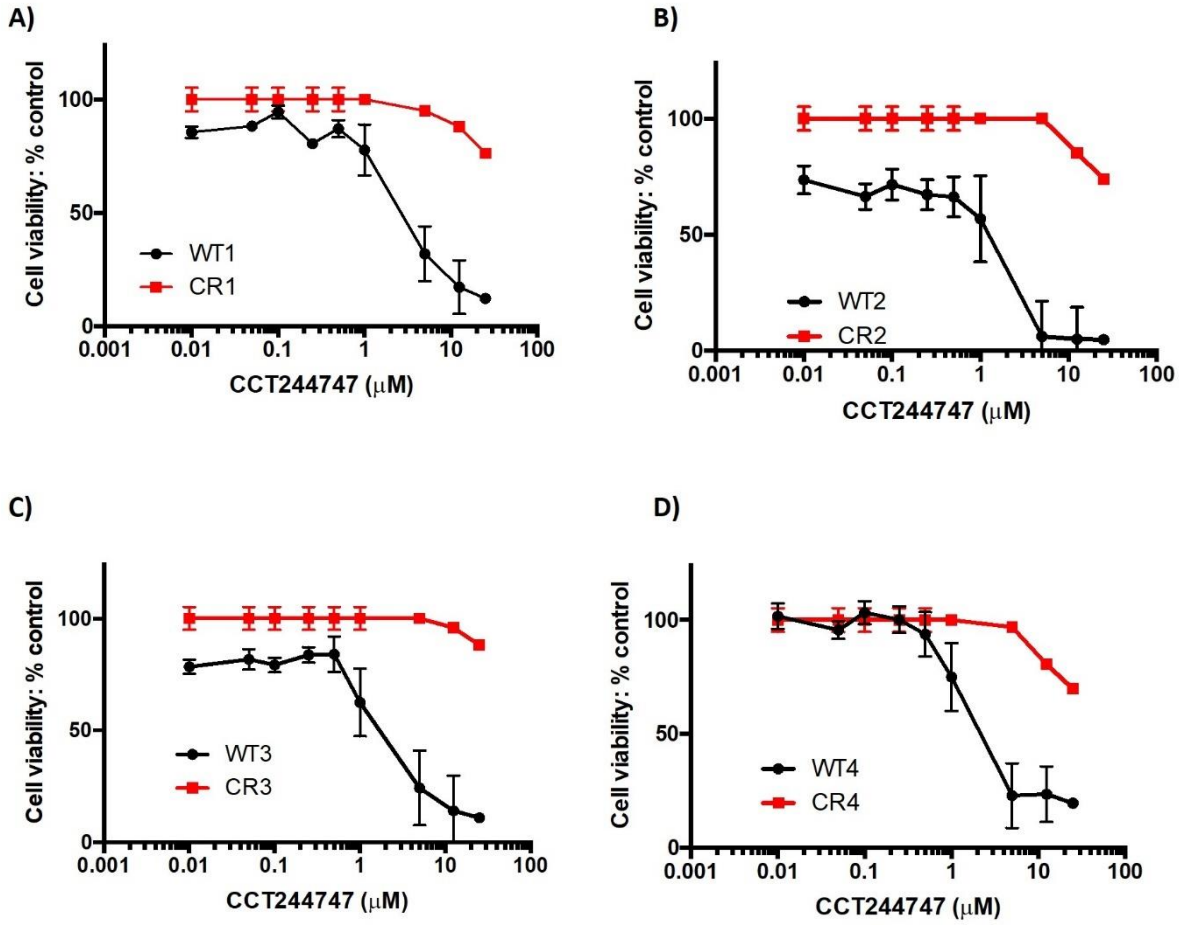

Figure 5.4. Generated CHK1 inhibitor resistant U2OS cell lines were confirmed as CCT244747 drug resistant using growth assays. Figure produced by Dr. J Hunter using GraphPad Prism and this figure plots cell viability change with increasing drug exposure. Conditions for these experiments were the same as previous - Fluorescence absorbance was recorded at 570nm after a 60-minute incubation of cells with the PrestoBlue reagent. Gain was set at 50% from the well containing the lowest cell number. Both WT and CHK1i resistant (CR) U2OS cells were treated with CCT244747 for 24 hours and PrestoBlue growth assays were performed. N=3 for all cell lines. A) is for WT and CR cell line 1; B) WT and CR cell line 2; C) for WT and CR cell line 3 and D) WT and CR cell line 4. Control consisted of untreated matched cells. All WT cell lines show a rapid decrease in cell viability at 1μM concentration. All CR cell lines show drug resistance with no drug response until 10μM response (x10 the dose level for the drug sensitive WT U2OS cell lines). At 10μM of drug exposure (which is a high level of drug exposure), cell viability can be affected by other off-target effects.

To further demonstrate CHK1 inhibitor resistance in the generated CHK1 inhibitor cell lines, clonogenic assays were performed for each cell line along with the WT control U2OS cell line. This assay tests the ability of a cell line to form colonies when seeded at very low density and is a very good measure of the survival following a drug challenge. It does not rely on the metabolic activity as a read-out as cell viability assays such as the PrestoBlue assay do (as discussed in Section 3.10.1), which are often seen as a caveat with that type of viability assay.

Briefly, cells were treated with 1µM CCT244747 CHK1 inhibitor then counted and seeded at very low densities after 24 hours to wait for colony formation. Controls for all experiments were DMSO treated matched cell lines. Cells were then fixed with Carnoys Fixative and stained with crystal violet before counting.

Results are shown in Figure 5.5. In all U2OS WT cells, treatment with 1µM CCT244747 resulted in a dramatic reduction in the number of surviving colonies. Importantly, all of the CR U2OS cell populations had a much greater clonogenic potential following CCT244747 treatment. All data shown are the mean of three independent experiments +/- SEM.

Taken together, the cell viability (Figure 5.4) and clonogenic survival data (Figure 5.5), confirmed that the cell lines generated were resistant to CCT244747. Going forward these could therefore be utilised as a model system to study acquired resistance to CHK1i.

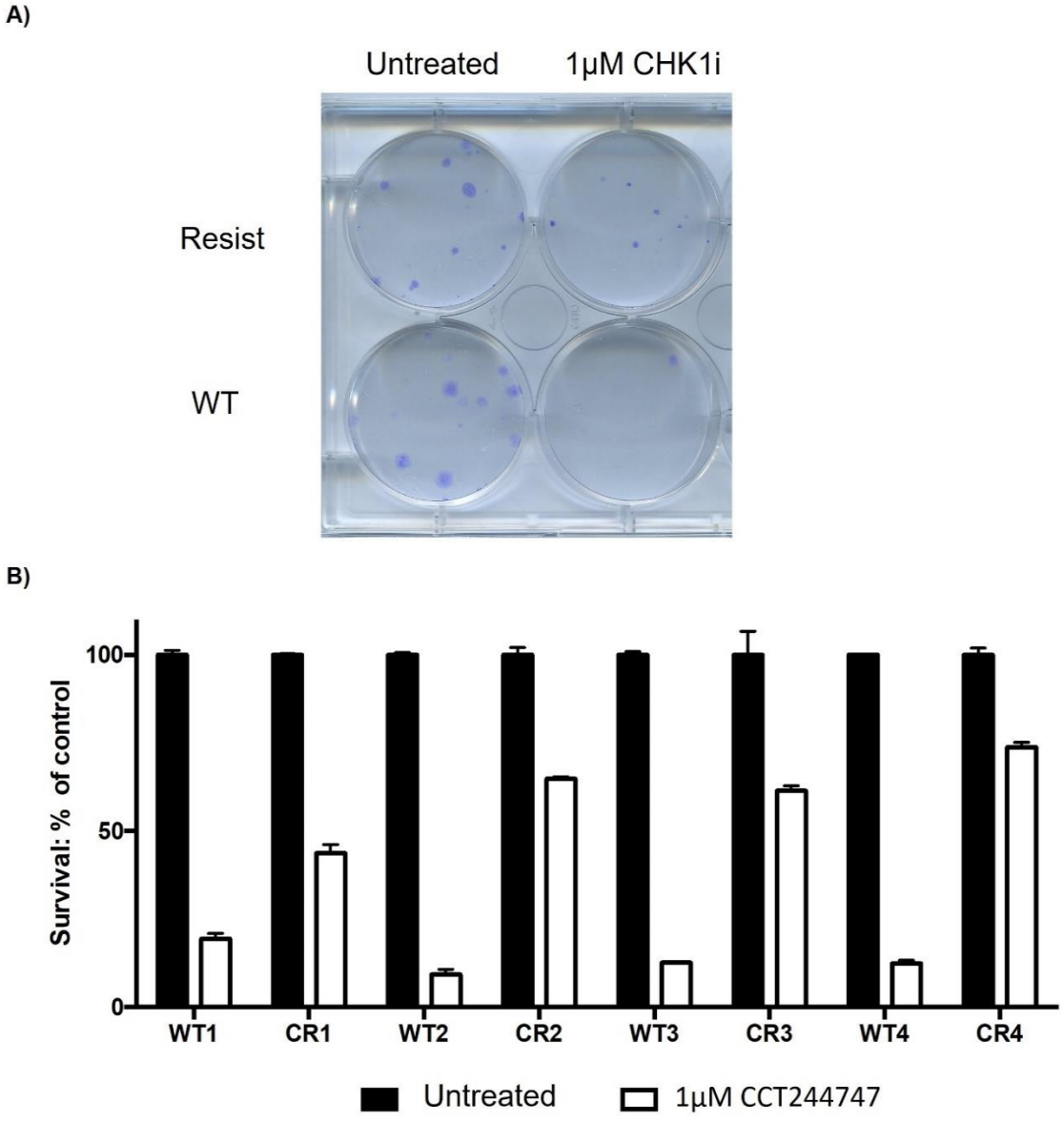

Figure 5.5. Generated CHK1 inhibitor resistant U2OS cell lines were confirmed as CCT244747 drug resistant using clonogenic assays. Both WT and CHK1i resistant (CR) U2OS cells were treated with 1μM CCT244747 and clonogenic cell survival assays were performed. Control for all cell lines were untreated matched cells. N=3 for all cell lines. A) Shows an example of colony formation in WT U2OS vs CR U2OS for cell line 1. B) Graph produced by Dr. J Hunter showing outcomes for all WT and generated CR U2OS cell lines. All WT cell lines show a rapid decrease in cell survival at 1μM concentration. U2OS cells do not typically form colonies well, therefore numbers for cell survival are also reduced in CR cell lines.

5.6. Morphological changes were seen in the generated U2OS CHK1i resistant cells in comparison to U2OS WT cell lines

Observation of the CR U2OS cells in culture revealed that they appeared to have morphological changes in comparison to the matched WT U2OS cell lines. In comparison to the WT U2OS cells, CHK1i resistant cells were observed to be more spaced out in culture and elongated in appearance. An example of this is shown in Figure 5.6 with WT and CR cell line 1. Cell growth was also seen to be slower in the CR cells.

The U2OS CHK1i resistant cell lines also appeared to behave differently to WT matched cell lines when splitting cell cultures. The CR cells were more adhesive and took longer to dissociate from the flask when in 1% trypsin. Following this observation, both U2OS WT and U2OS CR cell cultures were viewed under microscopy at 20X magnification whilst in 1% trypsin. Images were captured at intervals to monitor when cells had become unfixed. Figure 5.7 shows an example of the U2OS WT cell lines undergoing cell trypsinisation.

U2OS WT cells were fully free in suspension when captured at the 10 minute interval. In contrast, the U2OS CR cell lines took 15 minutes to become free in suspension. Figure 5.8 shows how the U2OS CR cells looked morphologically different in comparison to the WT cells and that CR cells took longer to become free in cell suspension. The U2OS CR cells appeared clumped in appearance rather than appearing in suspension as individual cells like the matched WT cell line.

Changes in cell shape are seen with the CR U2OS cells in comparison to the WT U2OS cells and the CR U2OS cells are more adherent in culture. The behaviour and morphological changes of the U2OS CHK1i resistant cell line led to the hypothesis that changes in the CR cell lines could be due to changes in epithelial–mesenchymal transition (EMT). Classical EMT results in the transition of epithelial cells with a mesenchymal phenotype (517,518). Cells undergoing EMT can change in morphological appearance with cell elongation and loss of cell-cell junction in culture (519).

A)

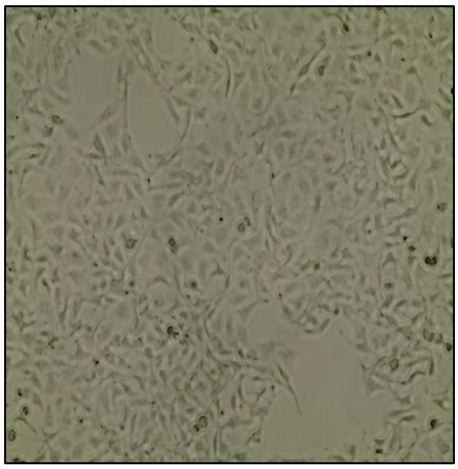

WT U2OS

B)

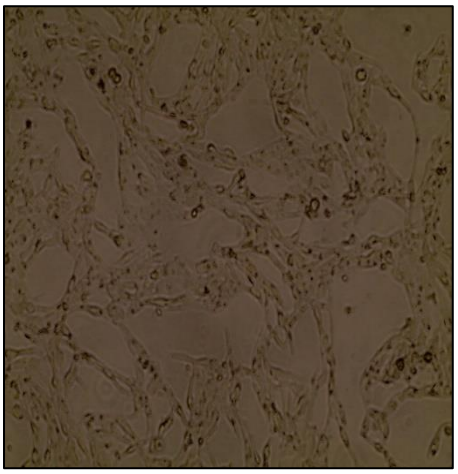

CR U2OS

Figure 5.6. U2OS CR cell lines behave differently in cell culture in comparison to U2OS WT. WT = Wild type U2OS (untreated cells), CR= CHK1i resistant cells. WT and CR cell line 1 used in this study. N=1. U2OS WT cells in A) were cultured in DMEM media alone. To generate CHK1i resistance, U2OS cells in B) were grown in DMEM media with increasing doses of the CHK1 inhibitor CCT244747 starting at 0.1µM to a maximum concentration of 5µM. Surviving cells from each concentration were monitored and the dose was increased when confluency level hit 50%. Surviving cells were then cultured in DMEM media and used for further studies. Cells were photographed at 20X microscopy. The WT cells are in a co-ordinated pattern in cell culture, however the CHK1i resistant cells appear elongated and do not form the same pattern when fixed.

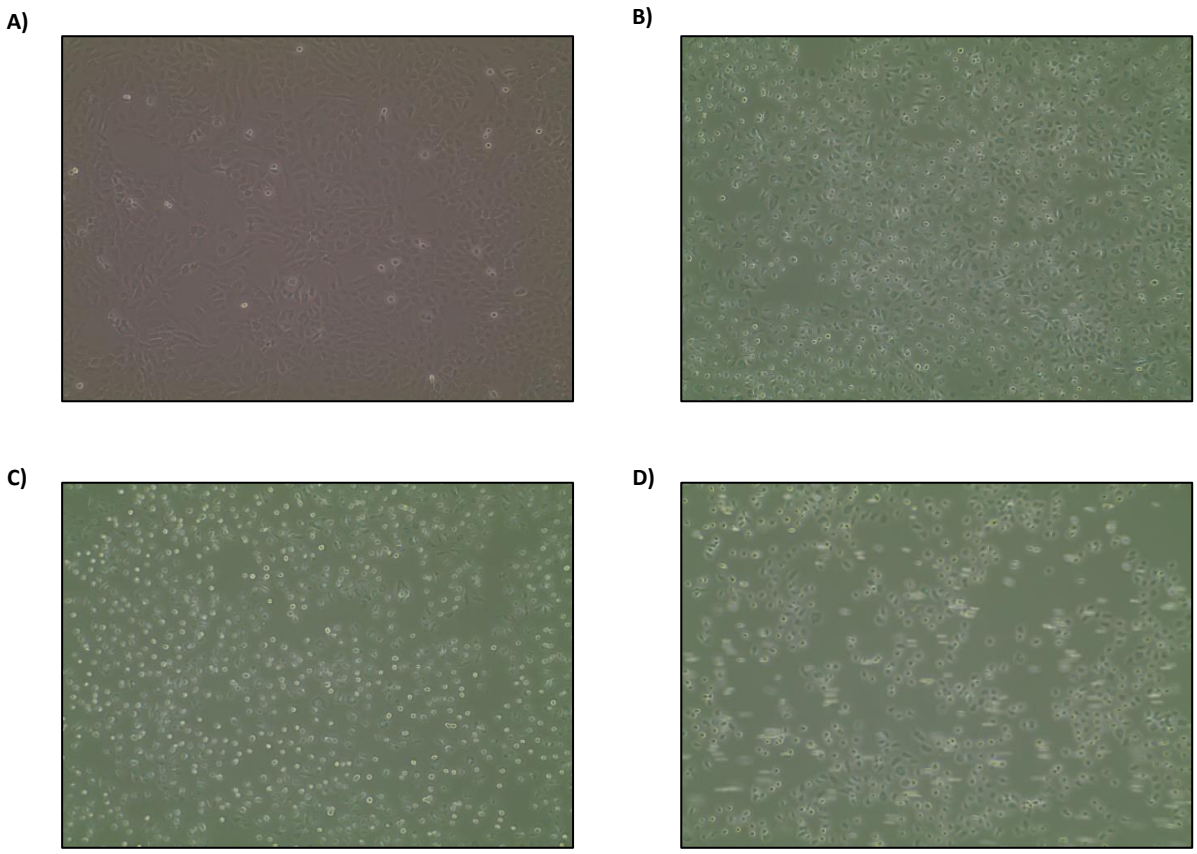

Figure 5.7. U2OS WT cells undergoing trypsinisation. N=1. WT cell line 1 used for this study. U2OS WT cells were cultured in DMEM media alone. Confluent U20S WT cells in A) were placed in 1% trypsin to remove the cells from fixation on the plate. Photos were captured under microscopy at intervals at 20X magnification. The pictures were taken at B) 5 minutes, C) 7 minutes, where the cells are starting to change in shape, and D) 10 minutes, where cells are now free in suspension.

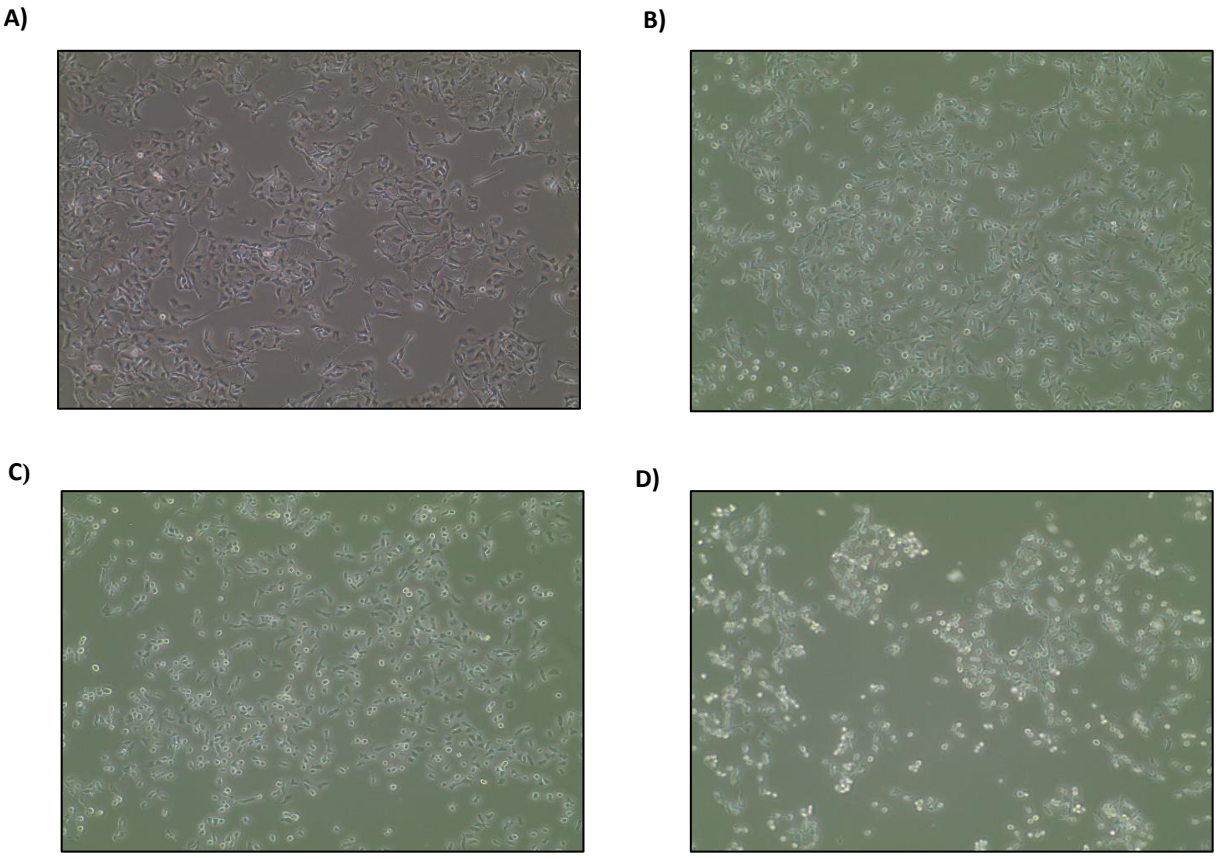

Figure 5.8. U2OS CHK1 inhibitor resistant cell lines undergoing trypsinisation behaved differently to U2OS WT cells. N=1. CR cell line 1 used in this study. To generate CHK1i resistance, U2OS cells were grown in DMEM media with increasing doses of the CHK1 inhibitor CCT244747 starting at 0.1µM to a maximum concentration of 5µM. Surviving cells from each concentration were monitored and the dose was increased when confluency level hit 50%. Surviving cells were then cultured in DMEM media and used for further studies. Confluent U2OS CHK1i resistant cells in A) were placed in 1% trypsin to remove the cells from fixation on the plate. Photos were captured under microscopy at intervals at 20X magnification. In comparison to the WT U2OS cells, no cell changes were viewed after 5 minutes. B) The photo was taken at 7 minutes with the cells still fixed to the plate. C) Photo taken at 12 minutes where the cells are starting to change in shape. D) Photo taken at 15 minutes where cells had started to become loose in suspension but were lifting in clumps rather than as individual cells.

5.7. Differences in epithelial-mesenchymal transition (EMT) were shown between the WT U2OS and CR U2OS cells

I have demonstrated in Section 5.6 that the CR U2OS cell line 1 appeared more elongated in culture and that the CR U2OS cells were more adhesive in comparison to matched WT U2OS cells. qPCR analysis of *SLUG* and *TWIST* was performed to further explore if changes in EMT could be present in the U2OS CHK1i resistant cell lines. SLUG and TWIST are both EMT-activating transcription factors (EMT-TFs) which can trigger EMT (517). SLUG can act as a repressor of e-cadherin, which is responsible for maintenance of cell-cell adhesion (520–522). TWIST is also a transcriptional repressor of e-cadherin and has also been described in the counteraction of p53 induced apoptosis (523–525).

Experiments were performed in WT and CR U2OS line 1 only and N=1 due to time constraints. Statistical analysis cannot be performed due to this only being one biological repeat with only 2 technical replicates. U2OS CR and matched U2OS WT cells were treated with 1µM or 5µM of the CHK1i CCT244747 for 24 hours. Controls were treated with matched doses of DMSO. Figure 5.9 shows the results. Figure 5.9A shows that the WT U2OS cells had higher starting levels of *SLUG* and a small reduction in levels post CHK1i treatment. The CR U2OS cells had a lower starting amount of *SLUG* present but very little change in *SLUG* levels were shown after CHK1i treatment.

In contrast, Figure 5.9B shows that WT U2OS cells have low levels of *TWIST* in comparison to CR U2OS cells. In addition, there appears to be a rise in *TWIST* levels in response to CHK1i treatment, in particular with the CR U2OS cells at 5µM CHK1i dose. This could indicate that the CR U2OS cell line has changes in EMT which have altered the cells both phenotypically and behaviourally. These experiments, however, are only preliminary and would need more extensive investigation to confirm this.

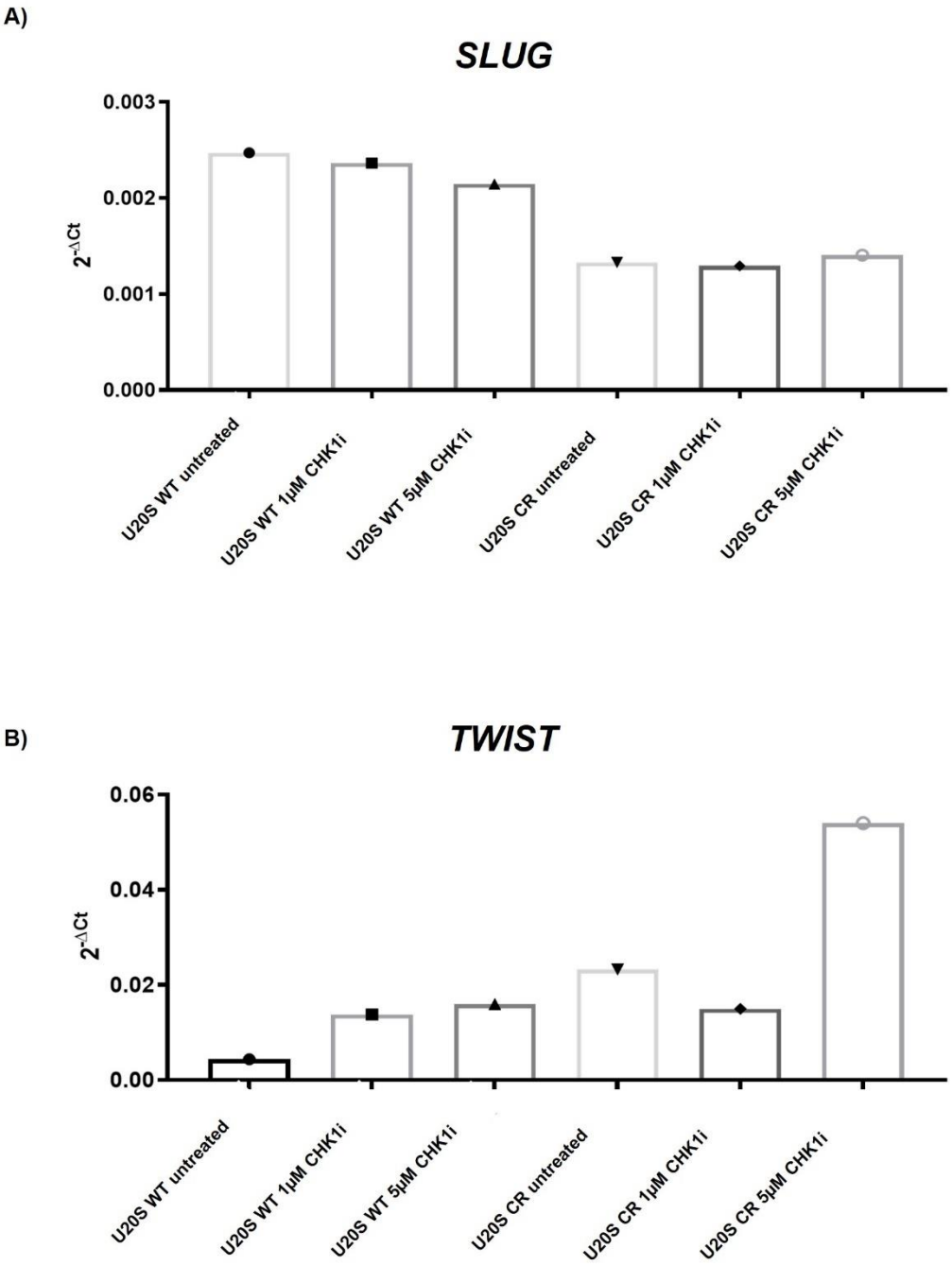

Figure 5.9. *SLUG* and *TWIST* levels are different between the U2OS WT and U2OS CR cell lines both at baseline and in response to CHK1i treatment. N=1. U2OS WT and U2OS CR cell line 1 were used in this study. Data were normalised using the 2-ΔCT method (R = 2–[ΔCP sample – ΔCP control]) using the gene *RPL13A* as reference. Statistical analysis cannot be performed due to this only being one biological repeat with only 2 technical replicates. U2OS WT and CR U2OS cell lines were treated with the CHK1i CCT244747 for 24 hours. Untreated cell lines were treated with the equivalent amount of DMSO. A) WT U2OS cells have higher starting levels of *SLUG* and have a small reduction with CHK1i treatment, whereas CR U2OS cells have a lower starting amount but there is little change after U2OS treatment. B) In contrast to A), WT U2OS cells have low levels of *TWIST* in comparison to CR U2OS cells. In addition, there appears to be a rise in *TWIST* levels in response to CHK1i treatment, in particular with the CR U2OS cells at 5μM CHK1i dose.

5.8. CHK1i resistant U2OS cells display different activation of key DDR genes in response to CHK1i treatment in comparison to WT U2OS cells

qPCR was also performed to look at changes within key DNA damage response genes. These genes were previously explored in the CHK1 sensitive and resistant mouse models in chapter 4. This was to examine how the DNA damage response behaves in the CHK1i resistant cells compared to the WT sensitive cells. Due to time constraints within this study, experiments were performed in WT and CR U2OS cell line 1 only and N=1 so the results here are only preliminary. Statistical analysis cannot be performed due to this only being one biological repeat with only 2 technical replicates. Figure 5.10 shows the qPCR results for *CHEK1*, *CLSPN* and for *CDC25A* both with CCT244747 CHK1i treatment and without. Untreated cells were dosed with the equivalent DMSO as control.

The U2OS WT cells show higher levels of *CHEK1* and *CLSPN* at baseline in comparison to the U2OS CR cells. Levels of both *CHEK1* and *CLSPN* reduce with CHK1i treatment in both WT and CR cells, in contrast to data obtained in the mouse models in chapter 4. *CDC25A* levels are slightly higher at baseline in untreated CR U2OS cells compared to the WT U2OS and there appears to be a slight increase in *CDC25A* after 1 µM CHK1i treatment in the CR U2OS cells. CDC25A levels decrease slightly in the WT U2OS cells after 1µM CHK1i treatment but a large change after CHK1i treatment is not demonstrated. More repeats would be needed to confirm these trends in the WT U2OS and CR U2OS cell lines.

The findings of low levels of *CLSPN* and *CHEK1* in the CHK1i resistant cells are similar to the trends shown in the Eµ-Myc/*c-Rel -/-* CHK1i resistant mouse models in chapter 4. There appears to be some alteration in the DNA damage response between the WT and CHK1i resistant cells at baseline. Significant changes were also not demonstrated in *CDC25A* levels between drug sensitive and drug resistant mouse models.

The WT U2OS and CR U2OS cell lines in this study were exposed to CHK1i for 24 hours whereas Eµ-Myc CHK1i sensitive mice treated with CHK1i at 8 hours showed the most prominent response. It would be beneficial to perform a time course as a follow up experiment in the cell lines to assess the time point of strongest CHK1i response.

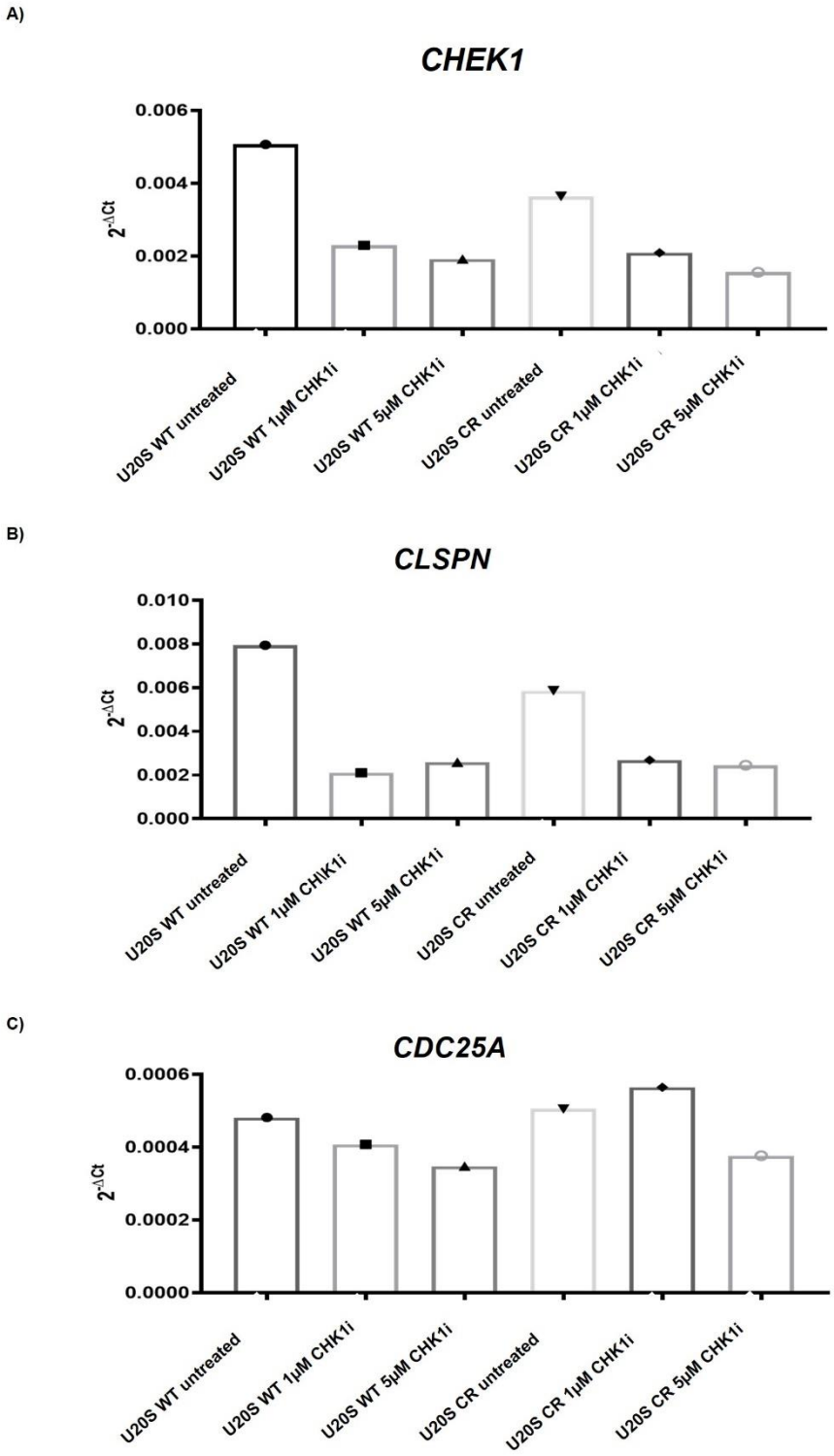

Figure 5.10. *CHEK1* and *CLSPN* show similar trends in gene expression at baseline and post CHK1i treatment in U2OS WT and U2OS CR cell lines, but a difference in *CDC25A* is demonstrated. N=1. WT and CR U2OS cell line 1 used in this study. Data were normalised using the 2-ΔCT method (R = 2–[ΔCP sample – ΔCP control]) using the gene *RPL13A* as reference. Statistical analysis cannot be performed due to this only being one biological repeat with only 2 technical replicates. U2OS WT and U2OS CR cells were treated with the CHK1i CCT244747 for 24 hours. Untreated cell lines were treated with the equivalent amount of DMSO. A) WT U2OS cells have higher starting levels of *CHEK1* in comparison to the CR U2OS cells and CR U2OS cells have a smaller relative change. B) Baseline *CLSPN* levels are also reduced in the CR U2OS cells, similar to demonstrated in the mouse models earlier. C) *CDC25A* levels only decrease slightly in the WT U2OS cells after 1μM CHK1i treatment and appear slightly higher after 1μM CHK1i treatment in the CR U2OS cells. These changes, however, appear to be small.

5.9. Changes in protein DDR expression are shown between the WT CHK1i sensitive U2OS cells and the CHK1i resistant U2OS cells

In the Eμ-Myc mouse models, changes demonstrated in protein were more evident than changes demonstrated in gene expression. To further explore the protein changes between WT U2OS cells and CR U2OS cells, western blot analysis was performed in key DDR genes at baseline. This was a preliminary study due to time constraints in this study, N=1 for U2OS WT and U2OS CHK1i resistant cell lines 1, 2 and 3. Results are shown in Figure 5.11.

Phosphorylated CHK1 serine 345 was not present. This was an expected result in unstimulated cells as they are not under additional replication stress. RelA and total CHK1 levels are higher in the WT U2OS cells in comparison to the CR U2OS matched cells. There also appears to be a reduction in CDK2 and PARP in the CR resistant cells. This could indicate that, as shown in the Eμ-Myc/*c-Rel -/-* CHK1i resistant mouse models in chapter 4, the DNA damage response pathways are downregulated in these CHK1 inhibitor resistant cell lines. The results are slightly different in each cell line however, with CDK2 levels being higher in CR cell line 1.

Further experiments are required to explore the protein expression differences between drug sensitive and drug resistant cell lines in more detail. This would involve looking at changes in the WT and CR U2OS cells in comparison after CHK1 inhibitor treatment.

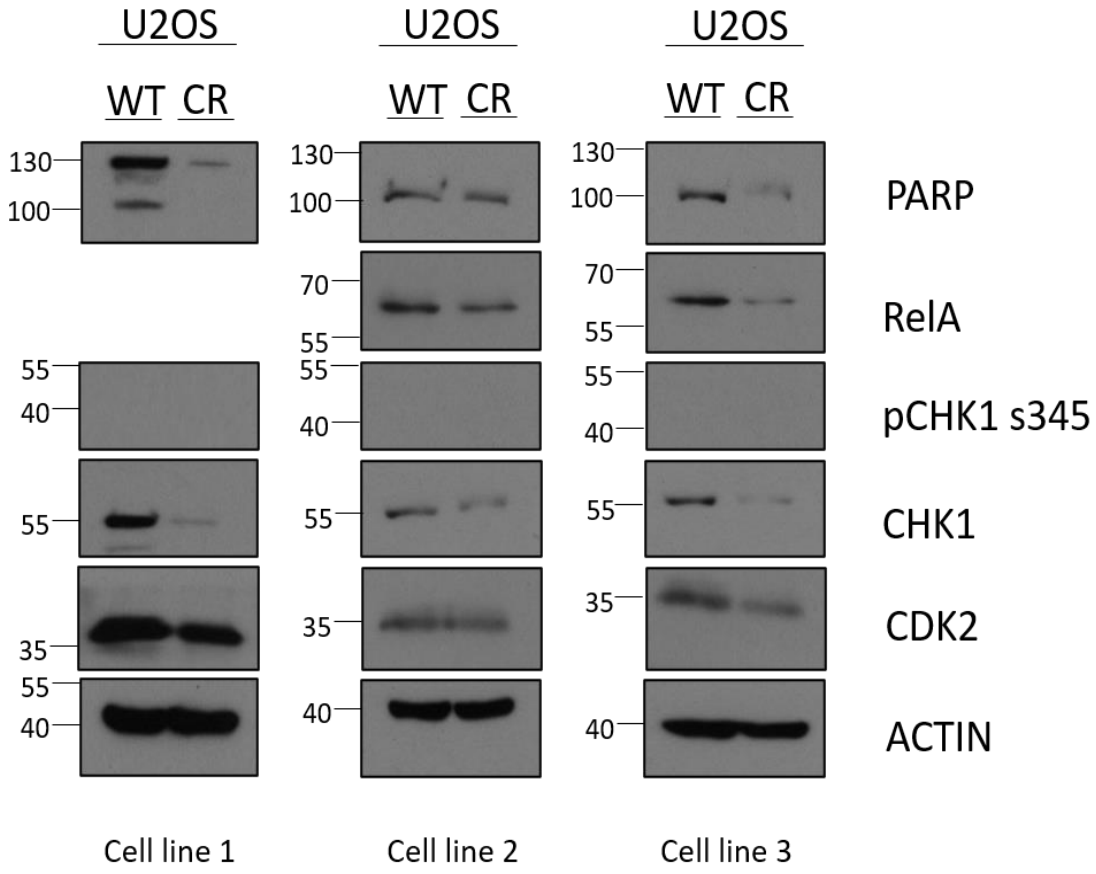

Figure 5.11. Western blot analysis of untreated U2OS WT and CHK1i resistant cells for DNA damage response markers. Preliminary protein analysis of untreated generated CR cells in comparison to matched WT U2OS cells (N=1 for each). A) Results for cell line 1; B) cell line 2 and C) cell line 3. pCHK1 s345 is not present; this is expected as cells have not been treated and therefore should not be activated at rest. CHK1 levels are reduced in CR cell lines as shown in the Eμ-Myc/*c-Rel -/-* mice in chapter 4. There also appears to be a reduction in baseline PARP, RelA and CDK2 in the CR cell lines in comparison to the WT U2OS cells.

5.10. Generated CHK1i resistant U2OS cells displayed more genomic instability in comparison to matched WT U2OS cells

Genomic DNA was extracted from both WT and CHK1i resistant cell lines. This was done with a view to sequencing the samples if time permitted. These samples differed from cfDNA samples as discussed in Chapter 6 as genomic DNA was extracted from the cells as opposed to small DNA fragments from plasma samples. DNA extractions on all 4 CHK1 resistant U2OS cell lines and their matched WT U2OS cells were performed. Sample quality was assessed using genomic DNA ScreenTape and analysed on the TapeStation (Agilent). Results are shown in Table 5.3.

WT U2OS cells had larger DNA fragment size in comparison to the CR cells. All DNA was extracted using the same DNA extraction kit at the same time. This could indicate that the CR cells are more genomically unstable in comparison to the WT cells and could be in keeping with a reduction in key DNA damage response proteins as shown in Figure 5.11. A downregulation of Claspin and CHK1 along with other DNA damage proteins could lead to less regulation of DNA repair and make cells more unstable when placed under replication stress.

Table 5.3. CHK1i resistant cell lines are more fragmented after genomic DNA extraction in comparison to matched WT U2OS cells. N=1. Genomic DNA was extracted from all cell lines and DNA quality was assessed using TapeStation. The WT cells all had large DNA fragment sizes post extraction, however in comparison the CR cells all had smaller initial fragment sizes after the same sample preparation.

Sample	Concentration (µg/µl)	Initial fragment size (bp)
WT1	52.8	>60000
WT2	94	>60000
WT3	323	>60000
WT4	537	>60000
CR1	57.7	20764
CR2	51.7	23030
CR3	48.1	23367
CR4	61.8	50664

5.11. RNA-seq has shown both similarities and differences in gene expression patterns in the CHK1i resistant cell lines

To further investigate gene expression trends in the CHK1i resistant U2OS cells, samples were prepared for RNA-seq analysis. WT and CR cell lines 1, 2, 3 and 4 were used in this study. N=1 for all samples. Samples were prepared as discussed in Section 3.3.8. RNA samples were run using the Illumina platform by Leigh Taylor at the Genomics Core Facility at Newcastle University. Due to time constraints data was not initially analysed in detail but was subsequently analysed by Dr. Peter Leary at Newcastle University Bioinformatics Support Unit (BSU). Findings from the data are summarised in this section.

Figure 5.12 shows the principle components analysis (PCA) of the RNA-seq data for the WT and CR U2OS cell lines. All of the WT untreated cells cluster together and have very similar gene expression patterns. This shows that the starting U2OS cells all have similar characteristics. Post CHK1i treatment, the WT gene expression profiles change, but again the gene expression changes in a similar way. This shows that the independent U2OS WT cell lines share characteristics and a similar response to CHK1 inhibition.

Results for the CR cells in Figure 5.12 appear to indicate 2 different gene expression populations that are different to the WT pattern. CHK1i resistant cell lines 1 and 4 (CR1 and CR4) cluster in a similar way, and CHK1i resistant cell lines 2 and 3 (CR2 and CR3) cluster similarly. In all of the CR cell lines, there is not a big change in gene expression post CHK1i treatment as demonstrated in the matched WT U2OS cells. These findings are similar to the trends demonstrated in the Eμ-Myc/*c-Rel -/-* mice. These results seem to indicate that there are not large gene expression changes post CHK1i treatment in the CHK1i resistant cell lines.

Figure 5.13 shows the gene expression patterns for *CLSPN* and *REL* from the RNA-seq analysis of WT and CHK1i resistant U2OS cell lines. Figure 5.13A shows that the untreated and CHK1i treated WT U2OS again cluster in groups displaying similar patterns for *CLSPN* expression. Cell lines CR2, CR3 and CR4 all have low *CLSPN* expression, similar to the Eμ-Myc/*c-Rel -/-* mice. CR1 displays higher levels of *CLSPN* compared to the other CHK1i resistant lines but lower levels than the WT groups.

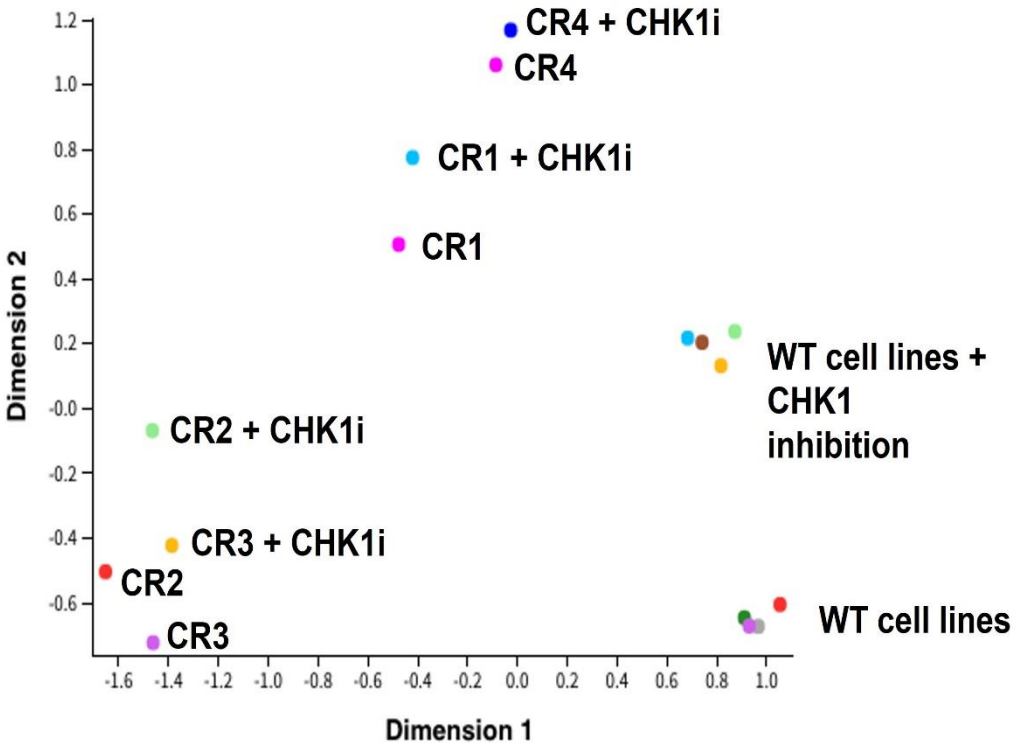

Figure 5.12. Principle components analysis (PCA) of RNA-seq data for WT U2OS and CHK1i resistant U2OS cell lines. Figure produced by Dr P. Leary. WT = Wild type; CR = CHK1i resistant. N=1. U2OS WT and CR U2OS cell lines were treated with 1μM CHK1i CCT244747 for 24 hours. Untreated cell lines were treated with the equivalent amount of DMSO. PCA of the RNA-seq data shows that all of the WT cells (untreated) cluster together and therefore in terms of their gene expression (GE) look very similar. Once treated with the CHK1i, the gene expression profiles of the WT cells all change, but all in a very similar way. Results for the CHK1i resistant cells appear to display 2 different populations - CR1 and CR4 cluster similarly, and CR2 and CR3 cluster similarly. In all CR U2OS cell lines, there are not big shifts in gene expression post CHK1i treatment. This is in contrast to the trends demonstrated in the WT U2OS cells.

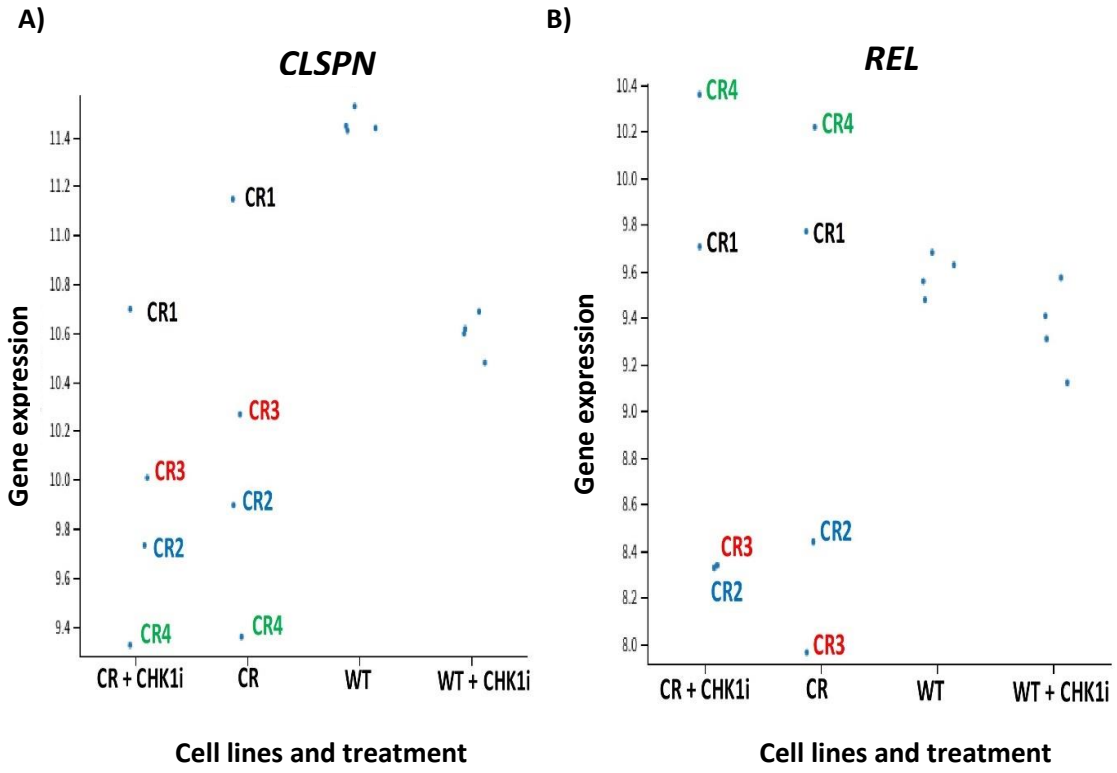

Figure 5.13. Gene expression plots for *CLSPN* and *REL* from RNA-seq analysis of WT and CHK1i resistant cell lines. Figure produced by Dr. Peter Leary. WT = Wild type; CR = CHK1i resistant. N=1. U2OS WT and CR U2OS cell lines were treated with 1µM CHK1i CCT244747 for 24 hours. Untreated cell lines were treated with the equivalent amount of DMSO.A) CR2, CR3 and CR4 all have low *CLSPN* expression, similar to the Eµ-Myc/*c-Rel -/-* mice. CR1 cells appear to have a slightly higher expression of *CLSPN*, but less than WT cell lines. Untreated WT U2OS cells all express higher *CLSPN* levels, which are reduced by treatment with the CHK1i. This is in contrast to the data for the Eµ-Myc mice shown in Table 4.1 where *CLSPN* levels increase after CHK1i treatment. The cell data here, however, represents single dose CHK1i treatment after 24 hours and results in the Eµ-Myc mice represent 9 days of CHK1i treatment. Gene expression in the CR cells does not change significantly post CHK1i treatment. B) *REL* expression – CR1 and CR4 cluster again as shown in the PCA in Figure 5.12, but the CR2 and CR3 cell lines appear to have very low *REL* (mimicking the Eµ-Myc/*c-Rel -/-* mice).

Gene expression profiles in the CR cells do not change significantly post CHK1i treatment. Figure 5.13B shows the results for *REL* expression. Again, the WT cell lines all cluster together in a similar pattern when untreated and separately cluster in a similar pattern post CHK1i treatment. CR1 and CR4 cell lines cluster again as shown in the PCA in Figure 5.12. The CR2 and CR3 cell lines have different gene expression patterns and appear to have very low *REL* expression, which again is shared with the Eμ-Myc/*c-Rel -/-* mice. Trends appear to be showing that CR2 and CR3 have some similar characteristics to the Eμ-Myc/*c-Rel -/-* mice, whereas CR1 and CR4 have different patterns of CHK1i resistance based on gene expression pattern.

Figure 5.14 shows the gene expression plots for *ATM* and *CHEK2* from the RNA-seq analysis of WT U2OS and CHK1i resistant U2OS cell lines. Figure 5.14A shows gene expression levels of *ATM* and Figure 5.14B shows gene expression levels of *CHEK2*. There is some variation in gene expression for *ATM* and *CHEK2* in the WT U2OS cell groups, but similar trends are demonstrated – *ATM* and *CHEK2* expression levels reduce after CHK1i treatment. CR1 and CR4 cell lines cluster together (as shown in the PCA in Figure 5.12) but cell lines CR2 and CR3 appear to have higher gene expression of *ATM* and *CHEK2* prior to CHK1i treatment. Levels remain high compared to WT U2OS cells after CHK1i treatment despite a small reduction in gene expression. This could indicate that CR2 and CR3 have an upregulation of the ATM/CHK2 pathway in an attempt to bypass CHK1 signalling.

The RNA-seq data has also confirmed that *USP1* was downregulated in CR2 and CR3 U2OS cells. This is again in keeping with the downregulation of *CLSPN* and *REL* in the CR2 and CR3 U2OS cells as shown in Figure 5.11 and 5.13, and as shown in the Eμ-Myc/*c-Rel -/-* mouse model in chapter 4. This data supports the idea of a shared mechanism of CHK1i resistance between the CR cell lines and the Eμ-Myc/*c-Rel -/-* mouse model. CR1 and CR4 are CHK1i resistant, however the resistance mechanism is different. Ongoing work in the Perkins' lab is being performed to investigate the resistance mechanisms in the CR cells in more detail.

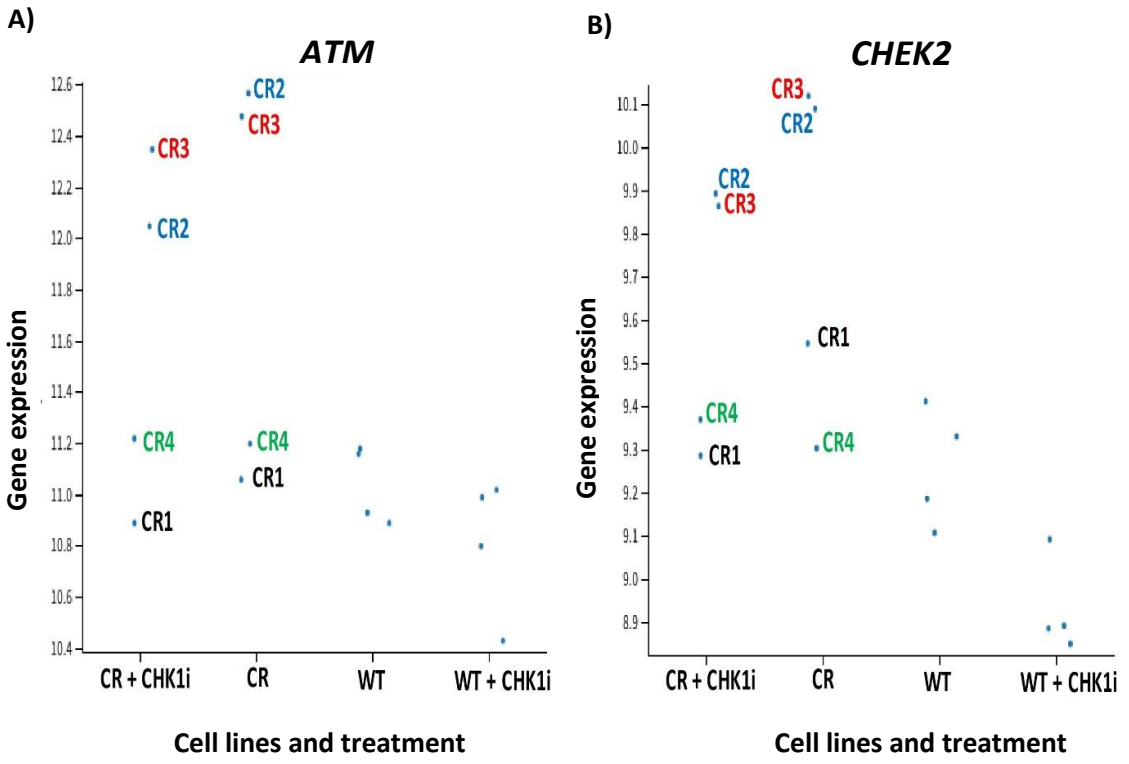

Figure 5.14. Gene expression plots for *ATM* and *CHEK2* from RNA-seq analysis of WT and CHK1i resistant cell lines. Figure produced by Dr. P. Leary. WT = Wild type; CR = CHK1i resistant. N=1. U2OS WT and CR U2OS cell lines were treated with 1μM CHK1i CCT244747 for 24 hours. Untreated cell lines were treated with the equivalent amount of DMSO.A) shows gene expression levels of *ATM* and B) shows gene expression levels of *CHEK2*. CR1 and CR4 cell lines cluster (as shown in the PCA in Figure 5.12) and cell lines CR2 and CR3 also cluster together. Cell lines CR2 and CR3 appear to have higher gene expression of *ATM* and *CHEK2*. This could indicate an upregulation of the ATM/CHK2 pathway in an attempt to bypass CHK1 signalling. WT U2OS cells show a reduction in both *ATM* and *CHEK2* expression after treatment with the CHK1i. This is in contrast to the data for the Eμ-Myc mice shown in Table 4.1 where *ATM* and *CHEK2* levels increase after CHK1i treatment, however, the cell data represents single dose CHK1i treatment and results in the Eμ-Myc mice are after 9 days CHK1i treatment.

5.12. Chapter Summary

In this chapter I have investigated a cell line which acquired resistance to CHK1 inhibition post CHK1i drug treatment. The U2OS cell line was the cell line selected as it is normally sensitive to CHK1 inhibition and has intact DDR pathways. It is important to be able to assess the baseline cell line characteristics when trying to assess and modify a drug response. This cell line can also be manipulated via transfection and siRNA analysis, making further follow up experiments possible within the same cell model. I have confirmed that the CR U2OS cells have become CHK1i resistant with use of cell survival assessments in comparison to the WT U2OS cells.

Changes in cell characteristics and behaviour were observed when growing the CHK1i resistant cells in culture. The CR U2OS cells appeared more elongated and clustered in comparison to the WT U2OS cells. In addition, changes were seen in cell adhesion during cell culture – the CR U2OS cells took longer to dissociate from the flask in the presence of trypsin. It is important to acknowledge that trypsin acts as a protease and prolonged exposure could lead to additional cell stress (526), therefore care must be taken to minimise exposure. Given the change in cell appearance and adhesion in culture, preliminary investigations into the EMT-TFs *SLUG* and *TWIST* were performed. *TWIST* levels were increased in the CR U2OS cells, but further characterisation of the cell line formally looking at EMT markers would be required to draw any conclusions.

WT U2OS cells showed a reduction in *CLSPN*, *ATM* and *CHEK2* after treatment with the CHK1i. This is in contrast to the data for the Eμ-Myc mice shown in Table 4.1 where *CLSPN, ATM* and *CHEK2* levels increase after CHK1i treatment. The cell data in Figure 5.13 and Figure 5.14, however, shows the RNA-seq results for single dose CHK1i treatment and the results in Table 4.1 for the Eμ-Myc mice represent qPCR results after 9 days of CHK1i treatment. The time difference in the CHK1i treatment course may have influenced the differences seen between the WT U2OS and the Eμ-Myc mice. Figure 4.9 shows data for *ATM* expression in the acute Eμ-Myc mouse model at 24 hours and there was no change in gene expression after treatment. This could indicate that there are some differences in

DDR gene expression post CHK1i treatment between the WT U2OS cells and the acute Eμ-Myc mouse model.

All of the CR U2OS cells have downregulated DDR protein expression, including CHK1. The CR U2OS cell lines, in particular CR2 and CR3, share characteristics with the Eμ-Myc/*c-Rel -/-* mouse model, including downregulation of *REL* and downregulation of *CLSPN*. There appears to be an upregulation in *ATM* and *CHEK2* expression in these cell lines which could indicate that the ATM/CHK2 pathway is upregulated to bypass CHK1 signalling and enhance cell survival. CR1 and CR4 cell lines appear to have different gene expression profiles and are likely to have a different pattern of CHK1i resistance. This highlights that, like in the Eμ-Myc/*RelA T505A* mouse model, there can be multiple mechanisms of CHK1i resistance.

RNA-seq has confirmed that CR U2OS lines also have downregulation of *USP1* as demonstrated in the mouse models. This has shown that there is a shared mechanism of resistance between the Eμ-Myc/*c-Rel -/-* mouse model displaying *de novo* drug resistance and the CR U2OS cell lines demonstrating acquired drug resistance.

Further suggested work

Most of the work in this chapter has been preliminary work due to the time constraints of this project. qPCR and western blot analysis performed in this study will need to be repeated to ensure that this is a true result.

The western blot I performed to look at DDR protein expression in the cell lines was pre-CHK1i treatment only. Therefore, I would want to further explore the protein expression in the CR U2OS cells in comparison to the WT U2OS cells in detail. This would further help to characterise the cell lines and see if other DDR pathway proteins are downregulated in response to the CHK1 inhibitor. Given the baseline reduction in expression my hypothesis would be that there would be a low level of DDR expression also in response to CHK1i treatment.

It would be useful to perform a time course in the CR U2OS cell lines to determine the optimal CHK1i treatment time. This has been determined as 8 hours in the Eμ-Myc/*c-Rel -/-* mouse model but this may be different in the cell models.

Given that *USP1* has also been shown to be downregulated in the CR U2OS cells it would be useful to validate this with follow up qPCR and western blot analysis to assess *USP1* gene and USP1 protein expression within this model. I would also investigate PI3K/AKT and MAPK pathways as well given the upregulation of AKT, ERK1, JNK1 and P38 MAPK shown in the proteomics data for the Eμ-Myc/*c-Rel -/-* mouse CHK1i resistant model. This would be to determine if these pathways are also upregulated in the CR U2OS cell lines, particularly in CR2 and CR3 which already share features with the Eμ-Myc/*c-Rel -/-* mouse model.

siRNA knockdown of *USP1* would be useful to perform in the WT U2OS cells. The siRNA knockdown cells could then be treated with CHK1 inhibitor to see if they have become resistant to CHK1 inhibition.

It would be useful to further interrogate the RNA-seq data to explore the mechanism of resistance for the CR1 and CR4 cell lines in more detail. It would be be interesting to see if there is evidence of cell survival pathway upregulation. Further investigations into the CHK1i resistance mechanisms in the CR U2OS cells are being performed by the Perkins' lab.

In this chapter I have shown that the CHK1i resistant U2OS cells with acquired CHK1i resistance share some characteristics with the Eμ-Myc/*c-Rel -/-* mouse model with *de novo* CHK1i resistance. In the next chapter, I extracted and quantifed cfDNA from samples obtained from patients on the SRA737 CHK1i study and assessed whether mutations in DDR related genes from human cfDNA samples can be detected.

6. Results 3: SRA737 trial sample preparation for cfDNA extraction and next generation sequencing

6.1. Introduction to chapter

The mutational profile of cancers can change significantly as disease progresses to promote cell survival and metastatic potential (40,44). The traditional method of tissue biopsy to capture mutational change on disease progression can be difficult due to patient fitness and tumour accessibility (263). Previous studies have demonstrated that cancer mutations can be detected in circulating cell free DNA (cfDNA) and tests are now routinely used in clinical practice for some cancers providing a personalised treatment approach (270,290–293).

cfDNA consists of DNA fragments present in the bloodstream and is thought to be released from cells undergoing necrosis and apoptosis (275–277). Normal physiological levels of cfDNA are low in healthy individuals but increased in pro-inflammatory conditions including cancer (276,277). Circulating tumour DNA (ctDNA) is the fraction of DNA specifically from tumour origin (283). This can provide information on the mutational status of a cancer and changes in tumour profile can be detected over time in successive samples (306,527).

Patients participating in the SRA737 clinical trial monotherapy arm had blood samples collected at different time points during their CHK1i treatment (207). Plasma was then spun from these samples for further cfDNA extraction. These cfDNA samples were for exploratory research purposes to see if mutations in genes linked to the DNA damage response could be detected during CHK1i treatment. The aim of this chapter is to see if mutations can be isolated from cfDNA from patients on CHK1i monotherapy and to develop the methods used to investigate gene changes in this patient group.

6.2. Chapter aims

Research aim 1 - to develop and validate methodologies needed for investigating genetic changes in patients treated with CHK1i therapy.

Research aim 2 - to see if mutations in the DDR can be identified in patients undergoing CHK1 inhibitor therapy on the SRA737 CHK1 inhibitor monotherapy trial.

6.3. Quantity of cfDNA can vary according to techniques used

Firstly, preliminary studies were also used to optimise the method used for cfDNA extraction. Plasma samples from healthy controls were spiked with genomic DNA from lung and colorectal cell lines to ensure that circulating free DNA can be detected and measured. Secondly, the number of centrifuge steps was altered during cfDNA elution, as was using different volumes of elution buffer (Figure 6.1A).

The addition of an extra centrifuge step was found to increase cfDNA yield. Using 50µl elution buffer volume per ml of plasma was found to give a higher total concentrated yield compared to 100µl/ml of elution buffer.

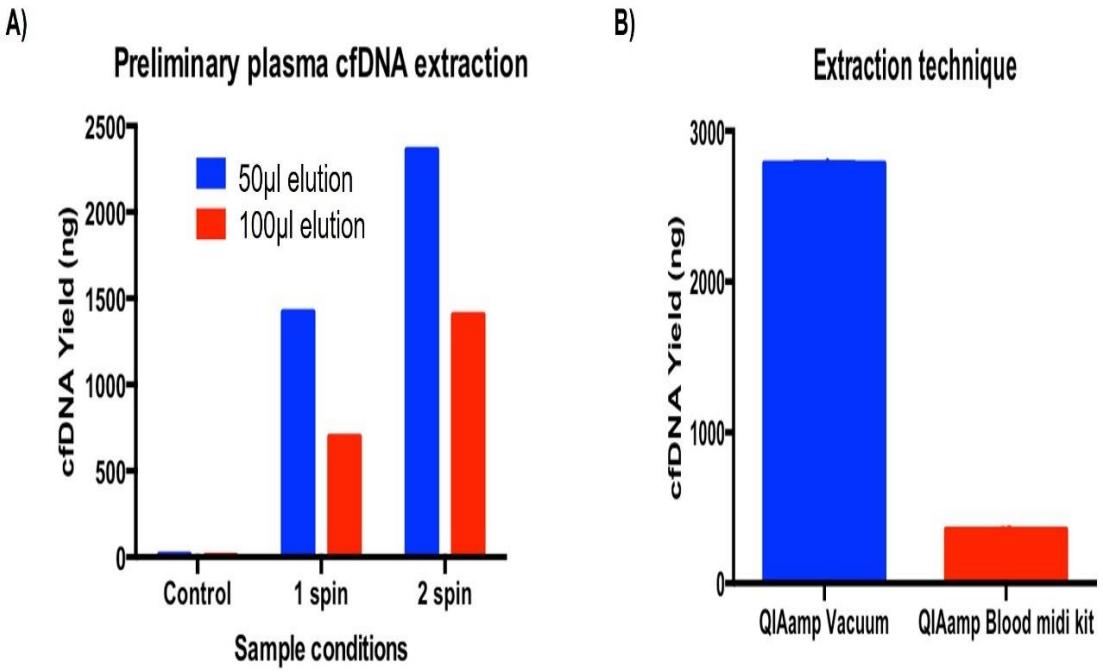

Figure 6.1. cfDNA yield varies according to the techniques and extraction kit used. A) Preliminary cfDNA extractions were performed using 1ml of healthy individual plasma samples spiked with DNA from lung and colorectal cell lines (N=1). Control samples have no added cellular DNA and contain low levels of cfDNA. Elution buffer volumes and elution centrifuge steps were modified to assess optimal extraction conditions. cfDNA yield was assessed by Qubit. B) Differences in yield of cfDNA compared from two different extraction kits and extraction method (N=2). Graph shows mean ± SD.

A comparison was also made between two different DNA extraction kits, the QIAamp Circulating Nucleic Acid Kit (QIAGEN) using a vacuum extraction method and the QIAamp Blood Mini Kit using centrifuge spins (QIAGEN; #51104). The comparison is shown in Figure 6.1B. QIAGEN kits were selected after discussions with other research centres and are commonly used in other cfDNA studies (528–532). Plasma from the same source sample was used to follow both protocols and DNA quantity was measured via Qubit post procedure. The QIAGEN QIAamp Circulating Nucleic Acid Kit using the QIAGEN QiaVac 24 plus vacuum manifold provided a greater DNA yield compared to the QIAamp Blood Midi Kit and therefore the vacuum method was used in subsequent extractions.

6.4. Quantity and quality of cfDNA shows intra-patient variability

Prior to using plasma samples from the SRA737 CHK1 inhibitor study, test plasma samples were used from the PROSPECT-NE study. This is a collection of samples from patients waiting for phase 1 clinical trial entry and who have donated plasma for investigative research. This patient population is similar to those enrolled onto the SRA737 CHK1 inhibitor study (533) and therefore it was assumed that cfDNA quantity and quality would be similar between the two patient groups.

cfDNA was extracted using the QIAamp Circulating Nucleic Acid Kit. cfDNA quantity was measured using the Qubit as discussed in Section 3.11.2 (Figure 6.2A). DNA quality and fragment size were measured using a TapeStation automated system, which uses gel electrophoresis and digital analysis to assess sample integrity (534). Samples show wide variation in the amount of cfDNA extracted, however, DNA fragment length in samples was shown to be consistent with a range between 130 and 150bp (Figure 6.2B).

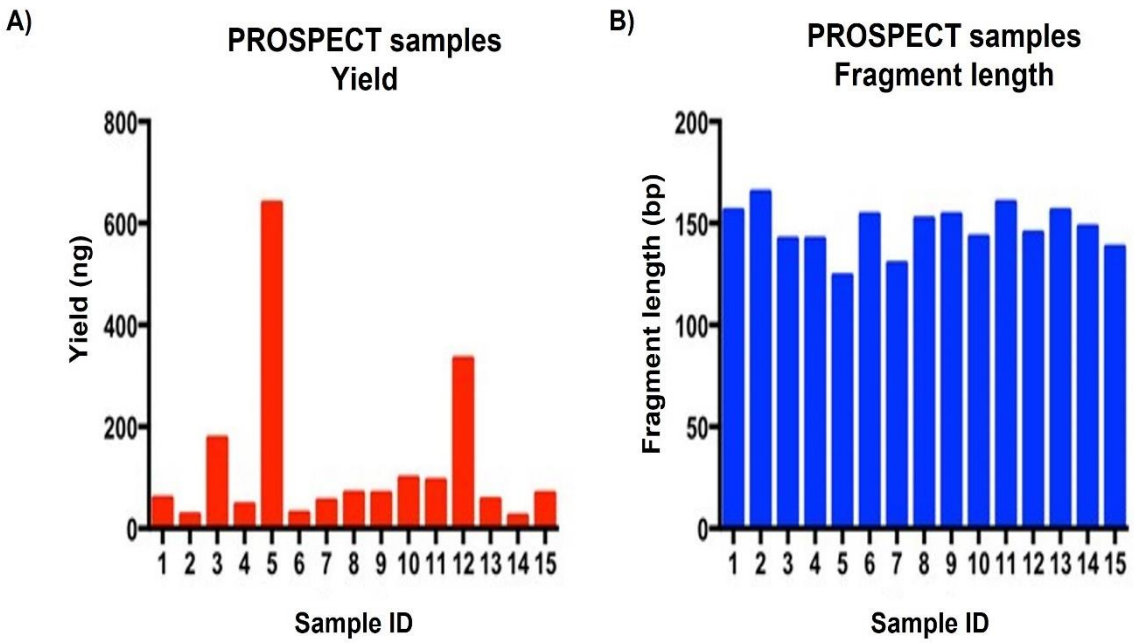

Figure 6.2. cfDNA quantity and quality varies between patients. A) Total yield of 15 separate cfDNA samples from PROSPECT-NE biobank patients suitable for phase 1 studies measured using Qubit fluorometer. B) Fragment size determined by TapeStation analysis for the matched samples.

Given the consistency of fragment size shown with the PROSPECT samples, the first 54 SRA737 samples were then extracted using the QIAamp Circulating Nucleic Acid Kit. These samples were from 30 patients in total. Variation was again seen with the quantity of cfDNA obtained from samples, but similar consistent trends were seen with the DNA fragment size. The main factor limiting the total cfDNA quantity gained from trial samples was having access to only a small starting volume of plasma (between 1 and 3mls per sample).

6.5. Design of gene panel for next generation sequencing

Given the preliminary data generated from the PROSPECT-NE samples, and those from the SRA737 trial showing low cfDNA yield, meetings were held with representatives from Illumina and the Core Genomics Facility staff at Newcastle University. This was to discuss the optimal design of the next generation sequencing panel. Factors taken into consideration prior to design included the low amount of DNA likely to be extracted from the SRA737 trial samples, the overall cost of the panel development and the depth of analysis required to determine mutation frequency opposed to background signal.

The panel designed consists of 32 key genes linked to the DNA damage response. Initially the panel selected contained 100 genes, but the preliminary plasma – cfDNA extractions showed that we would have insufficient DNA from the plasma volume available to proceed and therefore gene selection was scaled down. Genes were therefore selected according to their role in the DNA damage response, known interactions with NF-κB and direct interactions with CHK1. The genes selected are listed in Table 6.1.

After multiple discussions with Illumina and the Core Genomics Facility Team at Newcastle University, the decision was made to use an Illumina Nextera Rapid capture custom enrichment kit combined with TruSight Oncology reagents. This was based on the quantity of cfDNA extracted from samples and the recommendations from the team at Illumina. We discussed how to maximise data output with the amount of cfDNA extracted. Exome sequencing was selected to examine the coding regions of the genome and was feasible to be run with a low input of DNA. This type of kit also allowed the design of a custom-made exome sequencing panel for the 32 genes selected.

Table 6.1. Selected gene panel list for next generation sequencing of SRA737 patient samples. 32 genes were selected based on their interactions with CHK1 within the DNA damage response and interactions with NF-κB**.**

Gene	Protein	DNA Damage Response	Known interactions with NF-κB	Direct Target of CHK1	Function	Previously discussed in resistance?	Ref
ATR	ATR	✓	✓	✓	Cell cycle arrest and DNA damage repair in response to single stranded DNA damage	✓	(10,76,77, 224,325–328)
ATRIP	ATRIP	✓		✓	Binds to ATR and recruits CHK1		(53, 82,272,425, 537)
CHEK1	CHK1	✓	✓	✓	Cell cycle arrest in event of DNA damage in S and G2/M phases		(9,82,83,115,160,252,273)
CHEK2	CHK2	✓		✓	Cell cycle arrest in event of DNA damage in G1 phase		(49,76,116,123,333, 334)
CLSPN	Claspin	✓	✓	✓	Adaptor protein in recruitment of CHK1	✓	(224,230, 335,336)
HERC2	HERC2	✓		✓	Regulates claspin stability		(538,539)
RAD17	RAD17	✓			Recruits 9-1-1 complex onto chromatin after DNA damage		(75,77,80, 339)
RPA1	RPA1	✓			Binds and stabilises single-stranded DNA in the event of DNA damage		(75,77,79, 80)
TOPBP1	TOPBP1	✓			Rescue of stalled replication forks Checkpoint control		(75,77,79, 80)

Gene	Protein	DNA Damage Response	Known interactions with NF-κB	Direct Target of CHK1	Function	Previously discussed in resistance?	Ref
USP20	USP20	✓			Regulates Claspin stability Deubiquitinates hypoxia-inducible factor (HIF)-1 alpha causing angiogenesis/metastases		(243,538)
Wee1	WEE1	✓		✓	Negative regulator of entry into mitosis (G2 to M transition)	✓	(99,100)
C-Rel	C-Rel		✓		NF-κB Transcriptional activator Involved with Claspin regulation	✓	(202,209, 224)
Rel-A (P65)	REL-A (P65)		✓	✓	Forms the most abundant NF-κB complex Involved with Claspin regulation	✓	(244,252)
ABL1	ABL1	✓			Transcription factor - cell division, adhesion, differentiation, and response to stress		(61,210)
FANCA	FANCA	✓			Crosslink repair		(55,106)
FANCC	FANCC	✓			Crosslink repair		(55,66)
FANCE	FANCE	✓			Crosslink repair		(55,66)
FANCF	FANCF	✓			Crosslink repair Tumour suppressor		(55,106)
FANCG	FANCG	✓			Crosslink repair		(55,106)
CDC25A	CDC25A	✓		✓	Required for G1 to S phase progression of cell cycle	✓	(14,49,87, 123,191)

Gene	Protein	DNA Damage Response	Known interactions with NF-κB	Direct Target of CHK1	Function	Previously discussed in resistance?	Ref
CDC25B	CDC25B	✓		✓	Activates the cyclin dependent kinase CDC2 Required for entry into mitosis		(109,110, 115)
CDC25C	CDC25C	✓		✓	Directs dephosphorylation of cyclin B-bound CDC2 Triggers entry into mitosis Suppresses p53-induced growth arrest		(92,93,96, 125–127)
CCNE1	Cyclin E1	✓			Regulatory subunit of CDK2 Required for cell cycle G1/S transition	✓	(179,203)
c-MYC	c-Myc		✓		Proto-oncogene	✓	(197,198, 224,336)
MAPKAPK 2/ MK2	MK2	✓		✓	Cytokine production Endocytosis Reorganisation of the cytoskeleton Cell cycle control DNA damage response Transcriptional regulation	✓	(13,109, 110,192, 341)
PPM1A	PPM1A	✓	✓	✓	Dephosphorylates and negatively regulates MAP kinases		(540,541)
PRKDC	DNA-PKcs	✓			Non-homologous end joining Required for double-strand break repair		(64,67, 338)

Gene	Protein	DNA Damage Response	Known interactions with NF-κB	Direct Target of CHK1	Function	Previously discussed in resistance?	Ref
RAD51	RAD51	✓		✓	Homologous recombination and repair of DNA	✓	(49,130, 184,193)
TIMELESS	TIM	✓		✓	Involved in cell survival after damage/ stress Increase in DNA polymerase activity Maintenance of telomere length Role in circadian rhythm autoregulatory loop		(1,9,217, 218,339)
XRCC5	XRCC5/ Ku80	✓			DNA helicase II complex Binds preferentially to fork-like ends of double-stranded DNA Cell cycle-dependent		(65,67, 289)
XRCC6	XRCC6/ Ku70	✓			Single-stranded DNA dependent & ATP-dependent helicase		(65,67, 289)
BRCA1	BRCA1	✓	✓	✓	Central role in DNA repair Facilitates cellular responses to DNA damage		(43,65, 101–103, 289, 340–342)

6.6. Completion of sample plasma cfDNA extraction

In order to proceed with next generation sequencing, cfDNA had to be extracted from patient plasma samples. A total of 137 patient samples from 72 different patients were received from the SRA737 trial. The quality of samples received from the study was variable. Factors impacting on sample quality included variation in the plasma volume received (between 1ml and 3mls) and blood contamination of plasma samples. These factors were difficult to regulate as, although protocols for sample extraction were standardised, samples were taken and sent from multiple different clinical centres leading to some variation. The processes involved in sample extraction and preparation for sequencing are shown in Figure 6.3.

cfDNA was extracted from the plasma samples using the QIAGEN QIAamp Circulating Nucleic Acid Kit as discussed in Section 3.11.1 and eluted into 50µls/ml plasma of extraction buffer based on preliminary tests. Elution volume was therefore 50-150µl per sample. A maximum of 9 plasma samples were extracted at the same time in order to avoid cross contamination of samples and to minimise sample loss in the event of problems with the cfDNA extraction run.

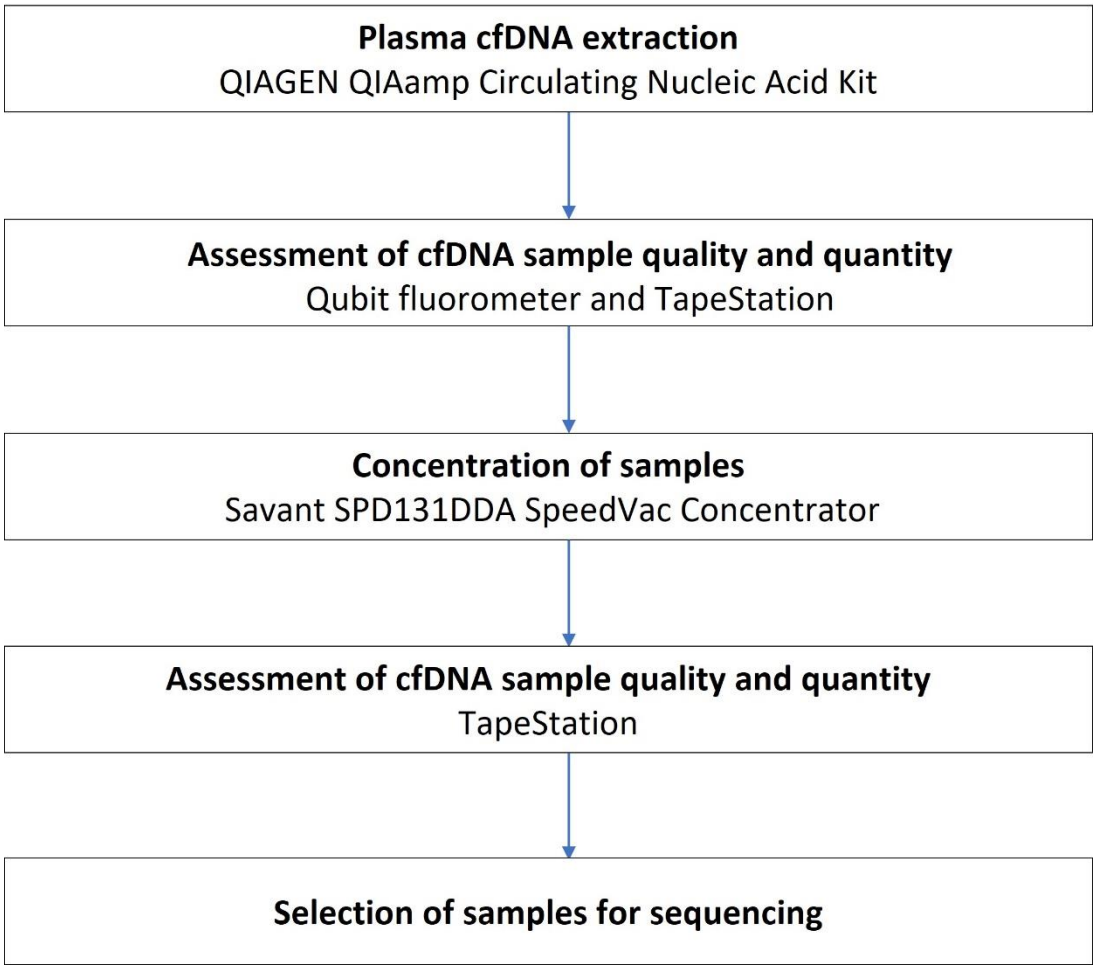

Figure 6.3. Flow chart summarising the steps taken to process cfDNA samples prior to sequencing. This involves concentration of the cfDNA samples and quality control.

6.7. Quality control of cfDNA samples

Quality control checks for quantity and sample integrity were required prior to next generation sequencing to ensure that samples were at the required standard to proceed. Post cfDNA extraction, samples were initially tested for cfDNA quantification using a Qubit fluorometer as per Section 3.11.2. This method gave total cfDNA quantification and allowed the estimation of sample suitability for next generation sequencing. Discussions with Illumina at this stage stated that 30ng of cfDNA were required for the sequencing panel. It was therefore hypothesised that samples recorded as having cfDNA less than 30ng with Qubit analysis would be unsuitable for sequencing.

Further quality control was performed on all samples using the TapeStation HS D1000 ScreenTapes (Agilent) as discussed in Section 3.11.3. This was to determine cfDNA fragment length as well as additional cfDNA quantification. Optimal cfDNA fragment length for library preparation was 75-250bp. If the fragment size was too large, DNA shearing would have to be considered as otherwise the adaptors would not preferentially bind to the cfDNA and impact on the library quality.

In comparison to the Qubit analysis, TapeStation software allows for selection of specific sample regions in order to provide a more accurate quantity reading within the required range. TapeStation analysis permitted cfDNA quantification measurements purely on the 75-250bp range of each sample. Figure 6.4 shows an example of sample quality control (QC) analysis of cfDNA fragment length and quality using the TapeStation software.

TapeStation analysis of samples showed a distribution of 2 main fragment peaks, as demonstrated in Figure 6.4. The samples all had a smaller peak with fragment size of approximately 100-200bp, and a second larger peak of fragment size 400-1000bp. These findings were reviewed and discussed with Illumina prior to commencement of library preparation. It was determined that provided there was enough cfDNA in the 75-250bp range that shearing would not be required. The amount of cfDNA required in this range was 30ng.

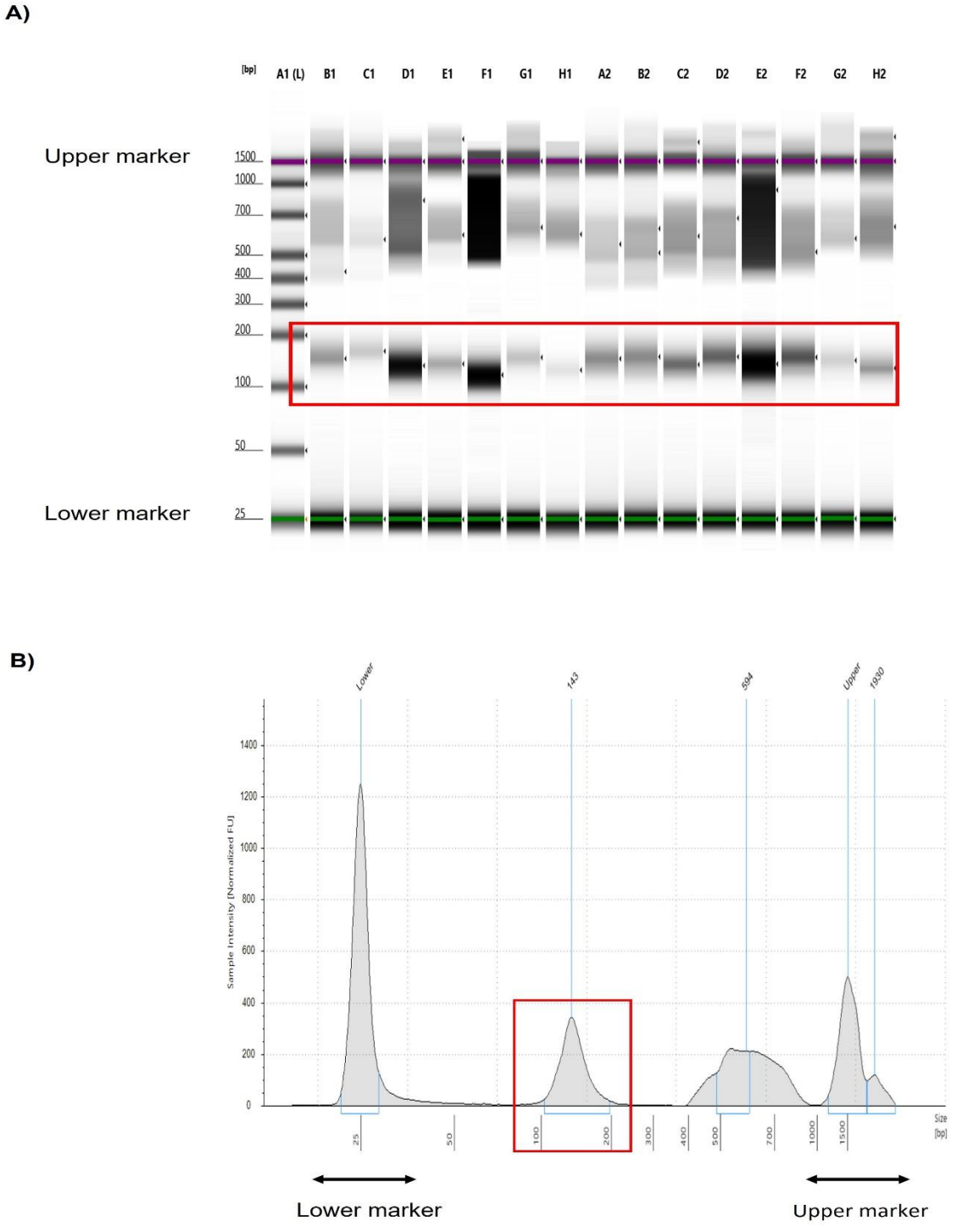

Figure 6.4. Example of TapeStation data. A) Gel electrophoresis image of multiple sample analysis from the TapeStation software. Columns B1-H2 show the samples and the spread of fragment size in each sample. The upper and lower bands represent upper and lower markers in each lane. The darker samples have higher concentrations of DNA. Highlighted is the band size thought to be most attributable to ctDNA and all samples have a clear band in the 100-200bp region. B) An example of individual sample analysis from TapeStation software. This demonstrates the spread of DNA fragment size, between upper and lower markers. Highlighted is the peak between 100bp and 200bp showing the average DNA fragment size. Samples also had a second peak in the 400-1000bp range, but current sequencing technology is not able to accurately analyse DNA fragments of this size.

Quantification of the 75-250bp fragment size using the TapeStation provided greater detail about sample quality within this range. Given that Qubit analysis provided total cfDNA content rather than a specific fragment size, most samples had less cfDNA in the 75-250bp range as determined by TapeStation analysis. Table 6.2 shows how cfDNA quantity varies between the two QC methods used. Although necessary, the requirement of samples to have at least 30ng of cfDNA in the 75-250bp range excluded many samples that were thought to be initially suitable as initial estimates were made based on total cfDNA content.

Further discussions with Illumina prior to library preparation determined that the 30ng of cfDNA in the required fragment range additionally needed to be in a maximum of 50µl starting volume. Given that samples had been prepared in 50µl/ml of plasma, many of the samples were not concentrated enough for library preparation use. Samples with a 75-250bp range cfDNA concentration of 0.6ng/µl or greater were adequate for library preparation, however all remaining samples were not adequately concentrated for sequencing.

Sample volumes were discussed with the team at the Genomics Core Facility at Newcastle University. The decision was made to vacuum spin samples with a volume greater than 50µl and a starting cfDNA concentration less than 0.6ng/µl. This was to concentrate samples and increase the number of cfDNA samples eligible for next generation sequencing.

Table 6.2. TapeStation results demonstrate more precision and selectivity for the required 75-250bp range in comparison to results from the Qubit fluorometer. The table shows all SRA737 samples and values for Qubit and TapeStation. Values shown for the Qubit analysis are for total cfDNA yield and TapeStation analysis for the 75-250bp range. Unhighlighted samples are greater than 30ng for the 75-250bp TapeStation range and therefore contain enough cfDNA for sequencing. Samples highlighted in grey were less than 30ng total yield for Qubit and for the 75-250bp range TapeStation readings. Samples highlighted in red were greater than 30ng total yield for Qubit but less than 30ng for the 75-250bp range TapeStation yield. Sample ID Key: first number = site, second number = patient number. Time points: D-7 to -4 (pre CHK1i), C3D1 (mid CHK1i treatment), EOS (end of study).

Sample (Site/patient number)	Time point	Elution Volume (µl)	Qubit Yield (ng)	75-250 bp Yield from TapeStation (ng)
011/002	D-7 to -4	100	164	45.9
011/003	D-7 to -4	100	48.8	13.1
011/006	D-7 to -4	50	18.7	4.9
011/006	C3D1	150	34.5	50.4
011/006	EOS	100	1010	749
011/010	D-7 to -4	150	19.8	3.5
011/010	C3D1	100	47.8	12.7
011/010	EOS	150	112.8	30.8
011/011	D-7 to -4	100	163	130
011/011	EOS	100	83.8	49.7
011/012	D-7 to -4	100	143	62.8
011/012	EOS	100	32	3.2
011/013	D-7 to -4	150	213	277.5
011/013	C3D1	100	268	253
011/018	D-7 to -4	100	28	22.1
031/001	D-7 to -4	150	237	162
031/001	C3D1	100	171	69.2
031/002	D-7 to -4	150	111.6	33.8
031/003	D-7 to -4	150	109.5	48.8
031/003	EOS	150	98.4	95.3
031/004	EOS	100	34.8	9.1

Sample (Site/patient number)	Time point	Elution Volume (µl)	Qubit Yield (ng)	75-250 bp Yield from TapeStation (ng)
031/004	D-7 to -4	150	42.9	15.6
031/004	C3D1	150	38.7	14.3
031/005	D-7 to -4	100	34.4	7.8
031/005	C3D1	100	26	7.2
031/005	EOS	150	68.1	21.2
031/007	D-7 to -4	100	18	4.8
031/007	C3D1	150	84.9	22.7
031/008	D-7 to -4	150	47.1	39.6
031/008	EOS	100	16.2	12.6
031/009	D-7 to -4	100	23	7.3
031/011	D-7 to -4	150	129.3	122.1
031/011	C3D1	150	140.1	171
031/011	EOS	100	64.8	40.4
031/013	D-7 to -4	100	73.2	73.5
031/013	EOS	100	62	29.8
031/019	C3D1	100	128	56.7
031/019	EOS	50	20.2	5.6
031/019	D-7 to -4	100	11.8	4.1
031/025	D-7 to -4	100	344	278
031/025	EOS	150	5100	2160
031/031	D-7 to -4	50	5.9	1.7
031/031	EOS	100	22.4	5.1
031/038	D-7 to -4	100	12.4	3.0
031/038	C3D1	100	20.4	5.9
031/038	EOS	100	26.6	15.4
031/040	D-7 to -4	150	27.3	11.5

Sample (Site/patient number)	Time point	Elution Volume (µl)	Qubit Yield (ng)	75-250 bp Yield from TapeStation (ng)
031/040	C3D1	100	18.4	6.5
031/040	EOS	100	23	10.2
031/042	D-7 to -4	100	26	6.4
031/042	C3D1	100	35.6	4.9
031/047	D-7 to -4	100	16.4	5.8
031/047	EOS	100	11.2	2.8
031/054	D-7 to -4	100	14.2	4.9
031/054	C3D1	100	12	2.5
031/060	D-7 to -4	100	10.8	6.3
031/060	C3D1	100	25	9.8
031/061	D-7 to -4	100	86.4	32.8
031/061	EOS	100	151	156
031/071	D-7 to -4	100	62.8	13.7
031/076	EOS	100	197	197
031/076	D-7 to -4	100	76.8	60
031/089	D-7 to 04	100	145	20.4
031/093	C3D1	100	11	3.6
031/093	D-7 to -4	100	22.8	4.8
039/003	D-7 to -4	100	35	7.1
039/003	EOS	100	19	5.7
039/010	D-7 to -4	150	45.6	13.8
039/010	C3D1	100	29.6	10
039/015	D-7 to -4	150	115.8	114.5
039/015	EOS	100	103	34.9
039/015	C3D1	100	89	31.2
039/029	D-7 to -4	100	18.8	16.7
039/029	EOS	100	38.2	27.3

Sample (Site/patient number)	Time point	Elution Volume (µl)	Qubit Yield (ng)	75-250 bp Yield from TapeStation (ng)
039/038	D-7 to -4	100	252	8.1
039/038	EOS	100	151	20.5
039/038	Unscheduled (D-7 to -4)	50	103	15.1
039/055	D-7 to -4	100	37.8	7.4
039/055	EOS	100	62	6.9
141/002	D-7 to -4	100	12.8	3.3
141/002	C3D1	100	26.8	5.8
141/002	EOS	100	45	4.5
141/003	D-7 to -4	100	672	104
141/005	D-7 to -4	100	151	6.8
141/005	EOS	100	514	263
141/012	D-7 to -4	100	30.2	14.8
141/012	EOS	100	736	340
143/007	C3D1	150	34.5	21.3
143/010	D-7 to -4	100	79	13
143/024	D-7 to -4	100	70.6	3.5
143/025	D-7 to -4	100	105	16.1
143/036	D-7 to -4	100	12	2.9
143/036	EOS	150	22.4	5.2
143/046	D-7 to -4	100	18.8	4.1
144/009	D-7 to -4	50	8.4	1.1
144/009	C3D1	50	7.9	1.2
144/016	D-7 to -4	50	38.1	5.3
144/016	C3D1	50	50.5	12.3
144/026	D-7 to -4	50	5.5	1.1
144/026	C3D1	50	5.4	1.7

Sample (Site/patient number)	Time point	Elution Volume (µl)	Qubit Yield (ng)	75-250 bp Yield from TapeStation (ng)
144/027	D-7 to -4	50	105	27.7
144/027	EOS	50	52	22.9
144/028	D-7 to -4	50	13.9	2.2
144/028	EOS	50	6.1	0.4
144/029	D-7 to -4	50	18.5	1.1
145/001	D-7 to -4	100	790	1660
145/001	EOS	100	4060	2550
146/001	D-7 to -4	100	51.6	13.4
146/001	C3D1	50	9.7	3.1
146/001	EOS	100	18.2	36.1
146/002	D-7 to -4	100	18.8	6.2
146/002	C3D1	100	14.2	5.8
148/001	D-7 to -4	100	182	49.9
148/001	EOS	100	456	326
148/002	D-7 to -4	100	146	35.2
148/015	D-7 to -4	50	15.2	3.0
148/015	EOS	100	61.6	6.9
148/017	D-7 to -4	100	22	11.2
148/017	C3D1	100	230	58.8
148/020	D-7 to -4	50	55.5	101
148/020	EOS	100	154	223
149/002	D-7 to -4	100	83.2	19.9
149/003	D-7 to -4	100	44	9.6
149/010	D-7 to -4	100	61.2	37.5
149/017	D-7 to -4	100	10	2.2

6.8. Concentration of samples using vacuum spin method

Prior to vacuum spinning SRA737 trial samples, preliminary tests were performed with 4 existing PROSPECT cfDNA samples. This was to verify that samples were adequately concentrated and to ensure that no complications occurred during the vacuum spin process. The starting sample volume was 145µl and the concentration per sample less than 0.5ng/µl.

Samples were transferred to Lo-Bind microcentrifuge tubes and vacuum spun using the Savant SPD131DDA SpeedVac Concentrator on a medium heat and predefined automatic setting on the machine. Samples were reviewed at 30 minute intervals to check sample volume, aiming for a final volume of 50µl. Total spin time required was 90 minutes, leading to a remaining volume of 47µl per sample. Samples were analysed using TapeStation HS D1000 ScreenTapes for fragment length and to calculate cfDNA after vacuum spin. The results are shown in Table 6.3.

Table 6.3. Preliminary SpeedVac results show increased concentration of cfDNA samples. Samples were vacuum spun for 90 minutes and checked using the TapeStation HS D1000 DNA ScreenTapes. 2µl of DNA from each sample were used for TapeStation analysis, leading to a remaining volume of 45µl. Fragment length decreased with vacuum spin but was still in the 75-250bp range required for sequencing. DNA post vacuum spin was more concentrated and in an adequate starting volume of buffer to proceed with library preparation.

PROSPECT sample ID	Pre SpeedVac mean fragment length (bp)	Post SpeedVac mean fragment length (bp)	Pre SpeedVac 75-250bp Concentration (ng/µl)	Post SpeedVac 75-250bp Concentration (ng/µl)	Total cfDNA in remaining 45µl sample
009 (1)	156	127	0.2	0.72	32.44
010 (2)	145	134	0.23	1.8	81
011 (3)	161	119	0.25	34.1	1534.5
013 (4)	158	116	0.28	1.73	77.85

Given that the preliminary PROSPECT samples were concentrated sufficiently enough to proceed with library preparation, SRA737 trial samples less than 0.6ng/µl were vacuum spun using the same conditions - medium heat and automatic setting. Samples were checked every 30 minutes until there was a remaining volume of 50µl. Samples were then checked via TapeStation for quality and quantity.

Despite maintaining the same initial conditions, sample concentration decreased significantly in the SRA737 trial samples post SpeedVac. Conditions were changed by adjusting the SpeedVac temperature setting to low. Samples then required a longer overall time to concentrate and were checked every 30 minutes for total change in volume as previously, aiming for a final volume of 50µl. Sample cfDNA concentration continued to decrease with these changes.

Concerns over total cfDNA sample loss were discussed with the team at the Genomics Core Facility at Newcastle University. The decision was made to continue despite sample loss as samples were required to be more concentrated in a smaller volume of buffer and alternative methods such as ethanol precipitation would also lead to a much greater sample loss. Table 6.4 shows representative pre and post SpeedVac results for SRA737 samples.

Table 6.4. Changes in SRA737 sample DNA quantity pre and post vacuum spin. Samples were concentrated using the SpeedVac until volumes were less than 50µl. Sample concentration was monitored every 30 minutes. The first 16 samples were spun at medium heat and the remaining samples were spun at low heat. Decrease in sample volume was not uniform in the same batch of samples. TapeStation values were obtained post vacuum spin and compared to pre vacuum spin levels. Levels of DNA quantity within the 75-250bp range often dropped dramatically in samples post vacuum spin, which is suggestive of sample loss. Sample ID Key: first number = site, second number = patient number.
Time points: D-7 to -4 (pre CHK1i), C3D1 (mid CHK1i treatment), EOS (end of study).

Sample (Site/patient number)	Time point	Elution volume (µl)	TapeStation 75-250 bp yield pre-vacuum spin (ng)	Total volume post- vacuum spin (µl)	TapeStation 75-250 bp yield post vacuum spin (ng)
011/002	D-7 to -4	100	45.9	48	38.3
011/003	D-7 to -4	100	13.1	48	7.5
011/006	C3D1	150	50.4	37	14.4
011/010	C3D1	100	12.7	48	4.8
011/010	EOS	150	30.8	37	7.8
011/011	EOS	100	49.7	50	33.4
011/012	D-7 to -4	100	62.8	48	128.2
011/012	EOS	100	3.2	46	0.3
031/001	C3D1	100	69.2	48	42.4
031/002	D-7 to -4	150	33.8	32	14.5
031/003	D-7 to -4	150	48.8	31	16.2
031/004	EOS	100	9.1	48	2.6
031/004	D-7 to -4	150	15.6	33	4.2
031/004	C3D1	150	14.3	33	5.3
031/005	D-7 to -4	100	7.8	48	2.2
031/005	EOS	150	21.2	33	35.6
031/008	D-7 to -4	150	39.6	34	3.5
031/011	EOS	100	40.4	48	44.5
031/013	D-7 to -4	100	73.5	49	97.5
031/013	EOS	100	29.8	49	39.2
031/042	C3D1	100	4.9	45	0.2
031/061	D-7 to -4	100	32.8	43	2
031/076	D-7 to -4	100	60	48	0.5
031/089	D-7 to 04	100	20.4	49	12.7
039/003	D-7 to -4	100	7.1	38	0.5
039/010	D-7 to -4	150	13.8	34	3.2
039/015	EOS	100	34.9	39	19.3
039/015	C3D1	100	31.2	40	5.9
039/029	EOS	100	27.3	38	0.3
039/038	D-7 to -4	100	8.1	38	0.1
039/038	EOS	100	20.5	38	92.3
039/055	D-7 to -4	100	7.4	39	1.1
039/055	EOS	100	6.9	40	0.2
141/002	EOS	100	4.5	40	0.04
141/005	D-7 to -4	100	6.8	38	0.2
141/012	D-7 to -4	100	14.8	34	0.2
143/007	C3D1	150	21.3	33	8.8
143/010	D-7 to -4	100	13	38	32.3
143/024	D-7 to -4	100	3.5	38	0
143/025	D-7 to -4	100	16.1	38	0
146/001	D-7 to -4	100	13.4	38	1.3
148/001	D-7 to -4	100	49.9	33	31.6
148/002	D-7 to -4	100	35.2	28	1.8
148/015	EOS	100	6.9	33	0
148/017	C3D1	100	58.8	38	2.6
149/002	D-7 to -4	100	19.9	38	0.4
149/003	D-7 to -4	100	9.6	34	0.3
149/010	D-7 to -4	100	37.5	34	0.9

6.9. Preliminary library preparation and sequencing

Prior to performing next generation sequencing on the SRA737 trial samples, a test library preparation and sequencing run was performed. This was the first attempt of cfDNA sequencing in Newcastle University and the kit was customised from Illumina, therefore it was necessary to check that the protocol for library preparation worked. As the overall concentration of samples had decreased, there were concerns about the suitability of samples for sequencing as many had dropped below the 30ng total content. In order to assess whether less cfDNA could be used in the library preparation, the decision was made to use serial dilutions of cfDNA on the initial test run. This was to see if the same quality of sequencing and read depth could be obtained. Figure 6.5 details the steps involved in the library preparation process.

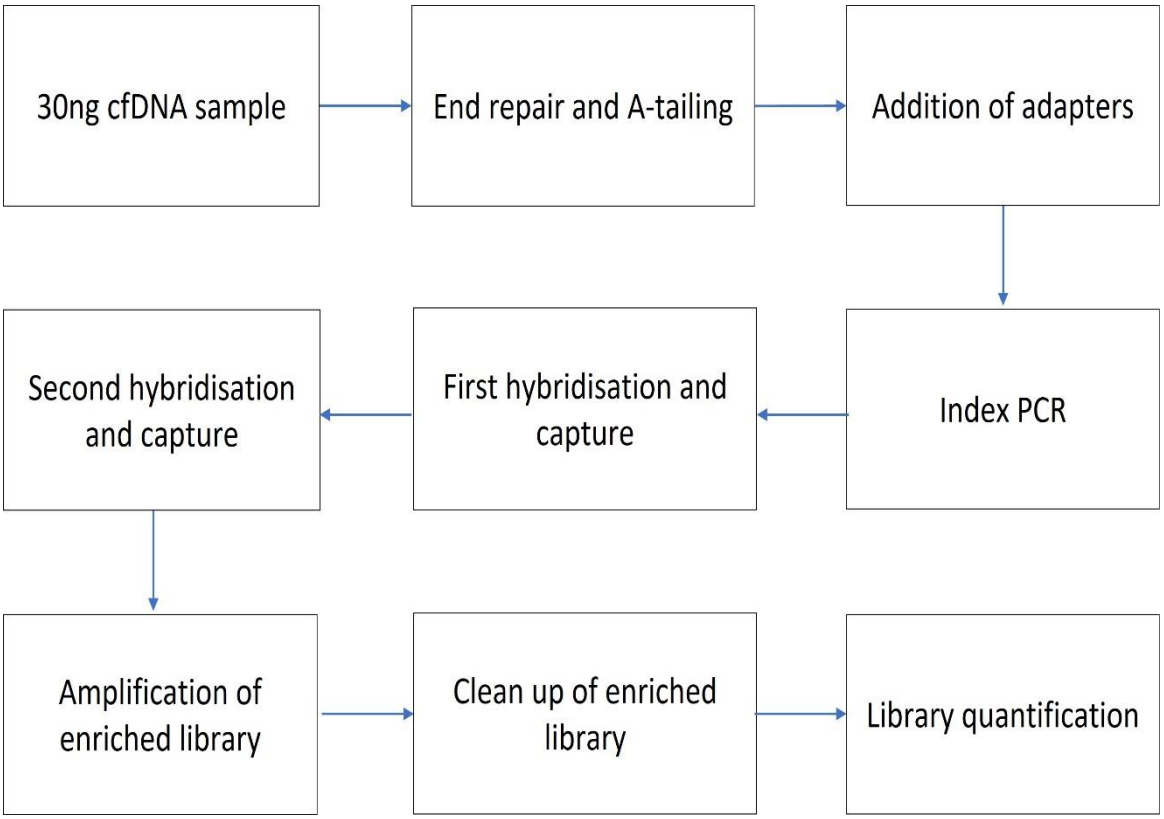

Figure 6.5. Library preparation of cfDNA samples prior to next generation sequencing using the Illumina Trusight 170 protocol. The preparation of cfDNA samples prior to next generation sequencing took 2 days. Day 1 finished with the first hybridisation and capture which required an overnight step. Day 2 finished with quantification of library samples using TapeStation analysis.

The initial library preparation and sequencing run was performed by Raf Hussain at the Genomics Core Facility, Newcastle University. I assisted with the library preparation. Given that this was the first attempt of cfDNA sequencing at Newcastle University, additional support was provided on site by Claire Logan, Illumina Representative. The Illumina Trusight 170 protocol was followed with modifications for the addition of unique molecular identifier (UMI) adaptors (see Section 3.11.5 for library preparation protocol).

UMIs are molecular tags that make each molecule in the initial DNA sample unique, therefore after amplification all molecules with the same UMI are from the same source fragment (535,536). The decision was made to include UMIs in discussions with Illumina to increase the accuracy with reads given the small starting quantity of cfDNA. Table 6.5 shows the samples selected for the initial sequencing run, based on concentration level and sample preparation.

Table 6.5. Samples selected for preliminary sequencing run. Samples chosen for the first run were selected to ensure that the library preparation worked and to see if differences in sample conditions impacted on the quality of sequenced data. Selection was made from highly concentrated PROSPECT trial samples used in the initial preparation test runs, PROSPECT samples that had undergone vacuum spinning, highly concentrated SRA737 trial samples and serial dilutions of PROSPECT sample 010. SRA737 sample ID Key: first number = site, second number = patient number. D-7 to -4 is pre SRA737 sample, C3D1 is mid SRA737 treatment sample and EOS is end of SRA737 study sample. TE buffer = 1X Tris EDTA buffer.

	Sequencing run ID	Sample ID	TapeStation (ng/µl)	Amount required for 30ng (µl)	TE buffer (µl)
Test PROSPECT samples	**1**	003	0.646	46.4	3.6
	2	005	0.891	33.7	16.3
	3	012	1.19	25.2	24.8
Vac spin	**4**	009	0.72	41.6	8.4
	5	010	1.8	16.7	33.3
SRA737 trial samples (Sample ID – site/patient number & time point)	**6**	011/013 D-7 to -4	1.85	16.2	33.8
	7	011/013 C3D1	2.53	11.9	38.1
	8	011/006 EOS	7.49	4.0	46.0
	9	031/061 EOS	1.56	19.2	30.8
	10	031/076 EOS	1.97	15.2	34.8
Diluted samples	**11**	010 15ng cfDNA	1.8	8.3	41.7
	12	010 7.5ng cfDNA	1.8	4.2	45.8

In order to monitor the progress of the library preparation, libraries were quantified using the TapeStation HS 5000 ScreenTape after the first hybridisation step and again after library clean-up. The review post hybridisation 1 (HYB1) showed that the library preparation appeared to be working as sample peak sizes on the TapeStation had shifted to the right as shown in Figure 6.6. This would be indicative of larger DNA fragments which would be expected post the addition of primers and adapters to the samples. This initial review showed potential additional peaks in samples with lower DNA concentration (15ng and 7.5ng) as shown in Figure 6.6, which could affect sample reading depth later.

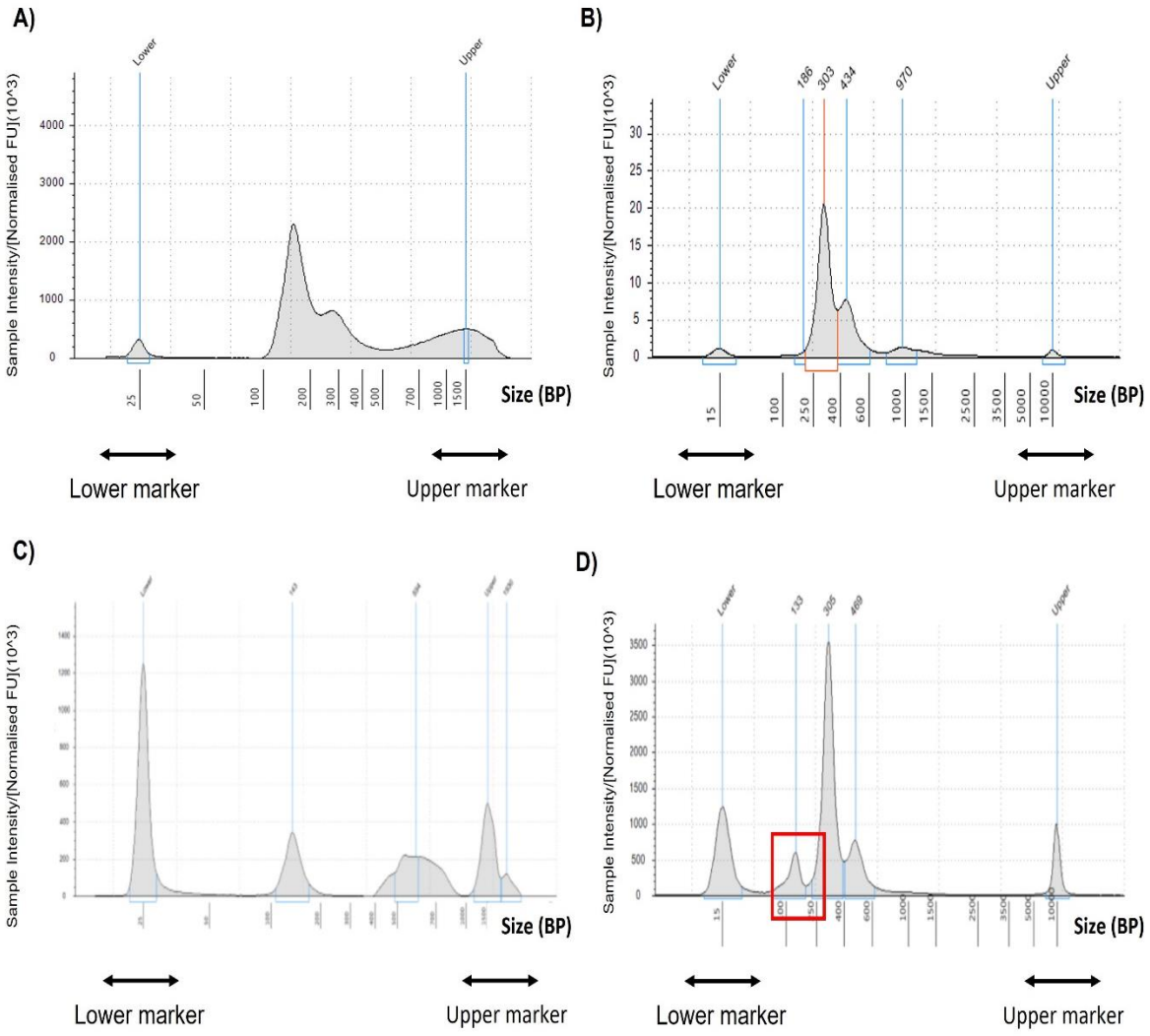

Figure 6.6. Differences in fragment size and sample peaks pre and post library preparation as determined by TapeStation. Representative samples from first sequencing run. The upper and lower bands represent upper and lower markers in each lane. A) SRA737 sample reading from HS D1000 ScreenTape showing distribution of fragment size prior to library preparation. B) Sample reading from HS D5000 ScreenTape for same samples as A), showing an increase in average peak size post library preparation. C) Initial PROSPECT-NE sample from HS D1000 ScreenTape. D) Sample dilution (7.5ng cfDNA instead of 30ng cfDNA) from sample in B) showing additional peak after library preparation (highlighted with red box).

The second library quantification was performed after the library clean up. The quality between libraries at this stage was consistent between samples with 30ng of cfDNA and viewed as adequate for sequencing. There was a possible dimerisation of primers in the samples with a lower concentration of cfDNA, particularly with the sample with only 7.5ng of cfDNA. This had to be taken into consideration as there was a potential of a loss of read depth in these samples as less primers would be available for library binding.

The decision had previously been made to run the cfDNA libraries on the NextSeq platform. The initial samples however were run on the MiSeq platform at the Genomics Core Facility, Newcastle University by Raf Hussain. The MiSeq platform was chosen for the initial run because it was faster and cheaper than the NextSeq platform, but we were still able to determine that the samples were successfully sequenced before committing costs to proceeding with a more expensive option. This option would also allow the analysis of the diluted samples in comparison to the concentrated parent sample and see if there was a loss in data at a lower sample concentration.

6.10. Summary of provisional cfDNA sequencing data

The first cfDNA sequencing run showed that samples could be successfully sequenced and provided information about sample dilution. The data obtained from the 15ng sample was of similar read depth and quality to the 30ng sample, however new low-level mutations appeared in the 7.5ng sample. This was determined to be an increase in the background false positive rate due to the low sample concentration. Samples with 7.5ng cfDNA were therefore excluded from sequencing runs.

Based on the initial sequencing run, SRA737 samples were selected for future sequencing runs (Table 6.6). All samples with a baseline cfDNA concentration of 0.6ng/µl in the 75-250bp range were included as these samples reached the threshold for 30ng total cfDNA concentration. Given that the 15ng sample provided data of similar read depth and quality to the 30ng concentration, samples with between 15ng and 30ng of cfDNA were included. As the number of suitable samples was small compared to the initial cohort, samples as low as 12ng total cfDNA were included. This increased the size of the cohort and provided more paired samples for some patients with samples already prepared for sequencing. The downside of including these samples was that the concentration may have not been enough for sequencing, but they were included with that known caveat.

In addition, to make up sequencing numbers, samples with sufficient cfDNA from the initial PROSPECT-NE study were also included. These samples are also from a phase 1 cohort and therefore a similar patient group to the patients on the SRA737 study, except samples are taken from patients not on treatment. The PROSPECT-NE patient group have not been selected based on mutational status, therefore it would be interesting to assess if mutations seen in SRA737 patients are also found in the PROSPECT-NE cohort. The sample numbers used are only small, but this is only an exploratory cfDNA study to see if we can detect mutations from our phase 1 cfDNA samples. 42 samples from the SRA737 study were sequenced in full.

Table 6.6. Summary of SRA737 samples selected for next generation sequencing. Samples with 0.6ng/µl cfDNA within the 75-250bp range were automatically included. Sample 61 was highly concentrated and required a 1:10 dilution in order to record concentration. Samples that needed to be concentrated were vacuum spun using the SpeedVac. A total of 32 samples reached the 30ng cfDNA standard. 5 further samples had between 15-30ng cfDNA and were included given that preliminary studies showed that these could be sequenced and sample quality remained good. A further 5 samples between 12 and 15ng were included to increase sample number as overall numbers used were small, with the risk taken that sample read depth may not be as good for these samples. SRA737 sample ID Key: first number = run ID, second number = site, third number = patient ID. D-7 to -4 is pre SRA737 sample, C3D1 is mid SRA737 treatment sample and EOS is end of SRA737 study sample.

Sample ID (Run ID_site_patient_time point)	TapeStation (ng/µl)	Amount of cfDNA used (ng)
1_011_006_C3D1	0.39	14.4
3_031_002_D7to4	0.453	14.4
4_031_003_D7to4	0.52	16.1
7_031_005_EOS	1.08	30
11_011_002_D7to4	0.798	30
14_011_011_EOS	0.668	30
15_011_012_D7to4	2.67	30
17_031_001_C3D1	0.884	30
20_031_011_EOS	0.928	30
21_031_013_D7to4	1.99	30
22_031_013_EOS	0.801	30
26_031_089_D7to4	0.26	12.7
28_039_015_EOS	0.496	19.3
32_039_038_EOS	2.43	30
38_143_010_D7to4	0.902	30
42_148_001_D7to4	0.958	30

Sample ID (Run ID_site_patient_time point)	TapeStation (ng/µl)	Amount of cfDNA used (ng)
49_031_019_C3D1	0.316	12
50_011_006_EOS	7.49	30
51_011_013_D7to4	1.85	30
52_011_013_C3D1	2.53	30
53_031_061_EOS	1.56	30
54_031_076_EOS	1.97	30
55_011_011_D7to4	1.31	30
56_031_001_D7to4	1.09	30
57_031_003_EOS	0.629	30
58_031_011_D7to4	0.83	30
59_031_011_C3D1	1.14	30
60_031_025_D7to4	2.95	30
61_031_025_EOS (1:10 dilution)	6.4	30
62_039_015_D7to4	0.763	30
63_141_003_D7to4	1.04	30
64_141_005_EOS	2.68	30
65_141_012_EOS	3.26	30
66_145_001_D7to4	16	30
67_145_001_EOS	24.1	30
68_148_001_EOS	3.55	30

Sample ID (Run ID_site_patient_time point)	TapeStation (ng/µl)	Amount of cfDNA used (ng)
69_148_020_D7to4	2.02	30
70_148_020_EOS	2.27	30
71_144_016_C3D1	0.25	12.3
72_039_038_D7to4	0.30	15.1
73_144_027_D7to4	0.55	27.7
74_144_027_EOS	0.46	22.9

6.11. Sequencing analysis of mutations detected in cfDNA

Dr. Iglika Ivanova from the Perkins' lab worked with Dr. Peter Leary at Newcastle University Bioinformatics Support Unit (BSU) to develop an analysis pipeline where variant calling could be made with high confidence. This was coordinated via the use of Mutect2 analysis software.

The main goal in the cfDNA arm of the study was to see if we could successfully extract cfDNA from the SRA737 patient samples. The secondary aim was to try and identify tumour mutations that changed as a result of SRA737 treatment. This has been limited by the variations in cfDNA yield caused by sample variability and small sample size as previously discussed in this chapter. Therefore, the number of paired samples (with high yield cfDNA from patients both before and after SRA737 treatment), was lower than initially anticipated at the start of this study.

The analysis of tumour associated mutations from cfDNA can be challenging due to the low number of 'variant' reads versus the background of 'normal' reads. Care has to be taken when comparisons are being made to a reference genome in order to exclude variants that might arise from SNPs already present in the patient. In addition, it is important to exclude variants that may be erroneous due to poor sample quality.

A summary of the Mutect2 analysis methods used are described below:

1) Normal-tumour mode

For this analysis, the D4to7 samples taken from patients prior to treatment with SRA737 were used as a control "normal" sample, while the C3D1/EOS samples (mid and end of study) were used as a "tumour" sample. This allowed the input variants from the D4to7 sample to be compared to the variants found in the samples treated with SRA737. This analysis was only done with paired samples as these could be matched from the same patients. One pair (011_006) was not analysed in this mode because it did not have a D4to7 sample to use as the initial control.

2) Individual analysis of all samples in the tumour-only mode

To allow inclusion of all sequenced samples, the cfDNA sequencing database was passed through Mutect2 software analysis using the Broad Picard Pipeline in tumour-only mode. This analysis was performed to identify enriching or arising gene variants in comparison to sequences from reference genomes. The software can identify insertions or deletions of nucleotide bases (INDELs), point mutations, and copy number variants (CNVs), where sections of the genome are duplicated or removed in comparison to the reference genome. The Mutect2 software deciphers whether mutations are germline or somatic via a somatic variant discovery tool. Germline mutations are ruled out due to a presence at near 50% or 100% in the sample. Sequencing variants are also eliminated by the software.

A disadvantage of 'tumour-only' mode of analysis is that it can produce a high rate of false positive results. This occurs as software is designed to identify mutations in solid tumours, comparing a WT cancer free sample to a tumour sample. The cfDNA database here includes pre-treatment patients who all have a pre-existing cancer diagnosis; therefore a 'normal' cancer-free comparison was not possible. Subsequent validation of the Mutect2 analysis was required to ensure that the software had correctly identified novel mutations either arising or being enriched after SRA737 treatment.

Steps undertaken for manual analysis of paired samples:

To be confident in the data produced by Mutect2, manual analysis was further performed by Dr. Iglika Ivanova. For both modes of analysis, the BSU provided a file containing all variants before Mutect2 applied filters and a file of the PASSED variants after the filters had been applied. Separate to this, a file explaining why a variant was not passed as a valid tumour mutation by Mutect2 was provided.

Steps undertaken during manual analysis of samples are described below:

Step 1. All multi allelic variants from files analysed in tumour-only mode were removed. These were clearly artefacts due to PCR slippage. There were also incidences where Mutect2 alignment was incorrect, making variant identification unreliable.

Step 2. The lists from the paired samples were combined and filtered both by name and genomic location. This analysis meant that variants picked up in both D4to7 and C3D1/EOS samples appeared in parallel. From this list, the allelic percentage of variant reads from the C3D1/EOS sample was divided by the allelic percentage of variant reads from the D4to7 sample. This calculated the fold change in the allelic fraction following CHK1i treatment. Variants with a fold change >2 were marked as enriched. Other variants were disregarded.

Step 3. Variants that were only found in one of the samples from the pairs were deemed as novel if they had an allelic fraction of <0.3-0.4. Anything above this level would be classed as a germline SNP and not picked up by Mutect2. This is because the variant would be unlikely to originate from the primary cancer. Silent mutations were also discarded.

Step 4. This list was checked against the variants PASSED by Mutect2 in normal-tumour mode and marked up.

Step 5. The list was checked against variants PASSED by Mutect2 in tumour-only mode. The database was then split into three categories:

A. Enriched and novel variants that were passed by Mutect2 in either normal-tumour mode or tumour-only mode.

B. Enriched variants that were NOT PASSED by Mutect2

C. Novel variants that were NOT PASSED by Mutect2

Mutations in Category A were deemed to be high confidence variants, while variants in B or C, despite passing manual analysis, were deemed to be lower confidence.

Steps undertaken for manual analysis of unpaired samples:

Steps 1 and 5 from above were applied for sample analysis.

6.12. cfDNA sequencing results

Sequencing of the cfDNA samples was to see if mutations in the DNA damage response could be picked up in cfDNA. Sample numbers were small; therefore, we cannot make strong conclusions about mutational change and how this impacts on drug sensitivity and resistance, but this may provide additional focus for further investigational studies.

The main focus for the cfDNA results was based on variants where the coding sequence of the gene was affected, particularly where the same mutation has arisen in different patients. These are summarised in Table 6.7. Patient samples frequently exhibited multiple coding sequence mutations as demonstrated below.

Appendix Table 1 shows the genes in which novel low allelic fraction variants appeared following SRA737 treatment. That is, variants present in the EOS but not D4to7/C3D1 paired patient samples (or C3D1 versus D4to7).

Table 6.7. Summary of coding sequence mutations identified as appearing after SRA737 treatment in paired patient samples. The table was prepared by Dr. Iglika Ivanova and Dr. Jill Hunter. A number of variants were also identified that were present in either untreated D4to7 samples or mid treatment samples (C3D1) but could no longer be detected in EOS samples. These mutations listed are present in end of study (EOS) cfDNA samples. SRA737 sample ID Key: first number = run ID, second number = site, third number = patient ID. D-7 to -4 is pre SRA737 sample, C3D1 is mid SRA737 treatment sample and EOS is end of SRA737 study sample.

Patient ID (Run ID_site_Patient_time point)	Sample time point	Treatment time (Days)	No. of mutations	Novel coding sequence mutations	Mutation
12_145_001_EOS (1)	End of study	348	2	BRCA1 Frame shift Deletion ATM Missense Mutation	p.K339fs p.A2274E
14_011_011_EOS (2)	End of study	77	2	CDC25B Frame shift Deletion CDC25B Frame shift Deletion	p.S117fs p.H122fs
20_031_011_EOS (3)	End of study	129	4	CDC25B Frame shift Deletion TIMELESS Frame shift Deletion XRCC5 Missense Mutation BRCA1 Frame shift Deletion	p.S115F p.A57fs p.K545R p.K339fs
3_031_003_EOS (4)	End of study	61	1	PRKDC Frame shift Deletion	p.R2704fs
32_039-038_EOS (5)	End of study	57	4	CDC25B Missense Mutation PRKDC Frame shift Deletion BRCA1 Frame shift Deletion RELA Frame shift Deletion	p.S117fs p.R2704fs p.K339fs p.A520fs

Patient ID (Run ID_site_Patient_time point)	Sample time point	Treatment time (Days)	No. of mutations	Novel coding sequence mutations	Mutation
74_144_027_EOS (6)	End of study	70	5	ATM Frame shift Insertion ATR In-Frame Insertion ATR Missense Mutation MYC Missense Mutation RELA Frame shift Deletion	p.T878fs p.2453_2454ins LN p.S2455I p.Q33H p.R324fs
17_031_001_C3D1 (7)	Mid cycle	63	3	PRKDC Frame shift Deletion WEE1 Missense Mutation MYC Frame shift Deletion	p.R2704fs p.S396N p.Q33del
7_011_013_C3D1 (8)	Mid cycle	63	1	PRKDC Frame shift Deletion	p.R2704fs
15_148_020_EOS (9)	End of study	Not known	0	Non-coding mutations only	
8_011_006_EOS (10)	End of study	224	0	Non-coding mutations only	

The list of mutations above highlights the diversity in mutational status between individual patients. This also may be due to the patients having different primary tumour types, as mutations can differ between tumour types. This is a selected tumour panel; therefore, genes have been specifically selected due to their role in the DNA damage response and interactions with CHK1.

Further mutations were also identified that were present prior to SRA737 treatment in the D4to7 samples and appeared to become enriched upon CHK1 inhibitor treatment. These are summarised in Table 6.8, where mutations were included if they represented coding sequence mutations. Sample numbers are small but again this shows that mutations that previously were of a low number in the initial samples can become more frequent after drug treatment, which can be shown with tumour heterogeneity in advanced cancers. Again, it would have been useful to know the preliminary driving mutation in the patient's cancers from the initial tumour biopsy to see how this may have changed over time, but unfortunately this information was not obtainable.

A number of variants were also identified that were present in either untreated D4to7 samples or mid treatment samples (C3D1) but could no longer be detected in EOS samples (Appendix Table 2). However, very few of these were found in coding regions as shown in Table 6.9

Table 6.8. Summary of coding sequence mutations identified as being enriched after SRA737 treatment in paired patient samples.
The table was produced by Dr. Iglika Ivanova and Dr. Jill Hunter. Samples in these 4 patients showed further enrichment after SRA737 treatment which could potentially impact on gene function.

Gene	Mutation type	Amino acid change	Protein change	No. independent samples	Fold Enrichment	Reported in COSMIC database?	Likely effect of mutation
ATR	Missense mutation	c.5039A>G	p.Y1680C	1	2.3	No	Inactivating. Within catalytic loop and ATP binding site
MYC	Missense mutation	c.99G>C	p.Q33H	1	4.3	No	Inactivating. Within N-terminal TAD
PRKDC	Frame shift deletion	c.8110delA	p.R2704fs	2	2.1 2.7	No pR2704G fs Reported (13cases)	Inactivating. Removes FAT and kinase domains

Table 6.9. Novel low allelic fraction coding sequence variants that disappear following SRA737 treatment (present in D4to7/C3D1 but not in paired EOS sample)
The table was produced by Dr. Iglika Ivanova and Dr. Jill Hunter. A number of variants disappeared after CHK1i treatment but very few of these mutations were found in coding regions.

Gene	Mutation type	Amino acid change	Protein change	Number of independent samples	Reported in COSMIC database?	Likely effect of mutation
CHEK1	Frame shift deletion	c.694delA	p.H122fs	1	No	Disruptive. Within kinase domain
MYC	Missense mutation	c.99G>C	p.Q33H	1	No	Inactivating. Within N-terminal TAD
PRKDC	Frame shift deletion	c.8110delA	p.R2704fs	2	No pR2704G fs Reported (13cases)	Inactivating. Removes FAT and kinase domains

Low allelic fraction variants were also identified in the non-paired samples (Appendix Table 3). Due to the lack of a paired sample, these have an intrinsically lower confidence value as having potentially arisen due to SRA737 treatment. These samples still however have value. The presence of specific variants that were identified from the paired samples in this set would support these variants as potentially being independently arising mutations that could play a role in the development of CHK1 inhibitor resistance. These samples could potentially have an important role in our selection of variants to take forward for future analysis.

6.13. Comparison of cfDNA samples with historical patient tumour samples

All patients entering the Sierra SRA737 trial had an initial gene analysis on trial entry. This was to see if there were any specific gene mutations which would make drug response more likely (207). Patients recruited to the more selected expansion part of the trial were selected based on DNA damage mutations and key drivers such as *RAS* and *MYC*, or mutations in tumour suppressors such as *TP53* and *RB1* (207).

It would have been useful to have the primary tumour type and mutational status of patients entering the clinical study as this could have shown preliminary trends and patterns in tumour groups. Early requests for access to this data were made to Sierra and requests were made throughout this project but unfortunately data was not shared. This meant that mutations seen in the cfDNA samples could not be confirmed as being present in the matched tumour tissue.

Some limited data was obtained for patients on the study based on discussions with a clinical trials unit included on the study. Table 6.10 shows the results. Given the limited number of samples included (6 samples from 2 patients), this data is just observational in nature, but it provides an insight into how diverse cancer mutations can be between cancer types and between individual patients.

Table 6.10. Primary tumour and mutational status in patient samples used for cfDNA sequencing.
This data shows an example for 2 patients included on the SRA737 study.

Patient ID (Site/patient)	Gender	Cancer type	Tumour mutation	Genetic profiling	Approx time on drug	Overall survival from 1st dose
039/015	F	High grade serous ovarian	*TP53*	*TP53* mutation, *CCNE1* gain	4 months	7 months
039/038	M	Colon cancer	*KRAS* WT, *BRAF* WT	*TP53* mutation, *PARK2*, MSI stable	Unknown	6 months

6.14. Chapter summary and discussion

This chapter has shown the establishment and optimisation of protocols for the extraction, quantification and quality control of cfDNA for the first time at Newcastle University. The optimisation steps and adaptations in the cfDNA extraction protocol have been important to ensure that good quality cfDNA was obtained and that the subsequent library preparation was successful before using the SRA737 trial samples. I have also shown that changes in genes associated with the DNA damage response can be isolated using a selected gene sequencing panel.

Due to time limitations, I have not looked into the mutations from the cfDNA samples in detail. Work within the Perkins' lab is investigating some of the key mutations. Figure 6.7 shows the functional domains of some of the genes of interest and the location of the mutations detected in cfDNA within them. The mutations in Figure 6.7 are likely to have an impact on gene function.

Figure 6.7A shows a frameshift mutation in close proximity to the *RelA* REL homology domain which facilitates dimerisation of subunits and DNA binding (208,210). A mutation within the transcription activation domain (TAD) could have an impact on target gene transcription (212). The mutation seen in 6.7A interestingly could potentially cause a *REL* knockout effect as seen in the EμMyc/*c-Rel -/-* mouse model, or a mutational change as demonstrated with a new amino acid change as seen in the EμMyc*/RelA T505A* mouse model.

Figure 6.7B shows a frameshift mutation located close to the FAT domain (FRAP, ATM and TRAAP) in *PRKDC*, which normally stabilises the DNA-PKcs catalytic domain (542). Figure 6.7C shows a *BRCA1* frameshift mutation detected close to the DNA binding domain. This domain can impact on the regulation of the intra S phase checkpoint and has a role in the maintenance of genomic instability (543). Figure 6.7D shows mutations discovered within the M-inducer phosphatase site of *CDC25B*. CDC25B is a regulator of G2/M phase cell progression and the M-inducer phosphatase site helps to facilitate this role (544).

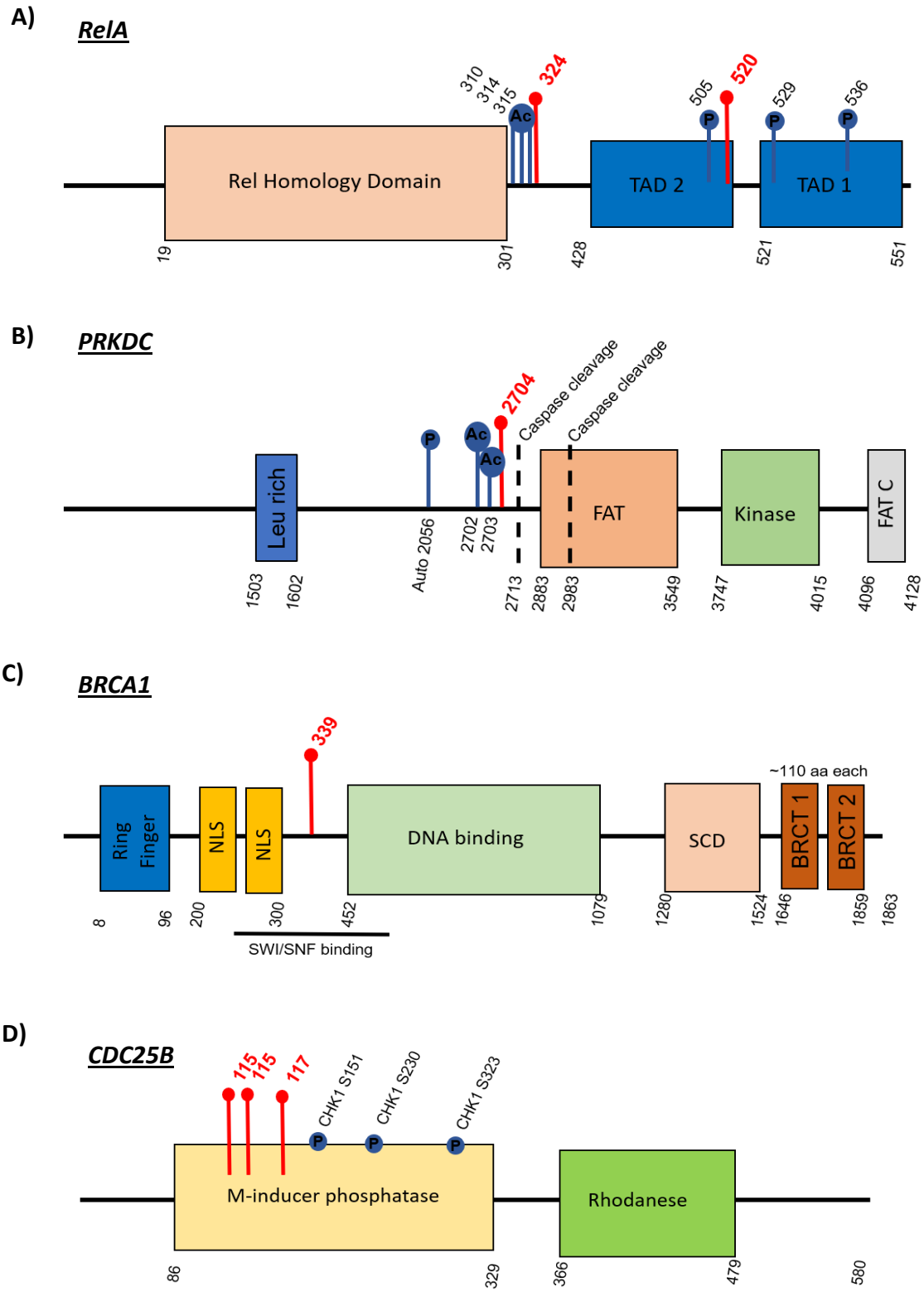

Figure 6.7. Schematics showing mutation location from SRA737 trial samples in functional domains of key genes. The schematics were obtained from Dr. Jill Hunter. Mutation sites are highlighted in red on the figures. A) Frameshift mutations in *RelA* close to the REL homology domain and involving the transcription activation domain (TAD); B) Frameshift mutation in *PRKDC* close to the FAT domain (FRAP, ATM and TRAAP); C) Mutation in *BRCA1* close to the DNA binding site; and D) Mutations in the M-inducer phosphatase domain in *CDC25B*, a regulator of mitotic progression. Based on site, these mutations are likely to inactivate the DNA damage response pathway. Key: Leu rich = leucine-rich region of *PRKDC* gene; NLS = Nuclear localisation sequences; BRCT = BRCA1 C-terminal domain; SCD = Serine cluster domain; SWI/SNF = SWItch/Sucrose Non-Fermentable chromatin remodelling complex.

Based on the site of these mutations, it is feasible that they could individually all cause a disruption of the associated pathway. This has the potential to turn off the pathway function, as demonstrated in the Eμ-Myc/*c-Rel -/-* mouse models and the resistant cell lines discussed in this project. Investigatation of these mutations in more detail is ongoing within the Perkins' lab.

Factors influencing cfDNA extraction

Variability in the starting volume of plasma in quantity was a factor that was difficult to control. The volume provided for each sample varied between 1ml and 3ml. The plasma samples were processed in different sites, therefore there may have been differences in the timing or the equipment used for plasma extraction. Most of the cfDNA extraction took place several months after the initial plasma extraction, therefore the starting plasma volume was not considered until samples had been extracted and quantified.

Approximately 30ng of cfDNA with fragment length of 75-250bp were required for library preparation, therefore many samples with low amounts of cfDNA were not suitable for sequencing. In addition, the low ctDNA concentration had implications for the design and development of the gene panel. Initial plans had to be scaled down from 100 genes to just 32. Ideally a more comprehensive sequencing panel would have been performed. With smaller selected panels, there are risks of missing the mutations of interest as they may not have been included. In future studies, it would be useful to request a larger starting volume of plasma for cfDNA extraction. It must still be considered that samples for experimental use will take less of a priority than essential monitoring for patients and there will be a limit to the plasma volume obtainable.

There are marked variations in cfDNA yield between patients. There are several possible reasons for this, some patient related and potentially some related to extraction method. Levels of cfDNA vary between patients and between different cancers (272). Patients with a higher tumour burden also have higher levels of cfDNA, this is likely due to increased tumour DNA shedding, inflammation and cellular necrosis (273).

Another pitfall in the study was the volume selected for the elution of cfDNA. Early experiments showed that 50µl of elution buffer per ml of plasma provided the optimal amount of cfDNA. Unfortunately, the cfDNA was not concentrated enough for the library preparation and sample was lost during the vacuum spinning process. In future studies, I would recommend that the cfDNA is eluted in a smaller volume of elution buffer to concentrate the cfDNA. 50µl would have been a better starting volume for these samples overall, but this may have to be reconsidered in future studies if a greater starting volume of plasma is included.

Initial plans were to have pre-treatment, mid-treatment and end of study samples for all patients but this was not possible. The plasma samples have been obtained from patients in a phase 1 study. This cohort of patients often have advanced malignancy and a high tumour burden; therefore, the clinical situation can rapidly change because of disease progression. Additionally, patients came off study due to drug intolerance or personal choice. Therefore, not all patients had 3 samples taken. This will always be a challenge of early phase studies, but most patients had samples taken at 2 separate time points.

Another challenge of phase 1 studies is that many of the patients will have had a non-therapeutic drug dose, therefore the potential likelihood of discovering mutations in response to the drug will be small. There is value, however, in using these samples to assess what mutations can be detected in cfDNA in patients and whether there is any change seen over time.

Patients in this phase 1 study also have different primary tumours. It is highly likely that there will be many different mutations present between patients and this can make it difficult to select key driver mutations to investigate further.

With gene panel design, in retrospect I would have included more of the genes shown to potentially have an impact in the mouse models and on the generated resistant cell lines as demonstrated in this thesis. This would include the inclusion of genes in the PI3K/AKT pathway including *AKT* and *AMPK*. I would have also included *USP1* and associated genes.

Unfortunately, the panel had to be selected in advance of data generated in Chapter 4 and Chapter 5. In addition, I initially wanted to create a more comprehensive gene sequencing panel but due to limitations with the volume of cfDNA extracted this was not feasible.

Further recommended work

There are multiple experiments that can be performed to further explore mutations from the cfDNA. This further work unfortunately could not be completed within the time scale of this project. Mutations isolated in patient samples could be further investigated in cellular models. This could help to identify if changes shown in the cfDNA are related to either CHK1i drug sensitivity or CHK1i drug resistance. This process could involve generation of siRNA knockouts of the genes of interest to analyse the gene impact on drug response.

Cellular models could also be generated to overexpress the gene of interest. This could be done using activated plasmid-based models. The advantage would be to see how a gene responds when overexpressed and whether this leads to drug resistance or sensitivity. A downfall of this is it could generate a new cellular response due to upregulation of normally dormant or non-dominant cellular pathways.

Another more specific use of gene modification could be with CRISPR CAS9 modification of cells. This would involve the design of templates with gene modifications based on the cfDNA results so that the exact mutations can be examined in cell lines (545,546). Specific CAS9 nucleases are generated to cut DNA at specific places in the gene and DNA templates designed with the desired mutation to try and incorporate through homologous recombination repair (546,547). The difficulty of designing cell models in this way is that generation of the required mutations take time and may have off target effects outside of the selected gene of interest.

Overall, I have been able to successfully extract, process and sequence cfDNA from plasma samples at Newcastle University. The Perkins' lab has also gained experienced with data handling and analysis of cfDNA samples. The main factors to consider with future cfDNA extraction will be to increase the starting volume of plasma and to limit the elution volume of the cfDNA to maximise the sample concentration. This will help to maximise the potential use of cfDNA for sequencing and enable more extensive gene exploration.

7. Discussion

This project has been undertaken using 3 distinct but complementary models. Firstly, I explored the potential mechanisms of CHK1i resistance in the NF-κB mutant Eμ-Myc/*c-Rel -/-* and Eμ-Myc/*RelA T505A* mouse models. The Eμ-Myc (WT) *c-MYC* driven model of B-cell lymphoma was known to be sensitive to CHK1 inhibition (147) whereas Eμ-Myc/*c-Rel -/-* and Eμ-Myc/*RelA T505A* display *de novo* drug resistance. Secondly, I examined the U2OS osteosarcoma cell line normally sensitive to CHK1 inhibitor treatment and characterised U2OS cell lines generated with acquired CHK1i resistance. Finally, I extracted cfDNA from patients undergoing treatment with the SRA737 CHK1 inhibitor to see if changes within key DNA damage response genes could be detected from these samples.

7.1. Common themes between models of CHK1i resistance

All 3 models used in this project show variation in the mechanisms behind CHK1i resistance. The Eμ-Myc/*c-Rel -/-* and Eμ-Myc/*RelA T505A* CHK1 inhibitor resistant mouse models both show evidence of primary CHK1i resistance, however we have confirmed that the mechanism behind this resistance is different. All of the WT U2OS cell lines had a similar profile pre- and post- CHK1 inhibition, whereas the U2OS cell lines with acquired CHKi resistance could be placed into 2 separate groups with different routes of CHK1i resistance.

Patient samples have the greatest heterogeneity in mutational status in comparison to the mouse models and resistant cell lines. This is because this group contains patients with multiple cancer diagnoses and will have different oncogene associated driver mutations and adaptations in DNA damage associated genes. This patient profile represents an early clinical phase trial patient population and highlights the challenge of looking for markers of response and resistance in a mixed patient group with intra and inter tumoral heterogeneity (548). Drug resistance is an ongoing challenge in cancers, whether acquired or resistant, and the development of new drugs to overcome resistance mechanisms continues (270,293,319,514).

7.2. Downregulation of the ATR/CHK1 pathway has been shown in both the Eμ-Myc/*c-Rel -/-* CHK1i resistant mouse model and in the CHK1i resistant U2OS cell lines

The downregulation of the ATR/CHK1 pathway appears to be a common theme within my data and the mouse model with findings between the *de novo* CHK1i resistance and the cell lines with acquired CHK1i resistance complement each other. Claspin levels are low in the Eμ-Myc/*c-Rel -/-* mouse model and CR2 and CR3 CHK1i resistant U2OS cell models which supports the earlier findings of the Perkins' lab. The NF-κB subunit *c-Rel* has previously been shown to regulate the transcription of Claspin (252), so it could be that the Eμ-Myc/*c-Rel -/-* model and also the CR2 and CR3 U2OS cells with downregulated *REL* are not able to upregulate Claspin and thus activate CHK1 in response to CHK1 inhibition. Given that the ATR/CHK1 is often a critical pathway required for genome stability, other mechanisms must be in place to promote cell survival.

Downregulation of *USP1* and *USP14* have also been found in the RNA-seq from the Eμ-Myc/*c-Rel* -/- mouse models. DUBs are important regulators of the cell cycle and have been shown to regulate Claspin expression at different stages of the cell cycle (252). USP1 has been shown to regulate the cell cycle via FANCD2, a regulator of CHK1 (475,478,549). It has also been suggested that USP1 can act directly as a DUB for CHK1 by protecting CHK1 from proteasomal degradation (479). Absence of *USP1* in this mouse model could indicate that degradation of CHK1 occurs in the absence of USP1 protection and CHK1 is therefore not activated.

I have not been able to show a proposed CHK1i resistance mechanism for Eμ-Myc/*RelA T505A* mouse model and the CR1 and CR4 U2OS cell lines from the investigations performed from this study but I have shown that the gene expression profiles are different in comparison to the Eμ-Myc/*c-Rel -/-* mice and the CR2 and CR3 U2OS cell lines. More investigations are required into establishing the mechanism of resistance in this mouse model and the cell lines.

Proposed future work

siRNA knockdown in CHK1i cell lines of *USP1* and *USP14* would be useful to determine the impact of these genes on CHK1i sensitivity and also to assess the role on DDR regulation. This could subsequently be performed through western blot analysis to establish how the siRNA knockdown changes the ATR/CHK1 pathway in comparison to WT CHK1i responsive cells from the same cell line.

7.3. cfDNA extraction and detection of DDR mutations in successive cfDNA samples in patients from the SRA737 CHK1i trial

I have been able to successfully extract and quantify cfDNA from patient plasma samples. I have also obtained some preliminary sequencing data from a next generation sequencing panel designed to look at DNA damage response markers and NF-κB markers. Preliminary differences have been described in the functional domains of *BRCA1*, *PRKDC*, *RelA* and *CDC25B* post CHK1i treatment as shown in Figure 6.7.

Based on the site of these mutations in key domains, it is feasible that they could individually all cause a disruption of the associated pathway. This could have the potential to turn off the pathway function, as demonstrated in the Eμ-Myc/*c-Rel -/-* mouse models and the resistant cell lines discussed in this project. Ongoing work is being performed to investigate these mutations in more detail. Assessing for mutations from phase 1 patient samples is complex. Patients will have received variable drug dosing with some patients receiving non-therapeutic levels of drug. Individuals also have complex intra- and inter-tumoral heterogeneity, with different driver mutations and survival pathways being activated based on both patient and tumour driven factors.

Proposed future work

There are multiple experiments that can be performed to further explore mutations from the cfDNA. Mutations of interest isolated from patient samples could be further investigated in cellular models. This process could involve generation of siRNA knockouts of the genes of interest to analyse the gene impact on drug response. Cellular models could also be generated to overexpress the gene of interest to see how this modifies the CHK1 inhibitor response.

Another more specific use of gene modification could be with CRISPR CAS9 modification of cells. This would involve the design of templates with gene modifications based on the cfDNA results so that the exact mutations can be examined in cell lines. The difficulty of designing cell models in this way is that generation of the required mutations take time and may have off target effects outside of the selected gene of interest.

Based on the site of these mutations, it is feasible that they could individually all cause a disruption of the associated pathway. This has the potential to turn off the pathway function, as demonstrated in the Eμ-Myc/*c-Rel -/-* mouse models and the resistant cell lines discussed in this project. Ongoing work is being performed to investigate these mutations in more detail.

7.4. Upregulation of PI3K/AKT and MAPK pathways has been shown in CHK1 inhibitor resistant models

Previously described mechanisms of CHK1 inhibitor drug resistance have shown that tumours develop patterns of bypass signalling or upregulation of alternative pathways in order to promote cell survival. For example, cancer cells in the MK-8776 study displaying drug resistance failed to dephosphorylate and activate CDK2 (203) and increased CDK1 activity in response to the CHK1 inhibitor LY2603618 (Rabusertib) was indicative of reduced drug sensitivity (204).

Proteomics data from the Eμ-Myc/*c-Rel -/-* model has demonstrated an upregulation of additional cell cycle pathways, including the proteins PI3K/AKT, ERK1, JNK1 and MAPK. Upregulation of additional cell cycle pathways could promote cancer cell survival in the Eμ-Myc/*c-Rel* -/- CHK1i resistant mouse model. These cell signalling pathways are however complex, and have been shown to interact both with the ATR/CHK1 pathway and with NF-κB signalling (114,490,496,550).

An upregulation in AKT correlates with previous investigations demonstrating that SRA737 plus a PARP inhibitor in combination led to AKT upregulation (116). In contrast to previous work, the mouse and cell work performed in this study has been performed using

the CHK1i CCT244747 as a single agent. This could indicate that in the Eμ-Myc/*c-Rel -/-* model, the upregulation of the oncogene MYC and adaptations in the NF-κB response from the knockout of *c-Rel* cause the AKT upregulation without combination drug therapy. It could also be that this resistance mechanism is predominantly driven by CHK1 inhibition with SRA737 rather than from in combination with a PARP inhibitor.

Figure 7.1 shows proposed mechanisms of CHK1i resistance based on the current findings from this project. This model is still currently work in progress. Figure 7.1A summarises how MYC-driven tumours, or tumours undergoing high levels of replication stress, become addicted to ATR-CHK1 signalling for cell survival. Levels of the adaptor protein Claspin are controlled by c-Rel. Claspin facilitates the phosphorylation of CHK1 by ATR, and potentially also the levels of USP1, the known CHK1 DUB. This cellular dependence on CHK1 signalling renders the cell sensitive to CHK1 inhibition by CCT244747 or SRA737, leading to tumour cell death.

Figure 7.1B shows that, based on the findings in this study, both acquired and *de novo* resistance to CHK1i is a two-step process. First there is loss of CHK1 protein, or loss of ATR/CHK1 pathway activity. This can be due to the loss of Claspin or loss of USP1, thus rendering the cell insensitive to CHK1 inhibition. Secondly, we have observed the upregulation of compensatory cell signalling pathways such as the PI3K/AKT pathway. This could allow tumour cells to survive the loss of CHK1.

Due to time constraints, these upregulated pathways and potential resistance mechanisms have not been examined in detail in this thesis. Further ongoing work is being performed by the Perkins' lab to investigate these pathways and resistance mechanisms.

A) **c-Rel expression drives USP1 and CLSPN expression, promoting CHK1 activity**

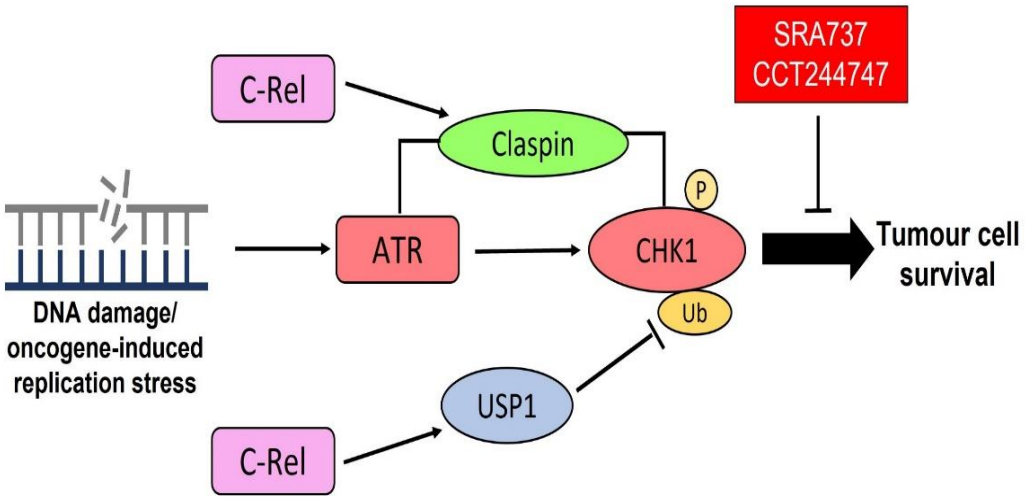

B) **Loss of c-Rel expression results in CHK1 inactivation and upregulation of the PI3K/AKT pathway**

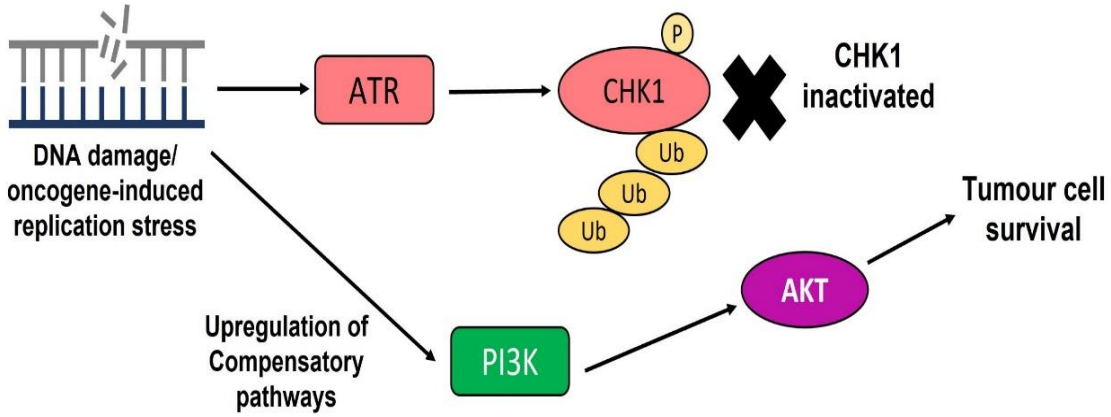

Figure 7.1. Summary of the proposed mechanisms of CHK1i resistance from this study. This model is a work-in-progress mechanism based on work in this project and the subsequent work within the Perkins' lab. A) Claspin is controlled by c-Rel in MYC-driven tumours and potentially other tumours with high levels of replication stress. Claspin activation facilitates the phosphorylation of CHK1 by ATR, and potentially the levels of USP1, which acts as a CHK1 DUB. Cell dependence on CHK1 signalling as shown in the Eμ-Myc mouse model renders the cell sensitive to CHK1 inhibition by CCT244747 or SRA737, leading to tumour cell death. B) The data in this study indicates that both *de novo* and acquired resistance to CHK1i is a two-step process. First there is loss of CHK1 protein, or ATR/CHK1 pathway activity due to the loss of Claspin or USP1, thus rendering the cell insensitive to CHK1 inhibition. Secondly, there is upregulation of compensatory pathways such as the PI3K/AKT pathway to allow the tumour cell to survive the loss of CHK1.

Proposed future work

I would investigate PI3K/AKT and MEK/ERK as mechanisms of CHK1i resistance in the Eμ-Myc/*c-Rel -/-* and CHK1i resistant cell lines in comparison to the corresponding CHK1i sensitive models. This could be done with western blot analysis of proteins and qPCR analysis of RNA levels prior to and after CHK1 inhibition. MEK inhibitors are already in clinical use in combination with BRAF inhibitors in malignant melanoma (319,338), therefore it would be interesting to see if there was a change in CHK1i response when MEK inhibitors were given in combination with CHK1i. Caution would have to be undertaken however in these drug combinations as side effect profiles and off target effects can change in models when drugs are administered in combination.

Cell models could be generated from the mouse models with siRNA knockdown of AKT and PI3K to see if cells respond differently to CHK1i inhibition and investigate if further drugs administered in combination with CHK1 inhibitors would change the response to CHK1 inhibitors.

Due to time constraints, only preliminary studies were conducted in this thesis examining USP1 and AKT. Subsequent work performed in the Perkins' lab by Dr. Jill Hunter and Scott Kerridge has confirmed AKT upregulation and USP1 downregulation in the Eμ-Myc/*c-Rel -/-* mouse model. Further treatment with CHK1i and PI3K inhibitors in combination has since been shown to overcome CHK1i resistance.

7.5. Potential future impact of study

This work has demonstrated that resistance mechanisms to CHK1 inhibitors are likely to be multiple and multifactorial and context dependent, although some common themes were seen between models. Each mutation within the DNA damage response, whether it be a tumour suppressor or oncogene activator, can lead to a reciprocal adaptation and mutation based on the initial tumour profile reflecting diversity in treatment response and tumour profile heterogeneity in clinical practice.

Cancer models in this study have demonstrated that increased CHK1 inhibitor sensitivity correlates with high levels of replication stress and with a dependence on the ATR/CHK1 pathway. In patients however, there is a diverse tumour mutational profile between patients, even before considering tumour and mutational profile selection. This was shown in the exploratory cfDNA samples from the SRA737 early clinical trial. Targeting CHK1 using CHK1 inhibitors as a single agent is therefore likely to be difficult and provide challenges in all-comers to clinical trials.

The ATR/CHK1 pathway is interconnected with multiple other cell signalling pathways in order to promote cell survival. It is likely that the upregulation of pathways such as PI3K/AKT and ERK as demonstrated in this study will lead to drug resistance in many patients. One of the mechanisms of resistance shown in this project has been loss of the target pathway. This has included loss of CHK1 protein itself, as well as other key components such as Claspin. Early results have shown that this could be mediated by the loss of USP1.

Loss of the target and upregulation of alternative pathways are both known resistance mechanisms to targeted cancer treatments (328,551,552). It may be that there is a group of patients, as shown in the animal and cell models in this study that will benefit from CHK1 inhibition as a single agent. More work would be required, however, to select the best patient cohort.

In order to combat resistance mechanisms, CHK1 inhibitors could be trialled in combination with other targeted agents, such as PI3K inhibitors, to try and overcome upregulation of the PI3K/AKT pathway. Some drugs already used in clinical practice, such as BRAF or MEK inhibitors, could be considered to target further upregulation within the Ras-Raf-MEK-ERK pathway. Initial work within this study has identified multiple mechanisms to CHK1 inhibitor treatment for further development and work is ongoing to explore these in more detail. One of the main challenges with combination therapy, however, is the potential for increased drug toxicity in patients. Drug side effects can impact on treatment tolerability and patient quality of life, and these are critical factors to consider when developing new cancer therapies.

Targeted cancer drug development continues to be an exciting and rapidly expanding part of oncology practice. Cancer therapeutic targets are likely to expand in the future, as more genetic and tumour mutational profiles are explored. Drug resistance continues to be a great challenge in oncology and research in this field remains vital for the improvement of patient outcomes in the future.

References

1. Gaillard H, García-Muse T, Aguilera A. Replication stress and cancer. *Nat Rev Cancer*. 2015; 15(5):276–80.

2. Chatterjee N, Walker GC. Mechanisms of DNA damage, repair, and mutagenesis. *Environ Mol Mutagen*. 2017; 58(5):235-263.

3. Shen Z. Genomic instability and cancer: an introduction. *J Mol Cell Biol.* 2011; 3(1):1–3.

4. Langie SAS, Koppen G, Desaulniers D, Al-Mulla F, Al-Temaimi R, Amedei A, κ Causes of genome instability: the effect of low dose chemical exposures in modern society. *Carcinogenesis.* 2015; 36(Suppl 1):S61-88.

5. Perez RP, Lewis LD, Beelen AP, Olszanski AJ, Johnston N, Rhodes CH, et al. Modulation of cell cycle progression in human tumors: A pharmacokinetic and tumor molecular pharmacodynamic study of cisplatin plus the Chk1 inhibitor UCN-01 (NSC 638850). *Clin Cancer Res.* 2006; 12(23):7079–85.

6. Rundle S, Bradbury A, Drew Y, Curtin N. Targeting the ATR-CHK1 Axis in Cancer Therapy. *Cancers*. 2017; 9(5):41.

7. Kastan MB, Bartek J. Cell-cycle checkpoints and cancer. *Nature*. 2004; 432(7015):316-23.

8. Hosoya N, Miyagawa K. Targeting DNA damage response in cancer therapy. *Cancer Sci.* 2014; 105(4):370–88.

9. Patil M, Pabla N, Dong Z. Checkpoint kinase 1 in DNA damage response and cell cycle regulation. *Cell Mol Life Sci*. 2013; 70(21):4009-21.

10. Vermeulen K, Van Bockstaele DR, Berneman ZN. The cell cycle: A review of regulation, deregulation and therapeutic targets in cancer. *Cell Prolif.* 2003; 36(3):131-49

11. Blow JJ, Tanaka TU. The chromosome cycle: coordinating replication and segregation. *EMBO Rep.* 2005; 6(11):1028–34.

12. Masai H, Matsumoto S, You Z, Yoshizawa-Sugata N, Oda M. Eukaryotic Chromosome DNA Replication: Where, When, and How? *Annu Rev Biochem.* 2010; 79(1):89–130.

13. Masai H, Yang CC, Matsumoto S. Mrc1/Claspin: a new role for regulation of origin firing. *Curr Genet*. 2017; 63(5):813–8.

14. Boos D, Frigola J, Diffley JFX. Activation of the replicative DNA helicase: Breaking up is hard to do. *Curr Opin Cell Biol*. 2012; 24(3):423-30.

15. Aze A, Zhou JC, Costa A, Costanzo V. DNA replication and homologous recombination factors: Acting together to maintain genome stability. *Chromosoma.* 2013; 122(5):401–13.

16. Brandsma I, Fleuren EDG, Williamson CT, Lord CJ. Directing the use of DDR kinase inhibitors in cancer treatment. *Expert Opin Investig Drugs.* 2017; 26(12):1341-1355.

17. Sørensen CS, Syljuåsen RG. Safeguarding genome integrity: the checkpoint kinases ATR, CHK1 and WEE1 restrain CDK activity during normal DNA replication. *Nucleic Acids Res.* 2012; 40(2):477–86.

18. Reinhardt HC, Yaffe MB. Kinases that control the cell cycle in response to DNA damage: Chk1, Chk2, and MK2. *Curr Opin Cell Biol*. 2009; 21(2):245–55.

19. Qiu Z, Oleinick NL, Zhang J. ATR/CHK1 inhibitors and cancer therapy. *Radiother Oncol.* 2017; 126(3):450–64.

20. De Bont R, van Larebeke N. Endogenous DNA damage in humans: A review of quantitative data. *Mutagenesis*. 2004; 19(3):169–85.

21. Basu AK. DNA damage, mutagenesis and cancer. *Int J Mol Sci*. 2018; 19(4):970.

22. Barnes JL, Zubair M, John K, Poirier MC, Martin FL. Carcinogens and DNA damage. *Biochem Soc Trans*. 2018; 46(5):1213-1224.

23. Clancy S. DNA Damage & Repair: Mechanisms for Maintaining DNA Integrity. *Nat Educ*. 2008; 1(1):3–5.

24. Rastogi RP, Richa, Kumar A, Tyagi MB, Sinha RP. Molecular Mechanisms of Ultraviolet Radiation-Induced DNA Damage and Repair. *J Nucleic Acids*. 2010; 2010:592980.

25. Mavragani IV, Nikitaki Z, Kalospyros SA, Georgakilas AG. Ionizing Radiation and Complex DNA Damage: From Prediction to Detection Challenges and Biological Significance. *Cancers* (Basel). 2019;11(11):1789.

26. Borrego-Soto G, Ortiz-López R, Rojas-Martínez A. Ionizing radiation-induced DNA injury and damage detection in patients with breast cancer. *Genet Mol Biol*. 2015; 38(4):420-32.

27. Ward JF. Ionizing Radiation Damage to DNA. In: *Advances in DNA Damage and Repair.* Springer US; 1999. p.431–9.

28. Wogan GN, Hecht SS, Felton JS, Conney AH, Loeb LA. Environmental and chemical carcinogenesis. *Semin Cancer Biol.* 2004; 14(6):473–86.

29. Kantidze OL, Velichko AK, Luzhin AV, Razin SV. Heat Stress-Induced DNA Damage. *Acta Naturae*. 2016; 8(2):75–8.

30. Neutelings T, Lambert CA, Nusgens BV, Colige AC. Effects of Mild Cold Shock (25°C) Followed by Warming Up at 37°C on the Cellular Stress Response. *PLoS One*. 2013; 8(7):e69687.

31. Odell ID, Wallace SS, Pederson DS. Rules of engagement for base excision repair in chromatin. *J Cell Physiol*. 2013; 228(2):258–66.

32. Tubbs A, Nussenzweig A. Endogenous DNA Damage as a Source of Genomic Instability in Cancer. *Cell*. 2017; 168(4):644–56.

33. Marteijn JA, Lans H, Vermeulen W, Hoeijmakers JHJ. Understanding nucleotide excision repair and its roles in cancer and ageing. *Nat Rev Mol Cell Biol*. 2014; 15(7):465–81.

34. Cortez D. Preventing replication fork collapse to maintain genome integrity. *DNA Repair* (Amst). 2015; 32:149–57.

35. Viguera E, Canceill D, Ehrlich SD. Replication slippage involves DNA polymerase pausing and dissociation. *EMBO J.* 2001; 20(10):2587–95.

36. Ashour ME, Atteya R, El-Khamisy SF. Topoisomerase-mediated chromosomal break repair: an emerging player in many games. *Nat Rev Cancer*. 2015; 15(3):137-51.

37. Pommier Y. Topoisomerase I inhibitors: Camptothecins and beyond. *Nat Rev Cancer*. 2006; 6(10):789-802.

38. Barnes DE, Lindahl T. Repair and Genetic Consequences of Endogenous DNA Base Damage in Mammalian Cells. *Annu Rev Genet*. 2004; 38(1):445–76.

39. Chan K, Resnick MA, Gordenin DA. The choice of nucleotide inserted opposite abasic sites formed within chromosomal DNA reveals the polymerase activities participating in translesion DNA synthesis. *DNA Repair* (Amst). 2013; 12(11):878–89.

40. Hanahan D, Weinberg RA. Hallmarks of cancer: The next generation. *Cell*. 2011; 144(5):646-74.

41. Menoyo A, Alazzouzi H, Schwartz S, Espín E, Armengol M, Yamamoto H. Somatic mutations in the DNA damage-response genes ATR and CHK1 in sporadic stomach tumors with microsatellite instability. *Cancer Res*. 2001; 61(21):7727–30.

42. Petropoulos M, Champeris Tsaniras S, Taraviras S, Lygerou Z. Replication Licensing Aberrations, Replication Stress, and Genomic Instability. *Trends Biochem Sci.* 2019; 44(9):752-764.

43. Ozeri-Galai E, Lebofsky R, Rahat A, Bester AC, Bensimon A, Kerem B. Failure of Origin Activation in Response to Fork Stalling Leads to Chromosomal Instability at Fragile Sites. *Mol Cell*. 2011; 43(1):122–31.

44. Macheret M, Halazonetis TD. DNA Replication Stress as a Hallmark of Cancer. *Annu Rev Pathol Mech Dis*. 2015; 10(1):425–48.

45. Zhang BN, Bueno Venegas A, Hickson ID, Chu WK. DNA replication stress and its impact on chromosome segregation and tumorigenesis. *Semin Cancer Biol*. 2019; 55:61-69.

46. Negrini S, Gorgoulis VG, Halazonetis TD. Genomic instability an evolving hallmark of cancer. *Nat Rev Mol Cell Biol*. 2010; 11(3):220-8.

47. Andreassen PR, Ren K. Fanconi Anemia Proteins, DNA Interstrand Crosslink Repair Pathways, and Cancer Therapy. *Curr Cancer Drug Targets*. 2009; 9(1):101-17.

48. Bhattacharjee S, Nandi S. DNA damage response and cancer therapeutics through the lens of the Fanconi Anemia DNA repair pathway. *Cell Commun Signal*. 2017; 15(1):41.

49. Pichierri P, Rosselli F. The DNA crosslink-induced S-phase checkpoint depends on ATR-CHK1 and ATR-NBS1-FANCD2 pathways. *EMBO J*. 2004; 23(5):1178–87.

50. Kotsantis P, Petermann E, Boulton SJ. Mechanisms of oncogene-induced replication stress: Jigsaw falling into place. *Cancer Discov*. 2018; 8(5):537-555.

51. Hills SA, Diffley JFX. DNA replication and oncogene-induced replicative stress. *Curr Biol*. 2014; 24(10):R435-44.

52. Medema RH, Macůrek L. Checkpoint control and cancer. *Oncogene.* 2012; 31(21):2601–13.

53. Smith J, Tho LM, Xu N, Gillespie DA. The ATM–Chk2 and ATR–Chk1 Pathways in DNA Damage Signaling and Cancer. *Adv Cancer Res.* 2010; 108:73-112.

54. How to solve the genome DNA damage - Nordic Biosite [Internet]. [cited 2021 Mar 23]. Available from: https://www.nordicbiosite.com/news/how-to-solve-the-genome-dna-damage.

55. Ciccia A, Elledge SJ. The DNA Damage Response: Making It Safe to Play with Knives. *Mol Cell*. 2010; 40(2):179-204.

56. Stojic L, Brun R, Jiricny J. Mismatch repair and DNA damage signalling. *DNA Repair* (Amst). 2004; 3(8–9):1091–101.

57. Gupta D, Heinen CD. The mismatch repair-dependent DNA damage response: Mechanisms and implications. *DNA Repair* (Amst). 2019; 78:60-69.

58. Fishel R. Mismatch repair. *J Biol Chem*. 2015; 290(44):26395-403.

59. Li Z, Pearlman AH, Hsieh P. DNA mismatch repair and the DNA damage response. *DNA Repair* (Amst). 2016; 38:94-101.

60. Wallace SS. Base excision repair: A critical player in many games. *DNA Repair* (Amst). 2014; 19:14–26.

61. Curtin NJ. DNA repair dysregulation from cancer driver to therapeutic target. *Nat Rev Cancer*. 2012; 12(12):801–17.

62. Krokan HE, Bjørås M. Base excision repair. *Cold Spring Harb Perspect Biol*. 2013; 5(4):a012583.

63. Lee TH, Kang TH. DNA oxidation and excision repair pathways. *Int J Mol Sci.* 2019; 20(23):6092.

64. Hoeijmakers JHJ. Genome maintenance mechanisms for preventing cancer. *Nature*. 2001; 411(6835):366-74.

65. Spivak G. Nucleotide excision repair in humans. *DNA Repair* (Amst). 2015; 36:13-18.

66. Gordon SM, Alon N, Buchwald M. FANCC, FANCE, and FANCD2 form a ternary complex essential to the integrity of the Fanconi anemia DNA damage response pathway. *J Biol Chem.* 2005; 280(43):36118–25.

67. Caldecott KW. Single-strand break repair and genetic disease. *Nat Rev Genet*. 2008; 9(8):619-31.

68. Schreiber V, Dantzer F, Amé JC, De Murcia G. Poly(ADP-ribose): Novel functions for an old molecule. *Nat Rev Mol Cell Biol*. 2006; 7(7):517-28.

69. Polo LM, Xu Y, Hornyak P, Garces F, Zeng Z, Hailstone R, et al. Efficient Single-Strand Break Repair Requires Binding to Both Poly(ADP-Ribose) and DNA by the Central BRCT Domain of XRCC1. *Cell Rep*. 2019; 26(3):573-581.

70. Chang HHY, Pannunzio NR, Adachi N, Lieber MR. Non-homologous DNA end joining and alternative pathways to double-strand break repair. *Nat Rev Mol Cell Biol.* 2017; 18(8):495–506.

71. Jackson SP, Bartek J. The DNA-damage response in human biology and disease. *Nature.* 2009; 461(7267):1071-8.

72. Lord CJ, Ashworth A. The DNA damage response and cancer therapy. *Nature.* 2012; 481(7381):287–94.

73. Scully R, Panday A, Elango R, Willis NA. DNA double-strand break repair-pathway choice in somatic mammalian cells. *Nat Rev Mol Cell Biol.* 2019; 20(11):698-714.

74. Pannunzio NR, Watanabe G, Lieber MR. Nonhomologous DNA end-joining for repair of DNA double-strand breaks. *J Biol Chem*. 2018; 293(27):10512-10523.

75. Hartlerode AJ, Scully R. Mechanisms of double-strand break repair in somatic mammalian cells. *Biochem J.* 2009; 423(2):157-68.

76. Sung P, Klein H. Mechanism of homologous recombination: Mediators and helicases take on regulatory functions. *Nat Rev Mol Cell Biol.* 2006; 7(10):739-50.

77. West SC. Molecular views of recombination proteins and their control. *Nat Rev Mol Cell Biol.* 2003; 4(6):435-45.

78. Krejci L, Altmannova V, Spirek M, Zhao X. Homologous recombination and its regulation. *Nucleic Acids Res*. 2012; 40(13):5795-818.

79. Prakash R, Zhang Y, Feng W, Jasin M. Homologous recombination and human health: The roles of BRCA1, BRCA2, and associated proteins. *Cold Spring Harb Perspect Biol*. 2015; 7(4):a016600.

80. Farmer H, McCabe N, Lord CJ, Tutt ANJ, Johnson DA, Richardson TB, et al. Targeting the DNA repair defect in BRCA mutant cells as a therapeutic strategy. *Nature*. 2005; 434(7035):917–21.

81. Cimprich KA, Cortez D. ATR: an essential regulator of genome integrity. *Nat Rev Mol Cell Biol*. 2008;9(8):616–27.

82. Benada J, Macurek L. Targeting the checkpoint to kill cancer cells. *Biomolecules*. 2015; 5(3):1912–37.

83. Paulsen RD, Cimprich KA. The ATR pathway: Fine-tuning the fork. *DNA Repair* (Amst). 2007; 6(7):953–66.

84. Toledo LI, Murga M, Fernandez-Capetillo O. Targeting ATR and Chk1 kinases for cancer treatment: A new model for new (and old) drugs. *Mol Oncol.* 2011; 5(4):368–73.

85. Bartek J, Lukas J. Chk1 and Chk2 kinases in checkpoint control and cancer. *Cancer Cell.* 2003; 3(5):421–9.

86. Zhang Y, Hunter T. Roles of Chk1 in cell biology and cancer therapy. *Int J Cancer*. 2014; 134(5):1013–23.

87. Chen T, Stephens PA, Middleton FK, Curtin NJ. Targeting the S and G2 checkpoint to treat cancer. Drug Discov Today. 2012;17(5–6):194–202.

88. Liu Q, Guntuku S, Cui XS, Matsuoka S, Cortez D, Tamai K, et al. Chk1 is an essential kinase that is regulated by Atr and required for the G2/M DNA damage checkpoint. *Genes Dev*. 2000; 14(12):1448–59.

89. Carrassa L, Damia G. Unleashing Chk1 in cancer therapy. *Cell Cycle*. 2011; 10(13):2121-8.

90. Syljuåsen RG, Sørensen CS, Hansen LT, Fugger K. et al. Inhibition of Human Chk1 Causes Increased Initiation of DNA Replication, Phosphorylation of ATR Targets, and DNA Breakage. *Mol Cell Biol.* 2005; 25(9):3553–62.

91. Kumagai A, Kim SM, Dunphy WG. Claspin and the activated form of ATR-ATRIP collaborate in the activation of Chk1. *J Biol Chem.* 2004; 279(48):49599–608.

92. Dai Y, Grant S. New insights into checkpoint kinase 1 in the DNA damage response signaling network. *Clin Cancer Res*. 2010; 16(2):376–83.

93. Goto H, Kasahara K, Inagaki M. Novel insights into chk1 regulation by phosphorylation. *Cell Struct Funct*. 2014; 40(1):43–50.

94. Kasahara K, Goto H, Enomoto M, Tomono Y, Kiyono T, Inagaki M. 14-3-3γ 3 mediates Cdc25A proteolysis to block premature mitotic entry after DNA damage. *EMBO J.* 2010; 29(16):2802–12.

95. Larner JM, Lee H, Little RD, Dijkwel PA, Schildkraut CL, Hamlin JL. Radiation down-regulates replication origin activity throughout the S phase in mammalian cells. *Nucleic Acids Res*. 1999; 27(3):803–9.

96. Liu P, Barkley LR, Day T, Bi X, Slater DM, Alexandrow MG, et al. The Chk1-mediated S-phase checkpoint targets initiation factor Cdc45 via a Cdc25A/Cdk2-independent mechanism. *J Biol Chem*. 2006; 281(41):30631–44.

97. Liu S, Bekker-Jensen S, Mailand N, Lukas C, Bartek J, Lukas J. Claspin Operates Downstream of TopBP1 To Direct ATR Signaling towards Chk1 Activation. *Mol Cell Biol.* 2006; 26(16):6056–64.

98. O'Connell MJ, Raleigh JM, Verkade HM, Nurse P. Chk1 is a wee1 kinase in the G2 DNA damage checkpoint inhibiting cdc2 by Y15 phosphorylation. *EMBO J*. 1997; 16(3):545–54.

99. Furnari B, Rhind N, Russell P. Cdc25 mitotic inducer targeted by Chk1 DNA damage checkpoint kinase. *Science*. 1997; 277(5331):1495–7.

100. Raleigh JM, O'Connell MJ. The G2 DNA damage checkpoint targets both Wee1 and Cdc25. *J Cell Sci*. 2000; 113(10):1727–36.

101. Schmitt E, Boutros R, Froment C, Monsarrat B, Ducommun B, Dozier C. CHK1 phosphorylates CDC25B during the cell cycle in the absence of DNA damage. *J Cell Sci.* 2006; 119(20):4269–75.

102. Lopez-Girona A, Furnari B, Mondesert O, Russell P. Nuclear localization of Cdc25 is regulated by DNA damage and a 14-3-3 protein. *Nature.* 1999; 397(6715):172–5.

103. Chen L, Liu TH, Walworth NC. Association of Chk1 with 14-3-3 proteins is stimulated by DNA damage. *Genes Dev*. 1999;13(6):675–85.

104. Shiromizu T, Goto H, Tomono Y, Bartek J, Totsukawa G, Inoko A, et al. Regulation of mitotic function of Chk1 through phosphorylation at novel sites by cyclin-dependent kinase 1 (Cdk1). *Genes to Cells*. 2006; 11(5):477–85.

105. Xu N, Hegarat N, Black EJ, Scott MT, Hochegger H, Gillespie DA. Akt/PKB suppresses DNA damage processing and checkpoint activation in late G2. *J Cell Biol.* 2010; 190(3):297–306.

106. Wang X, Kennedy RD, Ray K, Stuckert P, Ellenberger T, D'Andrea AD. Chk1-mediated phosphorylation of FANCE is required for the Fanconi anemia/BRCA pathway. *Mol Cell Biol*. 2007; 27(8):3098–108.

107. Guervilly J-H, Macé-Aimé G, Rosselli F, Tane Macé -Aimé G, Rosselli F, Macé-Aimé G, et al. Loss of CHK1 function impedes DNA damage-induced FANCD2 monoubiquitination but normalizes the abnormal G2 arrest in Fanconi anemia. *Hum Mol Genet*. 2008; 17(5):679–89.

108. Pichierri P. DNA cross-link-dependent RAD50/MRE11/NBS1 subnuclear assembly requires the Fanconi anemia C protein. *Hum Mol Genet*. 2002; 11(21):2531–46.

109. Bogliolo M, Lyakhovich A, Callén E, Castellà M, Cappelli E, Ramírez MJ, et al. Histone H2AX and Fanconi anemia FANCD2 function in the same pathway to maintain chromosome stability. *EMBO J*. 2007; 26(5):1340–51.

110. Tonic I, Yu WN, Park Y, Chen CC, Hay N. Akt activation emulates Chk1 inhibition and Bcl2 overexpression and abrogates G2 cell cycle checkpoint by inhibiting BRCA1 foci. *J Biol Chem.* 2010; 285(31):23790–8.

111. Stronach EA, Chen M, Maginn EN, Agarwal R, Mills GB, Wasan H, et al. DNA-PK mediates AKT activation and apoptosis inhibition in clinically acquired platinum resistance. *Neoplasia*. 2011; 13(11):1069–80.

112. Duan L, Perez RE, Hansen M, Gitelis S, Maki CG. Increasing cisplatin sensitivity by schedule dependent inhibition of AKT and Chk1. *Cancer Biol Ther.* 2014; 15(12):1600–12.

113. Shtivelman E, Sussman J, Stokoe D. A role for PI 3-kinase and PKB activity in the G2/M phase of the cell cycle. *Curr Biol*. 2002; 12(11):919–24.

114. Goodwin JF, Knudsen KE. Beyond DNA repair: DNA-PK function in cancer. *Cancer Discov.* 2014; 4(10):1126–39.

115. King FW, Skeen J, Hay N, Shtivelman E. Inhibition of Chk1 by activated PKB/Akt. *Cell Cycle.* 2004; 3(5):634–7.

116. Booth L, Roberts J, Poklepovic A, Dent P. The CHK1 inhibitor SRA737 synergizes with PARP1 inhibitors to kill carcinoma cells. *Cancer Biol Ther*. 2018; 19(9)786–96.

117. Gaestel M. MAPKAP kinases - MKs - Two's company, three's a crowd. *Nat Rev Mol Cell Biol*. 2006; 7(2):120–30.

118. Manke IA, Nguyen A, Lim D, Stewart MQ, Elia AEH, Yaffe MB. MAPKAP kinase-2 is a cell cycle checkpoint kinase that regulates the G2/M transition and S phase progression in response to UV irradiation. *Mol Cell.* 2005; 17(1):37–48.

119. Xiao Z, Xue J, Sowin TJ, Zhang H. Differential roles of checkpoint kinase 1, checkpoint kinase 2, and mitogen-activated protein kinase-activated protein kinase 2 in mediating DNA damage-induced cell cycle arrest: Implications for cancer therapy. *Mol Cancer Ther*. 2006; 5(8):1935–43.

120. Bulavin DV, Amundson SA, Fornace AJ. p38 and Chk1 kinases: Different conductors for the G2/M checkpoint symphony. *Curr Opin Genet Dev*. 2002; 12(1):92-7.

121. Jirmanova L, Bulavin DV, Fornace AJ. Inhibition of the ATR/Chk1 pathway induces a p38-dependent S-phase delay in mouse embryonic stem cells. *Cell Cycle*. 2005; 4(10):1428–34.

122. Vitale I, Senovilla L, Galluzzi L, Criollo A, Vivet S, Castedo M, et al. Chk1 inhibition activates p53 through p38 MAPK in tetraploid cancer cells. *Cell Cycle*. 2008; 7(13):1956–61.

123. Reinhardt HC, Aslanian AS, Lees JA, Yaffe MB. p53-Deficient Cells Rely on ATM- and ATR-Mediated Checkpoint Signaling through the p38MAPK/MK2 Pathway for Survival after DNA Damage. *Cancer Cell.* 2007; 11(2):175–89.

124. Shiloh Y, Ziv Y. The ATM protein kinase: regulating the cellular response to genotoxic stress, and more. *Nat Rev Mol Cell Biol*. 2013; 14(4):197–210.

125. Zhou BBS, Elledge SJ. The DNA damage response: Putting checkpoints in perspective. *Nature*. 2000; 408(6811):433-9.

126. Bekker-Jensen S, Lukas C, Kitagawa R, Melander F, Kastan MB, Bartek J, et al. Spatial organization of the mammalian genome surveillance machinery in response to DNA strand breaks. *J Cell Biol*. 2006; 173(2):195–206.

127. Blackford AN, Jackson SP. ATM, ATR, and DNA-PK: The Trinity at the Heart of the DNA Damage Response. *Mol Cell*. 2017; 66(6):801–17.

128. Lee JH, Goodarzi AA, Jeggo PA, Paull TT. 53BP1 promotes ATM activity through direct interactions with the MRN complex. *EMBO J*. 2010; 29(3):574–85.

129. Lukas C, Melander F, Stucki M, Falck J, Bekker-Jensen S, Goldberg M, et al. Mdc1 couples DNA double-strand break recognition by Nbs1 with its H2AX-dependent chromatin retention. *EMBO J*. 2004; 23(13):2674–83.

130. Ahn JY, Schwarz JK, Piwnica-Worms H, Canman CE. Threonine 68 phosphorylation by ataxia telangiectasia mutated is required for efficient activation of Chk2 in response to ionizing radiation. *Cancer Res.* 2000; 60(21):5934–6.

131. Falck J, Mailand N, Syljuåsen RG, Bartek J, Lukas J. The ATM-Chk2-Cdc25A checkpoint pathway guards against radioresistant DNA synthesis. *Nature*. 2001; 410(6830):842–7.

132. Smith HL, Southgate H, Tweddle DA, Curtin NJ. DNA damage checkpoint kinases in cancer. *Expert Rev Mol Med.* 2020 Jun 8;22:e2.

133. Ou YH, Chung PH, Sun TP, Shieh SY. p53 C-Terminal Phosphorylation by CHK1 and CHK2 Participates in the Regulation of DNA-Damage-induced C-Terminal Acetylation. *Mol Biol Cell.* 2005; 16(4):1684-1695.

134. Fischer M. Census and evaluation of p53 target genes. *Oncogene* 2017; 36(28):3943–56.

135. Hirao A, Kong YY, Matsuoka S, Wakeham A, Ruland J, Yoshida H, et al. DNA damage-induced activation of p53 by the checkpoint kinase Chk2. *Science.* 2000; 287(5459):1824–7.

136. Makredi JJ. The Mdm2–p53 relationship evolves: Mdm2 swings both ways as an oncogene and a tumor suppressor. *Genes Dev*. 2010; 24(15):1580–9.

137. Chehab NH, Malikzay A, Appel M, Halazonetis TD. Chk2/hCds1 functions as a DNA damage checkpoint in G1 by stabilizing p53. *Genes Dev.* 2000; 14(3):278–88.

138. Zannini L, Delia D, Buscemi G. CHK2 kinase in the DNA damage response and beyond. *J Mol Cell Biol*. 2014; 6(6):442–57.

139. Matsuoka S, Huang M, Elledge SJ. Linkage of ATM to cell cycle regulation by the Chk2 protein kinase. *Science*. 1998; 282(5395):1893–7.

140. Donzelli M, Draetta GF. Regulating mammalian checkpoints through Cdc25 inactivation. *EMBO Rep*. 2003; 4(7):671-7.

141. Lee JS, Collins KM, Brown AL, Lee CH, Chung JH. hCds1-mediated phosphorylation of BRCA1 regulates the DNA damage response. *Nature.* 2000; 404(6774):201–4.

142. Bahassi EM, Ovesen JL, Riesenberg AL, Bernstein WZ, Hasty PE, Stambrook PJ. The checkpoint kinases Chk1 and Chk2 regulate the functional associations between hBRCA2 and Rad51 in response to DNA damage. *Oncogene*. 2008; 27(28):3977–85.

143. Zhang J, Willers H, Feng Z, Ghosh JC, Kim S, Weaver DT, et al. Chk2 Phosphorylation of BRCA1 Regulates DNA Double-Strand Break Repair. *Mol Cell Biol.* 2004; 24(2):708–18.

144. Tan Y, Raychaudhuri P, Costa RH. Chk2 Mediates Stabilization of the FoxM1 Transcription Factor To Stimulate Expression of DNA Repair Genes. *Mol Cell Biol*. 2007; 27(3):1007–16.

145. Löbrich M, Jeggo PA. The impact of a negligent G2/M checkpoint on genomic instability and cancer induction. *Nat Rev Cancer*. 2007; 7(11):861–9.

146. Ma CX, Janetka JW, Piwnica-Worms H. Death by releasing the breaks: CHK1 inhibitors as cancer therapeutics. *Trends Mol Med.* 2011; 17(2):88–96.

147. Walton MI, Eve PD, Hayes A, Henley AT, Valenti MR, Brandon AKDH, et al. The clinical development candidate CCT245737 is an orally active CHK1 inhibitor with preclinical activity in RAS mutant NSCLC and Eμ-MYC driven B-cell lymphoma. *Oncotarget*. 2016; 7(3):3329-42.

148. O'Connor MJ. Targeting the DNA Damage Response in Cancer. *Mol Cell.* 2015; 60(4):547-60.

149. Chenard-Poirier M, Ingles Garces AH, Jones RH, Quinton A, Plummer ER, Drew Y, et al. A phase I study of SRA737 (formerly known as CCT245737) administered orally in patients with advanced cancer. *J Clin Oncol*. 2017; 35(suppl):TPS2607–TPS2607.

150 Walton MI, Eve PD, Hayes A, Valenti MR, De Haven Brandon AK, Box G, et al. CCT244747 is a novel potent and selective CHK1 inhibitor with oral efficacy alone and in combination with genotoxic anticancer drugs. *Clin Cancer R*es. 2012; 18(20):5650–61.

151. Manic G, Signore M, Sistigu A, Russo G, Corradi F, Siteni S, et al. CHK1-targeted therapy to deplete DNA replication-stressed, p53-deficient, hyperdiploid colorectal cancer stem cells. *Gut.* 2018; 67(5):903-917.

152. Bertoni F, Codegoni AM, Furlan D, Tibiletti MG, Capella C, Broggini M. CHK1 frameshift mutations in genetically unstable colorectal and endometrial cancers. *Genes Chromosom Cancer*. 1999; 26(2):176–80.

153. Doerr F, George J, Schmitt A, Beleggia F, Rehkämper T, Hermann S, et al. Targeting a non-oncogene addiction to the ATR/CHK1 axis for the treatment of small cell lung cancer. *Sci Rep.* 2017; 7(1):15511.

154. Verlinden L, Bempt I Vanden, Eelen G, Drijkoningen M, Verlinden I, Marchal K, et al. The E2F-regulated Gene Chk1 is highly expressed in triple-negative estrogen receptor-/progesterone receptor-/HER-2- breast carcinomas. *Cancer Res*. 2007; 67(14):6574–81.

155. Sriuranpong V, Mutirangura A, Gillespie JW, Patel V, Amornphimoltham P, Molinolo AA, et al. Global gene expression profile of nasopharyngeal carcinoma by laser capture microdissection and complementary DNA microarrays. *Clin Cancer Res*. 2004; 10(15):4944–58.

156. Thompson R, Eastman A. The cancer therapeutic potential of Chk1 inhibitors: how mechanistic studies impact on clinical trial design. *Br J Clin Pharmacol*. 2013; 76(3):358–69.

157. Daud AI, Ashworth MT, Strosberg J, Goldman JW, Mendelson D, Springett G, et al. Phase I dose-escalation trial of checkpoint kinase 1 inhibitor MK-8776 as monotherapy and in combination with gemcitabine in patients with advanced solid tumors. *J Clin Oncol*. 2015; 33(9):1060–6.

158. Herůdková J, Paruch K, Khirsariya P, Souček K, Krkoška M, Vondálová Blanářová O, et al. Chk1 Inhibitor SCH900776 Effectively Potentiates the Cytotoxic Effects of Platinum-Based Chemotherapeutic Drugs in Human Colon Cancer Cells. *Neoplasia*. 2017; 19(10):830–41.

159. Infante JR, Hollebecque A, Postel-Vinay S, Bauer TM, Blackwood EM, Evangelista M, et al. Phase I Study of GDC-0425, a checkpoint kinase 1 inhibitor, in combination with gemcitabine in patients with refractory solid tumors. *Clin Cancer Res*. 2017; 23(10):2423-2432.

160. McNeely S, Beckmann R, Bence Lin AK. CHEK again: Revisiting the development of CHK1 inhibitors for cancer therapy. *Pharmacol Ther*. 2014; 142(1):1–10.

161. Ho AL, Bendell JC, Cleary JM, Schwartz GK, Burris HA, Oakes P, et al. Phase I, open-label, dose-escalation study of AZD7762 in combination with irinotecan in patients with advanced solid tumors. *J Clin Oncol.* 2011; 29(suppl):3033.

162. Fuse E, Tanii H, Kurata N, Kobayashi H, Shimada Y, Tamura T, et al. Unpredicted clinical pharmacology of UCN-01 caused by specific binding to human alpha1-acid glycoprotein. *Cancer Res*. 1998;58 (15):3248–53.

163. Wickremsinhe ER, Hynes SM, Palmieri MD, Mitchell MI, Abraham TL, Rehmel JF, et al. Disposition and metabolism of LY2603618, a Chk-1 inhibitor following intravenous administration in patients with advanced and/or metastatic solid tumors. *Xenobiotica*. 2014; 44(9):827–41.

164. Calvo E, Braiteh F, Von Hoff D, McWilliams R, Becerra C, Galsky MD, et al. Phase I Study of CHK1 Inhibitor LY2603618 in Combination with Gemcitabine in Patients with Solid Tumors. *Oncology*. 2016; 91(5):251–60.

165. Sausville E, LoRusso P, Carducci M, Carter J, Quinn MF, Malburg L, et al. Phase I dose-escalation study of AZD7762, a checkpoint kinase inhibitor, in combination with gemcitabine in US patients with advanced solid tumors. *Cancer Chemother Pharmacol.* 2014; 73(3):539–49.

166. Gorecki L, Andrs M, Korabecny J. Clinical Candidates Targeting the ATR–CHK1–WEE1 Axis in Cancer. *Cancers* (Basel). 2021; 13(4):795.

167. Seto T, Esaki T, Hirai F, Arita S, Nosaki K, Makiyama A, et al. Phase I, dose-escalation study of AZD7762 alone and in combination with gemcitabine in Japanese patients with advanced solid tumours. *Cancer Chemother Pharmacol*. 2013; 72(3):619–27.

168. Blasina A, Hallin J, Chen E, Arango ME, Kraynov E, Register J, et al. Breaching the DNA damage checkpoint via PF-00477736, a novel small-molecule inhibitor of checkpoint kinase 1. *Mol Cancer Ther*. 2008; 7(8):2394–404.

169. Karp JE, Thomas BM, Greer JM, Sorge C, Gore SD, Pratz KW, et al. Phase I and pharmacologic trial of cytosine arabinoside with the selective checkpoint 1 inhibitor Sch 900776 in refractory acute leukemias. *Clin Cancer Res*. 2012;18(24):6723–31.

170. A Dose Escalation Study of Hydroxyurea in Combination With SCH900776 in Advanced Malignant Solid Tumors - ClinicalTrials.gov [Internet]. [cited 2021 Mar 30]. Available from:https://clinicaltrials.gov/ct2/show/NCT01521299.

171. Webster JA, Tibes R, Morris L, Blackford AL, Litzow M, Patnaik M, et al. Randomized phase II trial of cytosine arabinoside with and without the CHK1 inhibitor MK-8776 in relapsed and refractory acute myeloid leukemia. *Leuk Res*. 2017; 61:108–16.

172. Italiano A, Infante JR, Shapiro GI, Moore KN, LoRusso PM, Hamilton E, et al. Phase I study of the checkpoint kinase 1 inhibitor GDC-0575 in combination with gemcitabine in patients with refractory solid tumors. *Ann Oncol*. 2018; 29(5):1304–11.

173. Dent P. Investigational CHK1 inhibitors in early phase clinical trials for the treatment of cancer. *Expert Opin Investig Drugs.* 2019; 28(12):1095-1100.

174. Safety and Tolerability of IC83/LY2603618 Administered After Pemetrexed 500 mg/m2 Every 21 Days in Patients With Cancer - Study Results - ClinicalTrials.gov [Internet]. [cited 2021 Mar 30].
Available from: https://clinicaltrials.gov/ct2/show/results/NCT00415636

175. Barnard D, Diaz HB, Burke T, Donoho G, Beckmann R, Jones B, et al. LY2603618, a selective CHK1 inhibitor, enhances the anti-tumor effect of gemcitabine in xenograft tumor models. *Invest New Drugs*. 2016; 34(1):49–60.

176. Scagliotti G, Kang JH, Smith D, Rosenberg R, Park K, Kim SW, et al. Phase II evaluation of LY2603618, a first-generation CHK1 inhibitor, in combination with pemetrexed in patients with advanced or metastatic non-small cell lung cancer. *Invest New Drugs*. 2016; 34(5):625–35.

177. Wehler T, Thomas M, Schumann C, Bosch-Barrera J, Viñolas Segarra N, Dickgreber NJ, et al. A randomized, phase 2 evaluation of the CHK1 inhibitor, LY2603618, administered in combination with pemetrexed and cisplatin in patients with advanced nonsquamous non-small cell lung cancer. *Lung Cancer*. 2017; 108:212–6.

178. C14 Study in Oncology Patients With Advanced and/or Metastatic Solid Tumors - Full Text View - ClinicalTrials.gov [Internet]. [cited 2021 Mar 30]. Available from: https://clinicaltrials.gov/ct2/show/NCT01296568.

179. Manic G, Obrist F, Sistigu A, Vitale I. Trial Watch: Targeting ATM-CHK2 and ATR-CHK1 pathways for anticancer therapy. *Mol Cell Oncol.* 2015; 2(4):e1012976.

180. A Study of LY2603618 in Combination With Gemcitabine in Participants With Solid Tumors - Full Text View - ClinicalTrials.gov [Internet]. [cited 2021 Mar 30]. Available from: https://clinicaltrials.gov/ct2/show/NCT01341457.

181. A Drug Interaction Study to Assess the Effect of LY2603618 on the Metabolic Pathway of Desipramine - Full Text View - ClinicalTrials.gov [Internet]. [cited 2021 Mar 30]. Available from: https://clinicaltrials.gov/ct2/show/NCT01358968.

182. Plummer ER, Kristeleit RS, Cojocaru E, Haris NM, Carter L, Jones RH, et al. A first-in-human phase I/II trial of SRA737 (a Chk1 Inhibitor) in subjects with advanced cancer. *J Clin Oncol.* 2019; 37(suppl):3094–3094.

183. Banerji U, Plummer ER, Moreno V, Ang JE, Quinton A, Drew Y, et al. A phase I/II first-in-human trial of oral SRA737 (a Chk1 inhibitor) given in combination with low-dose gemcitabine in subjects with advanced cancer. *J Clin Onc*ol. 2019 May 20;37(suppl):3095–3095.

184. Hong D, Infante J, Janku F, Jones S, Nguyen LM, Burris H, et al. Phase I Study of LY2606368, a Checkpoint Kinase 1 Inhibitor, in Patients With Advanced Cancer. *J Clin Oncol.* 2016; 34(15):1764–71.

185. Patel MR, Hong DS, Bendell JC, Jones SF, Hamilton EP, Subbiah V, et al. A phase 1b dose-escalation study of prexasertib, a checkpoint kinase 1 (CHK1) inhibitor, in combination with cisplatin in patients with advanced cancer. *J Clin Oncol*. 2018; 36(Suppl):2579–2579.

186. Parmar K, Kochupurakkal BS, Lazaro JB, Wang ZC, Palakurthi S, Kirschmeier PT, et al. The CHK1 inhibitor prexasertib exhibits monotherapy activity in high-grade serous ovarian cancer models and sensitizes to PARP inhibition. *Clin Cancer Res*. 2019; 25(20):6127–40.

187. Lee JM, Nair J, Zimmer A, Lipkowitz S, Annunziata CM, Merino MJ, et al. Prexasertib, a cell cycle checkpoint kinase 1 and 2 inhibitor, in BRCA wild-type recurrent high-grade serous ovarian cancer: a first-in-class proof-of-concept phase 2 study. *Lancet Oncol*. 2018; 19(2):207–15.

188. Iwasa S, Yamamoto N, Shitara K, Tamura K, Matsubara N, Tajimi M, et al. Dose-finding study of the checkpoint kinase 1 inhibitor, prexasertib, in Japanese patients with advanced solid tumors. *Cancer Sci*. 2018; 109(10):3216–23.

189. Zeng L, Beggs RR, Cooper TS, Weaver AN, Yang ES. Combining Chk1/2 inhibition with cetuximab and radiation enhances in vitro and in vivo cytotoxicity in head and neck squamous cell carcinoma. *Mol Cancer Ther.* 2017; 16(4):591–600.

190. Winer ES, Stone RM. Novel therapy in Acute myeloid leukemia (AML): moving toward targeted approaches. *Ther Adv Hematol.* 2019; 10:2040620719860645.

191. Byers LA, Golden L, Zhang W, Lin AB, Forster M. P2.06-028 A Phase 2 Study of Prexasertib in Patients with Extensive Stage Small Cell Lung Cancer. *J Thorac Oncol.* 2017; 12(1):S1088–9.

192. A Study of Prexasertib (LY2606368) in Participants With Advanced Cancer - No Study Results Posted - ClinicalTrials.gov [Internet]. [cited 2021 Mar 31]. Available from: https://clinicaltrials.gov/ct2/show/results/NCT02778126.

193. Prexasertib in Treating Pediatric Patients With Recurrent or Refractory Solid Tumors - ClinicalTrials.gov [Internet]. [cited 2021 Mar 31]. Available from: https://clinicaltrials.gov/ct2/show/NCT02808650.

194. A Study of Prexasertib (LY2606368) in Combination With Ralimetinib in Participants With Advanced or Metastatic Cancer - ClinicalTrials.gov [Internet]. [cited 2021 Mar 31].Available from: https://clinicaltrials.gov/ct2/show/NCT02860780.

195. Hong DS, Moore K, Patel M, Grant SC, Burris HA, William WN, et al. Evaluation of prexasertib, a checkpoint kinase 1 inhibitor, in a phase ib study of patients with squamous cell carcinoma. *Clin Cancer Res*. 2018; 24(14):3263–72.

196. Brill E, Yokoyama T, Nair J, Yu M, Ahn YR, Lee JM. Prexasertib, a cell cycle checkpoint kinases 1 and 2 inhibitor, increases in vitro toxicity of PARP inhibition by preventing Rad51 foci formation in BRCA wild type high-grade serous ovarian cancer. *Oncotarget*. 2017; 8(67):111026–40.

197. A Study of Prexasertib (LY2606368) in Platinum-Resistant or Refractory Recurrent Ovarian Cancer - ClinicalTrials.gov [Internet]. [cited 2021 Mar 31]. Available from: https://clinicaltrials.gov/ct2/show/NCT03414047.

198. Do KT, Manuszak C, Thrash E, Giobbie-Hurder A, Hu J, Kelland S, et al. Immune modulating activity of the CHK1 inhibitor prexasertib and anti-PD-L1 antibody LY3300054 in patients with high-grade serous ovarian cancer and other solid tumors. *Cancer Immunol Immunother.* 2021; 70(10):2991-3000.

199. Prexasertib in Combination With MEC in Relapsed/Refractory AML and High Risk MDS - a Phase I Trial - ClinicalTrials.gov [Internet]. [cited 2021 Mar 31]. Available from: https://clinicaltrials.gov/ct2/show/NCT03735446

200. Evaluation of LY2606368 Therapy in Combination With Cyclophosphamide or Gemcitabine for Children and Adolescents With Refractory or Recurrent Group 3/Group 4 or SHH Medulloblastoma Brain Tumors - ClinicalTrials.gov [Internet]. [cited 2021 Mar 31]. Available from: https://clinicaltrials.gov/ct2/show/NCT04023669

201. LY3023414 and Prexasertib in Metastatic Triple-negative Breast Cancer - ClinicalTrials.gov [Internet]. [cited 2021 Mar 31]. Available from: https://clinicaltrials.gov/ct2/show/NCT04032080.

202. A Study of the Drugs Prexasertib, Irinotecan, and Temozolomide in People With Desmoplastic Small Round Cell Tumor and Rhabdomyosarcoma - ClinicalTrials.gov [Internet]. [cited 2021 Mar 31]. Available from: https://clinicaltrials.gov/ct2/show/NCT04095221.

203. Sakurikar N, Thompson R, Montano R, Eastman A. A subset of cancer cell lines is acutely sensitive to the Chk1 inhibitor MK-8776 as monotherapy due to CDK2 activation in S phase. *Oncotarget*. 2016; 7(2):1380–94.

204. van Harten AM, Buijze M, van der Mast R, Rooimans MA, Martens-de Kemp SR, Bachas C, et al. Targeting the cell cycle in head and neck cancer by Chk1 inhibition: a novel concept of bimodal cell death. *Oncogenesis.* 2019; 8(7):1–16.

205. Nair J, Huang TT, Murai J, Haynes B, Steeg PS, Pommier Y, et al. Resistance to the CHK1 inhibitor prexasertib involves functionally distinct CHK1 activities in BRCA wild-type ovarian cancer. *Oncogene.* 2020; 39(33):5520–35.

206. Restelli V, Chilà R, Lupi M, Rinaldi A, Kwee I, Bertoni F, et al. Characterization of a mantle cell lymphoma cell line resistant to the Chk1 inhibitor PF-00477736. *Oncotarget*. 2015; 6(35):37229–40.

207. Sierra Oncology I. A Phase 1/2 Trial of SRA737 in Subjects With Advanced Cancer. - clinicaltrials.gov. [Internet]. [cited 2021 Mar 31]. Available from: https://www.clinicaltrials.gov/ct2/show/NCT02797964.

208. Oeckinghaus A, Ghosh S. The NF-kappaB family of transcription factors and its regulation. *Cold Spring Harb Perspect Biol.* 2009; 1(4):a000034.

209. Mitchell S, Vargas J, Hoffmann A. Signaling via the NFκB system. *Wiley Interdiscip Rev Syst Biol Med.* 2018; 8(3):227-41.

210. Perkins ND. The diverse and complex roles of NF-κB subunits in cancer. *Nat Rev Cancer.* 2012 Jan 19;12(2):121-32.

211. Christian F, Smith EL, Carmody RJ. The Regulation of NF-κB Subunits by Phosphorylation. *Cells*. 2016; 18;5(1):12.

212. Hayden MS, Ghosh S. Shared Principles in NF-κB Signaling. *Cell.* 2008 Feb 8;132(3):344-62.

213. Basu S, Rosenzweig KR, Youmell M, Price BD. The DNA-dependent protein kinase participates in the activation of NFκB following DNA damage. *Biochem Biophys Res Commun.* 1998; 247(1):79–83.

214. Karin M. How NF-kB is activated: the role of the IkB kinase (IKK) complex. *Oncogene*. 1999; 18(49):6867-74.

215. Janssens S, Tschopp J. Signals from within: the DNA-damage-induced NF-κB response. *Cell Death Differ*. 2006; 13:773–84.

216. Hoffmann A, Levchenko A, Scott ML, Baltimore D. The IκB-NF-κB signaling module: Temporal control and selective gene activation. *Science*. 2002; 298(5596):1241–5.

217. Wang W, Mani AM, Wu Z-H. DNA damage-induced nuclear factor-kappa B activation and its roles in cancer progression. *J Cancer Metastasis Treat.* 2017; 3(3):45.

218. Perkins ND. Integrating cell-signalling pathways with NF-κB and IKK function. *Nat Rev Mol Cell Biol.* 2007; 8(1):49-62.

219. Hoesel B, Schmid JA. The complexity of NF-κB signaling in inflammation and cancer. *Mol Cancer*. 2013; 12(1):1–15.

220. Fang L, Choudhary S, Zhao Y, Edeh CB, Yang C, Boldogh I, et al. ATM regulates NF-κB-dependent immediate-early genes via RelA Ser 276 phosphorylation coupled to CDK9 promoter recruitment. *Nucleic Acids Res*. 2014; 42(13):8416–32.

221. Wu ZH, Shi Y, Tibbetts RS, Miyamoto S. Molecular linkage between the kinase ATM and NF-κB signaling in response to genotoxic stimuli. *Science.* 2006; 311(5764):1141–6.

222. Carroll BL, Pulkoski-Gross MJ, Hannun YA, Obeid LM. CHK1 Regulates NF-κB signaling upon DNA damage in p53- deficient cells and associated tumor-derived microvesicles. *Oncotarget.* 2016; 7(14):18159–70.

223. Rocha S, Garrett MD, Campbell KJ, Schumm K, Perkins ND. Regulation of NF-κB and p53 through activation of ATR and Chk1 by the ARF tumour suppressor. *EMBO J.* 2005; 24(6):1157–69.

224. Mayo MW, Madrid LV, Westerheide SD, Jones DR, Yuan XJ, Baldwin AS, et al. PTEN blocks tumor necrosis factor-induced NF-κB-dependent transcription by inhibiting the transactivation potential of the p65 subunit. *J Biol Chem.* 2002; 277(13):11116–25.

225. Gilmore TD. NF-κB and human cancer: What have we learned over the past 35 years? *Biomedicines.* 2021; 9(8):889.

226. Viennois E, Chen F, Merlin D. NF-κB pathway in colitis-associated cancers. T*ransl Gastrointest Cancer.* 2013; 2(1):21–9.

227. Voce DJ, Schmitt AM, Uppal A, McNerney ME, Bernal GM, Cahill KE, et al. Nfkb1 is a haploinsufficient DNA damage-specific tumor suppressor. *Oncogene*. 2015; 34(21):2807–13.

228. Naugler WE, Karin M. NF-κB and cancer - identifying targets and mechanisms. *Curr Opin Genet Dev.* 2008; 18(1):19-26.

229. Rahman KMW, Ali S, Aboukameel A, Sarkar SH, Wang Z, Philip PA, et al. Inactivation of NF-kappaB by 3,3'-diindolylmethane contributes to increased apoptosis induced by chemotherapeutic agent in breast cancer cells. *Mol Cancer Ther*. 2007; 6(10):2757–65.

230. Yang J, Pan WH, Clawson GA, Richmond A. Systemic Targeting Inhibitor of κB Kinase Inhibits Melanoma Tumor Growth. *Cancer Res*. 2007; 67(7):3127-3134.

231. Zou P, Kawada J, Pesnicak L, Cohen JI. Bortezomib Induces Apoptosis of Epstein-Barr Virus (EBV)-Transformed B Cells and Prolongs Survival of Mice Inoculated with EBV-Transformed B Cells. *J Virol.* 2007; 81(18):10029-10036.

232. Kawauchi K, Araki K, Tobiume K, Tanaka N. p53 regulates glucose metabolism through an IKK-NF-κB pathway and inhibits cell transformation. *Nat Cell Biol.* 2008; 10(5):611–8.

233. Huber MA, Azoitei N, Baumann B, Grünert S, Sommer A, Pehamberger H, et al. NF-κB is essential for epithelial-mesenchymal transition and metastasis in a model of breast cancer progression. *J Clin Invest.* 2004; 114(4):569-81.

234. Lin SY, Li K, Stewart GS, Elledge SJ. Human Claspin Works with BRCA1 to Both Positively and Negatively Regulate Cell Proliferation. *Proc Natl Acad Sci USA.* 2004; 101(17):6484–9.

235. Xia Y, Shen S, Verma IM. NF-κB, an active player in human cancers. *Cancer Immunol Res.* 2014; 2(9):823-30.

236. Webster GA, Perkins ND. Transcriptional Cross Talk between NF-κB and p53. *Mol Cell Biol.* 1999;19(5):3485–95.

237. Mauro C, Leow SC, Anso E, Rocha S, Thotakura AK, Tornatore L, et al. NF-κB controls energy homeostasis and metabolic adaptation by upregulating mitochondrial respiration. *Nat Cell Biol.* 2011; 13(10):1272–9.

238. Grasso CS, Wu YM, Robinson DR, Cao X, Dhanasekaran SM, Khan AP, et al. The mutational landscape of lethal castration-resistant prostate cancer. *Nature*. 2012; 487(7406):239–43.

239. Kurman RJ. Origin and molecular pathogenesis of ovarian high-grade serous carcinoma. *Ann Oncol*. 2013; 24(SUPPL.10):x16–21.

240. Meylan E, Dooley AL, Feldser DM, Shen L, Turk E, Ouyang C, et al. Requirement for NF-kappaB signalling in a mouse model of lung adenocarcinoma. *Nature.* 2009; 462(7269):104–7.

241. Bassères DS, Ebbs A, Levantini E, Baldwin AS. Requirement of the NF-κB Subunit p65/RelA for K-Ras-Induced Lung Tumorigenesis. *Cancer Res*. 2010; 70(9):3537-46.

242. Chini CCS, Wood J, Chen J. Chk1 is required to maintain Claspin stability. *Oncogene*. 2006; 25(30):4165–71.

243. Azenha D, Lopes MC, Martins TC. Claspin functions in cell homeostasis—A link to cancer? *DNA Repair* (Amst). 2017;59:27–33.

244. Smits VAJ, Cabrera E, Freire R, Gillespie DA. Claspin - checkpoint adaptor and DNA replication factor. *FEBS J.* 2019; 286(3):441–55.

245. Dobbelstein M, Sørensen CS. Exploiting replicative stress to treat cancer. *Nat Rev Drug Discov.* 2015; 14(6):405–23.

246. Scorah J, McGowan CH. Claspin and Chk1 regulate replication fork stability by different mechanisms. *Cell Cycle.* 2009; 8(7):1036–43.

247. Bianco JN, Bergoglio V, Lin YL, Pillaire MJ, Schmitz AL, Gilhodes J, et al. Overexpression of Claspin and Timeless protects cancer cells from replication stress in a checkpoint-independent manner. *Nat Commun.* 2019; 10(1):910.

248. D'Errico MP, Grimaldi L, Petruzzelli MF, Gianicolo EAL, Tramacere F, Monetti A, et al. N-terminal pro-B-type natriuretic peptide plasma levels as a potential biomarker for cardiac damage after radiotherapy in patients with left-sided breast cancer. *Int J Radiat Oncol Biol Phys*. 2012;82(2):e239-46.

249. Mamely I, van Vugt MA, Smits VA, Semple JI, Lemmens B, Perrakis A, et al. Polo-like Kinase-1 Controls Proteasome-Dependent Degradation of Claspin during Checkpoint Recovery. *Curr Biol.* 2006; 16(19):1950–5.

250. Mailand N, Bekker-Jensen S, Bartek J, Lukas J. Destruction of Claspin by SCFβTrCP Restrains Chk1 Activation and Facilitates Recovery from Genotoxic Stress. *Mol Cell.* 2006;23(3):307–18.

251. Iwanaga R, Komori H, Ishida S, Okamura N, Nakayama K, Nakayama KI, et al. Identification of novel E2F1 target genes regulated in cell cycle-dependent and independent manners. *Oncogene.* 2006; 25(12):1786–98.

252. Kenneth NS, Mudie S, Rocha S. IKK and NF-κB-mediated regulation of Claspin impacts on ATR checkpoint function. *EMBO J*. 2010; 29(17):2966–78.

253. Gewurz BE, Harper JW. DNA-Damage Control: Claspin Destruction Turns off the Checkpoint. *Curr Biol.* 2006 Nov 7;16(21):R932-4.

254. Allera-Moreau C, Rouquette I, Lepage B, Oumouhou N, Walschaerts M, Leconte E, et al. DNA replication stress response involving PLK1, CDC6, POLQ, RAD51 and CLASPIN upregulation prognoses the outcome of early/mid-stage non-small cell lung cancer patients. *Oncogenesis.* 2012; 1(10):e30-10.

255. Kobayashi G, Sentani K, Hattori T, Yamamoto Y, Imai T, Sakamoto N, et al. Clinicopathological significance of claspin overexpression and its association with spheroid formation in gastric cancer. *Hum Pathol.* 2019; 84:8–17.

256. Ito F, Yoshimoto C, Yamada Y, Sudo T, Kobayashi H. The HNF-1β-USP28-Claspin pathway upregulates DNA damage-induced Chk1 activation in ovarian clear cell carcinoma. *Oncotarget.* 2018; 9(25):17512–22.

257. Kobayashi G, Sentani K, Babasaki T, Sekino Y, Shigematsu Y, Hayashi T, et al. Claspin overexpression is associated with high-grade histology and poor prognosis in renal cell carcinoma. *Cancer Sci*. 2020; 111(3):1020–7.

258. Benevolo M, Musio A, Vocaturo A, Donà MG, Rollo F, Terrenato I, et al. Claspin as a biomarker of human papillomavirus-related high grade lesions of uterine cervix. *J Transl Med*. 2012; 10:132.

259. Cartwright T, Perkins ND, Wilson CL. NFKB1: a suppressor of inflammation, ageing and cancer. *FEBS J*. 2016; 283(10):1812–22.

260. Harris AW, Pinkert CA, Crawford M, Langdon WY, Brinster RL, Adams JM. The E mu-myc transgenic mouse. A model for High-incidence Spontaneous Lymphoma and Leukemia of Early B Cells. *J Exp Med*. 1988 Feb 1;167(2):353-71.

261. Hunter JE, Butterworth JA, Sellier H, Luli S, Floudas A, Moore AJ, et al. Regulation of checkpoint kinase signalling and tumorigenesis by the NF-κB regulated gene, CLSPN. *bioRxiv.* 2018. p. 358291.

262. Karampini E, McCaughan F. Circulating DNA in solid organ cancers-analysis and clinical application. *QJM.* 2016; 109(4):223–7.

263. Haber DA, Velculescu VE. Blood-based analyses of cancer: Circulating tumor cells and circulating tumor DNA. *Cancer Discov*. 2014; 4(6):650–61.

264. D'Arcangelo M, Margetts J, Greystoke A. The use of circulating biomarkers in early clinical trials in patients with cancer. *Biomark Med*. 2015; 9(10):1011–23.

265. Yap TA, Lorente D, Omlin A, Olmos D, De Bono JS. Circulating tumor cells: A multifunctional biomarker. *Clin Cancer Res.* 2014; 20(10):2553–8.

266. Schwarzenbach H, Hoon DSB, Pantel K. Cell-free nucleic acids as biomarkers in cancer patients. *Nat Rev Cance*r. 2011 Jun;11(6):426-37.

267. Ignatiadis M, Dawson SJ. Circulating tumor cells and circulating tumor DNA for precision medicine: Dream or reality? *Ann Oncol.* 2014; 25(12):2304-2313.

268. Elazezy M, Joosse SA. Techniques of using circulating tumor DNA as a liquid biopsy component in cancer management. *Comput Struct Biotechnol*. 2018 Oct 9;16:370-378.

269. Heitzer E, Ulz P, Geigl JB. Circulating tumor DNA as a liquid biopsy for cancer. *Clin Chem.* 2015; 61(1):112–23.

270. Thress KS, Paweletz CP, Felip E, Cho BC, Stetson D, Dougherty B, et al. Acquired EGFR C797S mutation mediates resistance to AZD9291 in non–small cell lung cancer harboring EGFR T790M. *Nat Med.* 2015; 21(6):560–2.

271. Lu J-L, Liang Z-Y. Circulating free DNA in the era of precision oncology: Pre- and post-analytical concerns. *Chronic Dis Transl Med.* 2016; 2(4):223–30.

272. Volik S, Alcaide M, Morin RD, Collins C. Cell-free DNA (cfDNA): Clinical Significance and Utility in Cancer Shaped By Emerging Technologies. *Mol Cancer Res.* 2016; 14(10):898–908.

273. Dawson SJ, Tsui DWY, Murtaza M, Biggs H, Rueda OM, Chin SF, et al. Analysis of Circulating Tumor DNA to Monitor Metastatic Breast Cancer. *N Engl J Med.* 2013; 368(13):1199–209.

274. Johann DJ, Steliga M, Shin IJ, Yoon D, Arnaoutakis K, Hutchins L, et al. Liquid biopsy and its role in an advanced clinical trial for lung cancer. *Exp Biol Med*. 2018; 243(3):262–71.

275. Siravegna G, Marsoni S, Siena S, Bardelli A. Integrating liquid biopsies into the management of cancer. *Nat Rev Clin Oncol.* 2017; 14(9):531–48.

276. Jahr S, Hentze H, Englisch S, Hardt D, Fackelmayer FO, Hesch R-D, et al. DNA Fragments in the Blood Plasma of Cancer Patients : Quantitations and Evidence for Their Origin from Apoptotic and Necrotic Cells. *Cancer Res*. 2001; 61(4):1659–65.

277. Diaz LA, Bardelli A. Liquid biopsies: Genotyping circulating tumor DNA. *J Clin Oncol*. 2014; 32(6):579–86.

278. Dawulieti J, Sun M, Zhao Y, Shao D, et al. Treatment of severe sepsis with nanoparticulate cell-free DNA scavengers. *Sci Adv*. 2020;6(22):eaay7148.

279. Butt AN, Swaminathan R. Overview of Circulating Nucleic Acids in Plasma/Serum. *Ann N Y Acad Sci*. 2008; 1137(1):236–42.

280. Bronkhorst AJ, Ungerer V, Holdenrieder S. The emerging role of cell-free DNA as a molecular marker for cancer management. *Biomol Detect Quantif.* 2019 Mar 18;17:100087.

281. Badeau M, Lindsay C, Blais J, Nshimyumukiza L, Takwoingi Y, Langlois S, et al. Genomics-based non-invasive prenatal testing for detection of fetal chromosomal aneuploidy in pregnant women. *Cochrane Database Syst Rev.* 2017; 11(11):CD011767.

282. Gil MM, Accurti V, Santacruz B, Plana MN, Nicolaides KH. Analysis of cell-free DNA in maternal blood in screening for aneuploidies: updated meta-analysis. *Ultrasound Obstet Gynecol.* 2017; 50(3):302-314.

283. Phallen J, Sausen M, Adleff V, Leal A, Hruban C, White J, et al. Direct detection of early-stage cancers using circulating tumor DNA. *Sci Transl Med.* 2017; 9(403):eaan2415.

284. Thierry AR, Mouliere F, El Messaoudi S, Mollevi C, Lopez-Crapez E, Rolet F, et al. Clinical validation of the detection of KRAS and BRAF mutations from circulating tumor DNA. *Nat Med*. 2014; 20(4):430–5.

285. Stroun M, Lyautey J, Lederrey C, Olson-Sand A, Anker P. About the possible origin and mechanism of circulating DNA: Apoptosis and active DNA release. *Clin Chim Acta*. 2001; 313(1-2):139-42.

286. Crowley E, Di Nicolantonio F, Loupakis F, Bardelli A. Liquid biopsy: monitoring cancer-genetics in the blood. *Nat Rev Clin Oncol.* 2013; 10(8):472–84.

287. Zill OA, Banks KC, Fairclough SR, Mortimer SA, Vowles JV, Mokhtari R, et al. The landscape of actionable genomic alterations in cell-free circulating tumor DNA from 21,807 advanced cancer patients. *Clin Cancer Res*. 2018; 24(15):3528–38.

288. Bettegowda C, Sausen M, Leary RJ, Kinde I, Wang Y, Agrawal N, et al. Detection of circulating tumor DNA in early- and late-stage human malignancies. *Sci Transl Med*. 2014; 6(224): 224ra24.

289. Kustanovich A, Schwartz R, Peretz T, Grinshpun A. Life and death of circulating cell-free DNA. *Cancer Biol Ther.* 2019; 20(8):1057-1067.

290. Abbosh C, Birkbak NJ, Wilson GA, Jamal-Hanjani M, Constantin T, Salari R, et al. Phylogenetic ctDNA analysis depicts early-stage lung cancer evolution. *Nature.* 2017; 545(7655):446–51.

291. Shaw JA, Brown J, Coombes RC, Jacob J, Payne R, Lee B, et al. Circulating tumor cells and plasma DNA analysis in patients with indeterminate early or metastatic breast cancer. *Biomark Med.* 2011; 5(1):87–91.

292. Oellerich M, Schütz E, Beck J, Kanzow P, Plowman PN, Weiss GJ, et al. Using circulating cell-free DNA to monitor personalized cancer therapy. *Crit Rev Clin Lab Sci.* 2017; 54(3):205–18.

293. Li W, Ren S, Li J, Li A, Fan L, Li X, et al. T790M mutation is associated with better efficacy of treatment beyond progression with EGFR-TKI in advanced NSCLC patients. *Lung Cancer.* 2014; 84(3):295–300.

294. Goodall J, Mateo J, Yuan W, Mossop H, Porta N, Miranda S, et al. Circulating cell-free DNA to guide prostate cancer treatment with PARP inhibition. *Cancer Discov.* 2017; 7(9):1006–17.

295. Butler TM, Spellman PT, Gray J. Circulating-tumor DNA as an early detection and diagnostic tool. *Curr Opin Genet Dev.* 2017; 42:14-21.

296. FoundationOne Liquid CDx | Foundation Medicine [Internet]. [cited 2022 Mar 20]. Available from: https://www.foundationmedicine.com/test/foundationone-liquid-cdx.

297. Ignatiadis M, Lee M, Jeffrey SS. Circulating tumor cells and circulating tumor DNA: Challenges and opportunities on the path to clinical utility. *Clin Cancer Res.* 2015; 21(21):4786-800.

298. Lipson EJ, Velculescu VE, Pritchard TS, Sausen M, Pardoll DM, Topalian SL, et al. Circulating tumor DNA analysis as a real-time method for monitoring tumor burden in melanoma patients undergoing treatment with immune checkpoint blockade. *J Immunother Cancer.* 2014; 2(1):1–7.

299. Tie J, Kinde I, Wang Y, Wong HL, Roebert J, Christie M, et al. Circulating tumor DNA as an early marker of therapeutic response in patients with metastatic colorectal cancer. *Ann Oncol.* 2015; 26(8):1715–22.

300. Dawson SJ, Tsui DWY, Murtaza M, Biggs H, Rueda OM, Chin SF, et al. Analysis of circulating tumor DNA to monitor metastatic breast cancer. *N Engl J Med*. 2013; 368(13):1199–209.

301. Murtaza M, Dawson SJ, Tsui DWY, Gale D, Forshew T, Piskorz AM, et al. Non-invasive analysis of acquired resistance to cancer therapy by sequencing of plasma DNA. *Nature.* 2013; 497(7447):108–12.

302. Karlovich C, Goldman JW, Sun JM, Mann E, Sequist LV, Konopa K, et al. Assessment of EGFR mutation status in matched plasma and tumor tissue of NSCLC patients from a phase I study of rociletinib (CO-1686). *Clin Cancer Res.* 2016;22(10):2386–95.

303. Wu YL, Sequist LV, Hu CP, Feng J, Lu S, Huang Y, et al. EGFR mutation detection in circulating cell-free DNA of lung adenocarcinoma patients: Analysis of LUX-Lung 3 and 6. *Br J Cancer.* 2017; 116(2):175–85.

304. Hochmair MJ, Buder A, Schwab S, Burghuber OC, Prosch H, Hilbe W, et al. Liquid-Biopsy-Based Identification of EGFR T790M Mutation-Mediated Resistance to Afatinib Treatment in Patients with Advanced EGFR Mutation-Positive NSCLC, and Subsequent Response to Osimertinib. *Target Oncol.* 2019; 14(1):75-83.

305. Pao W, Miller VA, Politi KA, Riely GJ, Somwar R, Zakowski MF, et al. Acquired resistance of lung adenocarcinomas to gefitinib or erlotinib is associated with a second mutation in the EGFR kinase domain. *PLoS Med*. 2005; 2(3):e73.

306. Thress KS, Brant R, Carr TH, Dearden S, Jenkins S, Brown H, et al. EGFR mutation detection in ctDNA from NSCLC patient plasma: A cross-platform comparison of leading technologies to support the clinical development of AZD9291. *Lung Cancer.* 2015; 90(3):509–15.

307. Lord CJ, Ashworth A. Mechanisms of resistance to therapies targeting BRCA-mutant cancers. *Nat Med.* 2013; 19(11):1381-8.

308. Quigley D, Alumkal JJ, Wyatt AW, Kothari V, Foye A, Lloyd P, et al. Analysis of Circulating Cell-Free DNA Identifies Multiclonal Heterogeneity of BRCA2 Reversion Mutations Associated with Resistance to PARP Inhibitors. *Cancer Discov*. 2017; 7(9):999–1005.

309. Weigelt B, Comino-Méndez I, De Bruijn I, Tian L, Meisel JL, García-Murillas I, et al. Diverse BRCA1 and BRCA2 reversion mutations in circulating cell-free DNA of therapy-resistant breast or ovarian cancer. *Clin Cancer Res.* 2017; 23(21):6708–20.

310. Pilié PG, Gay CM, Byers LA, O'Connor MJ, Yap TA. PARP inhibitors: Extending benefit beyond BRCA-mutant cancers. *Clin Cancer Res.* 2019; 25(13):3759–71.

311. Gomez MK, Illuzzi G, Colomer C, Churchman M, Hollis RL, O'connor MJ, et al. Identifying and overcoming mechanisms of PARP inhibitor resistance in homologous recombination repair-deficient and repair-proficient high grade serous ovarian cancer cells. *Cancers* (Basel). 2020; 12(6):1503.

312. Turajlic S, Xu H, Litchfield K, Rowan A, Chambers T, Lopes JI, et al. Tracking Cancer Evolution Reveals Constrained Routes to Metastases: TRACERx Renal. *Cell*. 2018; 173(3):581-594.

313. Hench IB, Hench J, Tolnay M. Liquid Biopsy in Clinical Management of Breast, Lung, and Colorectal Cancer. *Front Med.* 2018; 5:9.

314. Jamal-Hanjani M, Wilson GA, McGranahan N, Birkbak NJ, Watkins TBK, Veeriah S, et al. Tracking the Evolution of Non–Small-Cell Lung Cancer. *N Engl J Med*. 2017; 376(22):2109–21.

315. Turajlic S, Xu H, Litchfield K, Rowan A, Horswell S, Chambers T, et al. Deterministic Evolutionary Trajectories Influence Primary Tumor Growth: TRACERx Renal. *Cell*. 2018; 173(3):595-610.e11.

316. Lovly CM, Shaw AT. Implications for Therapeutic Strategies. *Clin Cancer Res*. 2015; 20(9):2249–56.

317. Buder A, Hochmair MJ, Schwab S, Bundalo T, Schenk P, Errhalt P, et al. Cell-Free Plasma DNA-Guided Treatment With Osimertinib in Patients With Advanced EGFR-Mutated NSCLC. *J Thorac Oncol*. 2018; 13(6):821–30.

318. Shi H, Moriceau G, Kong X, Lee MK, Lee H, Koya RC, et al. Melanoma whole-exome sequencing identifies V600E B-RAF amplification-mediated acquired B-RAF inhibitor resistance. *Nat Commun*. 2012; 3:724.

319. Flaherty KT, Infante JR, Daud A, Gonzalez R, Kefford RF, Sosman J, et al. Combined BRAF and MEK Inhibition in Melanoma with BRAF V600 Mutations. *N Engl J Med.* 2012; 367(18):1694–703.

320. Chase DM, Patel S, Shields K. Profile of olaparib in the treatment of advanced ovarian cancer. *Int J Womens Health*. 2016; 8:125–9.

321. Meador CB, Lovly CM. Liquid biopsies reveal the dynamic nature of resistance mechanisms in solid tumors. *Nat Med*. 2015; 21(7):663–5.

322. Helman E, Nguyen M, Karlovich CA, Despain D, Choquette AK, Spira AI, et al. Cell-Free DNA Next-Generation Sequencing Prediction of Response and Resistance to Third-Generation EGFR Inhibitor. *Clin Lung Cancer*. 2018; 19(6):518-530.e7.

323. Pao W, Girard N. New driver mutations in non-small-cell lung cancer. *Lancet Oncol.* 2011; 12(2):175-80.

324. Oxnard GR, Paweletz CP, Kuang Y, Mach SL, O'Connell A, Messineo MM, et al. Noninvasive detection of response and resistance in EGFR-mutant lung cancer using quantitative next-generation genotyping of cell-free plasma DNA. *Clin Cancer Res.* 2014; 20(6):1698-1705.

325. Heinrich MC, Maki RG, Corless CL, Antonescu CR, Harlow A, Griffith D, et al. Primary and secondary kinase genotypes correlate with the biological and clinical activity of sunitinib in imatinib-resistant gastrointestinal stromal tumor. *J Clin Oncol.* 2008; 26(33):5352-9.

326. Heinrich MC, Corless CL, Demetri GD, Blanke CD, Von Mehren M, Joensuu H, et al. Kinase mutations and imatinib response in patients with metastatic gastrointestinal stromal tumor. *J Clin Oncol.* 2003; 21(23):4342–9.

327. Zahreddine H, Borden KLB. Mechanisms and insights into drug resistance in cancer. *Front Pharmacol*. 2013; 4:28.

328. Housman G, Byler S, Heerboth S, Lapinska K, Longacre M, Snyder N, et al. Drug resistance in cancer: An overview. *Cancers* (Basel). 2014; 6(3):1769-92.

329. Wang X, Zhang H, Chen X. Drug resistance and combating drug resistance in cancer. *Cancer Drug Resist*. 2019; 2(2):141–60.

330. Noordermeer SM, van Attikum H. PARP Inhibitor Resistance: A Tug-of-War in BRCA-Mutated Cells. *Trends Cell Biol.* 2019; 29(10):820-834.

331. Turke A, Zejnullahu K, Wu Y, et al. Pre-existence and clonal selection of MET amplification in EGFR mutant NSCLC. *Cancer Cell.* 2010; 17:77–88.

332. Rosell R, Bivona TG, Karachaliou N. Genetics and biomarkers in personalisation of lung cancer treatment. *Lancet.* 2013; 382(9893):720–31.

333. Marcoux N, Gettinger SN, O'Kane G, Arbour KC, Neal JW, Husain H, et al. EGFR-mutant adenocarcinomas that transform to small-cell lung cancer and other neuroendocrine carcinomas: Clinical outcomes. *J Clin Oncol.* 2019; 37(4):278–85.

334. Saad N, Poudel A, Basnet A, Gajra A. Epidermal growth factor receptor T790M mutation-positive metastatic non-small-cell lung cancer: Focus on osimertinib (AZD9291). *Onco Targets Ther.* 2017; 10:1757-1766.

335. Cross DAE, Ashton SE, Ghiorghiu S, Eberlein C, Nebhan CA, Spitzler PJ, et al. AZD9291, an irreversible EGFR TKI, overcomes T790M-mediated resistance to EGFR inhibitors in lung cancer. *Cancer Discov*. 2014; 4(9):1046–61.

336. Arend RC, Jackson-Fisher A, Jacobs IA, Chou J, Monk BJ. Ovarian cancer: new strategies and emerging targets for the treatment of patients with advanced disease. *Cancer Biol Ther*. 2021; 22(2):89-105.

337. Chapman PB, Hauschild A, Robert C, Haanen JB, Ascierto P, Larkin J, et al. Improved Survival with Vemurafenib in Melanoma with BRAF V600E Mutation. *N Engl J Med.* 2011; 364(26):2507–16.

338. Welsh SJ, Corrie PG. Management of BRAF and MEK inhibitor toxicities in patients with metastatic melanoma. *Ther Adv Med Oncol.* 2015; 7(2):122-36.

339. Czeiger D, Shaked G, Eini H, Vered I, Belochitski O, Avriel A, et al. Measurement of circulating cell-free DNA levels by a new simple fluorescent test in patients with primary colorectal cancer. *Am J Clin Pathol.* 2011; 135(2):264–70.

340. Freidin MB, Freydina DV, Leung M, Fernandez AM, Nicholson AG, Lim E. Circulating tumor DNA outperforms circulating tumor cells for KRAS mutation detection in thoracic malignancies. *Clin Chem.* 2015; 61(10):1299–304.

341. Glenn TC. Field guide to next-generation DNA sequencers. *Mol Ecol Resour.* 2011; 11(5):759–69.

342. Gorgannezhad L, Umer M, Islam MN, Nguyen N-T, Shiddiky MJA. Circulating tumor DNA and liquid biopsy: opportunities, challenges, and recent advances in detection technologies. *Lab Chip.* 2018; 18(8):1174-1196.

343. Chan KCA, Yeung SW, Lui WB, Rainer TH, Lò YMD. Effects of preanalytical factors on the molecular size of cell-free DNA in blood. *Clin Chem.* 2005; 51(4):781–4.

344. Xue X, Teare MD, Holen I, Zhu YM, Woll PJ. Optimizing the yield and utility of circulating cell-free DNA from plasma and serum. *Clin Chim Acta.* 2009; 404(2):100–4.

345. Bronkhorst AJ, Aucamp J, Pretorius PJ. Cell-free DNA: Preanalytical variables. *Clin Chim Acta.* 2015; 450:243-53.

346. Yu Z, Kastenmüller G, He Y, Belcredi P, Möller G, Prehn C, et al. Differences between Human Plasma and Serum Metabolite Profiles. *PLoS One.* 2011; 6(7):e21230.

347. Lee TH, Montalvo L, Chrebtow V, Busch MP. Quantitation of genomic DNA in plasma and serum samples: Higher concentrations of genomic DNA found in serum than in plasma. *Transfusion*. 2001; 41(2):276–82.

348. Volik S, Alcaide M, Morin RD, Collins C. Cell-free DNA (cfDNA): Clinical Significance and Utility in Cancer Shaped By Emerging Technologies. *Mol Cancer Res*. 2016; 14(10):898–908.

349. Bronkhorst AJ, Aucamp J, Pretorius PJ. Adjustments to the preanalytical phase of quantitative cell-free DNA analysis. *Data Brief*. 2015; 6:326-9.

350. Trigg RM, Martinson LJ, Parpart-Li S, Shaw JA. Factors that influence quality and yield of circulating-free DNA: A systematic review of the methodology literature. *Heliyon*. 2018; 4(7):e00699.

351. Board RE, Williams VS, Knight L, Shaw J, Greystoke A, Ranson M, et al. Isolation and extraction of circulating tumor DNA from patients with small cell lung cancer. *Ann N Y Acad Sci*. 2008 Aug;1137:98-107.

352. El Messaoudi S, Rolet F, Mouliere F, Thierry AR. Circulating cell free DNA: Preanalytical considerations. *Clin Chim Acta.* 2013; 424:222-30.

353. Malentacchi F, Pizzamiglio S, Verderio P, Pazzagli M, Orlando C, Ciniselli CM, et al. Influence of storage conditions and extraction methods on the quantity and quality of circulating cell-free DNA (ccfDNA): The SPIDIA-DNAplas External Quality Assessment experience. *Clin Chem Lab Med.* 2015; 53(12):1935–42.

354. Page K, Hava N, Ward B, Brown J, Guttery DS, Ruangpratheep C, et al. Detection of HER2 amplification in circulating free DNA in patients with breast cancer. *Br J Cancer.* 2011; 104(8):1342–8.

355. Mouliere F, El Messaoudi S, Pang D, Dritschilo A, Thierry AR. Multi-marker analysis of circulating cell-free DNA toward personalized medicine for colorectal cancer. *Mol Oncol.* 2014; 8(5):927–41.

356. Wang BG, Huang HY, Chen YC, Bristow RE, Kassauei K, Cheng CC, et al. Increased plasma DNA integrity in cancer patients. *Cancer Res.* 2003; 63(14):3966–8.

357. Golenberg EM, Bickel A, Weihs P. Effect of highly fragmented DNA on PCR. *Nucleic Acids Res.* 1996; 24(24):5026–33.

358. Illumina. TruSeq Exome Library Prep Reference Guide 15059911 v01. 2015.

359. Lo YM, Zhang J, Leung TN, Lau TK, Chang AM, Hjelm NM. Rapid clearance of fetal DNA from maternal plasma. *Am J Hum Genet*. 1999; 64(1):218–24.

360. Thakur BK, Zhang H, Becker A, Matei I, Huang Y, Costa-Silva B, et al. Double-stranded DNA in exosomes: A novel biomarker in cancer detection. *Cell Res.* 2014; 24(6):766-9.

361. Kristensen LS, Hansen LL. PCR-based methods for detecting single-locus DNA methylation biomarkers in cancer diagnostics, prognostics, and response to treatment. *Clin Chem.* 2009; 55(8):1471-83.

362. Goodwin S, McPherson JD, McCombie WR. Coming of age: ten years of next-generation sequencing technologies. *Nat Rev Genet.* 2016; 17(6):333-51.

363. Forshew T, Murtaza M, Parkinson C, Gale D, Tsui DWY, Kaper F, et al. Noninvasive Identification and Monitoring of Cancer Mutations by Targeted Deep Sequencing of Plasma DNA. *Sci Transl Med.* 2012; 4(136):136ra68-136ra68.

364. Chen M, Zhao H. Next-generation sequencing in liquid biopsy: cancer screening and early detection. *Hum Genomics.* 2019; 13(1):34.

365. Kinde I, Wu J, Papadopoulos N, Kinzler KW, Vogelstein B. Detection and quantification of rare mutations with massively parallel sequencing. *Proc Natl Acad Sci U S A.* 2011; 108(23):9530–5.

366. Aravanis AM, Lee M, Klausner RD. Next-Generation Sequencing of Circulating Tumor DNA for Early Cancer Detection. *Cell*. 2017; 168(4):571-574.

367. Barbitoff YA, Polev DE, Glotov AS, Serebryakova EA, Shcherbakova IV, Kiselev AM, et al. Systematic dissection of biases in whole-exome and whole-genome sequencing reveals major determinants of coding sequence coverage. *Sci Rep.* 2020; 10(1):2057.

368. Diehl F, Li M, He Y, Kinzler KW, Vogelstein B, Dressman D. BEAMing: single-molecule PCR on microparticles in water-in-oil emulsions. *Nat Methods*. 2006; 3(7):551–9.

369. A Phase 1 Trial of SRA737 in Combination With Gemcitabine Plus Cisplatin or Gemcitabine Alone in Subjects With Advanced Cancer. ClinicalTrials.gov. 2017. [Internet] [cited 2021 Apr 04].
Available from: https://clinicaltrials.gov/ct2/show/NCT02797977.

370. National Cancer Institute. Common Terminology Criteria for Adverse Events (CTCAE) Version 4.0. 2009.

371. Skolnik JM, Barrett JS, Jayaraman B, Patel D, Adamson PC. Shortening the timeline of pediatric phase I trials: The rolling six design. *J Clin Oncol.* 2008; 26(2):190–5.

372. Le Tourneau C, Lee JJ, Siu LL. Dose Escalation Methods in Phase I Cancer Clinical Trials. *J Natl Cancer Inst*. 2009; 101(10):708–20.

373. Scher HI, Morris MJ, Stadler WM, Higano C, Basch E, Fizazi K, et al. Trial design and objectives for castration-resistant prostate cancer: Updated recommendations from the prostate cancer clinical trials working group 3. *J Clin Oncol*. 2016; 34(12):1402–18.

374. Cancer Genome Atlas Research Network. Integrated genomic analyses of ovarian carcinoma. *Nature.* 2011; 474(7353):609-15.

375. Alsop K, Fereday S, Meldrum C, DeFazio A, Emmanuel C, George J, et al. BRCA mutation frequency and patterns of treatment response in BRCA mutation-positive women with ovarian cancer: A report from the Australian ovarian cancer study group. *J Clin Oncol.* 2012; 30(21):2654–63.

376. Rahman B, Lanceley A, Kristeleit RS, Ledermann JA, Lockley M, McCormack M, et al. Mainstreamed genetic testing for women with ovarian cancer: First-year experience. *J Med Genet.* 2019; 56(3):195–8.

377. Mirza MR, Coleman RL, González-Martín A, Moore KN, Colombo N, Ray-Coquard I, et al. The forefront of ovarian cancer therapy: update on PARP inhibitors. *Ann Oncol.* 2020; 31(9):1148-1159.

378. Maemondo M, Inoue A, Kobayashi K, Sugawara S, Oizumi S, Isobe H, et al. Gefitinib or Chemotherapy for Non–Small-Cell Lung Cancer with Mutated EGFR. *N Engl J Med.* 2010; 362(25):2380–8.

379. Solomon BJ, Mok T, Kim D-W, Wu Y-L, Nakagawa K, Mekhail T, et al. First-Line Crizotinib versus Chemotherapy in *ALK* -Positive Lung Cancer. *N Engl J Med*. 2014; 371(23):2167–77.

380. Garon EB, Rizvi NA, Hui R, Leighl N, Balmanoukian AS, Eder JP, et al. Pembrolizumab for the Treatment of Non–Small-Cell Lung Cancer. *N Engl J Med.* 2015; 372(21):2018–28.

381. Gandhi L, Rodríguez-Abreu D, Gadgeel S, Esteban E, Felip E, De Angelis F, et al. Pembrolizumab plus Chemotherapy in Metastatic Non–Small-Cell Lung Cancer. N Engl J Med. 2018 May 31;378(22):2078–92.

382. Dempke WCM, Edvardsen K, Lu S. Brain Metastases in NSCLC - are TKIs Changing the Treatment Strategy? *Anticancer Res*. 2015; 35(11):5797-806.

383. Hammerman PS, Voet D, Lawrence MS, Voet D, Jing R, Cibulskis K, et al. Comprehensive genomic characterization of squamous cell lung cancers. *Nature*. 2012; 489(7417):519–25.

384. Collisson EA, Campbell JD, Brooks AN, Berger AH, Lee W, Chmielecki J, et al. Comprehensive molecular profiling of lung adenocarcinoma: The cancer genome atlas research network. *Nature*. 2014; 511(7511):543–50.

385. Koopman M, Kortman GAM, Mekenkamp L, Ligtenberg MJL, Hoogerbrugge N, Antonini NF, et al. Deficient mismatch repair system in patients with sporadic advanced colorectal cancer. *Br J Cancer.* 2009; 100(2):266–73.

386. Hissong E, Crowe EP, Yantiss RK, Chen YT. Assessing colorectal cancer mismatch repair status in the modern era: a survey of current practices and re-evaluation of the role of microsatellite instability testing. *Mod Pathol.* 2018; 31(11):1756–66.

387. Peltomäki P. Deficient DNA mismatch repair: A common etiologic factor for colon cancer. *Hum Mol Genet.* 2001; 10(7):735-40.

388. Conacci-Sorrell M, Ngouenet C, Anderson S, Brabletz T, Eisenman RN. Stress-induced cleavage of Myc promotes cancer cell survival. *Genes Dev.* 2014; 28(7):689–707.

389. Porru M, Pompili L, Caruso C, Biroccio A, Leonetti C. Targeting KRAS in metastatic colorectal cancer: current strategies and emerging opportunities. *J Exp Clin Cancer Res*. 2018; 37(1):57.

390. Kalkat M, De Melo J, Hickman KA, Lourenco C, Redel C, Resetca D, et al. MYC Deregulation in Primary Human Cancers. *Genes* (Basel). 2017; 8(6):151.

391. Gilad O, Nabet BY, Ragland RL, Schoppy DW, Smith KD, Durham AC, et al. Combining ATR suppression with oncogenic ras synergistically increases genomic instability, causing synthetic lethality or tumorigenesis in a dosage-dependent manner. *Cancer Res.* 2010; 70(23):9693–702.

392. Vermorken JB, Mesia R, Rivera F, Remenar E, Kawecki A, Rottey S, et al. Platinum-Based Chemotherapy plus Cetuximab in Head and Neck Cancer. *N Engl J Med*. 2008; 359(11):1116–27.

393. Lawrence MS, Sougnez C, Lichtenstein L, Cibulskis K, Lander E, Gabriel SB, et al. Comprehensive genomic characterization of head and neck squamous cell carcinomas. *Nature.* 2015; 517(7536):576–82.

394. Ferris RL, Blumenschein G, Fayette J, Guigay J, Colevas AD, Licitra L, et al. Nivolumab for Recurrent Squamous-Cell Carcinoma of the Head and Neck. *N Engl J Med*. 2016; 375(19):1856–67.

395. Chow LQM. Head and Neck Cancer. *N Engl J Med.* 2020; 382(1):60–72.

396. Morris V, Rao X, Pickering C, Foo WC, Rashid A, Eterovic K, et al. Comprehensive genomic profiling of metastatic squamous cell carcinoma of the anal canal. *Mol Cancer Res*. 2017; 15(11):1542–50.

397. Chung JH, Sanford E, Johnson A, Klempner SJ, Schrock AB, Palma NA, et al. Comprehensive genomic profiling of anal squamous cell carcinoma reveals distinct genomically defined classes. *Ann Oncol.* 2016; 27(7):1336–41.

398. Wheeler JMD, Bodmer WF, Mortensen NJ. DNA mismatch repair genes and colorectal cancer. *Gut.* 2000;47(1):148–53.

399. Zhao P, Li L, Jiang X, Li Q. Mismatch repair deficiency/microsatellite instability-high as a predictor for anti-PD-1/PD-L1 immunotherapy efficacy. *J Hematol Oncol*. 2019; 12(1):54.

400. Zhang S, Royer R, Li S, McLaughlin JR, Rosen B, Risch HA, et al. Frequencies of BRCA1 and BRCA2 mutations among 1,342 unselected patients with invasive ovarian cancer. *Gynecol Oncol.* 2011; 121(2):353–7.

401. Landen CN, Birrer MJ, Sood AK. Early events in the pathogenesis of epithelial ovarian cancer. *J Clin Oncol.* 2008; 26(6):995-1005.

402. Farolfi A, Gurioli G, Fugazzola P, Burgio SL, Casanova C, Ravaglia G, et al. Immune System and DNA Repair Defects in Ovarian Cancer: Implications for Locoregional Approaches. *Int J Mol Sci.* 2019; 20(10):2569.

403. Garon EB, Hellmann MD, Rizvi NA, Carcereny E, Leighl NB, Ahn MJ, et al. Five-year overall survival for patients with advanced non-small-cell lung cancer treated with pembrolizumab: Results from the phase i KEYNOTE-001 study. *J Clin Oncol.* 2019; 37(28):2518–27.

404. Animals (Scientific Procedures) Act 1986 [Internet]. [cited 2022 Mar 23]. Available from: https://www.legislation.gov.uk/ukpga/1986/14/contents

405. Guillen J. FELASA guidelines and recommendations. *J Am Assoc Lab Anim Sci.* 2012; 51(3):311-21.

406. Harris AW, Pinkert CA, Crawford M, Langdon WY, Brinster RL, Adams JM. The E mu-myc transgenic mouse. A model for high-incidence spontaneous lymphoma and leukemia of early B cells. *J Exp Med*. 1988; 167(2):353–71.

407. Moles A, Butterworth JA, Sanchez A, Hunter JE, Leslie J, Sellier H, et al. A RelA(p65) Thr505 phospho-site mutation reveals an important mechanism regulating NF-κB-dependent liver regeneration and cancer. *Oncogene.* 2016; 35(35):4623–32.

408. Wojciechowska-Durczyńska K, Krawczyk-Rusiecka K, Cyniak-Magierska A, Zygmunt A, Gałecka E, Lewiński A. Relative quantification of PIK3CA gene expression level in fine-needle aspiration biopsy thyroid specimens collected from patients with papillary thyroid carcinoma and non-toxic goitre by real-time RT-PCR. *Thyroid Res*. 2010; 3(1):5.

409. ATCC. Cell Culture Guides. ATCC online. 2016. [Internet]. [cited 2021 Apr 08]. Available from: https://www.atcc.org/resources/culture-guides.

410. Bicinchoninic Acid Assay - an overview | ScienceDirect Topics [Internet]. [cited 2021 Apr 23]. Available from: https://www.sciencedirect.com/topics/neuroscience/bicinchoninic-acid-assay

411. PrestoBlue® Cell Viability Reagent Documentation [Internet] [cited 2021 Feb 10]. Available from: https://www.thermofisher.com/order/catalog/product/A13261.

412. Bjerke M. Getting the Most From Your Plate-Based Assays - Critical Instrument Considerations for Luminescence-and Fluorescence-Based Assays. Promega, January 2014. [Internet] [cited 2019 April 04].
Available from: www.promega.com/discover.

413. Franken NAP, Rodermond HM, Stap J, Haveman J, van Bree C. Clonogenic assay of cells in vitro. *Nat Protoc.* 2006; 1(5):2315–9.

414. Clonogenic Assay - an overview | ScienceDirect Topics [Internet]. [cited 2021 Apr 24]. Available from: https://www.sciencedirect.com/topics/biochemistry-genetics-and-molecular-biology/clonogenic-assay

415. Nakayama Y, Yamaguchi H, Einaga N, Esumi M. Pitfalls of DNA quantification using DNA-binding fluorescent dyes and suggested solutions. *PLoS One*. 2016; 11(3) e0150528.

416. TapeStation DNA ScreenTape & Reagents | Agilent [Internet]. [cited 2021 Apr 24]. Available from: https://www.agilent.com/en/product/automated-electrophoresis/tapestation-systems/tapestation-dna-screentape-reagents

417. Negrini S, Gorgoulis VG, Halazonetis TD. Genomic instability — an evolving hallmark of cancer. *Nat Rev Mol Cell Biol.* 2010; 11(3):220–8.

418. Dominguez-Sola D, Gautier J. MYC and the control of DNA replication. *Cold Spring Harb Perspect Med*. 2014; 4(6):a014423

419. Cole KA, Huggins J, Laquaglia M, Hulderman CE, Russell MR, Bosse K, et al. RNAi screen of the protein kinome identifies checkpoint kinase 1 (CHK1) as a therapeutic target in neuroblastoma. *Proc Natl Acad Sci U S A.* 2011; 108(8):3336–41.

420. Krajewska M, Fehrmann RSN, Schoonen PM, Labib S, De Vries EGE, Franke L, et al. ATR inhibition preferentially targets homologous recombination-deficient tumor cells. *Oncogene.* 2015; 34(26):3474–81.

421. Petermann E, Caldecott KW. Cell Cycle Evidence That the ATR/Chk1 Pathway Maintains Normal Replication Fork Progression during Unperturbed S Phase. *Cell Cycle.* 2006; 5(19):2203-9.

422. Ohashi T, Idogawa M, Sasaki Y, Tokino T. p53 mediates the suppression of cancer cell invasion by inducing LIMA1/EPLIN. *Cancer Lett.* 2017; 390:58–66.

423. Nie Z, Du MQ, McAllister-Lucas LM, Lucas PC, Bailey NG, Hogaboam CM, et al. Conversion of the LIMA1 tumour suppressor into an oncogenic LMO-like protein by API2-MALT1 in MALT lymphoma. *Nat Commun.* 2015; 6:5908.

424. Wang X, Zou L, Lu T, Bao S, Hurov KE, Hittelman WN, et al. Rad17 Phosphorylation Is Required for Claspin Recruitment and Chk1 Activation in Response to Replication Stress. *Mol Cell.* 2006; 23(3):331–41.

425. Warmerdam DO, Kanaar R, Smits VAJ. Differential Dynamics of ATR-Mediated Checkpoint Regulators. *J Nucleic Acids.* 2010; 2010:319142.

426. Bartek J, Lukas C, Lukas J. Checking on DNA damage in S phase. *Nat Rev Mol Cell Biol.* 2004; 5(10):792–804.

427. Hunter JE, Butterworth JA, Zhao B, Sellier H, Campbell KJ, Thomas HD, et al. The NF-κB subunit c-Rel regulates Bach2 tumour suppressor expression in B-cell lymphoma. *Oncogene*. 2016; 35(26):3476–84.

428. Yang XH, Shiotani B, Classon M, Zou L. Chk1 and claspin potentiate PCNA ubiquitination. *Genes Dev.* 2008; 22(9):1147–52.

429. Buscemi G, Perego P, Carenini N, Nakanishi M, Chessa L, Chen J, et al. Activation of ATM and Chk2 kinases in relation to the amount of DNA strand breaks. *Oncogene*. 2004; 23(46):7691–700.

430. Hata AN, Niederst MJ, Archibald HL, Gomez-Caraballo M, Siddiqui FM, Mulvey HE, et al. Tumor cells can follow distinct evolutionary paths to become resistant to epidermal growth factor receptor inhibition. *Nat Med.* 2016; 22(3):262–9.

431. Xu YJ, Leffak M. ATRIP from TopBP1 to ATR-in vitro activation of a DNA damage checkpoint. *Proc Natl Acad Sci USA.* 2010; 107(31):13561–2.

432. Trovesi C, Manfrini N, Falcettoni M, Longhese MP. Regulation of the DNA damage response by cyclin-dependent kinases. *J Mol Biol.* 2013; 425(23):4756-66.

433. Strausfeld UP, Howell M, Descombes P, Chevalier S, Rempel RE, Adamczewski J, et al. Both cyclin A and cyclin E have S-phase promoting (SPF) activity in Xenopus egg extracts. *J Cell Sci*. 1996; 109(6):1555–63.

434. Hafezi S, Rahmani M. Targeting bcl-2 in cancer: Advances, challenges, and perspectives. *Cancers* (Basel). 2021; 13(6):1292.

435. Taylor P, Oakes V, Wang W, Harrington B, Lee WJ, Beamish H, et al. Cyclin A / Cdk2 regulates Cdh1 and claspin during late S / G2 phase of the cell cycle. *Cell Cycle*. 2014; 13:37–41.

436. Primo LMF, Teixeira LK. DNA replication stress: oncogenes in the spotlight. *Genet Mol Biol*. 2020; 43(suppl 1):20190138.

437. Cortez D, Guntuku S, Qin J, Elledge SJ. ATR and ATRIP: Partners in checkpoint signaling. *Science.* 2001; 294(5547):1713–6.

438. Crawley CD, Kang S, Bernal GM, Wahlstrom JS, Voce DJ, Cahill KE, et al. Cell Cycle S-phase-dependent p50/NF-κB1 phosphorylation in response to ATR and replication stress acts to maintain genomic stability. *Cell Cycle.* 2015; 14(4):566-76.

439. Oliveira DM, Mirante T, Mignogna C, Scrima M, Migliozzi S, Rocco G, et al. Simultaneous identification of clinically relevant single nucleotide variants, copy number alterations and gene fusions in solid tumors by targeted next-generation sequencing. *Oncotarget.* 2018; 9(32):22749–68.

440. Ran T, Ke S, Song X, Ma T, Xu Y, Wang M. WIPI1 promotes osteosarcoma cell proliferation by inhibiting CDKN1A. *Gene.* 2021; 782:145537.

441. Gorski JW, Ueland FR, Kolesar JM. CCNE1 amplification as a predictive biomarker of chemotherapy resistance in epithelial ovarian cancer. *Diagnostics* (Basel). 2020; 10(5):279.

442. Saldivar JC, Hamperl S, Bocek MJ, Chung M, Bass TE, Cisneros-Soberanis F, et al. An intrinsic S/G2 checkpoint enforced by ATR. *Science.* 2018; 361(6404):806-810.

443. Sur S, Agrawal DK. Phosphatases and Kinases Regulating CDC25 Activity in the Cell Cycle: Clinical Implications of CDC25 Overexpression and Potential Treatment . *Mol Cell Biochem*. 2016; 416(2):33–46.

444. Bian Z, Yu Y, Quan C, Guan R, Jin Y, Wu J, et al. RPL13A as a reference gene for normalizing mRNA transcription of ovarian cancer cells with paclitaxel and 10-hydroxycamptothecin treatments. *Mol Med Rep*. 2015; 11(4):3188–94.

445. Jeggo PA, Pearl LH, Carr AM. DNA repair, genome stability and cancer: a historical perspective. *Nat Rev Cancer*. 2016; 16(1):35–42.

446. Baber-Furnari BA, Rhind N, Boddy MN, Shanahan P, Lopez-Girona A, Russell P. Regulation of mitotic inhibitor Mik1 helps to enforce the DNA damage checkpoint. *Mol Biol Cell*. 2000;11(1):1–11.

447. Jin H, Rugira T, Ko YS, Park SW, Yun SP, Kim HJ. ESM-1 Overexpression is Involved in Increased Tumorigenesis of Radiotherapy-Resistant Breast Cancer Cells. *Cancers* 2020; 12(6):1363.

448. Kang YH, Ji NY, Han SR, Lee C Il, Kim JW, Yeom Y Il, et al. ESM-1 regulates cell growth and metastatic process through activation of NF-κB in colorectal cancer. *Cell Signal*. 2012; 24(10):1940–9.

449. Timofeeva OA, Tarasova NI, Zhang X, Chasovskikh S, Cheema AK, Wang H, et al. STAT3 suppresses transcription of proapoptotic genes in cancer cells with the involvement of its N-terminal domain. *Proc Natl Acad Sci U S A.* 2013; 110(4):1267–72.

450. Kim SY, Mori T, Chek MF, Furuya S, Matsumoto K, Yajima T, et al. Structural insights into vesicle amine transport-1 (VAT-1) as a member of the NADPH-dependent quinone oxidoreductase family. *Sci Rep.* 2021;11(1):2120.

451. Roth E, Frohman MA. Proliferative and metastatic roles for Phospholipase D in mouse models of cancer. *Adv Biol Regul.* 2018; 67:134–40.

452. Zhao Y, Cao X, Guo M, Wang X, Yu T, Ye L, et al. Neuralized E3 Ubiquitin Protein Ligase 3 Is an Inducible Antiviral Effector That Inhibits Hepatitis C Virus Assembly by Targeting Viral E1 Glycoprotein. *J Virol.* 2018; 92(21):e01123-18.

453. Fernández-Fernández L, Bellido-Martín L, De Frutos PG. Growth arrest-specific gene 6 (GAS6). An outline of its role in haemostasis and inflammation. *Thromb Haemost.* 2008; 100(4):604–10.

454. Wu G, Ma Z, Cheng Y, Hu W, Deng C, Jiang S, et al. Targeting Gas6/TAM in cancer cells and tumor microenvironment. *Mol Cancer.* 2018; 17(1):20.

455. Moskovskich A, Goldmann U, Kartnig F, Lindinger S, Konecka J, Fiume G, et al. The transporters SLC35A1 and SLC30A1 play opposite roles in cell survival upon VSV virus infection. *Sci Rep.* 2019; 9(1):10471.

456. El Ansari R, Alfarsi L, Craze ML, Masisi BK, Ellis IO, Rakha EA, et al. The solute carrier SLC7A8 is a marker of favourable prognosis in ER-positive low proliferative invasive breast cancer. *Breast Cancer Res Treat*. 2020; 181(1):1–12.

457. Monteiro FL, Baptista T, Amado F, Vitorino R, Jerónimo C, Helguero LA. Expression and functionality of histone H2A variants in cancer. *Oncotarget.* 2014;5(11):3428-3443.

458. Yu J, Ershler M, Yu L, Wei M, Hackanson B, Yokohama A, et al. TSC-22 contributes to hematopoietic precursor cell proliferation and repopulation and is epigenetically silenced in large granular lymphocyte leukemia. *Blood.* 2009; 113(22):5558–67.

459. Andrade WA, Silva AM, Alves VS, Salgado APC, Melo MB, Andrade HM, et al. Early endosome localization and activity of RasGEF1b, a toll-like receptor-inducible Ras guanine-nucleotide exchange factor. *Genes Immun.* 2010; 11(6):447–57.

460. MSANTD2 Gene - GeneCards | MSD2 Protein | MSD2 Antibody [Internet]. [cited 2022 Apr 11]. Available from: https://www.genecards.org/cgi-bin/carddisp.pl?gene=MSANTD2

461. Poncette L, Bluhm J, Blankenstein T. The role of CD4 T cells in rejection of solid tumors. *Curr Opin Immunol.* 2022; 74:18–24.

462. Yang X, Wu W, Pan Y, Zhou Q, Xu J, Han S. Immune-related genes in tumor-specific CD4+ and CD8+ T cells in colon cancer. *BMC Cancer.* 2020; 20(1):585.

463. Oh DY, Fong L. Cytotoxic CD4+ T cells in cancer: Expanding the immune effector toolbox. *Immunity.* 2021; 54(12):2701–11.

464. Lyu L, Wang M, Zheng Y, Tian T, Deng Y, Xu P, et al. Overexpression of FAM234B Predicts Poor Prognosis in Patients with Luminal Breast Cancer. *Cancer Manag Res.* 2020;12:12457.

465. Li Y-L, Tian H, Jiang J, Zhang Y, Qi X-W. Multifaceted regulation and functions of fatty acid desaturase 2 in human cancers. *Am J Cancer Res*. 2020; 10(12):4098-4111.

466. Suzuki N, Yoshioka N, Uekawa A, Matsumura N, Tozawa A, Koike J, et al. Transcription factor POU6F1 is important for proliferation of clear cell adenocarcinoma of the ovary and is a potential new molecular target. *Int J Gynecol Cancer*. 2010; 20(2):212–9.

467. Dho SH, Lee K-P, Jeong D, Kim C-J, Chung K-S, Kim JY, et al. GPR171 expression enhances proliferation and metastasis of lung cancer cells. *Oncotarget.* 2016; 7(7):7856–65.

468. Fujiwara Y, Torphy RJ, Sun Y, Miller EN, Ho F, Borcherding N, et al. The GPR171 pathway suppresses T cell activation and limits antitumor immunity. *Nat Commun* 2021; 12(1):5857.

469. Arimura Y, Ikura M, Fujita R, Noda M, Kobayashi W, Horikoshi N, et al. Cancer-associated mutations of histones H2B, H3.1 and H2A.Z.1 affect the structure and stability of the nucleosome. *Nucleic Acids Res*. 2018; 46(19):10007–18.

470. Zhang S, Guo K, Liang Y, Wang K, Liu S, Yang X. ADGRG1 Is a Predictor of Chemoresistance and Poor Survival in Cervical Squamous Carcinoma. *Front Oncol.* 2021;11:671895.

471. Singh AK, Lin HH. The role of GPR56/ADGRG1 in health and disease. *Biomed J.* 2021; 44(5):534–47.

472. Lunning MA, Green MR. Mutation of chromatin modifiers; an emerging hallmark of germinal center B-cell lymphomas. *Blood Cancer J.* 2015;5(10):e361–e361.

473. piR-42653-001 Gene - GeneCards | piR-42653-001 RNA Gene [Internet]. [cited 2022 Apr 11]. Available from: https://www.genecards.org/cgi-bin/carddisp.pl?gene=piR-42653-001,

474. Love MI, Huber W, Anders S. Moderated estimation of fold change and dispersion for RNA-seq data with DESeq2. *Genome Biol.* 2014; 15(12):550.

475. Fraile JM, Quesada V, Rodríguez D, Freije JMP, López-Otín C. Deubiquitinases in cancer: New functions and therapeutic options. *Oncogene.* 2012; 31(19):2373-88.

476. Huang TT, Nijman SMB, Mirchandani KD, Galardy PJ, Cohn MA, Haas W, et al. Regulation of monoubiquitinated PCNA by DUB autocleavage. *Nat Cell Biol*. 2006; 8(4):341–7.

477. Huang TT, D'Andrea AD. Regulation of DNA repair by ubiquitylation. *Nat Rev Mol Cell Biol*. 2006; 7(5):323-34.

478. Kim H, D'Andrea AD. Regulation of DNA cross-link repair by the Fanconi anemia/BRCA pathway. *Genes Dev.* 2012; 26(13):1393-408.

479. Guervilly JH, Renaud E, Takata M, Rosselli F. USP1 deubiquitinase maintains phosphorylated CHK1 by limiting its DDB1-dependent degradation. *Hum Mol Genet.* 2011; 20(11):2171–81.

480. Sharma A, Almasan A. USP14 regulates dna damage response and is a target for radiosensitization in non-small cell lung cancer. *Int J Mol Sci*. 2020; 21(17):6383.

481. Xia X, Huang C, Liao Y, Liu Y, He J, Guo Z, et al. Inhibition of USP14 enhances the sensitivity of breast cancer to enzalutamide. *J Exp Clin Cancer Res*. 2019; 38(1):220.

482. Liao Y, Liu N, Hua X, Cai J, Xia X, Wang X, et al. Proteasome-associated deubiquitinase ubiquitin-specific protease 14 regulates prostate cancer proliferation by deubiquitinating and stabilizing androgen receptor. *Cell Death Dis*. 2017; 8(2):e2585.

483. Martins RG, Parvathaneni U, Bauman JE, Sharma AK, Raez LE, Papagikos MA, et al. Cisplatin and radiotherapy with or without erlotinib in locally advanced squamous cell carcinoma of the head and neck: a randomized phase II trial. *J Clin Oncol.* 2013; 31(11):1415–21.

484. Zhao X, Wu X, Wang H, Yu H, Wang J. USP53 promotes apoptosis and inhibits glycolysis in lung adenocarcinoma through FKBP51-AKT1 signaling. *Mol Carcinog*. 2020; 59(8):1000–11.

485. Gui D, Dong Z, Peng W, Jiang W, Huang G, Liu G, et al. Ubiquitin-specific peptidase 53 inhibits the occurrence and development of clear cell renal cell carcinoma through NF-κB pathway inactivation. *Cancer Med*. 2021; 10(11):3674–88.

486. Liu C, Wang L, Chen W, Zhao S, Yin C, Lin Y, et al. USP35 activated by miR let-7a inhibits cell proliferation and NF-κB activation through stabilization of ABIN-2. *Oncotarget.* 2015; 6(29):27891-906.

487. Kim M, Kim JM. The role of USP1 autocleavage in DNA interstrand crosslink repair. *FEBS Lett.* 2016 ;590(3):340–8.

488. Szklarczyk D, Gable AL, Lyon D, Junge A, Wyder S, Huerta-Cepas J, et al. STRING v11: protein-protein association networks with increased coverage, supporting functional discovery in genome-wide experimental datasets. *Nucleic Acids Res*. 2019;47 (D1):D607–13.

489. Hemmings BA, Restuccia DF. PI3K-PKB/Akt pathway. *Cold Spring Harb Perspect Biol.* 2012; 4(9): a011189.

490. Tsuruo T, Naito M, Tomida A, Fujita N, Mashima T, Sakamoto H, et al. Molecular targeting therapy of cancer: drug resistance, apoptosis and survival signal. *Cancer Sci.* 2003; 94(1):15–21.

491. Llopis A, Salvador N, Ercilla A, Guaita-Esteruelas S, Del Barco Barrantes I, Gupta J, et al. The stress-activated protein kinases p38α/β and JNK1/2 cooperate with Chk1 to inhibit mitotic entry upon DNA replication arrest. *Cell Cycle.* 2012; 11(19):3627–37.

492. Roskoski R. ERK1/2 MAP kinases: Structure, function, and regulation. *Pharmacol Res.* 2012; 66(2):105–43.

493. Roberts PJ, Der CJ. Targeting the Raf-MEK-ERK mitogen-activated protein kinase cascade for the treatment of cancer. *Oncogene.* 2007; 26(22):3291-310.

494. Lindforss U, Zetterquist H, Papadogiannakis N, Olivecrona H. Persistence of K-ras mutations in plasma after colorectal tumor resection. *Anticancer Res*. 2005; 25(1 B):657–61.

495. Riely GJ, Marks J, Pao W. KRAS mutations in non-small cell lung cancer. *Proc Am Thorac Soc.* 2009; 6(2):201–5.

496. Papa S, Bubici C, Zazzeroni F, Pham CG, Kuntzen C, Knabb JR, et al. The NF-κB-mediated control of the JNK cascade in the antagonism of programmed cell death in health and disease. *Cell Death Differ.* 2006; 13(5):712-29.

497. Kefaloyianni E, Gaitanaki C, Beis I. ERK1/2 and p38-MAPK signalling pathways, through MSK1, are involved in NF-kappaB transactivation during oxidative stress in skeletal myoblasts. *Cell Signal*. 2006; 18(12):2238–51.

498. Papa S, Zazzeroni F, Pham CG, Bubici C, Franzoso G. Linking JNK signaling to NF-κB: a key to survival. *J Cell Sci*. 2004; 117(22):5197–208.

499. Cao Z, Liao Q, Su M, Huang K, Jin J, Cao D. AKT and ERK dual inhibitors: The way forward? *Cancer Lett*. 2019; 459:30–40.

500. Han F, Li CF, Cai Z, Zhang X, Jin G, Zhang WN, et al. The critical role of AMPK in driving Akt activation under stress, tumorigenesis and drug resistance. *Nat Commun.* 2018; 9(1):4728.

501. Papadopoli D, Pollak M, Topisirovic I. The role of GSK3 in metabolic pathway perturbations in cancer. *Biochim Biophys Acta Mol Cell Res.* 2021; 1868(8):119059.

502. Kurosu T, Nagao T, Wu N, Oshikawa G, Miura O. Inhibition of the PI3K/Akt/GSK3 pathway downstream of BCR/ABL, Jak2-V617F, or FLT3-ITD downregulates DNA damage-induced Chk1 activation as well as G2/M arrest and prominently enhances induction of apoptosis. *PLoS One.* 2013; 8(11):e79478.

503. Linseman DA, Butts BD, Precht TA, Phelps RA, Le SS, Laessig TA, et al. Glycogen synthase kinase-3β phosphorylates bax and promotes its mitochondrial localization during neuronal apoptosis. *J Neurosci.* 2004; 24(44):9993–10002.

504. Beurel E, Grieco SF, Jope RS. Glycogen synthase kinase-3 (GSK3): Regulation, actions, and diseases. *Pharmacol Ther*. 2015; 148:114-31.

505. Suzuki T, Bridges D, Nakada D, Skiniotis G, Morrison SJ, Lin JD, et al. Inhibition of AMPK Catabolic Action by GSK3. *Mol Cell.* 2013; 50(3):407–19.

506. Ma Y, Cui D, Xiong X, Inuzuka H, Wei W, Sun Y, et al. SCFβ-TrCP ubiquitinates CHK1 in an AMPK-dependent manner in response to glucose deprivation. *Mol Oncol*. 2019; 13(2):307–21.

507. Calpe E, Codony C, Baptista MJ, Abrisqueta P, Carpio C, Purroy N, et al. ZAP-70 enhances migration of malignant B lymphocytes toward CCL21 by inducing CCR7 expression via IgM-ERK1/2 activation. *Blood.* 2011; 118(16):4401–10.

508. Torchia MLG, Dutta D, Mittelstadt PR, Guha J, Gaida MM, Fish K, et al. Intensity and duration of TCR signaling is limited by p38 phosphorylation of ZAP-70T293 and destabilization of the signalosome. *Proc Natl Acad Sci U S A.* 2018; 115(9):2174–9.

509. Sjölin-Goodfellow H, Frushicheva MP, Ji Q, Cheng DA, Kadlecek TA, Cantor AJ, et al. The catalytic activity of the kinase ZAP-70 mediates basal signaling and negative feedback of the T cell receptor pathway. *Sci Signal.* 2015; 8(377):ra49.

510. Au-Yeung BB, Shah NH, Shen L, Weiss A. ZAP-70 in Signaling, Biology, and Disease. *Annu Rev Immunol*. 2018; 36:127-156.

511. Hargrove JL, Schmidt FH. The role of mRNA and protein stability in gene expression. *FASEB J.* 1989; 3(12):2360–70.

512. Goldbraikh D, Neufeld D, Eid-Mutlak Y, Lasry I, Gilda JE, Parnis A, et al. USP1 deubiquitinates Akt to inhibit PI3K-Akt-FoxO signaling in muscle during prolonged starvation. *EMBO Rep*. 2020; 21(4):e48791.

513. Zhang Z, Qinghui Y, Zhang Y, Zhang J, Xin Z, Haiying M, et al. USP1 regulates AKT phosphorylation by modulating the stability of PHLPP1 in lung cancer cells. *J Cancer Res Clin Oncol.* 2012; 138(7):1231–8.

514. Dannenberg J-H, Berns A. Drugging Drug Resistance. *Cell.* 2010; 141(1):18–20.

515. Huang RS, Ratain MJ. Pharmacogenetics and pharmacogenomics of anticancer agents. *CA Cancer J Clin.* 2009; 59(1):42–55.

516. Unger FT, Witte I, David KA. Prediction of individual response to anticancer therapy: Historical and future perspectives. *Cell Mol Life Sci*. 2015; 72(4):729-57.

517. Brabletz T, Kalluri R, Nieto MA, Weinberg RA. EMT in cancer. *Nat Rev Cancer*. 2018; 18(2):128-134.

518. Liu X, Yun F, Shi L, Li ZH, Luo NR, Jia YF. Roles of signaling pathways in the epithelial-mesenchymal transition in cancer. *Asian Pac J Cancer Prev.* 2015; 16(15):6201-6.

519. Lamouille S, Xu J, Derynck R. Molecular mechanisms of epithelial-mesenchymal transition. *Nat Rev Mol Cell Biol.* 2014; 15(3):178-96.

520. Steinbichler TB, Dudas J, Ingruber J, Glueckert R, Sprung S, Fleischer F, et al. Slug Is A Surrogate Marker of Epithelial to Mesenchymal Transition (EMT) in Head and Neck Cancer. *J Clin Med.* 2020; 9(7):2061.

521. Wang Y, Shi J, Chai K, Ying X, Zhou B. The Role of Snail in EMT and Tumorigenesis. *Curr Cancer Drug Targets.* 2014; 13(9):963–72.

522. Bolós V, Peinado H, Pérez-Moreno MA, Fraga MF, Esteller M, Cano A. The transcription factor Slug represses E-cadherin expression and induces epithelial to mesenchymal transitions: A comparison with Snail and E47 repressors. *J Cell Sci.* 2003; 116(3):499-511.

523. Wallerand H, Robert G, Pasticier G, Ravaud A, Ballanger P, Reiter RE, et al. The epithelial-mesenchymal transition-inducing factor TWIST is an attractive target in advanced and/or metastatic bladder and prostate cancers. *Urol Oncol.* 2010; 28(5):473-9.

524. Grzegrzolka J, Biala M, Wojtyra P, Kobierzycki C, Olbromski M, Gomulkiewicz A, et al. Expression of EMT markers SLUG and TWIST in breast cancer. *Anticancer Res.* 2015; 35(7):3961–8.

525. Lavon I, Pikarsky E, Gutkovich E, Goldberg I, Bar J, Oren M, et al. Nuclear factor-κB protects the liver against genotoxic stress and functions independently of p53. *Cancer Res*. 2003; 63(1):25–30.

526. Kurashina Y, Imashiro C, Hirano M, Kuribara T, Totani K, Ohnuma K, et al. Enzyme-free release of adhered cells from standard culture dishes using intermittent ultrasonic traveling waves. *Commun Biol*. 2019; 2(1):393.

527. Garcia-Murillas I, Schiavon G, Weigelt B, Ng C, Hrebien S, Cutts RJ, et al. Mutation tracking in circulating tumor DNA predicts relapse in early breast cancer. *Sci Transl Med.* 2015; 7(302): 302ra133.

528. Streubel A, Stenzinger A, Stephan-Falkenau S, Kollmeier J, Misch D, Blum TG, et al. Comparison of different semi-automated cfDNA extraction methods in combination with UMI-based targeted sequencing. *Oncotarget*. 2019; 10(55):5690–702.

529. Sorber L, Zwaenepoel K, Deschoolmeester V, Roeyen G, Lardon F, Rolfo C, et al. A Comparison of Cell-Free DNA Isolation Kits: Isolation and Quantification of Cell-Free DNA in Plasma. *J Mol Diagnostics*. 2017; 19(1):162–8.

530. Fleischhacker M, Schmidt B, Weickmann S, Fersching DMI, Leszinski GS, Siegele B, et al. Methods for isolation of cell-free plasma DNA strongly affect DNA yield. *Clin Chim Acta*. 2011; 412(23–24):2085–8.

531. Chen Y-L, Lin C-C, Yang S-C, Chen W-L, Chen J-R, Hou Y-H, et al. Five Technologies for Detecting the EGFR T790M Mutation in the Circulating Cell-Free DNA of Patients With Non-small Cell Lung Cancer: A Comparison. *Front Oncol.* 2019; 9:631.

532. Devonshire AS, Whale AS, Gutteridge A, Jones G, Cowen S, Foy CA, et al. Towards standardisation of cell-free DNA measurement in plasma: Controls for extraction efficiency, fragment size bias and quantification. *Anal Bioanal Chem*. 2014; 406(26):6499–512.

533. Molecular PROfiling in Early Clinical Trials- North East (PROSPECT-NE) - Health Research Authority [Internet]. [cited 2018 Sep 16]. Available from: https://www.hra.nhs.uk/planning-and-improving-research/application-summaries/research-summaries/molecular-profiling-in-early-clinical-trials-north-east-prospect-ne/.

534. Hussing C, Kampmann M-L, Mogensen HS, Børsting C, Morling N. Quantification of massively parallel sequencing libraries – a comparative study of eight methods. *Sci Rep.* 2018; 8(1):1110.

535. Sena JA, Galotto G, Devitt NP, Connick MC, Jacobi JL, Umale PE, et al. Unique Molecular Identifiers reveal a novel sequencing artefact with implications for RNA-Seq based gene expression analysis. *Sci Rep.* 2018; 8(1):13121.

536. Kivioja T, Vähärautio A, Karlsson K, Bonke M, Enge M, Linnarsson S, et al. Counting absolute numbers of molecules using unique molecular identifiers. *Nat Methods*. 2012; 9(1):72–4.

537. Toledo L, Neelsen KJ, Lukas J. Replication Catastrophe: When a Checkpoint Fails because of Exhaustion. *Mol Cell*. 2017; 66(6):735–49.

538. Zhu M, Zhao H, Liao J, Xu X. HERC2/USP20 coordinates CHK1 activation by modulating CLASPIN stability. *Nucleic Acids Res.* 2014; 42(21):13074–81.

539. Yuan J, Luo K, Deng M, Li Y, Yin P, Gao B, et al. HERC2-USP20 axis regulates DNA damage checkpoint through Claspin. *Nucleic Acids Res*. 2014; 42(21):13110–21.

540. Lu X, An H, Jin R, Zou M, Guo Y, Su PF, et al. PPM1A is a RelA phosphatase with tumor suppressor-like activity. *Oncogene.* 2014; 33(22):2918–27.

541. Lu Z, Wan G, Guo H, Zhang X, Lu X. Protein phosphatase 1 inhibits p53 signaling by dephosphorylating and stabilizing Mdmx. *Cell Signal.* 2013; 25(4):796–804.

542. Mohiuddin IS, Kang MH. DNA-PK as an Emerging Therapeutic Target in Cancer. *Front Oncol*. 2019; 9:635.

543. Masuda T, Xu X, Dimitriadis EK, Lahusen T, Deng CX. "DNA binding region" of BRCA1 affects genetic stability through modulating the intra-S-phase checkpoint. *Int J Biol Sci.* 2016; 12(2):133–43.

544. Karlsson C, Katich S, Hagting A, Hoffmann I, Pines J. Cdc25B and Cdc25C differ markedly in their properties as initiators of mitosis. *J Cell Biol*. 1999; 146(3):573–83.

545. Zhang F, Wen Y, Guo X. CRISPR/Cas9 for genome editing: Progress, implications and challenges. *Hum Mol Genet*. 2014 Sep 15;23(R1):R40-6.

546. Doudna JA, Charpentier E. The new frontier of genome engineering with CRISPR-Cas9. *Science.* 2014; 346(6213):1258096–1258096.

547. Sánchez-Rivera FJ, Jacks T. Applications of the CRISPR-Cas9 system in cancer biology. *Nat Rev Cancer.* 2015; 15(7):387–95.

548. Swanton C. Intratumor heterogeneity: Evolution through space and time. *Cancer Res*. 2012; 72(19):4875–82.

549. García-Santisteban I, Peters GJ, Giovannetti E, Rodríguez JA. USP1 deubiquitinase: cellular functions, regulatory mechanisms and emerging potential as target in cancer therapy. *Mol Cancer.* 2013; 12(1):91.

550. Cacheux W, Rouleau E, Briaux A, Tsantoulis P, Mariani P, Richard-Molard M, et al. Mutational analysis of anal cancers demonstrates frequent PIK3CA mutations associated with poor outcome after salvage abdominoperineal resection. *Br J Cancer.* 2016; 114(12):1387–94.

551. Rosell R, Chaib I, Santarpia M. Targeting MET amplification in EGFR-mutant non-small-cell lung cancer. *Lancet Respir Med.* 2020; 8(11):1068-1070.

552. Benderra MA, Aspeslagh S, Postel-Vinay S, Bigot L, De Baere T, Loriot Y, et al. Acquired EGFR mutation as the potential resistance driver to crizotinib in a MET-Mutated Tumor. *J Thorac Oncol*. 2016; 11(2):e21-3.

Appendices

Appendix Table 1.

Novel low allelic fraction variants that appear following SRA737 treatment (present in the EOS but not D4to7/C3D1). SRA737 sample ID Key: first number = Analysis ID, second number = site, third number = patient ID. D-7 to -4 is pre SRA737 sample, C3D1 is mid SRA737 treatment sample and EOS is end of SRA737 study sample.

Patient ID+A3:C112 (Analysis ID_Site_patient_time point)	Hugo_Symbol	Variant_Classification
22_031_013_EOS	ABL1	5'UTR
14_011_011_EOS	ABL1	Intron
17_031_001_C3D1	ABL1	Intron
3_031_003_EOS	ATM	3'UTR
22_031_013_EOS	ATM	3'UTR
74_144_027_EOS	ATM	Frame_Shift_Ins
3_031_003_EOS	ATM	Intron
3_031_003_EOS	ATM	Intron
32_039-038_EOS	ATM	Intron
13_148_001_EOS	ATM	Intron
13_148_001_EOS	ATM	Missense_Mutation
74_144_027_EOS	ATR	In_Frame_Ins
3_031_003_EOS	ATR	Intron
3_031_003_EOS	ATR	Intron
8_011_006_EOS	ATR	Intron
8_011_006_EOS	ATR	Intron
74_144_027_EOS	ATR	Missense_Mutation
3_031_003_EOS	BRCA1	3'UTR
8_011_006_EOS	BRCA1	3'UTR
22_031_013_EOS	BRCA1	Frame_Shift_Del
61_031_025_EOS	BRCA1	Frame_Shift_Del
12_145_001_EOS	BRCA1	Frame_Shift_Del
17_031_001_C3D1	BRCA1	Intron

Patient ID+A3:C112 (Analysis ID_Site_patient_time point)	Hugo_Symbol	Variant_Classification
32_039-038_EOS	BRCA1	Intron
13_148_001_EOS	BRCA1	Intron
14_011_011_EOS	CCNE1	Intron
17_031_001_C3D1	CDC25A	3'UTR
74_144_027_EOS	CDC25A	3'UTR
15_148_020_EOS	CDC25A	3'UTR
8_011_006_EOS	CDC25A	3'UTR
14_011_011_EOS	CDC25A	Intron
32_039-038_EOS	CDC25A	Intron
7_011_013_C3D1	CDC25B	3'UTR
61_031_025_EOS	CDC25B	3'UTR
32_039-038_EOS	CDC25B	3'UTR
14_011_011_EOS	CDC25B	Frame_Shift_Del
14_011_011_EOS	CDC25B	Frame_Shift_Del
20_031_011_EOS	CDC25B	Frame_Shift_Del
14_011_011_EOS	CDC25B	Intron
20_031_011_EOS	CDC25B	Intron
32_039-038_EOS	CDC25B	Intron
32_039-038_EOS	CDC25B	Missense_Mutation
74_144_027_EOS	CDC25C	Intron
17_031_001_C3D1	CHEK1	Intron
32_039-038_EOS	CLSPN	5'Flank
7_011_013_C3D1	CLSPN	Intron
17_031_001_C3D1	CLSPN	Intron
3_031_003_EOS	CLSPN	Intron
3_031_003_EOS	CLSPN	Intron
22_031_013_EOS	CLSPN	Intron
12_145_001_EOS	CLSPN	Intron

Patient ID+A3:C112 (Analysis ID_Site_patient_time point)	Hugo_Symbol	Variant_Classification
13_148_001_EOS	CLSPN	Intron
15_148_020_EOS	CLSPN	Intron
8_011_006_EOS	CLSPN	Intron
14_011_011_EOS	FANCA	3'UTR
7_011_013_C3D1	FANCA	3'UTR
15_148_020_EOS	FANCA	3'UTR
15_148_020_EOS	FANCA	3'UTR
14_011_011_EOS	FANCA	Intron
17_031_001_C3D1	FANCA	Intron
8_011_006_EOS	FANCA	Intron
8_011_006_EOS	FANCA	Intron
14_011_011_EOS	FANCC	3'UTR
14_011_011_EOS	FANCC	3'UTR
3_031_003_EOS	FANCC	3'UTR
13_148_001_EOS	FANCC	3'UTR
14_011_011_EOS	FANCE	Intron
3_031_003_EOS	FANCG	3'UTR
22_031_013_EOS	FANCG	3'UTR
12_145_001_EOS	FANCG	3'UTR
13_148_001_EOS	HERC2	Intron
8_011_006_EOS	HERC2	Intron
17_031_001_C3D1	MAPKAPK2	3'UTR
12_145_001_EOS	MAPKAPK2	3'UTR
74_144_027_EOS	MYC	Missense_Mutation
28_039_015_EOS	none	
17_031_001_C3D1	PPM1A	Intron
7_011_013_C3D1	PRKDC	Frame_Shift_Del
17_031_001_C3D1	PRKDC	Frame_Shift_Del

Patient ID+A3:C112 (Analysis ID_Site_patient_time point)	Hugo_Symbol	Variant_Classification
3_031_003_EOS	PRKDC	Frame_Shift_Del
32_039-038_EOS	PRKDC	Frame_Shift_Del
3_031_003_EOS	PRKDC	Intron
20_031_011_EOS	PRKDC	Intron
22_031_013_EOS	RAD51	3'UTR
3_031_003_EOS	REL	3'UTR
13_148_001_EOS	REL	3'UTR
7_011_013_C3D1	REL	Intron
61_031_025_EOS	RELA	Frame_Shift_Del
74_144_027_EOS	RELA	Frame_Shift_Del
8_011_006_EOS	RPA1	Intron
8_011_006_EOS	TIMELESS	5'UTR
20_031_011_EOS	TIMELESS	Frame_Shift_Del
3_031_003_EOS	TOPBP1	Intron
22_031_013_EOS	TOPBP1	Intron
12_145_001_EOS	TOPBP1	Intron
13_148_001_EOS	TOPBP1	Intron
13_148_001_EOS	TOPBP1	Intron
7_011_013_C3D1	Unknown	IGR
17_031_001_C3D1	Unknown	IGR
15_148_020_EOS	Unknown	IGR
8_011_006_EOS	USP20	Intron
8_011_006_EOS	WEE1	3'UTR
17_031_001_C3D1	WEE1	Missense_Mutation
12_145_001_EOS	XRCC5	Intron
20_031_011_EOS	XRCC5	Missense_Mutation
3_031_003_EOS	XRCC6	Intron
3_031_003_EOS	XRCC6	Intron

Patient ID+A3:C112 (Analysis ID_Site_patient_time point)	Hugo_Symbol	Variant_Classification
20_031_011_EOS	XRCC6	Intron

Appendix Table 2.

Novel low allelic fraction variants that disappear following SRA737 treatment (present in D4to7/C3D1 but not in paired EOS sample). SRA737 sample ID Key: first number = Analysis ID, second number = site, third number = patient ID. D-7 to -4 is pre SRA737 sample, C3D1 is mid SRA737 treatment sample and EOS is end of SRA737 study sample.

Patient ID (Analysis ID_Site_patient_time point)	Hugo_Symbol	Variant_Classification
6_011_013_D7to4	ATM	3'UTR
6_031_025_D7to4	ATM	3'UTR
7_039_015_D7to4	ATM	3'UTR
6_031_025_D7to4	ATM	Intron
6_031_025_D7to4	ATM	Intron
1_011_006_C3D1	ATR	Intron
2_031_001_D7to4	BRCA1	3'UTR
2_031_001_D7to4	BRCA1	Intron
1_011_006_C3D1	BRCA1	Intron
5_031_011_C3D1	CDC25A	3'UTR
7_039_015_D7to4	CDC25A	3'UTR
1_011_006_C3D1	CDC25A	3'UTR
42_148_001_D7to4	CDC25A	Intron
73_144_027_D7to4	CDC25B	3'UTR
1_011_006_C3D1	CDC25B	3'UTR
4_031_003_D7to4	CDC25B	Intron
4_031_003_D7to4	CHEK1	Frame_Shift_Del
21_031_013_D7to4	CHEK2	3'UTR
6_031_025_D7to4	CHEK2	Intron
4_031_003_D7to4	CLSPN	Intron
5_031_011_C3D1	CLSPN	Intron
6_031_025_D7to4	CLSPN	Intron
6_031_025_D7to4	CLSPN	Intron

Patient ID (Analysis ID_Site_patient_time point)	Hugo_Symbol	Variant_Classification
1_011_006_C3D1	CLSPN	Intron
6_011_013_D7to4	FANCA	Intron
6_031_025_D7to4	FANCA	Intron
4_031_003_D7to4	FANCC	3'UTR
4_031_011_D7to4	FANCC	3'UTR
6_031_025_D7to4	FANCC	3'UTR
6_031_025_D7to4	FANCC	3'UTR
1_011_011_D7to4	FANCC	Intron
1_011_006_C3D1	FANCC	Intron
7_039_015_D7to4	FANCE	Intron
1_011_011_D7to4	FANCG	3'UTR
5_031_011_C3D1	FANCG	3'UTR
7_039_015_D7to4	FANCG	3'UTR
14_148_020_D7to4	FANCG	3'UTR
1_011_011_D7to4	HERC2	Intron
2_031_001_D7to4	HERC2	Intron
7_039_015_D7to4	HERC2	Intron
1_011_006_C3D1	HERC2	Missense_Mutation
2_031_001_D7to4	MAPKAPK2	3'UTR
6_011_013_D7to4	MAPKAPK2	Intron
6_031_025_D7to4	MAPKAPK2	Intron
73_144_027_D7to4	MAPKAPK2	Intron
1_011_011_D7to4	MYC	Missense_Mutation
72_039_038_D7to4	none are novel	
5_031_011_C3D1	PRKDC	Frame_Shift_Del
42_148_001_D7to4	PRKDC	Frame_Shift_Del
1_011_011_D7to4	PRKDC	Intron
4_031_003_D7to4	RPA1	3'UTR

Patient ID (Analysis ID_Site_patient_time point)	Hugo_Symbol	Variant_Classification
4_031_003_D7to4	RPA1	3'UTR
1_011_006_C3D1	RPA1	3'UTR
1_011_011_D7to4	TIMELESS	Intron
5_031_011_C3D1	TOPBP1	Intron
73_144_027_D7to4	TOPBP1	Intron
11_145_001_D7to4	TOPBP1	Intron
1_011_006_C3D1	TOPBP1	Intron
11_145_001_D7to4	Unknown	IGR
1_011_006_C3D1	XRCC6	Intron
1_011_011_D7to4	ZNF276	3'UTR

Appendix Table 3.

Low allelic fraction variants in the non-paired samples. SRA737 sample ID Key: first number = Analysis ID, second number = site, third number = patient ID. D-7 to -4 is pre SRA737 sample, C3D1 is mid SRA737 treatment sample and EOS is end of SRA737 study sample.

Patient ID (Analysis ID_Site_patient_time point)	Hugo_Symbol	Variant_Classification
8_141_003_D7to4	ATM	3'UTR
8_141_003_D7to4	ATM	3'UTR
7_031_005_EOS	ATM	Intron
7_031_005_EOS	ATM	Intron
8_141_003_D7to4	ATM	Intron
38_143_010_D7to4	ATM	Intron
3_031_002_D7to4	ATM	Missense_Mutation
3_031_002_D7to4	ATM	Missense_Mutation
8_141_003_D7to4	ATM	Missense_Mutation
10_031_076_EOS	ATM	Missense_Mutation
9_141_005_EOS	ATM	Splice_Site
10_031_076_EOS	ATM	Splice_Site
9_031_061_EOS	ATR	Intron
9_141_005_EOS	ATR	Intron
10_141_012_EOS	ATR	Intron
38_143_010_D7to4	ATR	Intron
15_011_012_D7to4	ATR	Missense_Mutation
8_141_003_D7to4	BRCA1	3'UTR
16_011_002_D7to4	BRCA1	3'UTR
3_031_002_D7to4	BRCA1	Frame_Shift_Del
26_031_089_D7to4	BRCA1	Frame_Shift_Del
8_141_003_D7to4	BRCA1	Intron
8_141_003_D7to4	BRCA1	Intron
9_141_005_EOS	BRCA1	Intron

Patient ID (Analysis ID_Site_patient_time point)	Hugo_Symbol	Variant_Classification
10_031_076_EOS	BRCA1	Intron
16_011_002_D7to4	BRCA1	Intron
26_031_089_D7to4	BRCA1	Intron
49_031_019_C3D1	BRCA1	Missense_Mutation
8_141_003_D7to4	CCNE1	Intron
8_141_003_D7to4	CCNE1	Intron
10_031_076_EOS	CDC25A	3'UTR
10_141_012_EOS	CDC25A	3'UTR
16_011_002_D7to4	CDC25A	Nonsense_Mutation
7_031_005_EOS	CDC25B	3'UTR
38_143_010_D7to4	CDC25B	3'UTR
49_031_019_C3D1	CDC25B	3'UTR
7_031_005_EOS	CDC25B	Frame_Shift_Del
38_143_010_D7to4	CDC25B	Frame_Shift_Del
7_031_005_EOS	CDC25B	Intron
9_141_005_EOS	CDC25B	Intron
10_031_076_EOS	CDC25B	Intron
15_011_012_D7to4	CDC25B	Intron
9_031_061_EOS	CDC25B	Missense_Mutation
3_031_002_D7to4	CDC25C	3'UTR
7_031_005_EOS	CDC25C	Intron
11_5_013_15ng_input	CHEK2	Frame_Shift_Ins
3_031_002_D7to4	CLSPN	Intron
8_141_003_D7to4	CLSPN	Intron
9_141_005_EOS	CLSPN	Intron
10_141_012_EOS	CLSPN	Intron
11_5_013_15ng_input	CLSPN	Intron
8_141_003_D7to4	CLSPN	Missense_Mutation

Patient ID (Analysis ID_Site_patient_time point)	Hugo_Symbol	Variant_Classification
9_141_005_EOS	FANCA	3'UTR
10_141_012_EOS	FANCA	3'UTR
15_011_012_D7to4	FANCA	3'UTR
8_141_003_D7to4	FANCA	Intron
9_141_005_EOS	FANCA	Intron
10_141_012_EOS	FANCA	Intron
10_141_012_EOS	FANCA	Intron
10_141_012_EOS	FANCA	Intron
9_141_005_EOS	FANCC	3'UTR
15_011_012_D7to4	FANCC	3'UTR
38_143_010_D7to4	FANCC	3'UTR
49_031_019_C3D1	FANCC	3'UTR
9_141_005_EOS	FANCC	5'UTR
15_011_012_D7to4	FANCC	Intron
10_031_076_EOS	FANCE	Frame_Shift_Del
3_031_002_D7to4	FANCE	Intron
3_031_002_D7to4	FANCE	Intron
9_141_005_EOS	FANCE	Intron
49_031_019_C3D1	FANCE	Intron
49_031_019_C3D1	FANCE	Intron
8_141_003_D7to4	FANCE	Missense_Mutation
9_031_061_EOS	FANCF	3'UTR
10_031_076_EOS	FANCG	3'UTR
10_141_012_EOS	FANCG	3'UTR
15_011_012_D7to4	FANCG	3'UTR
49_031_019_C3D1	FANCG	Intron
8_141_003_D7to4	HERC2	Intron
10_031_076_EOS	HERC2	Intron

Patient ID (Analysis ID_Site_patient_time point)	Hugo_Symbol	Variant_Classification
10_141_012_EOS	HERC2	Intron
11_5_013_15ng_input	HERC2	Intron
16_011_002_D7to4	HERC2	Intron
26_031_089_D7to4	HERC2	Intron
3_031_002_D7to4	HERC2	Missense_Mutation
8_141_003_D7to4	MAPKAPK2	3'UTR
9_141_005_EOS	MAPKAPK2	3'UTR
9_031_061_EOS	MAPKAPK2	Intron
3_031_002_D7to4	MYC	Missense_Mutation
7_031_005_EOS	MYC	Missense_Mutation
8_141_003_D7to4	MYC	Missense_Mutation
10_031_076_EOS	MYC	Missense_Mutation
49_031_019_C3D1	MYC	Missense_Mutation
71_144_016_C3D1	none	
8_141_003_D7to4	PPM1A	3'UTR
9_031_061_EOS	PPM1A	3'UTR
49_031_019_C3D1	PPM1A	3'UTR
49_031_019_C3D1	PPM1A	3'UTR
3_031_002_D7to4	PRKDC	Frame_Shift_Del
7_031_005_EOS	PRKDC	Frame_Shift_Del
9_031_061_EOS	PRKDC	Frame_Shift_Del
9_141_005_EOS	PRKDC	Frame_Shift_Del
10_031_076_EOS	PRKDC	Frame_Shift_Del
15_011_012_D7to4	PRKDC	Frame_Shift_Del
26_031_089_D7to4	PRKDC	Frame_Shift_Del
38_143_010_D7to4	PRKDC	Frame_Shift_Del
49_031_019_C3D1	PRKDC	Frame_Shift_Del
8_141_003_D7to4	PRKDC	Intron

Patient ID (Analysis ID_Site_patient_time point)	Hugo_Symbol	Variant_Classification
11013_15ng_input	PRKDC	Intron
11013_15ng_input	PRKDC	Intron
49_031_019_C3D1	PRKDC	Intron
49_031_019_C3D1	PRKDC	Intron
49_031_019_C3D1	PRKDC	Intron
8_141_003_D7to4	PRKDC	Missense_Mutation
49_031_019_C3D1	PRKDC	Missense_Mutation
9_141_005_EOS	REL	3'UTR
9_141_005_EOS	REL	3'UTR
3_031_002_D7to4	RPA1	3'UTR
10_031_076_EOS	RPA1	3'UTR
10_031_076_EOS	RPA1	3'UTR
15_011_012_D7to4	RPA1	3'UTR